The role of cell-type selective synaptic connections in rhythmic neuronal network activity in the hippocampus

Doctor of Philosophy (D. Phil.) Thesis
Trinity Term, 2014

Linda Katona
Brasenose College

MRC Anatomical Neuropharmacology Unit
Department of Pharmacology
University of Oxford
Oxford, UK

„A világ megismerése érdekes, hasznos, gyönyörködtető, félelmes vagy tanulságos;

önmagunk megismerése a legnagyobb utazás, a legfélelmesebb felfedezés,

a legtanulságosabb találkozás."

(Márai Sándor)

Abstract

The role of cell-type selective synaptic connections in rhythmic neuronal network activity in the hippocampus

Linda Katona, Brasenose College
Thesis submitted for the degree of Doctor of Philosophy, Trinity Term, 2014.

Structural and functional changes in the hippocampal neuronal network of the brain allow organisms to adapt to the environment. Such plasticity leads to the encoding of newly acquired information and the replacement or updating of stored knowledge by new experience. Information is carried by the output of active pyramidal cell assemblies during transient network oscillations. In the CA1 area, the activity of pyramidal cells is regulated by at least twenty-two distinct types of GABAergic interneuron with different molecular expression profiles and innervating defined pyramidal cell compartments. The *in vivo* spike-timing of identified types of GABAergic cell in freely moving rodents has been largely unknown until recently. Although thousands of interneurons have been reported from large scale extracellular recordings their cell type identity has remained uncertain.

How do different types of GABAergic cell regulate pyramidal cell output during behaviour? In order to test the hypothesis that differences in connectivity and molecular composition amongst cell types reflect the specialisation of their functions, I have recorded single pyramidal cells and GABAergic interneurons extracellularly in the CA1 area of freely moving rats during theta- and sharp wave associated ripple-oscillations (SWRs), and subsequently I have labelled the recorded neurons using the juxtacellular technique (Lapray et al., 2012). My main findings are: **1.** I have identified PV+ basket, axo-axonic, bistratified and O-LM cells, together with an "unconventional interneuron". **2.** Behaviour and network states differentiate the activities of GABAergic cell types in freely moving rats. **3.** During sleep, PV+ basket and bistratified cells fire at higher rates than axo-axonic and O-LM cells, and unlike axo-axonic and O-LM cells, strongly increase spiking during SWRs. **4.** Axo-axonic and O-LM cells decrease firing during sleep relative to awake states and are inhibited during all or most SWRs, respectively. **5.** During movement, axo-axonic and PV+ basket cells fire with similarly high frequencies but on complementary segments of the descending slope of theta cycles. **6.** Bistratified and O-LM cells fire cooperatively during movement at the troughs of theta oscillations but with different frequencies. **7.** The "unconventional interneuron", in contrast to the other identified cell types, has a low spike rate and becomes activated exclusively during SWRs. **8.** Behaviour and rhythmic network events differentiate GABA and peptide release to distinct membrane domains of pyramidal cells. **9.** My results have validated many of the spike-timing characteristics determined under urethane anaesthesia (Klausberger and Somogyi, 2008; Somogyi, 2010), although, in average, firing rates are higher under physiological, drug-free conditions.

My results demonstrate specialisations of distinct types of GABAergic interneuron during network operations. Distinct cell types contribute to the rhythmic redistribution of GABAergic action on different pyramidal cell membrane domains, at both slower and faster time scales, from the axon initial segment through the cell body down to the distal apical tuft and back, which is necessary for the rhythmic separation of network function during different stages of mnemonic processing.

Acknowledgements

This thesis is a testimony to my undertakings in neuroscience, specifically in the investigation of hippocampal GABAergic interneuron types, and I address it as a token of my gratitude to my two supervisors Professor Peter Somogyi and Professor Thomas Klausberger. Thank you for guiding my development as a scientist through rigorous teaching and relentless mentorship showcasing the spirit of excellence throughout the years. Much of this work would not have been possible without the dedicated teaching, patient listening and friendly support that I have received from Dr. Damien Lapray, for which I am forever thankful.

Since my arrival to the Somogyi laboratory I have been fortunate to meet wonderful people who provided me with a very supportive and a flourishing scientific environment and from whom I learned great expertise and professionalism. For current and past members of the group and Unit, for the visiting scientists and students and collaborators, I wish to thank you all for your contributions: Dr. Tim Viney, Dr. Jozsef Somogyi, Dr. Yannis Dalezios, Dr. Balint Lasztoczi, together with Kristina Detzner (Wagner), Ben Micklem, David Roberts, Abhilasha Joshi, Szabi Biro, Dr. Daniel Swiejkowski, Dr. Rob Stewart, Mike Crump, Dr. Gunes Unal, Klara Peto, Liz Norman and Katie Whitworth, Mary Gilgunn-Jones, Jenny Cooke, Agnieszka Swiejkowska and Jo Stocker; Dr. Katja Hartwich and Dr. Zsolt Borhegyi for allowing me to analyse their data, Laszlo Papp for the microdrive-driven tetrodes, Dr. Laszlo Marton for a subset of electron microscopic samples, Szabi Biro and Dr. Timea Szabadi for the 3D Neurolucida reconstructions. I am also grateful to Prof. Jozsef Csicsvari, Dr. David Dupret, Dr. Alvaro Tejero-Cantero, Colin McNamara, Dr. Alessia Manganaro, Dr. Thomas Bienvenu and Dr. Mira Lapray for the sometimes heated discussions which helped in my scientific endeavours, as well as, for all the unforgettable fun moments and true friendship which enriched my experience in this “city of dreaming spires”.

To all my friends, old and new, and the ladies in the Oxford University Blues Basketball team many thanks.

Finally, I wish to dedicate this written testimony also to those closest to me and who I treasure in my heart. My beloved family and Colin, thank you for being my solid rock and believing in me. I am blessed with your love. Köszönöm, drága családom, szeretetetek számomra áldás.

Contents

Figures

Tables

List of abbreviations

A

AC, autocorrelogram

AIS, axon initial segment

AMPA, α-amino-3-hydroxy-5-methyl-4-isoxazolepropionic acid receptor

ANOVA, analysis of variance

C

CA1, Cornu Ammonis 1

CA2, Cornu Ammonis 2

CA3, Cornu Ammonis 3

CB, calbindin

CB1, cannabinoid receptor type 1

CCK, cholecystokinin

CDF, cumulative distribution function

CGE, caudal ganglionic eminence

COUP-TFII, chicken ovalbumin upstream promoter type II

CR, celretinin

Cy3, cyanine 3

Cy5, cyanine 5

D

DAB, 3,3'-diaminobenzidine

DG, dentate gyrus

E

EC, entorhinal cortex

EEG, electroencephalography

Elfn1, extracellular leucine-rich repeat fibronectin containing protein type 1

EM, electron microscopy

ErbB4, tyrosine-protein kinase receptor

F

Fog-2, zinc finger protein transcription factor

G

GABA, gamma-Aminobutyric acid

$GABA_A$, gamma-Aminobutyric acid type A receptor

$GABA_B$, gamma-Aminobutyric acid type B receptor

H

HCN, hyperpolarization-activated cyclic nucleotide-gated channel

HRP, horseradish peroxidase enzyme

I

IF, instantaneous frequency

ISI I-III, interneuron specific interneuron types I-III

ISI, inter-spike intervals

L

LED, light-emitting diode

LFP, local field potential

LOSC, low oscillatory periods

LTD, long-term depression

LTP, long-term potentiation

M

MBS, Main Beam Splitters

MGE, medial ganglionic eminence

mGluR1a, metabotropic glutamate receptor 1a

mGluR7a, metabotropic glutamate receptor 7a

N

NHS, normal horse serum

NMDA, N-methyl-D-aspartate receptor

NOS, nitric oxide synthase

NPY, neuropeptide tyrosine

O

O-LM, oriens–lacunosum moleculare

P

PB, phosphate buffer

PV+, parvalbumin immunopositive

S

s.d., standard deviaton

s.e.m., standard error of the mean

Satb1, special AT-rich sequence-binding protein 1

SOM, somatostatin

sst2R, sst3R, sst4R, somatostatin receptors 2,3,4

SWRs, sharp wave associated ripple oscillations

T

TBS-TX, tris buffered saline with Triton X-100®

V

VIP, vasoactive intestinal polypeptide

1 General introduction

Brains adapt to the environment using mnemonic processing which induces structural and functional changes in the hippocampal neuronal circuitry and supports survival. Such plasticity allows the encoding of newly acquired information and the replacement or updating of stored knowledge by new experience.

I have explored the roles of identified hippocampal cell types in learning-induced changes during rhythmic network events in freely moving rats. Specifically, I have tested the hypothesis that distinct types of GABAergic interneuron have different effects on pyramidal cell firing during exploration and sleep.

In chapter 1, I first summarise current knowledge about the hippocampal formation and its involvement in learning and navigation. This is followed by an overview of the synaptic organisation of the hippocampal neuronal network. Glutamatergic pyramidal cells and distinct types of GABAergic interneuron have been investigated *in vitro* and *in vivo* under anaesthesia, but very little is known about their firing activities in natural brain states. Next, I review our understanding about hippocampal oscillatory network states and, finally, I present my research aims.

It was proposed that the *assembly* of pyramidal cells activated simultaneously by an external event becomes the *engram/memory trace* associated with that

particular stimulus (Hebb, 1949). The contribution of specific cell types to the temporal ordering of pyramidal cells into assemblies is mostly unknown. I have studied the behaviour related spike-timing of hippocampal neurons during theta- and sharp wave associated ripple oscillations. The goal of my explorations is to improve our understanding about the behaviour-dependent organisation of the hippocampal "chronocircuit".

1.1 Hippocampus and mnemonic processing

1.1.1 Hippocampal roles

Changes in behaviour are determined by transient brain states. In the cerebral cortex the emergence and termination of different brain states is governed by the cooperative activity of large groups of neuron. Computations in such complex neuronal networks process sensation, initiate action and lead to learning through plasticity; their malfunction underlies brain disorders.

The medial temporal lobe has been identified as a part of the cortex responsible for associative learning (Aggleton, 2012; Zola-Morgan and Squire, 1985). In its centre lies the hippocampal formation (Figure 1-1Aa), the brain region governing the *encoding* of new information and the *consolidation* of this new knowledge into a memory (Eichenbaum et al., 2012; Milner et al., 1998; Squire, 2009b; Squire et al., 2004). Studies of patients suffering from anterograde and/or retrograde amnesia (e.g., H.M., R.B.) caused by bilateral removal of the hippocampi (Figure 1-1Ab,c) demonstrated the importance of the hippocampal formation in mnemonic processing (Scoville and Milner, 1957; Squire, 2009a; Zola-Morgan et al., 1986). Furthermore, the need of the hippocampus for the retention of relational information has been extensively demonstrated in rodents. Using spatial navigation tasks it has been shown

that hippocampal lesions generate memory impairment in all mammalian species (Burgess et al., 2002; Deacon and Rawlins, 2006; Fortin et al., 2002; Kirby and Rawlins, 2003; Lisman, 1999; Manns and Eichenbaum, 2006; Morris et al., 1982; Olton, 1977; Olton et al., 1986; Squire et al., 2004; Zhang et al., 2004).

What are the cellular and molecular mechanisms related to mnemonic functions? Neurons use electrical and chemical signals to transfer information between each other. The site of this communication is called the synapse. A novel experience is encoded in the brain as a specific pattern of *short-term* synaptic changes between neurons. These short-term changes are transformed into *long-term* changes via molecular mechanisms termed long-term potentiation (LTP) (Bliss and Lømo, 1973; Kandel and Spencer, 1961) and long-term depression (LTD) (Castellucci et al., 1970; Mulkey and Malenka, 1992). The relationship between LTP/LTD and memory consolidation has been demonstrated by *in vitro* and *in vivo* animal studies and it involves glutamate receptors and changes in transmitter release probability (Bannerman et al., 2014; Bekinschtein et al., 2010; Debanne and Thompson, 1996; Dudek and Bear, 1992; Krug et al., 1985; Magee and Johnston, 1997; McHugh et al., 1996; Morris, 2013; Morris et al., 2013; Nakazawa et al., 2002; Nakazawa et al., 2003; Silva et al., 1992a; Silva et al., 1992b; Thomas et al., 1998).

When do these synaptic modifications occur? In the hippocampal formation, rhythmic network states of different frequencies are thought to provide the temporal framework for the different phases of mnemonic processing (see section 1.3). During exploration, theta frequency oscillations (5-12 Hz) are prominent in the hippocampal local field potential (Buzsaki et al., 1983). Specialised neurons, the *place cells*, are active during theta oscillations at times when the rat traverses defined portions of the environment, the *place fields* (O'Keefe and Dostrovsky, 1971). New experiences along

the path may induce short-term synaptic changes between novel sequences of place cells (Buzsáki, 1989). Connections modified during exploration become consolidated during subsequent slow wave sleep (Buzsáki, 1996). The sequences of place cell assemblies activated by the progressive traversal of place fields is replayed in a temporally compressed manner during the much shorter cycles of sharp wave associated ripple frequency (130-230 Hz) oscillations (Bendor and Wilson, 2012; Pavlides and Winson, 1989; Skaggs and McNaughton, 1996; Wilson and McNaughton, 1994).

1.1.2 Brain disorders and the hippocampus

Hippocampal abnormalities correlate with a variety of mental disorders such as epilepsy, Alzheimer's disease, schizophrenia, autism and anxiety disorders. The very low threshold for seizures makes the hippocampus prone to aberrant oscillatory activity emerging during epilepsy (Green and Scheetz, 1964; Kitchigina et al., 2013). Under normal conditions, large synchronous excitatory events in the local field potential (Johnston and Brown, 1986) are supressed by GABAergic and/or peptidergic interneurons (Cammarota et al., 2013; Kovac and Walker, 2013). It has been shown that distinct GABAergic cell types are lost or become dysfunctional in epileptic rats (Buckmaster and Jongen-Rêlo, 1999; Feldt Muldoon et al., 2013; Huusko et al., 2013; Peng et al., 2013; Sun et al., 2014). In schizophrenia, a variety of hippocampal alterations have been reported including tissue shrinkage, defects in myelin sheaths, abnormal neuron clustering and changes in neurotransmitter signalling (del Pino et al., 2013; Fisahn et al., 2009; Lewis et al., 2005; Neddens et al., 2011). Furthermore, functional impairment of specific interneuron types has been linked to perturbed oscillations (Cunningham et al., 2006; Koutsoukos et al., 2013; Nakazawa et al., 2012;

Uhlhaas and Singer, 2006; Whittington et al., 2011b). Moreover, hippocampal cell death in Alzheimer's disease leads to spatial and episodic memory impairment and the inability to form new associations (Hyman et al., 1984; Jeong, 2004; Moretti et al., 2011).

Common factors started unfolding in these mental disorders. Aberrant oscillatory activities correlate with interneuron malfunction which then results in cognitive impairments (Basar and Guntekin, 2008; Uhlhaas and Singer, 2006; Uhlhaas and Singer, 2012). Determining the activity of distinct GABAergic interneuron types during normal versus anomalous rhythmic network states could potentially elucidate some of the mechanisms of mental illnesses and lead to treatment. Clinical studies together with the use of rodent models of human diseases are important for early diagnosis and future therapies.

1.1.3 Organisation of the hippocampal formation

The hippocampal formation (Figure 1-1B) is a cluster of cortical structures within the limbic system (Amaral and Witter, 1989; Squire, 2004; Squire et al., 2004; van Strien et al., 2009) including the entorhinal cortex (EC)(Kerr et al., 2007), the para- and presubiculum, subiculum, hippocampal areas CA1-3 (Lorente De No, 1934) and dentate gyrus (DG) (Amaral et al., 2007). Together, these areas contribute to the formation of declarative memories (Aggleton et al., 2012). High-level, multisensory information reaches the hippocampal formation via glutamatergic pathways (Figure 1-1C) through the retrosplenial or peri- and postrhinal cortices (Burwell, 2000; Naber et al., 2001b; Wyass and Van Groen, 1992). The information is passed along the sequence of EC-DG-hippocampus-subiculum-EC while it is transformed into memory engrams (Buzsáki, 1996; Eichenbaum and Lipton, 2008; Manns and Eichenbaum,

2006). These engrams are then sent back for long-term storage from the deep layers of the EC to the cortical areas originally projecting to the hippocampal formation. Other, direct cortical projections from the hippocampus to e.g., the medial prefrontal cortex also have great behavioural significance. In addition, the hippocampal formation sends information to, and controls large areas of the subcortical forebrain, including the hypothalamus, the accessory olfactory bulb and the nucleus accumbens.

There is a progression of excitatory pathways within the hippocampal formation (Figure 1-1C,D). Stellate cells in the entorhinal cortical layer 2 project to DG (Ruth et al., 1982, 1988; Steward and Scoville, 1976) and to areas CA2-3 via the *perforant path* (Steward, 1976; Yeckel and Berger, 1990). It has been proposed that projections originating from the medial and lateral EC provide segregated information to the hippocampus about the spatial *context* and the experience-specific *content*, respectively (Henriksen et al., 2010; Knierim et al., 2014). Neurons in layer 3 give rise to a topographical *perforant path* projection targeting CA1 and the subiculum (Yeckel and Berger, 1995). Granule cells in the DG send their axon bundles termed *mossy fibres* to CA3 stratum lucidum (Claiborne et al., 1986) and in the mouse also to CA2 (Kohara et al., 2014). In the CA3 area, pyramidal cells at different septo-temporal levels are heavily interconnected via recurrent collaterals creating the *associational path* (Ramon y Cajal, 1893; Witter, 2007) including the CA2 area. Moreover, these same pyramidal cells send their *Schaffer collaterals* to the CA1 area (Ishizuka et al., 1990; Li et al., 1994; Sik et al., 1993; Witter, 2007; Wittner et al., 2007) which is paralleled by a projection from CA2 pyramidal cells (Kohara et al., 2014; Shinohara et al., 2012). In contrast to the CA3 area, CA1 pyramidal cells have fewer recurrent collaterals (Amaral et al., 1991; Deuchars and Thomson, 1996; Takács et al., 2012), and target mainly the subiculum (Amaral et al., 1991), the deep layers of the EC (Naber et al., 2001a) and project to many

subcortical structures. Subiculum is also connected to the entorhinal cortical deep layers (Ishizuka, 2001; Naber and Witter, 1998) and is one of the main output structures of the hippocampal formation to subcortical areas.

In addition to the connections listed above, there are several *back-projections*; e.g., CA3 to DG (Ishizuka et al., 1990), *commissural pathways* and projections to and from subcortical areas; e.g., thalamus (Dolleman-Van der Weel and Witter, 2000; Swanson and Cowan, 1977; Wouterlood et al., 1990); amygdala (Pitkanen et al., 2000). Furthermore, hippocampal computations require these glutamatergic projections to be regulated by GABAergic, cholinergic and other neuromodulatory pathways from the medial septum, supramammillary nuclei, raphe nuclei and locus coeruleus, amongst others. I present more information about these pathways in later chapters, in order to keep the introduction focused.

1.1.4 The dorsal hippocampal CA1 area

The hippocampus can be divided into functionally distinct regions along its dorso-ventral and medio-lateral axes (Fanselow and Dong, 2010; Thompson et al., 2008). The dorsal portion of the hippocampus (Figure 1-1D) is thought to be involved in spatial navigation related tasks, whereas the ventral part is more interconnected with brain areas processing object-features and emotions (Bannerman et al., 2003; Bannerman et al., 2004; Zhang et al., 2004).

My work focuses on the CA1 area of the dorsal hippocampus and its intensely studied neuronal network (Figure 1-1D). This brain region has a laminar structure composed of four layers: strata oriens, pyramidale, radiatum and lacunosum moleculare, in the dorsal-to-ventral direction. Cell bodies of glutamatergic pyramidal cells constitute the compact middle layer and give rise to radial running dendrites that

cross the entire hippocampus. GABAergic interneurons with diverse dendritic and axonal trees populate all layers.

Because the different afferents are themselves segregated by layers (Amaral and Witter, 1989; Rawlins and Green, 1977; van Strien et al., 2009), the area is convenient for the study of input-pathways-specific activation of different types of neuron. There are two major glutamatergic inputs to the CA1 area. The synaptic terminals of the *perforant path* are found mostly in stratum lacunosum moleculare and to a smaller extent in stratum oriens forming type I synapses on spines of pyramidal cell dendrites, as well as on interneurons. These fibres originating from the medial or lateral EC have a preferential topographic organisation, where the former terminate in the portion of CA1 closer to CA3 and the latter project to the distal portions neighbouring the subiculum (Kerr et al., 2007; Yeckel and Berger, 1990). The second major glutamatergic projection, the *Schaffer collaterals* (Schaffer, 1892) terminate on the pyramidal cell spines in strata radiatum and oriens (Kim et al., 2012) as well as on interneurons. These glutamatergic pathways are mirrored by GABAergic, cholinergic and neuromodulatory topographical projections from subcortical areas some of which terminate mainly on local GABAergic interneurons distributed across different layers (Freund, 1989; Freund, 1992; Gulyás et al., 1990; Nyakas et al., 1987).

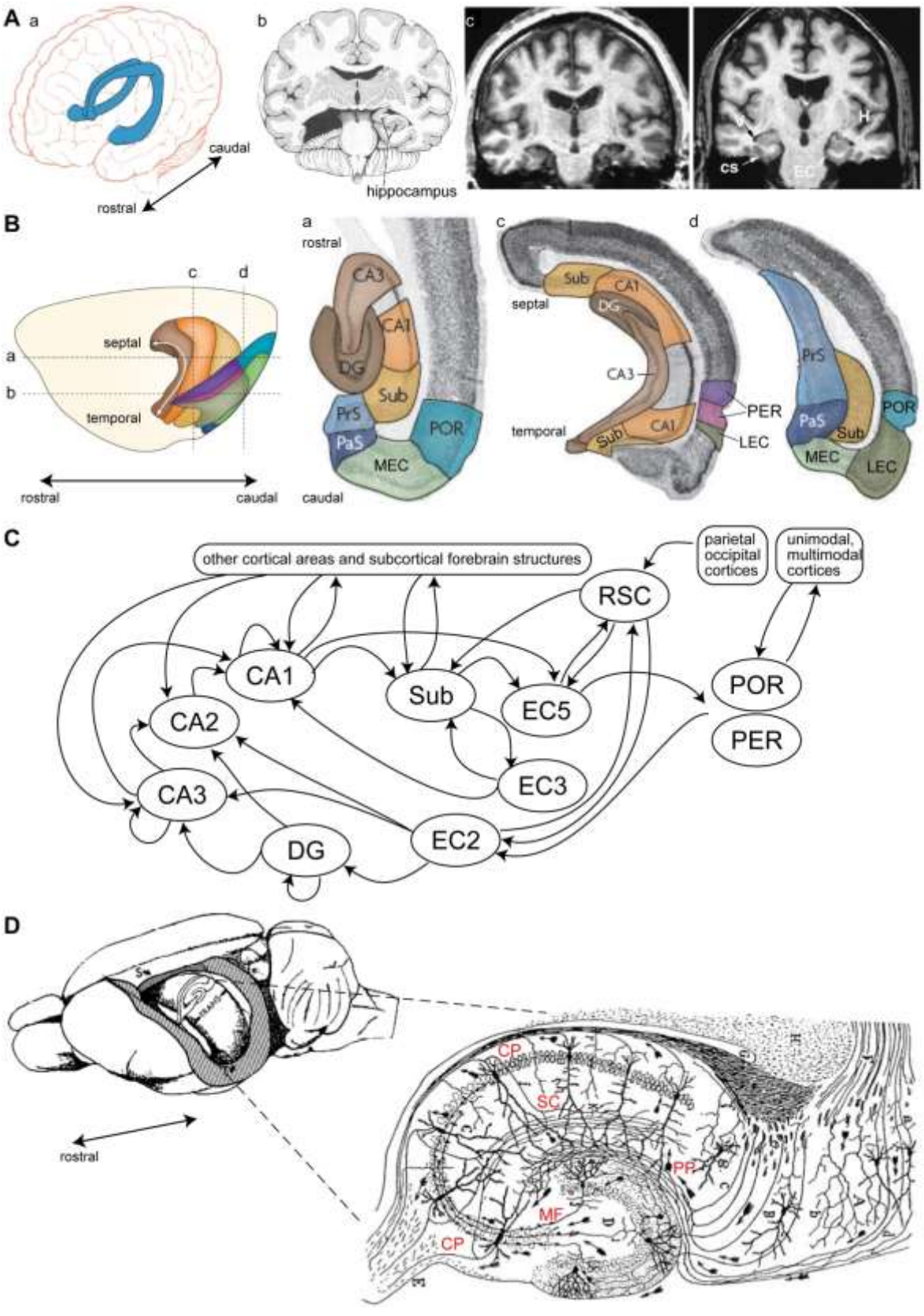
A
a
caudal
rostral
b
hippocampus
c
cs
H
B
a
b
c
d
septal
temporal
rostral
caudal
CA3
CA1
DG
Sub
PrS
PaS
POR
MEC
LEC
PER
C
other cortical areas and subcortical forebrain structures
parietal occipital cortices
unimodal, multimodal cortices
RSC
CA1
Sub
EC5
POR
CA2
PER
CA3
EC3
DG
EC2
D
rostral
CP
SC
PP
MF

Figure 1-1 Hippocampus and mnemonic processing.

A. a, Schematic view of the human brain and hippocampus (blue). b, Diagram of a coronal human brain section showing the attempted medial temporal lobe resection for patient H.M. suffering of epilepsy. After the bilateral removal of a large part of his medial temporal lobes, H.M. developed severe anterograde amnesia [modified from (Scoville and Milner, 1957)]; c, T1-weighted MRI brain scans of H.M (left) and a control subject (right). Note, that most of the hippocampal formation, including the entorhinal cortex and other cortical areas, are missing in H.M. [modified from (Corkin et al., 1997)]. **B, C.** The rat hippocampal formation [modified from (van Strien et al., 2009); (a), horizontal and (c,d) coronal cut brain sections] and its simplified connectivity diagram including input-output regions (C). DG, dentate gyrus; EC2, entorhinal cortical layer 2; EC3, entorhinal cortical layer 3; EC5, entorhinal cortical layer 5; LEC, lateral entorhinal cortex; MEC, medial entorhinal cortex; PaS, parasubiculum; PER, perirhinal cortex; POR, postrhinal cortex; PrS, presubiculum; RSC, retrosplenial cortex; Sub, subiculum. **D.** Major glutamatergic input and output pathways of the dorsal hippocampus [modified from (Amaral and Witter, 1989) and (Ramon y Cajal, 1911)]. Note arrows indicating the direction of impulses as predicted by Ramon y Cajal. CP, commissural pathways; MF, mossy fibres; PP, perforant path; SC, Schaffer collaterals.

1.2 Neuronal network connectivity in the hippocampal CA1 area

1.2.1 Pyramidal cells

The majority of the neurons in the hippocampus are glutamatergic pyramidal cells named after the shape of their somata (Ramon y Cajal, 1893). The cell bodies form a compact layer in the middle of the structure and their dendrites extend in dorsal and ventral directions into strata oriens as well as radiatum and lacunosum moleculare, respectively (Figure 1-2). The somatic and dendritic membranes of pyramidal cells are very densely covered by spines, the loci of short- and long-term synaptic changes between connected neurons (Ishizuka et al., 1995). Pyramidal cells in the CA1 area project to extrahippocampal areas including subiculum and deep layers of the entorhinal cortex (Amaral et al., 1991; Naber et al., 2001a). Their axons give rise to local CA1 collaterals which branch into a plexus in stratum oriens and rarely in stratum pyramidale and only exceptionally in stratum radiatum. They innervate mainly interneurons and less frequently other pyramidal cells (Amaral et al., 1991; Deuchars and Thomson, 1996; Takács et al., 2012). Pyramidal cells receive type I, mostly glutamatergic synapses onto their spines and type II GABAergic synapses onto their somatic and dendritic shaft membranes (Klausberger, 2009; Megias et al., 2001; Miles et al., 1996; Papp et al., 2001).

At least three types of pyramidal cell can be identified (Figure 1-2) based on somatic location and calbindin expression (Bezaire and Soltesz, 2013; Somogyi, 2010). Immunopositivity for certain transcription factors, activity patterns during behaviour and projection areas demonstrate diversification of the pyramidal cell population (Epsztein et al., 2011; Kohara et al., 2014; Krook-Magnuson et al., 2012; Mizuseki et al., 2011; Thompson and Best, 1989).

1.2.2 Synaptic organisation of GABAergic interneuron types

The hippocampal code is created by the output of pyramidal cells which, in the CA1 area, is determined by at least twenty-two distinct types of GABAergic interneuron (Bezaire and Soltesz, 2013; Freund and Buzsáki, 1996; Somogyi, 2010; Somogyi et al., 2014). These GABAergic cells (Figure 1-2) populate all hippocampal layers and exert their inhibitory effects (Glickfeld et al., 2009) via $GABA_A$ (Fritschy and Panzanelli, 2014; Olsen and Sieghart, 2009) and $GABA_B$ receptors (Benarroch, 2012; Lewis, 2010; Terunuma et al., 2014). The majority have dendrites and axon collaterals only within the CA1 area but there are some long-range projecting GABAergic neurons, which have axonal targets in subcortical and extrahippocampal cortical regions (Ferraguti et al., 2005; Fuentealba et al., 2008b; Jinno, 2009; Jinno et al., 2007; Melzer et al., 2012). The fast spread of inhibition between distant brain regions mediated by the latter may provide precise interregional timing for anatomically distributed pyramidal cells in synchronous activity (Buzsáki and Chrobak, 1995; Fujisawa and Buzsáki, 2011).

Based on the dendritic and axonal arborisations, molecular expression profiles and the action potential firing which until recently has been recorded *in vitro* or *in vivo* under urethane anaesthesia, distinct cell types were identified (Figure 1-2): axo-axonic cells, targeting exclusively the axon initial segment of pyramidal cells (Buhl et al., 1994b; Klausberger et al., 2003; Li et al., 1992; Somogyi et al., 1985; Somogyi et al., 1983; Takács et al., 2014); three types of basket cell named after their terminals wrapping around the somata and proximal dendrites of pyramidal cells (Acsády et al., 1996a; Armstrong and Soltesz, 2012; Buhl et al., 1994a; Freund and Katona, 2007; Halasy et al., 1996; Harris et al., 1985; Katsumaru et al., 1988b; Klausberger et al., 2003; Klausberger et al., 2005; Kosaka et al., 1987; Kosaka et al., 1985; Lorente De No, 1934; Nunzi et al., 1985; Ramon y Cajal, 1893; Takács et al., 2014); fifteen types of dendrite-

targeting interneuron e.g., bistratified and oriens-lacunosum moleculare cells (Baude et al., 1993; Klausberger et al., 2003; Klausberger et al., 2004), some also long-range projecting e.g., trilaminar neurons, double projection and oriens-retrohippocampal projecting cells (Ferraguti et al., 2005; Jinno et al., 2007; Sik et al., 1995); and three types of interneuron exclusively targeting other GABAergic interneurons (ISI I-III)(Acsády et al., 1996b; Gulyás et al., 1996; Gulyás et al., 2003). According to the timing of their action, some interneuron types fire action potentials with high temporal precision and others have more variable spiking patterns and are under strong neuromodulatory control (Armstrong and Soltesz, 2012; Freund and Katona, 2007; Glickfeld and Scanziani, 2006). Differences in the spike-timing correlate with distinct intrinsic cellular properties and specialised input synaptic organisation (e.g., the calcium binding protein parvalbumin is expressed by the former but not by the latter). These, in turn, derive from differential origin and cell fate regulating genetic programs of the interneuron types (Fishell, 2007; Tricoire et al., 2011). It appears that with the exception of the axon initial segment, the entire postsynaptic membrane surface of pyramidal cells is modulated by GABA on two complementary temporal scales. Why has such diversity evolved? Perhaps this dichotomy is required to provide a switch between reliability and plasticity by dynamically shifting the inhibitory control of pyramidal cells by different GABAergic cell types.

The *in vivo* activity of identified types of GABAergic interneuron in the drug-free brain has been largely unknown until recently. Although thousands of interneurons have been reported from recordings by extracellular electrodes their identity has remained subject to conjecture. How do different types of GABAergic cell regulate pyramidal cell output? Is the neuronal spike-timing behaviour dependent? I set about to test the hypothesis that distinct GABAergic interneurons have behaviourally

differentiated temporal control over pyramidal cell firing. The fine-tuned inhibition provided by the segregated GABA release onto specific membrane domains of pyramidal cells (Klausberger and Somogyi, 2008; Soltesz, 2005; Somogyi, 2010; Somogyi et al., 2014) may control their action potential generation and it may govern learning-related synaptic plasticity during behaviour (Dupret et al., 2010; Dupret et al., 2013; Spruston, 2008). In order to investigate these questions I recorded the spike-timing of pyramidal cells and diverse types of GABAergic interneuron in freely moving rats.

I report five types of GABAergic interneuron, which I recorded and identified in freely moving rats. My observations presented in chapters 3, 4 and 5 were grouped according to the postsynaptic pyramidal cell compartments targeted by the GABAergic cells. Previous experiments performed under urethane anaesthesia demonstrated that different types of interneuron release GABA at specific times during hippocampal network oscillations (Klausberger and Somogyi, 2008). I have confirmed several of the activity patterns in freely moving rats. Before presenting the evidence, I will first introduce the network oscillatory events occurring in the hippocampus during behaviour.

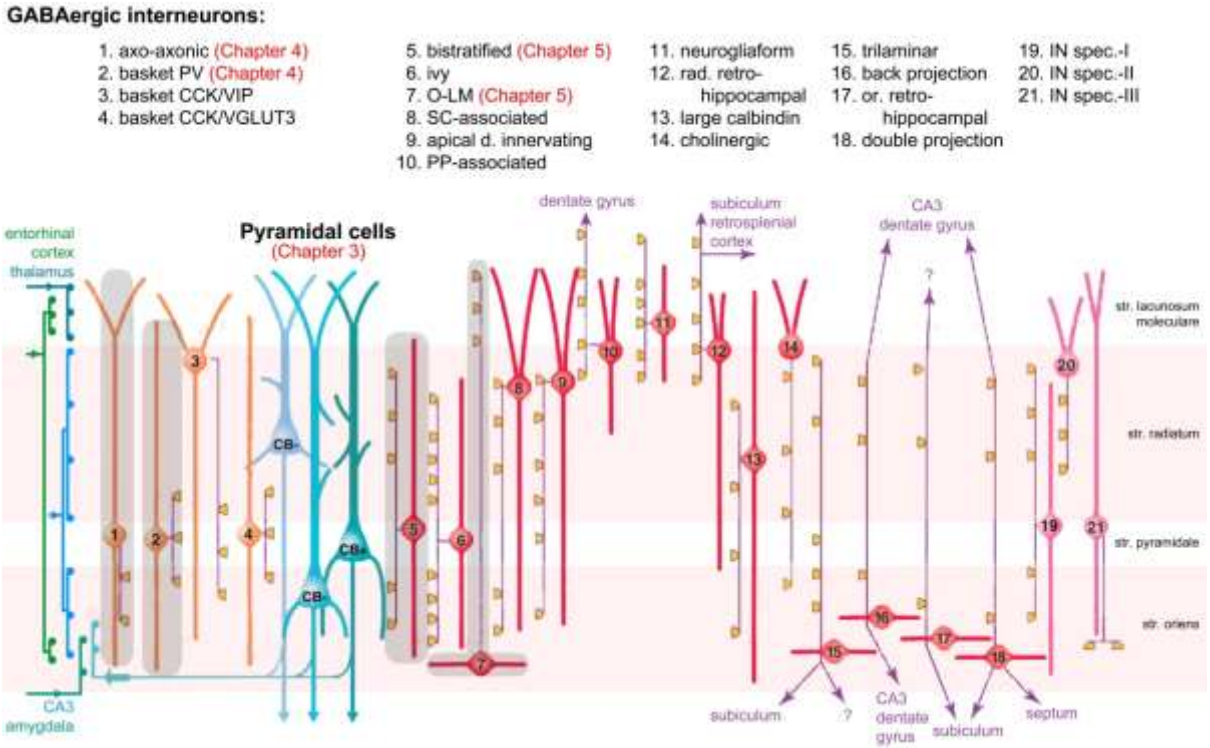

Figure 1-2 Neuronal network connectivity in the CA1 area of the rat hippocampus.

At least 22 distinct types of GABAergic interneuron (somata and dendrites orange, red and pink; axons purple; boutons yellow) govern the activity of three types of pyramidal cell (blue and green). Some interneurons associate their output synapses with the perisomatic region of pyramidal cells (1-4, orange; the "unconventional interneuron" not shown; see chapter 4), others with the dendrites mirroring either the Schaffer collateral/commissural (5,6,8,9,13,14, red) or the entorhinal pathway termination zones (7,10,11,12, red). Long-range projecting GABAergic cells (15-18, red) target related brain structures within the temporal lobe or the medial septum. Cells 19-21 (red) innervate mainly or exclusively other interneurons. Note on the left layer specific termination patterns of five glutamatergic inputs to the CA1 area (terminals, green and blue filled circles) [modified from (Klausberger and Somogyi, 2008; Somogyi, 2010)]. In this thesis I have studied axo-axonic, PV+ basket, bistratified and O-LM interneurons (highlighted in grey) together with some pyramidal cells in freely moving rats. -, immunonegative; +, immunopositive; CB, calbindin; CCK, cholecystokinin; d, dendrite; IN, interneuron; O-LM, oriens-lacunosum moleculare cell; or, oriens; PP, perforant path; PV, parvalbumin; rad, radiatum; SC, Schaffer collateral; spec, specific; VGLUT3, vesicular glutamate transporter 3; VIP, vasoactive intestinal polypeptide.

1.3 Rhythmic neuronal network activity in the dorsal hippocampal CA1

In the hippocampus, the integration of synaptic currents from different sources gives rise to rhythmic network events. It has been recognised that the emergence of oscillations at specific frequencies (e.g., theta, 5-12 Hz) correlates with specific behavioural states (e.g., exploration) (Berger, 1929; Buzsaki et al., 1983; Vanderwolf, 1969). Furthermore, it was suggested that different hippocampal rhythms segregate specific phases of mnemonic processing (Buzsáki, 1989; Hasselmo, 1999; Sutherland and McNaughton, 2000). Theta frequency oscillations regulate the plasticity of CA1 pyramidal cell inputs from EC and CA3 constituting information encoding and retrieval. During sharp wave associated ripples, population bursts of pyramidal cells induce long-term potentiation in the local network and in output targets, which may represent memory consolidation.

In this section I will introduce hippocampal theta (5-12 Hz), gamma (30-100 Hz) and ripple frequency (130-230 Hz) oscillations. The thesis will have a focus on the first and the last. In the final chapter, the emergence of such rhythmic events and their significance will be discussed based on my observations about the spike-timing of identified types of neuron recorded in freely moving rodents. I did not carry out analysis of gamma oscillations due to technical limitations of the recording conditions.

1.3.1 Theta frequency oscillations and mnemonic processing

During exploratory behaviour and rapid eye movement sleep, membrane oscillations at theta frequencies (5-12 Hz) of large populations of hippocampal neuron emerge in the local field potential (LFP) and are related to mnemonic processing (Buzsáki, 2002; Buzsaki and Moser, 2013; Clemens et al., 2009; Grosmark et al., 2012;

Jacobs et al., 2007; Jones and Wilson, 2005; Lisman and Jensen, 2013; Montgomery et al., 2009; O'Keefe, 1993; O'Neill et al., 2013; Poch et al., 2011; Staudigl and Hanslmayr, 2013; Vanderwolf, 1969). Theta oscillatory cycles are generated by periodic activation of active current sources and sinks in the perisomatic region and the distal dendritic tuft of pyramidal cells, respectively. Theta-rhythmic excitatory afferents arriving from the entorhinal cortex create the active inward current (sink) contrasting phase-shifted perisomatic outward currents (source) generated by theta-modulated GABA released by interneurons (Brankačk et al., 1993; Buzsáki, 2002; Leung, 1984). The theta rhythm binds together distant cortical areas co-operatively (Young and McNaughton, 2009) and it is governed by a network of subcortical regions (e.g., thalamus, medial septum, hypothalamic areas, raphe nuclei) via glutamatergic, cholinergic and GABAergic long range projections (Freund and Antal, 1988; Hajós et al., 2003; Hangya et al., 2009; Lawrence, 2008; Leao et al., 2012; Léránth and Frotscher, 1987; Lovett-Barron et al., 2014; Pan and McNaughton, 2004; Rawlins et al., 1979; Tóth et al., 1997; Vertes, 1982; Vertes et al., 2001; Viney et al., 2013). Indeed, as demonstrated in rodents, lesions and pharmacological manipulations of these areas can abolish hippocampal theta oscillations (Kramis et al., 1975; Lawson and Bland, 1993; Woodnorth and McNaughton, 2002a; Woodnorth and McNaughton, 2002b). Theta oscillatory cycles are coherent across the entire hippocampus but their phase measured in the LFP shifts along the septo-temporal and medio-lateral hippocampal axes in a travelling wave (Hartwich et al., 2009; Lubenov and Siapas, 2009; Patel et al., 2012).

While rodents explore a given environment the majority of pyramidal cells in the CA1 area are silent. The pyramidal cells that are active, can fire at any phase of the theta cycle, but fire at highest rate at the trough of the oscillatory cycles (Buzsaki, 2006). When an animal enters a place field, pyramidal place cells coding for that

location start firing around the peak of the theta cycle recorded in the pyramidal layer (O'Keefe and Recce, 1993). On subsequent cycles the phases of the action potentials shift towards earlier phases showing phase precession (O'Keefe and Recce, 1993; Skaggs et al., 1996). Most types of GABAergic interneuron fire with higher rates during theta oscillations than pyramidal cells and some release GABA phase-locked to the ongoing theta rhythm (Czurkó et al., 2011; Klausberger et al., 2003; Klausberger et al., 2004; Klausberger et al., 2005) as also shown recently *in vivo* in freely moving rats and awake head-fixed mice (Lapray et al., 2012; Varga et al., 2012; Viney et al., 2013). Some interneurons recorded with tetrodes have been shown to gradually advance their firing in phase during consecutive theta cycles (Ego-Stengel and Wilson, 2007; Maurer et al., 2006), but the identity of these cells remains unknown.

According to a model, the different phases of theta oscillations segregate different stages in cognitive processing (Hasselmo et al., 2002). The *encoding of information* mainly occurs at theta peaks driven by the entorhinal cortex and the *retrieval* of existing contextual associations takes place at theta troughs driven by the CA3 area (Douchamps et al., 2013; Manns et al., 2007; Wells et al., 2013). I aim to determine the contribution of distinct types of GABAergic interneuron to the different stages of memory operations. In my recordings, I have determined the relationships between neuronal discharge patterns and the power, frequency and phase of theta oscillations. How might GABA released to distinct domains of pyramidal cells contribute to the selection of active place cells? Does interneuron firing support the temporal ordering of neurons into memory encoding assemblies? I will attempt to answer some of these questions based on my experimental results in the following chapters.

1.3.2 Gamma frequency oscillations and cognitive processing

Gamma frequency (30-100 Hz) oscillations are present in all cortical structures (Buzsaki et al., 1983; Chrobak and Buzsáki, 1998a; Hájos and Paulsen, 2009; Stumpf, 1965; Vanderwolf, 1969; Whittington et al., 2011a) and in many different species including humans (Canolty et al., 2006; Jacobs et al., 2007; Le Van Quyen et al., 2010; Tallon-Baudry et al., 1996). These have been proposed to support attention (Engel and Singer, 2001; Fries et al., 2001), working memory (Fries, 2009; Howard et al., 2003; Lisman and Idiart, 1995) and participate in memory encoding and retrieval (Lisman and Idiart, 1995; Montgomery and Buzsáki, 2007; Sederberg et al., 2007). Both, the timing of $GABA_A$ receptor-mediated inhibitory postsynaptic currents and the *in vivo* membrane time constants of pyramidal cells support the 10-30 ms duration of a gamma cycle (Bazelot et al., 2010; Destexhe and Paré, 1999; Glickfeld et al., 2009; Léger et al., 2004; Mann et al., 2005). Moreover, this time period is also the optimal window for synaptic plasticity (Magee and Johnston, 1997; Markram et al., 1997; Pouille and Scanziani, 2004). Neurons firing together during the same gamma cycle strengthen their connections and become members of an "assembly" (Harris et al., 2003) representing an association. Based on these parameters, it has been proposed that gamma oscillations represent the optimal "temporal units" segregating the sequences of pyramidal cell "assemblies" (Fries et al., 2007; Harris, 2005; Harris et al., 2003) that support cognitive performance (Buzsáki and Draguhn, 2004; Buzsáki and Wang, 2012; Colgin and Moser, 2010; Lisman and Jensen, 2013).

In the hippocampal CA1, different gamma frequency oscillations exist nested within the slower frequency theta oscillations (Belluscio et al., 2012; Lisman and Buzsáki, 2008; Sirota et al., 2008; Tort et al., 2009). The differentiation of gamma rhythms of different frequencies is controversial due to the discrepancies in

terminology, recording techniques, experimental conditions and the studied species (Colgin et al., 2009; Lasztoczi and Klausberger, 2014). In freely moving rats (Colgin et al., 2009), fast gamma oscillations (65-140 Hz) were detected in the pyramidal cell layer coupled to the trough of theta cycles. Because of the detected synchronisation of the oscillations in the CA1 area with those in the medial entorhinal cortical layer 3, these gamma oscillations were hypothesised to facilitate the transmission of spatial information to the hippocampal place cells (Chrobak and Buzsáki, 1998a; Colgin et al., 2009). Although, the entorhinal input to CA1 is weakest at the trough of the theta cycle (Mizuseki et al., 2009), it cannot be excluded that some specific subpopulation of entorhinal neurons (Kitamura et al., 2014) may be active at this time and hence may contribute to the detected gamma synchrony. In the same tetrode recordings (Colgin et al., 2009), gamma oscillations of 25-55 Hz were recognised on the descending slope of subsequent theta cycles. During these oscillatory episodes, the CA1 area was synchronised with the CA3 area indicating a possible role of the oscillations in memory retrieval (Colgin et al., 2009). Recently, using silicone probe measurements, "$\text{gamma}_{\text{perisomatic}}$" (centre frequency of 46 Hz) and "$\text{gamma}_{\text{apical tuft}}$" (centre frequency of 29 Hz) were identified in the CA1 area of urethane anaesthetised rats and in awake head-fixed mice (Lasztoczi and Klausberger, 2014). "$\text{Gamma}_{\text{perisomatic}}$" oscillations, localised to stratum pyramidale, were coupled to the late descending slope and trough of theta cycles and their generation requires the interaction between perisomatic-targeting PV+ basket cells and their postsynaptic pyramidal cell partners (Bartos et al., 2007; Fries et al., 2007; Lasztoczi and Klausberger, 2014; Mann et al., 2005; Oren et al., 2010). Driven by inputs from the CA3 area (Csicsvari et al., 2003; Zemankovics et al., 2013) these rhythmic events are likely to supervise the transfer of retrieved contextual associations to downstream regions (Lasztoczi and Klausberger, 2014). "$\text{Gamma}_{\text{apical}}$

$_{tuft}$" oscillations in stratum lacunosum moleculare are coupled to the peak and early descending slope of theta cycles, when initiation of synaptic plasticity in the apical tuft of CA1 pyramidal cell dendrites is optimal, suggesting that these oscillatory episodes might support the encoding of novel information (Lasztoczi and Klausberger, 2014). Projection cells in layer 3 of the medial entorhinal cortex form synapses on the distal apical tuft of CA1 pyramidal cells. Lasztoczi et al (2014) determined that the spiking of such cells, as a population, is coupled to the "gamma$_{apical\ tuft}$" oscillations measured in the CA1 indicating the contribution of the projection neurons to this gamma rhythm. It is hard to reconcile the observations from the two reports. Although the slower rhythm in the first study (Colgin et al., 2009) shows certain similarities with "gamma$_{perisomatic}$"(Lasztoczi and Klausberger, 2014), it is not possible to establish any relationship between the two studies because of the different methodologies used. Furthermore, the timing of the interaction between the CA1 area and the medial entorhinal cortex is controversial being defined at the trough of theta cycles in the first report (Colgin et al., 2009) but at the peak of theta cycles in the latter (Lasztoczi and Klausberger, 2014). In order to conclude the source and roles of the different frequency gamma oscillatory components additional drug-free experiments are needed.

The action potential discharge of CA1 pyramidal cells and different types of identified GABAergic interneuron has been intensely studied *in vitro* during pharmacologically induced gamma oscillations and *in vivo* under urethane anaesthesia (Fisahn et al., 1998; Lasztoczi and Klausberger, 2014; Lasztoczi et al., 2011; Penttonen et al., 1998; Soltesz and Deschenes, 1993; Tukker et al., 2007; Tukker et al., 2013). The strongly oscillatory-phase coupled spike-timing of PV+ basket and bistratified cells suggests their importance in the gamma entrainment of pyramidal cell somatic and dendritic membranes, respectively. Recently, the coupling of O-LM cell firing to the

higher frequency gamma oscillations (90-130 Hz) has been demonstrated in awake head-fixed mice (Varga et al., 2012). These cells innervate the apical dendritic tufts of pyramidal cells, the same membrane domain that receives gamma rhythmic glutamatergic drive from the entorhinal cortex. What the role, if any, GABA released by O-LM cells could have in gamma oscillations remains to be clarified. This same study has confirmed the strong relationship between PV+ basket cell firing and gamma oscillations in the drug-free hippocampus.

Because of technical limitations that I detail in chapter 4, in my experiments, it was not possible to analyse single cell spike-timing in relation to gamma oscillations. Our knowledge about the contribution of identified GABAergic interneuron types to gamma rhytmogenesis and pyramidal cell assembly formation in freely moving animals remains quite limited.

1.3.3 Sharp wave associated ripple oscillations and memory consolidation

During slow wave sleep, awake immobility or consummatory behaviour "large negative slow waves" emerge in the CA1 local field potential in association with "a sinusoidal ripple consisting of 4-10 waves with periods of 4-8 ms and a burst of firing in the theta units located in stratum pyramidale and oriens", as reported by O'Keefe and Nadel (1978). The sharp waves, most prominent in stratum radiatum, are initiated by population bursts of groups of CA3 pyramidal cells which via their Schaffer collaterals (Csicsvari et al., 2000; Nakashiba et al., 2009) excite pyramidal cells and GABAergic interneurons in the CA1 area. Consequently, the somatic and dendritic membranes of targeted pyramidal cells become entrained to high frequency "ripple"-like oscillations (120-230 Hz) by GABAergic PV+ basket and bistratified cells, the "theta

units", respectively (Bragin et al., 1999; Buzsaki et al., 1992; Buzsaki et al., 1983; Klausberger et al., 2003; Klausberger et al., 2004; Varga et al., 2012).

During sharp wave associated ripples (SWRs), transient memories represented by assemblies of co-firing CA1 pyramidal cells are transferred to neocortex for long-term storage (Buzsáki, 1989; Hasselmo, 1999). Pyramidal cells firing together within one theta cycle, during exploration, often become *reactivated* during subsequent sleep- and/or awake-SWRs during the 50-100 ms ripple cycles (Lee and Wilson, 2002; Nádasdy et al., 1999; O'Neill et al., 2006; O'Neill et al., 2008; Pavlides and Winson, 1989; Skaggs and McNaughton, 1996; Wilson and McNaughton, 1994). The order of replay of active pyramidal cell sequences can be the same as during the exploration or it can get reversed (Csicsvari et al., 2007; Diba and Buzsaki, 2007; Foster and Wilson, 2006; O'Neill et al., 2006). A temporal compression of pyramidal cell associations probably could initiate LTP required for *memory consolidation* (Bendor and Wilson, 2012; Buzsáki, 1996; Dupret et al., 2010; Ego-Stengel and Wilson, 2010; Girardeau et al., 2009; Jadhav et al., 2012). The coherence of SWRs in the CA1 area and its downstream regions e.g., pre- and parasubiculum, entorhinal cortical deep layers (Chrobak and Buzsáki, 1996; Chrobak and Buzsáki, 1998b) highlights the role of these network events in relaying transient information to cortical structures. Furthermore, this function is also suggested by the correlation between hippocampal SWRs and neocortical spindle oscillations regulating neuronal firing during sleep in the neocortex (Clemens et al., 2007; Clemens et al., 2011; Isomura et al., 2006; Siapas and Wilson, 1998).

Unidentified types of hippocampal interneuron show differential SWR-related firing responses in non-anaesthetised rats; some become activated, others become inhibited during the fast frequency events and some do not change their firing rates

(Csicsvari et al., 1999a, b; Csicsvari et al., 2000). Until recently, the identity of SWR-responsive and non-responsive GABAergic interneurons and their contribution to pyramidal cell firing could only be determined *in vitro* or *in vivo* in urethane anaesthetised rodents (Fuentealba et al., 2008a; Fuentealba et al., 2008b; Hájos et al., 2013; Jinno et al., 2007; Klausberger et al., 2003; Klausberger et al., 2004; Klausberger et al., 2005; Ylinen et al., 1995a). Recent technological advances allow us to investigate neuronal firing patterns of identified cells in the drug-free brain (Lapray et al., 2012; Varga et al., 2012; Viney et al., 2013). My work aims to dissect further interneuron-type specific contributions to pyramidal cell output control during SWRs.

1.4 Aims

During my D.Phil. studies, I attempted to dissect the contribution of GABAergic interneuron types to the encoding and consolidation of information in the hippocampus of rats during exploration and natural slow wave sleep. Testing the hypothesis of functional specialisation of distinct types of interneuron, I examined the timing of action potential discharge, indicative of GABA released onto functionally different postsynaptic domains of pyramidal cells during behaviour.

My results contribute to improving our understanding of GABAergic/peptidergic regulation of pyramidal cell firing *in vivo* provided by PV+ basket, axo-axonic, dendrite-targeting bistratified and O-LM cells and one "unconventional interneuron" during drug-free theta oscillations and sharp wave-ripples *in vivo*.

I carried out the following experiments:

- performed extracellular recordings and juxtacellular neurobiotin-labelling of single cells in the hippocampal CA1 area of freely moving rats;
- recorded the local field potentials (LFPs) from the hippocampus and cortical areas in parallel during behaviour;
- determined cell-type specific firing patterns during movement, sleep and quiet wakefulness;
- determined the network oscillatory-state dependent spike-timing of different types of neuron;
- identified urethane induced changes in neuronal activity and in the LFP by comparing my data set with previously reported and identified CA1 interneurons recorded *in vivo* under anaesthesia.

As detailed in chapter 2, to achieve my objectives, I have used a powerful combination of techniques: electrophysiological and statistical analyses of spike trains and LFP, anatomical examination of axonal and dendritic arborisations and immunohistochemical identification of molecular expression profiles of single cells. My main results are reported in chapters 3-5 and their significance is discussed in the final chapter 6 concluded with an "Outlook".

2 Experimental procedures

2.1 *In vivo* electrophysiological techniques

2.1.1 Experimental subjects

Most procedures involving experimental animals were performed in accordance with the Animals (Scientific Procedure) Act, 1986 (UK) and associated regulations under approved project licence (30/2719) at the University of Oxford. Furthermore, additional data included and analysed by me in chapters 3-5, was recorded by colleagues in Vienna under the approval of the Animal Care and Use Committee of the Medical University, Vienna and the Austrian Federal Ministry of Science and Research.

Data reported is from thirty-six Sprague-Dawley rats (n=35 male; n=1 female) recorded between 8 am and 8 pm. Animals were housed in groups of 2–4 per cage in Oxford (n=34 rats; 19–21C°; 55% humidity; reverse light/dark cycle, lights on from 8 pm – 8 am) or Vienna (n=2 rats; diurnal cycle, lights on from 6 am – 6 pm). One to seven days before the experiments started rats were housed in a cage on their own with *ad libitum* access to food pellets and water. During some recording sessions, the rats in Vienna received chocolate chip rewards.

2.1.2 Surgical procedures

Implantations of the head-mounted recording setup (Figure 2-1B), craniotomies and duratomies were performed (Figure 2-1A) mounted in a stereotaxic

frame (Kopf Instruments) under isoflurane (IsoFlo, Abbott) anaesthesia using analgesic (subcutaneous injection of 0.05 ml Rimadyl, Pfizer or Dipidolor, Janssen-Cilag; 2 ml per 125 ml of drinking water provided for 48 h after surgery) and antibiotic (intraperitoneal injection of 0.1 ml 2.5% wt/vol Baytril, Bayer Vital) treatments. Breathing was monitored visually by the experimenter and body temperatures were maintained at 37°C with a heating pad connected to a homeothermic monitor (Harvard Apparatus).

After exposing and cleaning the skull, a cylindrical micro-drive holder was attached above the left parietal cortex using dental acrylic (Refobacin R, Biomet). A main connector was placed above the frontal part of the skull, supported by five stainless steel screws attached to the bone. EEG and reference-ground signals were connected to this head stage from one screw above the right prefrontal cortex (bregma -4 mm rostro-caudal, bregma +2 mm medio-lateral) and another above the cerebellum, respectively (Figure 2-1B). All this was embedded in dental acrylic and was coated with blue light–polymerised cement (Tetric EvoFlow, Ivoclar Vivadent).

Following at least three days of recovery, successive craniotomy and duratomy were completed above the right hemisphere under anaesthesia (Figure 2-1A). To prevent excessive tissue growth on subsequent days, 0.1 mg/ml of Mitomycin C was applied on the dura mater for 10 min between these two steps. Next, either a single wire electrode (50 μm tungsten, California Fine Wire; n=23 rats) fixed on the skull or movable by a miniature drive (Haiss et al., 2010) or a microdrive movable tetrode (n=11 rats) (Neuronelektrod Kft., Budapest, Hungary) was lowered into the hippocampus or cortex (Figure 2-1A). While connected to the head stage, these electrodes and/or tetrodes were used to record local field potentials (LFPs). A layer of silicone (Kwik-Sil, World Precision Instruments) was used to protect the cortical

surface overnight and between recordings. During recordings, this was replaced by wax for the ease of advancement of the glass electrode.

2.1.3 In vivo extracellular single cell recording and juxtacellular neurobiotin-labelling in freely moving rats

Recording sessions started after a recovery period of up to 7 days (Figure 2-1A). Rats were anaesthetised briefly by isoflurane and a miniature preamplifier (ELC mini-preamplifier, NPI Electronic), two LED arrays and an accelerometer (Supertech Instruments; n= 25 rats) were connected to the head stage. A glass electrode (10-20 MΩ) filled with neurobiotin (1.5 or 3% wt/vol in 0.5 M NaCl) was advanced using a hydraulic (Narishige) or piezoelectric (Kleindiek Nanotechnik) (Lee et al., 2006) microdrive to record single cell activity and LFPs in the hippocampus (Figure 2-1B). Recordings commenced 1h after recovery from anaesthesia in either a darkened room (Oxford) or one with partially obscured windows (Vienna) using a recording arena (Oxford, n=7 rats, 40 x 40 cm floor, 27 cm walls; or n=25 rats, 50 x 50 cm floor, 27 cm walls; Vienna n=2 rats, 40 x 60 cm floor, 30 cm walls) to which the rats were naive on the first day (Figure 2-1C). Two video cameras captured the activity of the rats that were free to move around; one infra-red sensitive for behavioural analysis and another one for position tracking using the head-mounted LED arrays (Position Tracking System, v14.02.08, courtesy of K. Allen). Recordings were performed for 1–12 days (5 ±4 d) after duratomy (Figure 2-1A). After having recorded a neuron, the pipette was advanced towards the cell into a juxtacellular position and labelling using neurobiotin was attempted (Pinault, 1996). The neuron was rhythmically entrained by the injection of increasing amplitude square-pulsed current (Figure 2-1D). The stimulation was performed using ELC-03M amplifier with active bridge compensation. At this point, the

neurobiotin ejected from the pipette was thought to be taken up by the cell. When labelling was judged successful, the pipette was retracted slowly and the neuron was left to recover from the entrainment. I have considered a labelling attempt successful if the firing of the cell was rhythmically entrained by the current stimulation for at least 30 sec and if, after ending the stimulation, the cell kept firing action potentials but at a slowly decreasing rate until it approximately recovered its pre-labelling spiking pattern. The rats were then briefly anaesthetised in the stereotaxic frame while the recording equipment was removed (Figure 2-1A). Following a post-labelling period of up to 3 h the animals were deeply anaesthetised using isoflurane followed by intraperitoneal injection of an overdose of Pentobarbital (JML Biopharm; 20% w/v solution; dose: 400 µl/100 g) and perfusion fixed (Figure 2-1A). If no stable neurons were found, sessions were finished by simply removing the recording devices (Figure 2-1A). Each day, only one anaesthesia and electrode was allowed to be used according to the limits of our licence, and a maximum of 12 recordings could be performed. Accordingly, if for the 12 recording days I was unable to label an interneuron, I attempted to record and label a pyramidal cell on the last day, before perfusing the animal.

2.1.4 Recording technical specifications / Data acquisition

Amplification of 1000x (BF-48DGX and DPA-2FS, NPI Electronic) was used and signals were digitised at 1 or 20 kHz (Power1401 A/D board, Cambridge Electronics Design). Measurements from the glass electrode were online band-pass filtered according to three different frequency ranges (0.3 Hz–10 kHz, wide-band; 0.3–500 Hz, LFP; 0.8–5 kHz, action potentials). Signals from the EEG and hippocampal/cortical electrodes or tetrodes were band pass filtered (0.3–300 Hz or 0.3 Hz–10 kHz).

Elimination of 50 Hz noise without phase-shift was provided by Hum Bugs (Quest Scientific Instruments). Movements along three spatial axes were recorded in three separate channels by the accelerometer as voltage deflections and were digitised at 1 or 20 kHz. Acquisition of all signals, except tracking, went in parallel using Spike2 software (v7.01, Cambridge Electronics Design).

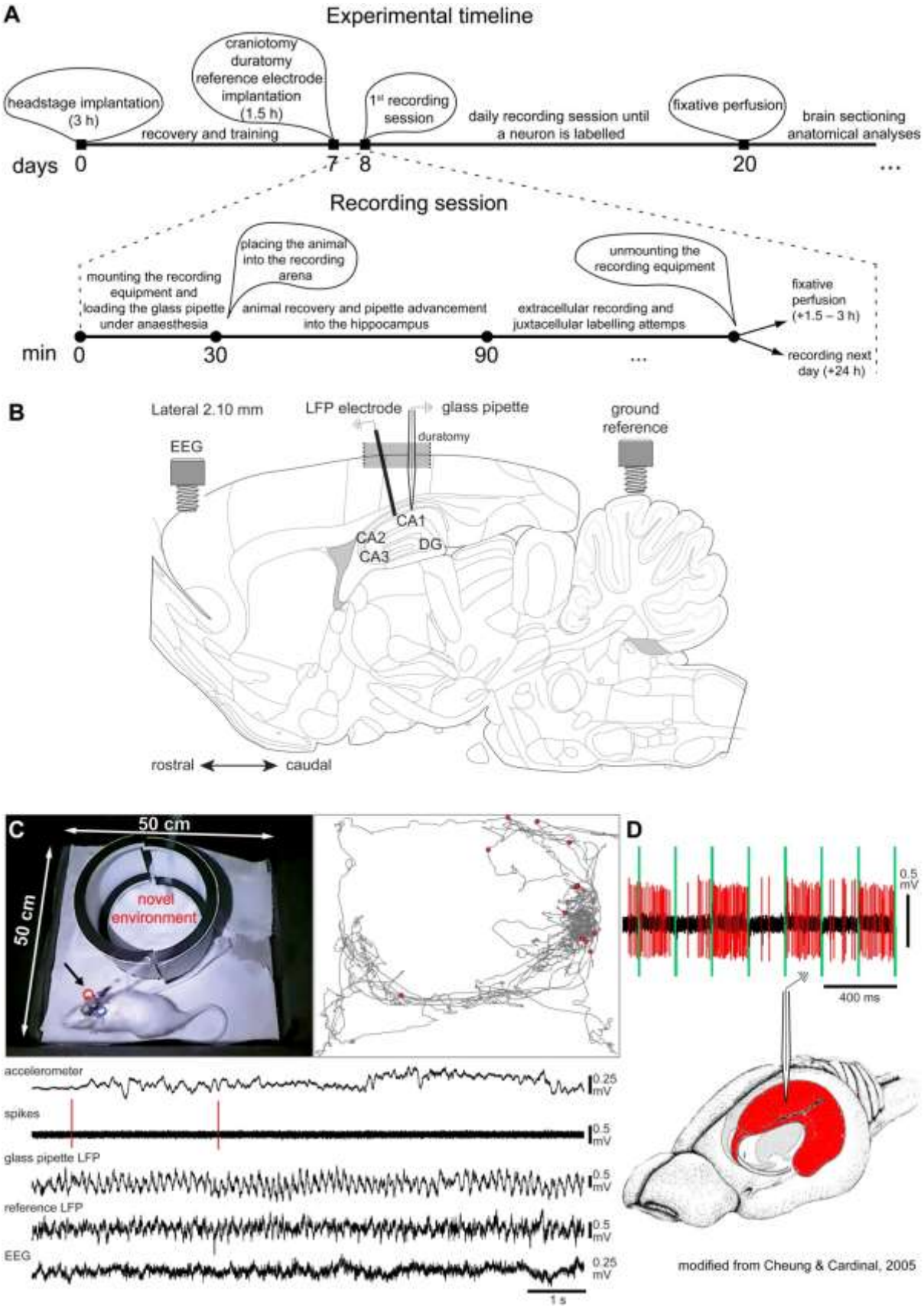
A
Experimental timeline
headstage implantation (3 h)
craniotomy duratomy reference electrode implantation (1.5 h)
recovery and training
1st recording session
daily recording session until a neuron is labelled
fixative perfusion
brain sectioning anatomical analyses
days 0 7 8 20 ...
Recording session
mounting the recording equipment and loading the glass pipette under anaesthesia
placing the animal into the recording arena
animal recovery and pipette advancement into the hippocampus
unmounting the recording equipment
extracellular recording and juxtacellular labelling attemps
fixative perfusion (+1.5 – 3 h)
recording next day (+24 h)
min 0 30 90 ...
B
Lateral 2.10 mm
LFP electrode
glass pipette
ground reference
EEG
duratomy
CA1
CA2
CA3
DG
rostral
caudal
C
50 cm
50 cm
novel environment
accelerometer
0.25 mV
spikes
0.5 mV
glass pipette LFP
0.5 mV
reference LFP
0.5 mV
EEG
0.25 mV
1 s
D
0.5 mV
400 ms
modified from Cheung & Cardinal, 2005

Figure 2-1 In vivo extracellular single cell recording and neurobiotin-labelling in freely moving rats.

A. Experimental time frame and recording schedule. **B.** Placement of recording electrodes (sagittal brain section) including the glass pipette lowered into the hippocampal CA1 area. **C.** Rat exploring the experimental arena. *Top left*, Recorded signals were passed through the head mounted stage made in house (black arrow) and fed back via a cable to the recording devices. LEDs connected to the left (blue) and right (red) side of the head stage are used for automated position tracking using a video camera installed on top of the arena. A second camera using infrared lighting captures the animal's behaviour in the arena. *Top right,* The trajectory (grey) of the animal while recording a pyramidal cell (LK10k) with action potentials (APs, red dots) superimposed on the path. *Bottom,* Example of the acquisition process in Spike2 with traces from the pyramidal cell recording. Action potentials (red, second row from top; band pass filter 0.8-5 kHz) and LFPs (third row from top; band pass filter 0.3-300 Hz) were recorded from the hippocampal CA1 area using a glass pipette mounted on the rat's head. Reference CA1 LFPs (second row from bottom; band pass filter 0.3-300 Hz) and frontal cortical LFPs (bottom row, EEG; band pass filter 0.3-300 Hz) were recorded from two other electrodes chronically implanted before the recording sessions started (see A and B). Note the rhythmic oscillatory state of the hippocampal LFPs (second and third rows from bottom) known as the theta rhythm (5-12 Hz) prominent during spatial navigation (top trace). Pyramidal cells in general decrease their firing rates during this brain state compared to their activity during slow wave sleep. The firing rate might suddenly increase if the rat happens to run through the part of the arena (place field), which is encoded by the cell assembly including the pyramidal cell under recording (place cell). For this pyramidal cell (LK10k), no place related firing was observed in this environment. **D.** Example trace from the juxtacellular labelling of a recorded GABAergic interneuron (LK06ah) in stratum oriens of the CA1 area in hippocampus. Representative period of action potential discharge (red vertical lines) rhythmically entrained by the injection of increasing amplitude square-pulsed current (start and end of pulses in green). The ejected neurobiotin was taken up by the current-driven interneuron.

2.2 Anatomical techniques

2.2.1 Brain fixation and sectioning

One to three h after cell labelling, rats were transcardially perfused first briefly with saline and then for ~20 min with fixative solution consisting of 4% paraformaldehyde (wt/vol, Sigma-Aldrich), 15% saturated picric acid (vol/vol, Sigma-Aldrich), 0.05% glutaraldehyde (wt/vol, distilled grade, TAAB Laboratories Equipment Ltd) in 0.1 M phosphate buffer at pH ~ 7.2.

Brains were removed from the skull and, if well fixed, as assessed by the firmness, absence of blood and the yellow colouring provided by picric acid, were washed in phosphate buffer (PB) and sectioned, otherwise they were post-fixed. For the latter the incubation lasted for up to 12 h in a fixative solution lacking glutaraldehyde at ~4°C. Next, brains were reduced to the size of a block containing the right hippocampus then these blocks were glued to the cutting stage and coronal brain sections were produced (70 μm nominal thickness, VT1000s vibratome, Leica Instruments) in the caudal to rostral direction numbered accordingly (Figure 2-2A). Sections were washed in PB (3 x 10 min) then subsets of every fourth section were selected for neurobiotin visualisation. These were washed in tris buffered saline with Triton X-100® detergent (TBS-TX, 0.3% wt/vol, Sigma-Aldrich; 3 x 10 min) to enhance reagent penetration. The rest of the sections were preserved in PB with 0.05% wt/vol sodium azide at ~4°C. Before use they were always washed in PB (3 x 10 min) to remove the preservative.

2.2.2 Streptavidin reactions and immunohistochemistry

For the visualisation of neurobiotin, the selected subsets of sections were incubated in 0.5 ml streptavidin-conjugated Alexa 488 in TBS-TX, either at room

temperature for 4 h or at ~4°C overnight. In case of two additional interneurons I used streptavidin-conjugated DyLight 405 or DyLight 594. After washing in TBS-TX (3 x 10 min) sections were mounted on glass slides for examination using the mounting medium for fluorescence Vectashield (Vector Laboratories) and permanently sealed around the cover slips with nail polish.

Furthermore, using the indirect primary antibody detection method in combination with fluorochrome-conjugated secondary antibodies, the expression of cell-type specific molecules was tested on individual labelled neurons and control tissue. Mixtures of up to four primary antibodies, raised in different species, and appropriate secondary antibodies were used on each individual section. The immunohistochemical reactions were started by washing the stored sections in TBS-TX (3 x 10 min) and blocking nonspecific antibody binding sites with 20% vol/vol normal horse serum (NHS, Vector Laboratories) in TBS-TX for 1h at room temperature. Next, sections were incubated in TBS-TX containing 1% vol/vol NHS and primary antibodies raised against the antigens of interest at appropriate dilutions for two days at ~4°C. After a wash (3 x 10 min) in TBS-TX, sections were further incubated either for 4 h at room temperature or overnight at ~4°C in TBS-TX containing 1% NHS, streptavidin-conjugated fluorochromes and respective secondary antibodies at appropriate dilutions. Finally, sections were washed (3 x 10 min) in TBS-TX and mounted as previously described for microscopic examination.

Using immunohistochemistry, I tested for the expression of several peptides, receptors, transcription factors and other proteins. These results are summarised in the following three chapters in Table 3.1, Table 4.1 and Table 5.1, respectively. Secondary antibodies were raised in donkey, swine and rabbit against immunoglobulin G of the species of origin of the primary antibodies and conjugated to Alexa 405,

DyLight405 (blue); Alexa 488, DyLight488 (green); cyanine 3 (Cy3), DyLight594 (red); and cyanine 5 (Cy5), DyLight649 (infra-red); or horseradish peroxidase enzyme (HRP). The donkey-anti-rabbit-Alexa405 and secondary antibodies conjugated to Alexa488 were purchased from Invitrogen. The donkey-anti-chicken-Alexa488, the donkey-anti-guinea-pig-Alexa488 and secondary antibodies conjugated to Cy3, Cy5, DyLight405, DyLight488, DyLight594 and DyLight649 fluorophores were purchased from Stratech. For a list of all primary and secondary antibody solutions and dilutions used with respective specificity references see Table 2.1 and Table 2.2.

Specificity

Although sometimes difficult, neurobiotin labelling can be distinguished from endogenous biotin primarily because of the continuous pattern of cytoplasmic labelling and often also because of the difference in signal strength. Antibody specificity tests are referenced in Table 2.1. The best control reactions known at present are those using tissue from animals that lack the protein e.g., 'knock-out' mice. Some primary antibodies have been tested this way. I accepted antibodies to recognise the claimed molecule where the staining pattern and subcellular localisation corresponded to the predicted subcellular compartment e.g., plasma membrane using other antibodies to the same protein (Lorincz and Nusser, 2008b). Nevertheless, in immunohistochemistry, there is always some uncertainty as to the identity of the detected molecular species.

I have performed controls for the immunohistochemical methods of my experiments. Typically I evaluated the reaction in a second section from a different brain as minimal control. In some cases I produced negative controls by leaving out the primary antibodies from reactions performed on sections from different brains, and

testing if all specific labelling was abolished. An important test is when using several primary antibodies on the same section, to exclude the possibility of cross-reaction by secondary antibodies with several primary antibodies from different species. Because of convincing results with these antibodies in our laboratory using highly cross-absorbed secondary antibodies from reputable suppliers, I did not perform this latter control. When assessing the quality of reactions there are multiple factors to consider. The quality of tissue fixation and the degree of reagent penetration are the two most important factors influencing the outcome.

2.2.3 Wide-field epifluorescence- and confocal laser scanning microscopy

The immunohistochemical reactions were first evaluated using wide-field epifluorescence microscopy. This was performed using Leitz DMRB microscope (Leica) with epifluorescence illumination (Hg arc lamp, HBO, Osram) and PL Fluotar 20x/0.5 and 40x/0.7 lenses. The light was spectrally filtered using dichroic mirrors to obtain optimally separated excitation and emission bandwidths for different fluorophores: Alexa405 (excitation: 405/20 nm; emission: 460/50 nm; beam splitter: 425 nm), Alexa488 (excitation: 480/40 nm; emission: 527/30 nm; beam splitter: 505 nm), Cy3 (excitation: 545/30 nm; emission: 610/75 nm; beam splitter: 565 nm) and Cy5 (excitation: 620/60 nm; emission: 700/75 nm; beam splitter: 660 nm). For documentation and qualitative evaluation of the reactions, images were taken using a Hamamatsu Photonics ORCA ER digital camera controlled by OpenLab software v.5.5.0 (Improvision). Exposure times were individually set for each image depending on the signal strength and the recorded wavelength. Further editing was only done to brightness and contrast levels and was applied for the entire frame.

To improve image resolution and increase contrast, when needed, reactions were further examined using confocal laser scanning microscopy. This technique uses point illumination and a confocal aperture or pinhole. Point illumination is achieved by focusing laser light by the imaging objective lens. The pinhole positioned in the image plane eliminates the out-of-focus light from the specimen. The light sensor can detect only the light that passes through the pinhole. Thus, a point-like detection becomes possible quantitatively described by the point spread function. The diameter of the pinhole is variable, and has a key role in resolution and depth discrimination in the acquired image. It also determines the number of photons detected, therefore it is an important parameter to be set before scanning.

It is possible to image a thin optical slice with this technique, which then allows a great number of slices to be recorded at different focal planes of a 70 μm thick section. Thus a stack is created along the optical axis (Z). To optimise sampling for digitisation the Nyquist criterion has to be met. In case of laser scanning microscopy for optimal pixellation in the XY plane two pixels are allocated to the widths of the point spread function at half maximum intensity. In Z direction this means elevation of the specimen with half the distance of the optical slice thickness. If the number of sampling points is smaller than the given Nyquist value then information will be lost. A greater number of sampling points leads to oversampling.

The generation of an optimal Z stack with one fluorophore in one spectral channel involves the following steps:

1. A focused laser beam deflected in the X and Y directions line-by-line scans the specimen.

2. A single (Ch) or an array (ChS) of photomultiplier tubes (PMT) detects the fluorescence emitted by the scanned tissue.

3. The detected light intensity is digitized and displayed pixel-by-pixel on the screen.

For confocal microscopy an AxioImager.Z1 microscope (Carl Zeiss) was used equipped with LSM 710 scan head and DIC M27 Plan-Apochromat 40x/1.3 oil, 63x/1.4 oil and alpha Plan-Apochromat 100x/1.46 oil objectives. Using appropriate lasers and the special features of the microscope, various fluorophores were spectrally separated (Figure 2-2B,C) and, thus recorded either simultaneously i.e. more than one channel (Ch) per scan track (T) or sequentially i.e. single channel per track. Channel settings for Alexa405 (405-30 solid state laser: 405 nm), for Alexa488 (Argon laser: 488 nm), for Cy3 (HeNe laser: 543 nm), for DyLight594 (HeNe laser: 594 nm) and for Cy5 (HeNe laser: 633 nm) varied by application. After deciding on the number of tracks and channels within one track, appropriate Main Beam Splitters (MBS) were selected resulting in an optimally detected emission spectral range. I have included such relevant information into the figure legends of the individual images. Pinhole size was adjusted to 0.66-1.17 Airy units resulting in 0.6-0.7 μm optical slice thickness. The scanner was calibrated to pixel registration of 100 nm in X, Y and of 200 nm in Z directions. Image pixellation varied with the lens (see above) and the digital magnification applied. All confocal image acquisition and analysis was done using ZEN 2008 software, v5.0 (Carl Zeiss). Brightness and contrast were adjusted in the whole stack and for each channel separately. To reduce noise and enhance contrast levels images were filtered (median algorithm, kernel size X, Y=3; kernel size Z, channel=1). When needed stacks were maximum intensity projected along the Z axis.

Spectral identification of fluorophores

I have tested channel separation by spectral identification of potential cross-talk in detected dyes (Figure 2-2C). For instance, COUP-TFII labelling was tested in Cy5 channel in a neurobiotin-filled interneuron soma imaged in DyLight594 channel (LK12o, Figure 4-4B). Initially, I used sequential frame scanning (T1-Ch1: MBS 458/514/594; detected emission spectral range: 598-641 nm; T2-Ch2: MBS 488/543/633; detected emission spectral range: 640-757 nm) with the 594 nm and 633 nm lasers, respectively. Signals detected in channel mode showed double positivity for neurobiotin and for COUP-TFII. However the high intensity of the neurobiotin-streptavidin-DyLight594 reaction raised the possibility of shine-through in the detected Cy5 channel. Next, I switched to lambda scanning mode using the 633 nm laser (ChS: MBS 488/543/633; detected emission spectral range: 415-727 nm) to identify the spectral components in the detected signal. At this stage the entire detection range was divided into 32 bins resulting in nominally 9.7 nm bin width. In the stack of 32 images each XY picture represents the signal from a particular bin. I could confirm the origin of the signal for COUP-TFII from the bins corresponding to the Cy5 spectral range (>= 644 nm).

2.2.4 HRP reactions and immunohistochemistry

For neurobiotin visualisation (Figure 2-2A), I used a method providing high contrast, the avidin-biotin combined horseradish peroxidase (HRP) reaction with 3,3'-diaminobenzidine (DAB) as chromogen and either 0.002% wt/vol hydrogen peroxide (H_2O_2) as substrate, or H_2O_2 generated continuously from glucose by glucose oxidase (Sigma-Aldrich).

Brain sections, either stored in PB and preservative or previously reacted using immunohistochemistry were processed for transmitted light microscopy. Those in the latter group were washed in TBS-TX (3 x 10 min). The rest were washed in 0.1 M PB or TBS (3 x 10 min) and processed according to a "freezing-thawing" protocol. This involved first incubating the section in sucrose solution in 0.1 M PB for 15 min (10% wt/vol, Sigma-Aldrich) then for up to 2 h in 20% wt/vol for cryoprotection, followed by quickly freezing it with liquid nitrogen and thawing in 0.1 M PB. The last two steps were repeated twice. Either way the aim was to make the cell membranes more permeable to the reagents.

Next, sections were incubated for 2 days in avidin and biotinylated peroxidase complex (1:100, Vectastain ABC Elite kit, Vector Laboratories) formed over a pre-incubation period in TBS-TX for 30 min at room temperature. If the sections were previously treated with streptavidin then these were first incubated in biotinylated peroxidase in TBS-TX (1:100; Vectastain ABC Elite kit, Vector Laboratories) either overnight at ~4°C or for 4 h at room temperature, to amplify the signal.

After an additional wash (3 x 10 min in 0.1 M PB) the sections were left in dark for 15 min in 0.05% wt/vol DAB (Sigma-Aldrich, stock 5 mg/ml) solution containing 0.02% wt/vol glucose (Sigma-Aldrich), 0.004% wt/vol ammonium chloride (Sigma-Aldrich; stock 0.4% wt/vol) and 0-0.04% ammonium-Nickel-sulphate (Sigma-Aldrich; stock 1% wt/vol). The amount of the latter component was judged based on how well-stained the processes were likely to come up depending on the strength of the neurobiotin signal in the labelled cell. The reaction was started by adding ~ 4 units of glucose oxidase enzyme (Sigma-Aldrich) to the solution. The peroxidase enzyme catalyses the oxidation of DAB by hydrogen peroxide and at appropriate concentration forms a brown polymer precipitate. The glucose oxidase enzyme is used to provide a

gradual supply of hydrogen peroxide from glucose, oxygen and water. After 40-60 min, selected sections were mounted in 0.1 M PB and checked under the light microscope for stained processes that could be followed through the entire section thickness.

After successful reactions and following washing, sections were flattened on the bottom of glass vials and incubated in 0.2-1% wt/vol osmium tetroxide (TAAB; 4% wt/vol stock OsO_4) in 0.1 M PB for 60 min. The concentration depended on the level of background staining. Sections were washed and gradually dehydrated with increasing ethanol concentrations (50% and 70% for 10 min each; 90% and 95% for 5 min each; 100% for 2 x 10 min). Sections selected for electron microscopy were further contrast enhanced by 'en-bloc' staining in 2% wt/vol uranyl acetate (TAAB) for 40 min in 70% ethanol before the 90% ethanol step. For resin embedding, the sections were immersed in propylene oxide (VWR International) for 2 x 10 min in order to enhance resin penetration. This was followed by submerging the sections in epoxy resin (Durcupan ACM Fluka, Sigma-Aldrich) for overnight. Finally, sections were carefully mounted on hand-greased glass slides, covered under a coverslip and left at ~60°C for 48 h for the resin to polymerise.

2.2.5 Light- and electron microscopy

Conventional transmitted light microscopy was performed using either a Leitz Dialux22 microscope (Leica) equipped with NPL Fluotar 10x/0.3, 25x/0.55, 40x/0.78 and PL Apo 100x/1.32 oil objectives or the AxioImager.Z1 microscope (Carl Zeiss) described above. In the case of the former, images were taken using Canon EOS 40D camera controlled by an EOS Canon Utility software v2.9.0.0. Otherwise the documentation was done using AxioCam HRm CCD camera and AxioVision 2009, Rel.4.8.1 software.

Electron microscopy (EM) is a technology that allows us to achieve much greater resolving power than optical microscopy since it uses electrons instead of photons for imaging. Its advantage is in the much shorter equivalent wavelength of electrons compared to the photons. On the other hand EM is technically more demanding and more time-consuming. For EM studies, first I selected 70 μm thick sections from the labelled cells and performed the enzyme reactions on them followed by epoxy resin embedding. After light microscopic evaluation, I selected a small region and re-embedded it into a block of resin for cutting serial EM sections. The cutting of EM sections was done by Kristina Detzner and David Roberts and they provided the thin serial sections mounted on pioloform coated single-slot grids, which I studied using Philips CM 100 transmission electron microscope. To document the images I used Digital Micrograph software (Gatan) and a Gatan Ultrascan 1000 CCD camera.

2.2.6 Single cell reconstruction techniques

Neurons (n=5; see Figure 4-2A, Figure 4-4A, Figure 5-2A,G, Figure 5-4A) were manually traced using a microscope-attached drawing tube using a Pl Apo 63x/1.4 oil immersion objective. Some were digitally reconstructed in 3D (Figure 2-2A) from resin-embedded, osmium-treated serial coronal cut brain sections (70 μm nominal thickness) using Neurolucida (MBF Bioscience). A Nikon Eclipse 80i transmitted light microscope and Lucivid microdisplay (MBF Bioscience) was used in continuous mode equipped with a VC Plan Apo 100x/1.4 oil immersion objective. The three dimensional reconstruction of an interneuron allows to quantitatively evaluate it for future comparison with other cell types. Hippocampal laminar boundaries can be marked digitally and dendritic and axonal proportions quantified appropriately.

Neuronal processes can be also manually traced from individual sections. These drawings then are merged and projected onto different planes with the layer boundaries marked. This is photographed and scanned for further processing in Photoshop (Adobe Systems). I have traced LK08c and LK12o using this method.

During my MSc studies I learned and carried out 3D reconstructions of recorded cells. In this thesis the illustrated cells were reconstructed by Szabolcs Biro (LK20p and LK27d) and Dr. Timea Szabadi (LK06ah) with the agreement of my supervisors.

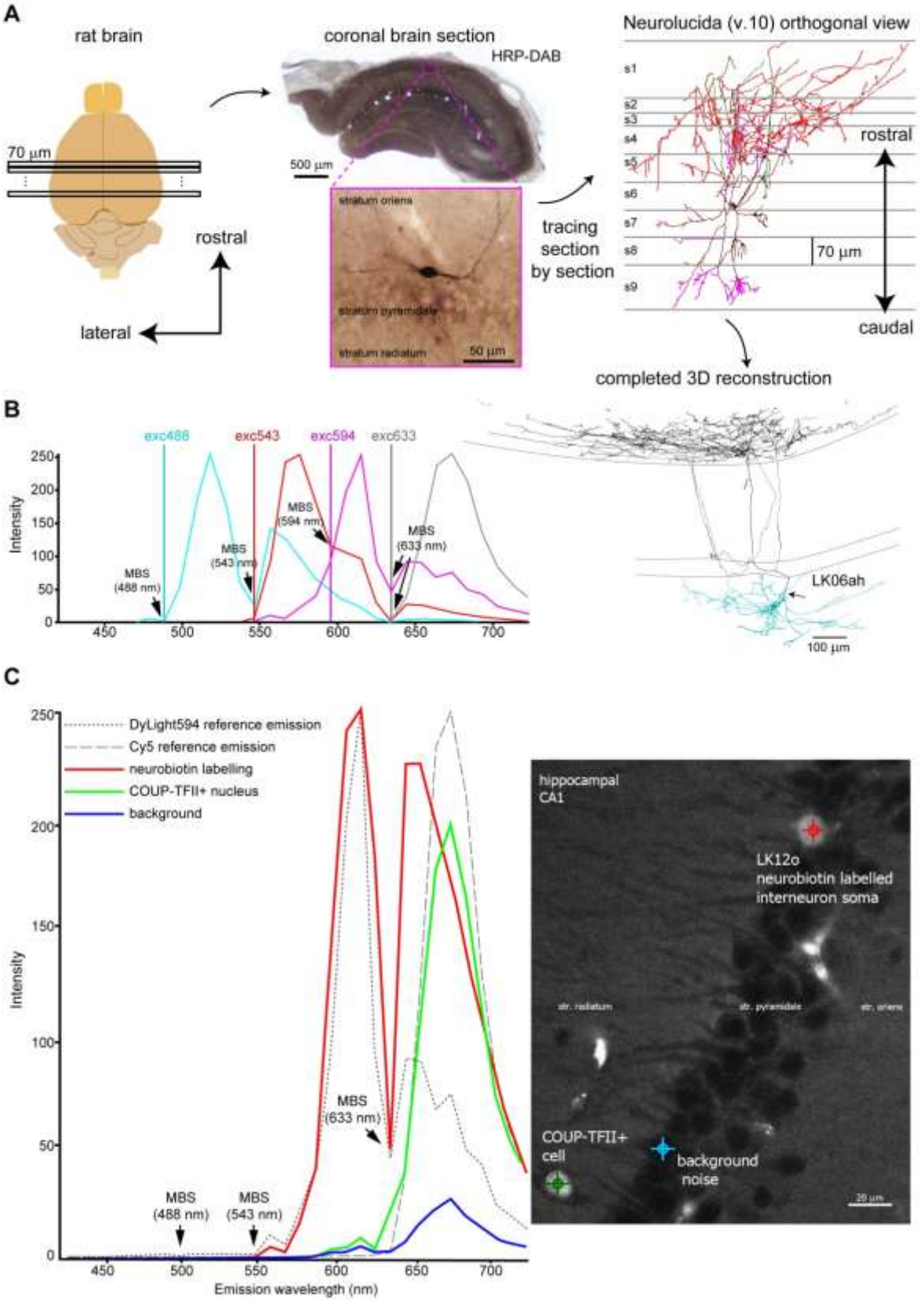
A
rat brain
70 µm
rostral
lateral
coronal brain section
HRP-DAB
500 µm
stratum oriens
stratum pyramidale
stratum radiatum
50 µm
tracing section by section
Neurolucida (v.10) orthogonal view
s1
s2
s3
s4
s5
s6
s7
s8
s9
rostral
70 µm
caudal
completed 3D reconstruction
B
exc488
exc543
exc594
exc633
Intensity
MBS (488 nm)
MBS (543 nm)
MBS (594 nm)
MBS (633 nm)
LK06ah
100 µm
C
DyLight594 reference emission
Cy5 reference emission
neurobiotin labelling
COUP-TFII+ nucleus
background
Intensity
MBS (633 nm)
MBS (488 nm)
MBS (543 nm)
Emission wavelength (nm)
hippocampal CA1
LK12o neurobiotin labelled interneuron soma
str. radiatum
str. pyramidale
str. oriens
COUP-TFII+ cell
background noise
20 µm

Figure 2-2 Anatomical analyses and spectral imaging using confocal laser scanning microscopy.

A. Three-dimensional reconstruction of neurobiotin-filled neurons. Fixed brains are cut into 70 μm-thick serial coronal sections. Using the HRP-DAB protocol (see above) neurobiotin labelled processes are visualised for conventional light microscopy. Next, cell bodies, dendrites and axon collaterals are traced using Neurolucida software section by section. Each data point is registered according to X, Y and Z coordinates and is finally merged into a three dimensional data structure. **B.** Excitation wavelengths (vertical lines) and emission bandwidths of different fluorophores (Al488/DyLight488; Cy3/DyLight543; DyLight594; Cy5/DyLight633). **C.** *Left,* Grey lines illustrate the spectral identity of DyLight594 and Cy5 dyes. Coloured curves represent the emissions from (i) the soma of the neurobiotin-labelled interneuron (red, LK12o); (ii) a neighbouring unlabelled COUP-TFII immunopositive nucleus (green) and (iii) an immunonegative soma of a pyramidal neuron (blue) as control for background (excitation using 633 nm HeNe laser; MBS 488/543/633 nm). *Right,* Crosses mark the sites of the measurements. Note that the signal emitted by the labelled cell body is a mix of DyLight594 and Cy5 emissions because of the width and intensity levels of the emission curve (red). After peaking at ~600 nm as expected based on the DyLight594 reference emission curve (dotted line) the signal intensity in the labelled neuron is still very high at ~650 nm which can only be explained by Cy5 emission as demonstrated on the respective reference emission curve (dashed line). Therefore I concluded that there is genuine Cy5 signal at the marked site (red), indicating COUP-TFII expression in the interneuron under investigation. Intensity is given in arbitrary units. Eight bit digital images were taken in which contrast is represented in 256 steps. Minimum intensity = 0 and maximum = 255.

Table 2.1 Primary antibody information.

Molecule	Host species	Internal ref No.	Dilution	Stock protein concentration (µg/ml)	Source	Source code
Ca2+/calmodulin-dependent protein kinase II (CaMKII)	Mouse	1312	1:500	1000	Abcam, Cambridge, UK **(www.abcam.com)**	ab22609
Calbindin (CB)	Rabbit	989	1:5000	antiserum	Swant, Bellinzona, Switzerland **(www.swant.com)**	CB-38 (lot 5.5)
Calretinin (CR)	Goat	1116	1:1000	antiserum	Swant, Bellinzona, Switzerland **(www.swant.com)**	CG1
Calretinin (CR)	Rabbit	1102	1:1000	antiserum	Swant, Bellinzona, Switzerland **(www.swant.com)**	7699/3H (lot 18299)
Cannabinoid receptor type 1 (CB1R)	Rabbit	1272	1:1000	380	Prof. M. Watanabe, FRONTIER INSTITUTE Co. Ltd, Hokkaido, Japan	(Kind gift)
Chicken ovalbumin upstream promoter transcription factor 2 (COUP-TFII)	Mouse	1096	1:250	1000	Perseus Proteomics Inc., Tokyo, Japan **(www.ppmx.com)**	PP-H7147-00
Cholecystokinin precursor protein (CCK)	Guinea pig	1306	1:500	380	Prof. M. Watanabe, FRONTIER INSTITUTE Co. Ltd, Hokkaido, Japan	(Kind gift)
Extracellular leucine-rich repeat fibronectin containing protein 2 (Elfn2)	Rabbit	1432	1:500	antiserum	Sigma-Aldrich, St. Louis, MO, USA **(www.sigma-aldrich.com)**	HPA000781
$GABA_A$ receptor alpha1 subunit ($GABA_Aa1$)	Rabbit	946	1:500	406	Prof. W. Sieghart, Brain Research Institute, Vienna, Austria.	P16
Metabotropic glutamate receptor 1a (mGluR1a)	Goat	1266	1:750	1220	Prof. M. Watanabe, FRONTIER INSTITUTE Co. Ltd, Hokkaido, Japan	(Kind gift)
Metabotropic glutamate receptor 1a (mGluR1a)	Guinea pig	1267	1:500, 1:1000, 1:2000	660	Prof. M. Watanabe, FRONTIER INSTITUTE Co. Ltd, Hokkaido, Japan	(Kind gift)
Metabotropic glutamate receptor 7a (mGluR7a)	Rabbit	960	1:1000, 1:2000	500	Prof. R. Shigemoto, Division of Cerebral Structure, Nat. Inst. Physiol. Sci., Okazaki, Japan	(Kind gift)
Multizinc finger protein (Fog-2)	Rabbit	1369	1:200	200	Santa Cruz Biotechnology Inc., Santa Cruz,CA, USA	sc-10755
Muscarinic acetylcholine receptor 2 (M2R)	Rat	981	1:250, 1:400	1.4	EMD Millipore Corporation, Billerica, MA, USA **(www.millipore.com)**	MAB367
Neuropeptide Y (NPY)	Rabbit	1011	1:5000	antiserum	ImmunoStar Inc. (DiaSorin), Hudson, WI, USA	22940 (lot 208001)
Nitric oxide synthase (nNOS)	Mouse	1167	1:1000	ascites 35900	Sigma-Aldrich, St. Louis, MO, USA	N2280 Lot 081K4815
Parvalbumin (PV)	Goat	1258	1:1000, 1:2000	antiserum	Swant, Bellinzona, Switzerland **(www.swant.com)**	PVG-214 (lot 3.6)
Parvalbumin (PV)	Guinea pig	1310	1:5000	antiserum	Synaptic Systems, Entwicklung und Produktion mbH, Goettingen, Germany	195 004 (lot5)
Parvalbumin (PV)	Mouse	922	1:5000	antiserum	Swant, Bellinzona, Switzerland **(www.swant.com)**	235 (lot 10-11 F)

Molecule (continued)	Host species (continued)	Internal ref No. (continued)	Dilution (continued)	Stock protein concentration (µg/ml) (continued)	Source (continued)	Source code (continued)
Parvalbumin (PV)	Rabbit	835	1:500	antiserum	Swant, Bellinzona, Switzerland **(www.swant.com)**	PV-28 Lot 5.5
Preproenkephalin (PPE)	Guinea pig	1037	1:500	0.4	Dr. T. Kaneko, Kyoto University, Japan	
Pro-cholecystokinin (proCCK)	Rabbit	1090	1:500	350	Prof. M. Watanabe, FRONTIER INSTITUTE Co. Ltd, Hokkaido, Japan	(Kind gift)
Reelin	Mouse	1112	1:500	1000	EMD Millipore Corporation, Billerica, MA, USA	MAB5364 Lot LV1566698
Somatostatin (SM)	Mouse	1276	1:200, 1:400, 1:500	140	GeneTex Inc., Irvine, CA, USA **(www.genetex.com)**	GTX71935 (clone SOM-
Somatostatin (SM)	Rat	815	1:500	1000	EMD Millipore Corporation, Billerica, MA, USA	MAB354
Special AT-rich sequence-binding protein 1 (Satb1)	Goat	1394	1:200	200	Santa Cruz Biotechnology Inc., Santa Cruz,CA, USA **(www.scbt.com)**	sc-5989
Special AT-rich sequence-binding protein 1 (Satb1)	Rabbit	1393	1:1000	1000	Abcam, Cambridge, UK **(www.abcam.com)**	ab70004
Special AT-rich sequence-binding protein 2 (Satb2, SATBA4B10)	Mouse	1341	1:100	100	Abcam, Cambridge, UK **(www.abcam.com)**	ab51502
Tyrosine-protein kinase receptor (ErbB4)	Mouse	1353	1:1000	200	Thermo Fisher Scientific, Kalamazoo, MI, USA **(www.labvision.com)**	MS-270-P, clone H4.77.16
Vasoactive intestinal polypeptide (VIP)	Mouse	1053	1:50000	antiserum	Dr. G. Ohning, Cure, UCLA, USA	55

Molecule (repeated)	Host species (repeated)	Description	Antibody specificity information	Notes
Ca2+/calmodulin-dependent protein kinase II (CaMKII)	Mouse	Monoclonal, partially purified, native rat protein.	Western blot (Wang and Maler, 1998); Abcam.	
Calbindin (CB)	Rabbit	Polyclonal, recombinant rat calbindin D-28k.	Knockout test (Airaksinen et al., 1997); characterisation in rat hippocampus (Sloviter, 1989).	
Calretinin (CR)	Goat	Polyclonal, recombinant human calretinin.	Western blot (Schwaller et al., 1999a).	
Calretinin (CR)	Rabbit	Polyclonal, recombinant human calretinin containing a 6-his tagged N-terminus.	Knockout test (Schiffmann et al., 1999); Western blot (Schiffmann et al., 1999); Swant.	
Cannabinoid receptor type 1 (CB1R)	Rabbit	Affinity purified.	Immunoblot (Fukudome et al., 2004).	
Chicken ovalbumin upstream promoter transcription factor 2 (COUP-TFII)	Mouse	Monoclonal, recombinant human COUP-TFII.	Knockout test (Qin et al., 2007). Cross reacts with mouse and rat COUP-TFII and does not recognise COUP-TFI or EAR2.	
Cholecystokinin precursor protein (CCK)	Guinea pig	Polyclonal, CCK-8.	Personal communication with Prof. M. Watanabe.	Labelling patterns similar to that seen by several other previously characterized antibodies recognizing the same molecules.
Extracellular leucine-rich repeat fibronectin containing protein 2 (Elfn2)	Rabbit	Polyclonal, human ELFN2, recombinant protein epitope signature tag.	Protein array test and Western blot (Sylwestrak and Ghosh, 2012); developed and validated by the Human Protein Atlas project.	Labels interneurons via cross-reactivity with Elfn1.
$GABA_A$ receptor alpha1 subunit ($GABA_Aa1$)	Rabbit	Rat sequence aa1-9.	Western blot (Zezula and Sieghart, 1991).	
Metabotropic glutamate receptor 1a (mGluR1a)	Goat		Personal communication with Prof. M. Watanabe.	In some interneurons it labels a reticular pattern instead of labelling the plasma membrane.
Metabotropic glutamate receptor 1a (mGluR1a)	Guinea pig	Affinity purified.	RNA- and immunoblot (Nakamura et al., 2004; Sato et al., 2004).	In some interneurons it labels a reticular pattern instead of labelling the plasma membrane.
Metabotropic glutamate receptor 7a (mGluR7a)	Rabbit	Rat mGluR7, affinity purified, aa874-915.	Receptor-null mice (Klausberger et al., 2005); immunoblot (Shigemoto et al., 1997; Shigemoto et al., 1996).	
Multizinc finger protein (Fog-2)	Rabbit	Polyclonal, epitope aa880-1126 mapping at the C-terminus of FOG-2 of mouse origin.	Western blot (Dale et al., 2007; Roche et al., 2008); Santa Cruz.	
Muscarinic acetylcholine receptor 2 (M2R)	Rat	Monoclonal, purified, i3 loop of m2 receptor fusion protein aa225-359, fused to Glutathione S-transferase, clone M2-2-B3	Western blot (Levey et al., 1995); PCR (Chaudhuri et al., 2005).	
Neuropeptide Y (NPY)	Rabbit	Polyclonal, NPY conjugated to bovine thyroglobulin with glutaraldehyde.	Radioimmunoassay and column chromatography (Allen et al., 1983); absorption-tested by manufacturer to 6 other peptides, no cross-reactivity observed.	Strong immunoreactivity observed in subpopulations of hippocampal interneurons, no significant background. Labelling as with other antibodies.
Nitric oxide synthase (nNOS)	Mouse	Monoclonal, recombinant rat neuronal NOS fragment aa1-181, clone NOS-B1.	Western blot (Sigma).	Labelling pattern as published with other antibodies.
Parvalbumin (PV)	Goat	Polyclonal, rat muscle PV.	Knockout test (Swant); Western blot (personal communication with E. Celio); (Constantinople et al., 2009); immunoblot (Swant).	
Parvalbumin (PV)	Guinea pig	Polyclonal, recombinant full length rat PV.	Western blot (Synaptic Systems).	
Parvalbumin (PV)	Mouse	Monoclonal, purified carp muscle PV.	Radioimmunoassay and immunoblot (Celio et al., 1988).	

Molecule (repeated continued)	Host species (repeated continued)	Description (continued)	Antibody specificity information (continued)	Notes (continued)
Parvalbumin (PV)	Rabbit	Purified rat PV.	Knockout test (Schwaller et al., 1999b); HPLC, radioimmunoassay, dot blot and Western blot (Kägi et al., 1987); double immunodiffusion, immunoreplica techique (Celio and Heizmann, 1981).	
Preproenkephalin (PPE)	Guinea pig		Dot blot (Lee et al., 1997).	
Pro-cholecystokinin (proCCK)	Rabbit	C terminus aa9 of proCCK.	Personal communication with Prof. M. Watanabe.	Labelling pattern as published with other
Reelin	Mouse	Monoclonal, recombinant reelin, aa164-496, clone G10.	Western blot (de Bergeyck et al., 1998); Millipore.	
Somatostatin (SM)	Mouse	Monoclonal, conjugated to protein carrier, human SOM.	Labelling pattern same as with rat antibody Chemicon MAB364 (Kubota et al., 2011).	Labels dendrites and axon stronger than other SOM antibodies.
Somatostatin (SM)	Rat	Monoclonal, unpurified, aa1-14 of cyclic SOM conjugated to bovine thyroglobulin using carbodiimide, clone YC7	(Kubota et al., 2011); no signal in preabsorption test for rat antibody (Jinno and Kosaka, 2000).	
Special AT-rich sequence-binding protein 1 (Satb1)	Goat	Polyclonal, N-terminus, human SATB1.	Knockout test and Western blot (Balamotis et al., 2012).	Same labelling as with rabbit antibody ab70004 (Huang et al., 2011). Labels in addition Satb2-expressing nuclei in CA1 when used at 1:100 dilution. Weakly labels hilar neuron nuclei.
Special AT-rich sequence-binding protein 1 (Satb1)	Rabbit	Polyclonal, aa18 near N-terminus, human SATB1.	Knockout test (Balamotis et al., 2012); no signal for knockout for a similar rabbit antibody; original rabbit antibody (Dickinson et al., 1992); Western blot (different band than Satb2 at P1); colocalization with NeuN, neuron specific.	Labels interneurons exclusively in hippocampus.
Special AT-rich sequence-binding protein 2 (Satb2, SATBA4B10)	Mouse	Monoclonal, recombinant fragment C-terminal, human SATB2.	Knockout test (Britanova et al., 2005; Dobreva et al., 2006); knockout test and Southern blot (Britanova et al., 2006).	Same labelling as rabbit antibody ab34735 with additional signal for Satb1. Labels pyramidal cells and a subpopulation of interneurons in CA1, consistent with the combination of specific Satb2
Tyrosine-protein kinase receptor (ErbB4)	Mouse	Monoclonal, extracellular fragment, recombinant human c-erbB4/HER-4 oncoprotein.	Knockout test (Vullhorst et al., 2009); Western blot (Chen et al., 1996; Neddens et al., 2011).	Cortical GABA circuit development controlled by ErbB4 signalling (Fazzari et al., 2010).
Vasoactive intestinal polypeptide (VIP)	Mouse	Monoclonal, raised in mouse against VIP.	Radioimmunoassay (Wong et al., 1996).	

Table 2.2 Secondary antibodies with respective dilutions (all raised in donkey).

Primary antibody species	Alexa 405	DyLight 405	Alexa 488	DyLight 488	Cy3	DyLight 549	DyLight 594	Cy5	DyLight 649
guinea pig	1:250			1:500 1:1000	1:400		1:500	1:250 1:1000	1:250
goat	1:200	1:250			1:400			1:250	
mouse	1:250				1:400			1:250	
rabbit	1:100 1:250 1:1000		1:1000		1:400		1:500	1:250	
rat	1:250			1:800	1:400			1:250	
streptavidin		1:200	1:1000				1:1000		

2.3 Computational and statistical analyses

2.3.1 Detecting behavioural states

I segmented recording sessions according to slow wave sleep, paradoxical sleep, movement and quiet wakefulness using data from the electrophysiological and behavioural recordings in freely moving rats, as follows (Figure 2-3). In the recordings without the use of the accelerometer, I imported the LED array-tracking data into Spike2 (v7.06a, Cambridge Electronic Design, Cambridge, UK) for movement detection.

First, motionless periods were analysed for the detection of sleep episodes. During slow wave sleep (Figure 2-3A), the cortical LFP oscillates at low delta frequencies (<3 Hz) and it is enriched in spindle oscillations (7-14 Hz) therefore I examined the EEG channel for the occurrence of such spindle-rich sleep periods. After downsampling the data to 1 kHz I digitally band pass filtered it (finite impulse response, Gaussian window, 1024 coefficients, transition gap 2.5 Hz) at delta and spindle frequencies and calculated the power (root mean square amplitude, r.m.s.) in the latter for 4 s sliding windows. The beginning and end of delta frequency oscillatory epochs coincided with the 40% threshold (of maximum r.m.s.) in the spindle channel hence these periods were allocated as slow wave sleep (2015 s; n=11 rats).

During paradoxical sleep (Figure 2-3B), both the cortical and the hippocampal LFPs oscillate at theta frequencies (5-12 Hz). These episodes occur always subsequently to slow wave sleep periods and include muscle twitches. I detected 8 s in n=1 rat of paradoxical sleep in total. Between the different sleep stages transitions were identified when spindles in the cortical LFP were simultaneously recorded with theta oscillations in the hippocampal LFP.

During wakefulness, the EEG channel becomes desynchronised, spindles disappear and the signal amplitude drops. In the hippocampal LFP theta oscillations (5-12 Hz) and SWRs (130-230 Hz) alternate, but are not exclusive. Based on data from motion tracking, I identified periods of movement (488 s; n=12 rats) which included slight head movements and running (Figure 2-3C), whereas motionless awake episodes were categorised as quiet wakefulness (Figure 2-3C; 1402 s; n=12 rats).

I excluded periods suggestive of the mechanical influence of the glass electrode on the firing of the recorded cell.

2.3.2 Detecting oscillatory network states

To detect theta oscillatory epochs (5-12 Hz), SWRs (130-230 Hz) and low oscillatory periods (LOSC) in drug-free rats, I analysed the hippocampal LFP by developing algorithms or using those written by Drs J. Tukker and B. Lasztoczi in Spike2 and MATLAB (Wavelet Toolbox, v7.9-R2009b, MathWorks), respectively.

Following digitally band pass filtering the LFP (finite impulse response, FIR, Gaussian window, 1024/2048 coefficients, transition gap 2.5 Hz) at delta (2-4 Hz), theta and ripple frequencies, I selected theta periods (n=629 s; n=12 rats) based on the theta to delta frequency power ratio using Fast-Fourier transforms (FFT, 1024 points, 2 s Hanning windows). A ratio greater than four in three consecutive windows was identified as a theta epoch. Theta cycles were defined between two consecutive troughs during the selected periods. I adjusted the beginnings and ends of theta epochs manually, based on the regularity of the oscillation.

For detecting SWRs, the threshold was set to power values (r.m.s. in 10 ms sliding windows) of 5 x s.d. above the mean power. The start and end of ripples were set to time points where the r.m.s. crossed 1 x s.d. above the mean power. Peaks were

determined as local power maxima between detected start and end points using a peak-finding algorithm (Klausberger et al., 2003). I verified manually each such segmented time period (n=54 s; n=12 rats).

During LOSC, there is a drop in power for all oscillatory rhythms in the hippocampal LFP. To detect such events, I digitally band pass filtered the LFP using settings from above at 5-15 Hz, 15-30 Hz, 30-70 Hz and 70-120 Hz frequencies and I calculated the r.m.s power for each in 1 s sliding windows. LOSC periods (160 s; n=11 rats) were identified where the power dropped in all four channels simultaneously by 1 x s.d. below the mean for at least 300 ms. Detection began when the second channel went below threshold and ended when the third channel reached above threshold.

Similarly like above, periods suggestive of the mechanical influence of the glass electrode on the firing of the recorded cell were excluded from further analyses.

2.3.3 Spike train analyses

Following spike detection and sorting in Spike2, I developed algorithms using MATLAB to calculate parameters of interest for cell type identification and for comparison between distinct neuron types. During some recordings, I recognised artefacts produced by the advancement of the glass electrode closer to the neuron, which suggested mechanical injury or 'irritation' to the recorded neuron. The action potential waveform changed (e.g. double peaks; very short or no refractory period; etc.) and the firing rate of the neuron increased to aberrantly high values. This could happen even when the electrode was clearly extracellular to the neuron. Occasionally, even the local field potential recorded with the same electrode was affected (e.g. started to artificially oscillate at low frequencies; action potential waveforms appeared in the signal; etc.). I only included artefact-free time periods in the analysis. I

determined average firing rates for individual cells during different behavioural and oscillatory network states by counting, for a given state and cell, the total number of spikes and dividing this by the total length of time. Similarly, I calculated autocorrelograms (AC) for comparisons between cell types and investigated rhythmicity in their spiking (Figure 3-1-Figure 3-3, Figure 4-5, Figure 4-6, Figure 5-5-Figure 5-7). These graphs represent the timing between each consecutive action potential in a spike train. Moreover, the preferential timing of action potential discharges during different phases of theta oscillatory cycles and the SWR-related firing of individual neurons proved to be very informative with regard to cell type identity. I further studied likely changes in firing dynamics during SWRs compared to time periods lacking such events (see below). I completed the statistical analyses presented in this thesis using SPSS, MATLAB (Statistical Toolbox) and SAS (v9.3).

For each neuron, I computed the autocorrelograms of spiking activity and I measured the inter-spike intervals (ISI), the periods between two consecutive action potentials, and analysed their distributions (1 ms bin width) with respect to distinct behavioural and network states (Figure 4-5B-D, Figure 4-6D-F, Figure 5-5B, Figure 5-6A,B, Figure 5-7C). The autocorrelograms or the ISI data of cells of a given type were averaged and the mean $\pm$ s.e.m. was considered as the representative autocorrelogram or ISI distribution for the cell type (Figure 5-6). Additionally, I calculated point estimates (median $\pm$ interquartile range) for the individual ISI distributions for each interneuron during each state (Table 4.3, Table 5.5). I derived also a measure for the instantaneous frequencies (IF) of firing using the reciprocal of the ISIs and studied their distribution (bin width: 1Hz; domains of theta, beta, gamma and fast frequencies were highlighted) per cell type.

2.3.4 State-dependent firing rate and spike count comparisons

In order to account for possible correlations between measurements from the same cell during different behavioural and network oscillatory states, I performed repeated-measures ANOVA analyses (Figure 5-5A, Figure 5-7A). For consistency, the total number of cells was always included, even when for a given neuron either the behavioural states or the network oscillatory states were incomplete (e.g., in chapter 5, for LK20p sleep data is missing; for TV21f LOSC data is missing). Using the PROC MIXED procedure in SAS, I fitted a linear mixed effects model to the data with restricted maximum likelihood estimation.

$$Y_{ijk} = \mu + \alpha_i + \beta_j + (\alpha\beta)_{ij} + \varepsilon_{ijk},$$

where Y_{ijk} is the observed firing rate or spike count during SWRs of cell k of cell type i during within-factor behavioural/network-oscillatory state j; μ is the overall average firing rate or overall average spike count; α_i is the effect of cell type i; β_j is the effect of within-factor behavioural/network-oscillatory state j; $(\alpha\beta)_{ij}$ is the interaction effect between cell type and within-factor behavioural/network-oscillatory state; ε_{ijk} is random noise; all units are in Hz or counts. I defined the model with compound symmetry with the assumption that the variability is similar between different cell types and the correlation is equal between different behavioural/network oscillatory states. As *post hoc* pairwise comparisons within the same model, differences of least squares means between cell types were calculated for each level of within-factors of behavioural/network oscillatory states, and vice versa. Due to the low number of cells statistical significance was assessed without adjustments for multiple comparisons. As an alternative model used for validation, I implemented an adjustment for the

denominator degrees of freedom because of the small sample sizes using the Kenward-Roger (KR) method (Kenward and Roger, 1997). Since the results of the original model were not significantly different from those of the alternative adjusted model, I decided to report the conclusions given by the former. For all statistical methods used in this thesis p-values and confidence intervals were calculated according to $\alpha=0.05$. Note that before fitting the model I normalised the SWR-related spike counts (countX) using the following calculation: $\log_{10}(1+\text{countX})$. As an alternative calculation, I applied the mixed model to SWR-related median number of action potentials. The conclusions were similar to those given by mean spike counts, therefore I report the latter. I confirmed the prediction of the model using one-way ANOVA and Kruskal Wallis tests (Table 5.4).

2.3.5 Theta oscillations related spike-timing of interneurons

Following the segmentation of spike trains according to theta epochs present in the hippocampal LFP, theta cycles were detected and spikes were sorted into 18° theta-phase bins, cycle-by-cycle. The definition of the phase relationship between single cell firing and theta activity is as follows. For every spike time (t_s) the phase was computed between the preceding (t_i) and following (t_{i+1}) theta trough times using:

$$\text{phase}_s = [(t_s - t_i)/(t_{i+1} - t_i)] \times 360°$$

Thus each spike was assigned an instantaneous phase between two troughs (0 and 360°). I plotted the spike-timing relative to the theta cycles in the CA1 stratum pyramidale or oriens on circular phase histograms (18° bins; n=20; Figure 4-6C, Figure 5-7B). For each neuron, after computing the theta phases of the recorded spikes I determined whether the cell was theta modulated using Rayleigh's method (Zar, 1999). If the theta phases resulted in a non-uniform distribution around the theta cycle, I

calculated the cell's mean phase angle and the depth of the cell's theta modulation using normalised vector addition. Next, by averaging data across individual cells of the same type I quantified the mean depth of theta modulation and the preferential mean theta phase of firing for a given cell type (circular mean $\pm$ circular standard deviation) using circular statistics and compared these parameters between distinct cell types using two-sample permutation tests (Good, 2000).

2.3.6 SWRs related firing activity

After determining the average firing rate of a neuron during SWRs I have also counted the mean and median number of action potentials occurring during individual events. SWRs were further segregated into those that occurred during sleep and those happening during wakefulness. These counts were compared between distinct cell types and behavioural states as described above using repeated-measures ANOVA analysis (Figure 4-6B, Figure 5-8C). Moreover, for a given cell type, I computed the average spiking probability histogram (5 ms bin width) during the ± 500 ms periods surrounding the peak of SWRs. If another SWR occurred during these 500 ms time windows, its period was omitted from the calculation. In order to gain insight into the detailed spiking responses per individual event, I created raster plots of the action potential firing aligned to the peak SWR power using coloured lines delineating the beginnings and ends of aligned SWRs and surrounding SWR episodes. Sweeps were sorted according to when SWRs occurred, starting from the bottom with those during sleep and finishing with awake-SWRs.

2.3.7 SWR-dependent firing rate changes of interneurons

In order to quantify the variability (e.g., cells firing with rates above average during some SWRs but being silent during others) in firing of a given neuron dependent on SWRs, I developed two novel methods. I aimed to obtain a more detailed quantification, over the entire domain of firing frequencies, of the differences in SWR-related firing rates versus firing rates outside SWR events. Previous procedures mostly use time-normalised averaging of firing during SWRs, or simply SWR-peaks-aligned averaging.

Method 1

Firing rates were calculated for the *n* detected SWRs and their distribution displayed as a cumulative distribution function (CDF) (Figure 4-2G, Figure 4-3I, Figure 4-4N, Figure 5-8F,G, Figure 5-9A,B). For some cells these appeared Poisson-like. Next, I created a population of 1000 x *n* surrogate time windows (surrogate 'SWRs') as follows: 1. Periods of movement and of detected SWRs were excluded from the total recording time. The resulting sleep or rest states were considered as periods for SWRs to occur. 2. I generated random numbers to mark time points within these periods when surrogate 'SWRs' could occur. 3. I placed intervals of detected single SWR lengths, one-by-one, at the marked time points over the recorded spike train. Once a period was taken by a surrogate 'SWR' it was not available for the subsequent ones. 4. After creating a surrogate for each detected SWR, I calculated individual firing rates and displayed their distribution as a CDF. These four steps were repeated 1000 times resulting in 1000 CDFs (grey) representing the spiking of a given neuron outside detected SWRs. Next, I computed the average of surrogate 'SWRs' as the median value (solid black line) at each frequency bin and I also plotted the 95% confidence intervals

(dashed black lines). Finally, I compared for each neuron, the detected and derived firing rate distributions using a 2-sample Kolmogorov-Smirnov test. A probability of ≤0.05 indicated a significantly different firing rate distribution during detected SWRs from that calculated during outside SWR periods. A shift to the left or right of the measured firing rate distribution relative to the mean of the surrogate sets indicated a decreased or increased firing probability.

Method 2.

I altered the calculation of the mean firing rate of a given neuron during the detected *n* SWRs by summing all spikes during the *n* SWRs and dividing this by the sum of durations of the *n* SWRs. A set of 1000 x *n* surrogate 'SWRs' was generated as above and the mean firing rate of each surrogate set was calculated, representing the spiking of a given neuron outside detected SWRs. In each sweep, I counted spikes during *n* surrogate 'SWRs' and I divided this by the sum of time lengths of *n* SWRs. Then I compared the CDF of the 1000 surrogate mean firing rates with the real mean firing rate during detected SWRs (insets Figure 4-2G, Figure 4-3I, Figure 4-4N, Figure 5-8F,G, Figure 5-9A,B). The crossing between the two lines shows the probability of the measured mean firing rate falling within or outside the population of surrogate rates obtained outside detected SWRs. If the probability was ≤0.05 then the mean firing rate of a given neuron during SWRs was considered significantly different from the firing rate during periods outside SWRs. From this second method I derived a *SWR activity index* as the ratio between the measured mean firing rate and the average of the population of surrogate rates calculated from outside detected SWRs.

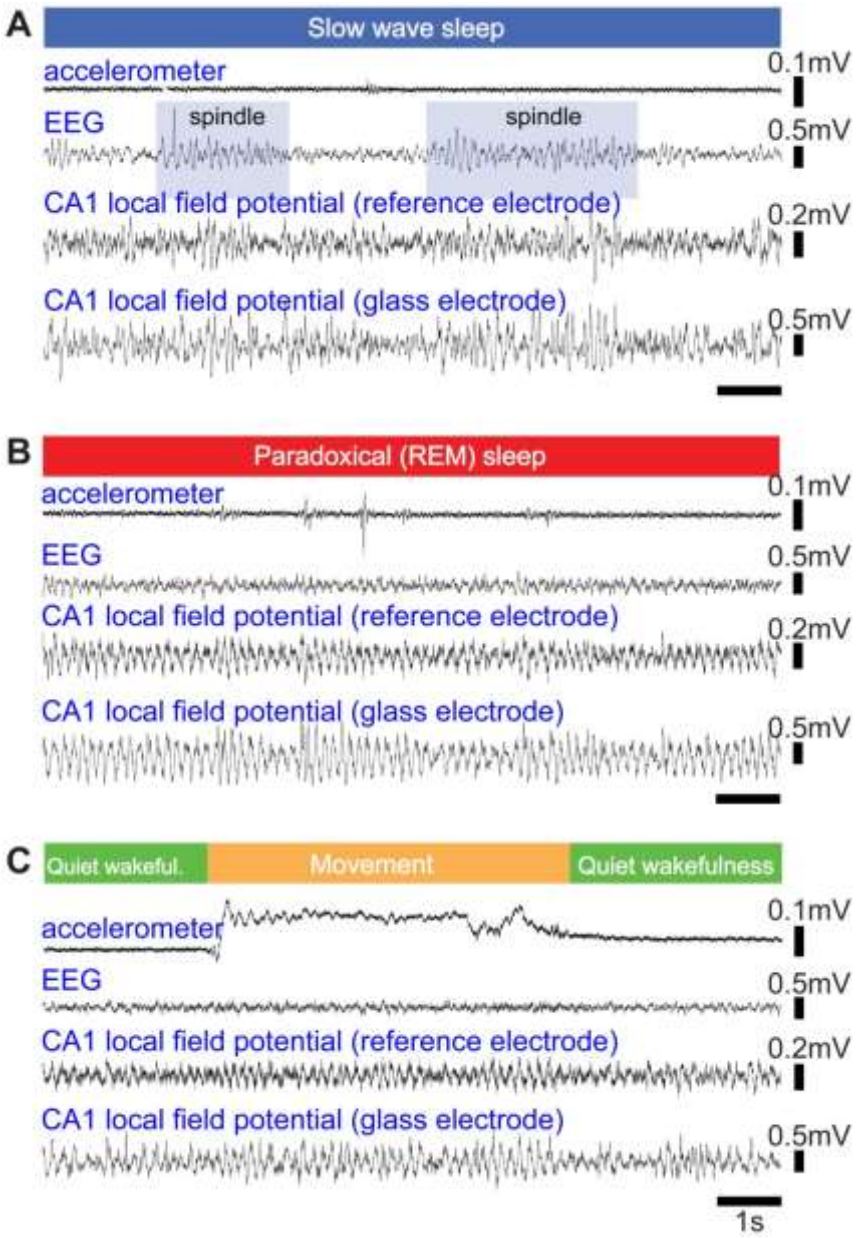

Figure 2-3 Behavioural state segmentation.

A. Motionless periods (accelerometer flat) were analysed for the detection of slow wave sleep. The cortical LFP (EEG) oscillates at low delta frequencies (<3 Hz) and it is enriched in spindle oscillations (7-14 Hz). Periods of high power (root mean square, r.m.s.) in the delta- and spindle frequency bands were detected as slow wave sleep. **B.** During paradoxical sleep, both the cortical (EEG) and the hippocampal (CA1 local) LFPs oscillate at theta frequencies (5-12 Hz). **C.** During wakefulness, the EEG channel becomes desynchronised, spindles disappear and the signal amplitude drops. In the hippocampal LFP theta oscillations (5-12 Hz) and SWRs (130-230 Hz) alternate, but are not exclusive. Movement was detected based on motion tracking (accelerometer) and it included slight head movements and running. Motionless awake episodes were categorised as quiet wakefulness. Modified from Fig. 4 in (Lapray et al., 2012).

3 The hippocampal neuronal network: pyramidal cells and GABAergic interneurons

3.1 Introduction

The cooperation of synaptically connected groups of hippocampal neurons is essential for mnemonic processing (Squire et al., 2004). The majority of such neurons are glutamatergic pyramidal cells. Their output encodes novel associations that are consolidated in the neocortex (Buzsáki, 1989, 1996). The emergence of the hippocampal code is regulated by a smaller population of GABAergic interneurons which show great diversity (Somogyi, 2010). In the CA1 area, we can differentiate at least twenty-two distinct types of such cell which are hypothesised to temporally organise pyramidal cell firing via inhibition. Their selective influence is twofold, *spatial* because axon collaterals of distinct interneuron types innervate different pyramidal cell compartments; and *temporal* because GABA is released, under anaesthesia, only at specific times by different types of interneuron (Somogyi et al., 2014). However, the firing activity of GABAergic cells in the drug-free brain is mostly unknown.

In order to test the hypothesis that differences in connectivity and molecular composition amongst cell types reflect the segregation of functions, I have recorded single pyramidal cells and GABAergic interneurons extracellularly in the CA1 area of freely moving rats (Lapray et al., 2012). This was followed by neurobiotin-labelling of the recorded neurons using the juxtacellular technique (Pinault, 1996). The data allows me to study the pyramidal cell output code and its GABAergic regulation in correlation

with behaviour. I summarise the results of my explorations in the next section and evaluate their importance. The next two chapters contain my original observations about the action of identified GABAergic cell types and the interpretation of their function.

3.2 Spike-timing of hippocampal neurons in freely moving rats

From a total of twenty-nine *in vivo* experiments (n=28 in freely moving rats; n=1 under urethane anaesthesia) I have attempted recording and labelling single neurons in the CA1 area of freely moving rats in twenty-six cases (n=21 rats implanted by me; n=5 rats implanted by colleagues). In two additional experiments I have focused exclusively on recording local field potentials using tetrodes. In this short chapter I summarise these investigations (Table 3.1, Figure 3-1, Figure 3-2 and Figure 3-3).

From a population of thirty-nine putative pyramidal cells and fifty putative non-pyramidal cells recorded in the hippocampus I have labelled and identified four (LK01v, LK08d, LK14v and LK18m) and nine cells (n=8 GABAergic interneurons; n=1 granule cell in dentate gyrus, LK26h), respectively (Table 3.1). Three O-LM (LK01ab, LK06ah, LK13k), one PV-expressing basket cell (LK08c), one "unconventional interneuron" (LK12o), two bistratified (LK20p, LK27d) and one axo-axonic cell (LK24g) were successfully identified (see chapters 4 and 5). I only attempted labelling pyramidal cells when by the end of the last recording day (Figure 2-1A) no single GABAergic cell could be labelled in the animal.

3.2.1 Cell-type specific responses during behavioural transitions and oscillatory network states

In this section, I report differences in the spike-timing of different types of hippocampal neuron. Note that only those recordings were analysed (Figure 3-1-Figure 3-3) and included in Table 3.1 in which the separation of action potentials could be performed and the neurons were active for a sufficient length of time. When possible, I segmented the spike trains according to behavioural states and I detected periods of rhythmic network events.

In order to categorise non-labelled neurons as pyramidal cells or interneurons, I compared the extracellularly measured action potential waveforms, the autocorrelograms (Figure 3-1A,C, Figure 3-2 and Figure 3-3) and the activity patterns during different behavioural periods. I validated the separation criteria using data from labelled neurons. Pyramidal cell spikes (1.8 ± 0.4 ms, mean $\pm$ s.d.) measured from the positive peak of the spike to the second smaller positive peak at the end of the spike, as illustrated in Suppl. Fig. 7 in (Royer et al., 2012), are broader (Mann-Whitney U test, Z=-2.722, p=0.006; n=6 cells for each group) than those of interneurons (1.0 ± 0.2 ms). The overall firing rate of pyramidal cells (1.9 ± 2.4 Hz) is lower (Mann-Whitney U test, Z=-2.619, p=0.009; n=5 cells for each group) than that of interneurons (22.1 ± 16.7 Hz), although there is high variability within the latter population, as expected because of the diversity of cell types.

I have confirmed that the activity patterns of single neurons depend on behavioural and network oscillatory states (Buzsaki, 2006; O'Keefe and Conway, 1978; Ranck, 1973; Vanderwolf, 1969). Pyramidal cells are more active during slow wave sleep (Figure 3-1A *top*) firing complex-spike bursts (inter-spike intervals < 6 ms;

Figure 3-1B *top inset*) during sharp wave associated ripples (SWRs). Note that these neurons fire only during some of the SWRs and spiking in complex bursts is not restricted to sleep periods. During awake states, when active, pyramidal cells preferentially fire on the trough of theta oscillations (Figure 3-1C *top left*), but they can fire at any phase. Sometimes the spikes are triggered at earlier and earlier phases of consecutive theta cycles starting and finishing at the peak of the oscillatory waveform (Figure 3-1C *top right*). This phenomenon termed phase precession was discovered in pyramidal cell spike trains (O'Keefe and Recce, 1993; Skaggs et al., 1996) and then demonstrated also for non-identified GABAergic interneurons (Ego-Stengel and Wilson, 2007; Maurer et al., 2006). Some of the recorded putative pyramidal neurons might have been place cells, but because of the short duration of my recordings and the lack of running of the animal, the preferential place related firing of neurons could not be assessed quantitatively.

I recorded variable firing rates and different activation patterns for distinct types of identified and putative GABAergic interneuron (Figure 3-1A-C, Figure 3-2, Figure 3-3, Figure 4-2C-E, Figure 4-3E-G, Figure 4-4J-L, Figure 5-2E,F, Figure 5-4G,H). Some are more active during slow wave sleep, similar to pyramidal cells and increase their spike rates significantly during SWRs (Figure 3-1A *middle,* Figure 4-2E, Figure 5-2F). A putative trilaminar cell (LK26a) recorded in stratum oriens fires bursts of 10 to 15 action potentials with instantaneous rates >200 Hz (Figure 3-1B *middle inset*). The similar behavioural- and network state-dependent activity of this non-labelled cell with one identified by my colleague (Dr. D. Lapray, unpublished observation) is predictive of its identity. Other GABAergic interneurons fire with higher rates during wakefulness, especially in correlation with theta oscillations (Figure 3-1C *bottom*, Figure 4-3E,F, Figure 5-2E,F, Figure 5-4G). The spike discharge of the majority of

putative interneurons I have recorded is theta rhythmic (Figure 3-1C *bottom,* Figure 4-2D, Figure 4-3F). Some fire one action potential per theta cycle, others up to 11 and at different preferential phases along the theta cycle. Furthermore, some cells do not fire continuously during theta epochs or they do not couple their spike-timing to the oscillatory wave.

Because I recorded mostly in the direction from alveus down to the hippocampal fissure, my sample might be biased towards neurons in the more dorsal hippocampal layers of the CA1 area (Figure 4-1, Figure 5-1 and Table 3.1). Moreover, interneuron density is quite high in the alveus and stratum oriens. Most GABAergic interneurons in stratum oriens (Figure 3-2) are theta rhythmic and are activated during SWRs and have been identified as dendrite-targeting projection cells. In the pyramidal cell layer (Figure 3-3A,B), I encountered predominantly fast-spiking interneurons some of which I identified as parvalbumin-expressing basket (LK08c), axo-axonic (LK24g) or bistratified cells (LK20p, LK27d). While recording, I experienced clusters of interneurons along the electrode track. I have confirmed the spatial clustering of interneurons after brain removal and fixation using immunohistological processing. At least two other non-labelled GABAergic cells were found in close proximity to the neurobition-labelled interneuron, often having different molecular expression profiles (Figure 4-4D). Occasionally, because of the densely packed layer, I could not avoid labelling neighbouring pyramidal cells together with the current pulse entrained interneuron. Fortunately, based on the presence of dendritic spines and by tracing the neurobiotin-labelled dendritic and axonal processes back to their respective cell bodies, the identity of each neuron could be determined. In strata radiatum and lacunosum moleculare I rarely observed action potential discharges (Figure 3-3C,D). Most frequently the spike trains resembled those

of pyramidal neurons. Possible explanations include that cell density is much lower in these layers and that the activity of the interneurons is much lower at least during certain behavioural states.

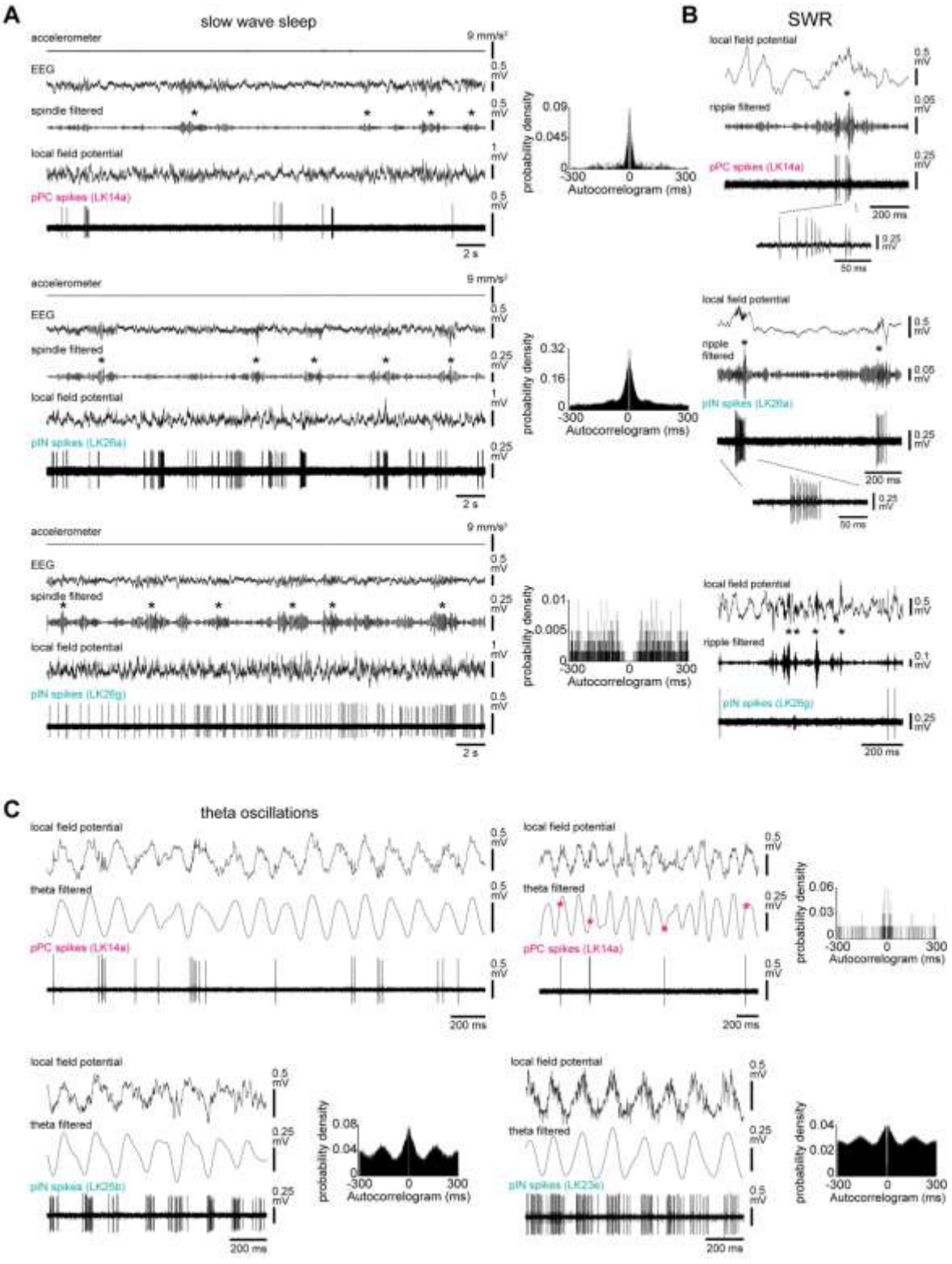
A
slow wave sleep
accelerometer
9 mm/s²
EEG
0.5 mV
spindle filtered
0.5 mV
local field potential
1 mV
pPC spikes (LK14a)
0.5 mV
2 s
probability density
0.09
0.045
0
-300
0
300
Autocorrelogram (ms)
accelerometer
9 mm/s²
EEG
0.5 mV
spindle filtered
0.25 mV
local field potential
1 mV
pIN spikes (LK26a)
0.25 mV
2 s
probability density
0.32
0.16
0
-300
0
300
Autocorrelogram (ms)
accelerometer
9 mm/s²
EEG
0.5 mV
spindle filtered
0.25 mV
local field potential
1 mV
pIN spikes (LK26g)
0.5 mV
2 s
probability density
0.01
0.005
0
-300
0
300
Autocorrelogram (ms)
B
SWR
local field potential
0.5 mV
ripple filtered
0.05 mV
pPC spikes (LK14a)
0.25 mV
200 ms
50 ms
local field potential
0.5 mV
ripple filtered
0.05 mV
pIN spikes (LK26a)
0.25 mV
200 ms
50 ms
local field potential
0.5 mV
ripple filtered
0.1 mV
pIN spikes (LK26g)
0.25 mV
200 ms
C
theta oscillations
local field potential
0.5 mV
theta filtered
0.5 mV
pPC spikes (LK14a)
0.5 mV
200 ms
local field potential
0.5 mV
theta filtered
0.25 mV
pPC spikes (LK14a)
0.5 mV
200 ms
probability density
0.06
0.03
0
-300
0
300
Autocorrelogram (ms)
local field potential
0.5 mV
theta filtered
0.25 mV
pIN spikes (LK26b)
0.25 mV
200 ms
probability density
0.08
0.04
0
-300
0
300
Autocorrelogram (ms)
local field potential
0.5 mV
theta filtered
0.25 mV
pIN spikes (LK23e)
0.5 mV
200 ms
probability density
0.04
0.02
0
-300
0
300
Autocorrelogram (ms)

Figure 3-1 Discharge patterns of putative pyramidal cells and GABAergic interneurons in the hippocampal CA1 area of freely moving rats.

A. Cell-type specific firing activity during slow wave sleep marked by the occurrence of spindle oscillations (9-14 Hz, asterisk) in the EEG. Note sparse spiking of the pyramidal cell (top, LK14a), firing at lower rates than the two putative GABAergic interneurons (middle and bottom). A putative trilaminar cell (LK26a) discharges high frequency bursts, occasionally. In contrast, the cell recorded in stratum pyramidale (LK26g) fires action potentials at regular intervals. Note the differences in the autocorrelograms of spike-timing (right). **B.** Cell-type specific firing during sharp wave associated ripple oscillations (SWR, 130-230 Hz, asterisk). During certain SWRs, the pyramidal cell (top) fires complex-spikes (top inset). SWR-related bursts (middle inset) of 10-15 action potentials are fired by trilaminar cells with instantaneous rates >200 Hz, like those recorded for LK26a (middle). Some GABAergic interneurons do not fire during SWR events (bottom). **C.** Cell-type specific activity patterns during theta oscillations (5-12 Hz). Although pyramidal cells can fire at any phase, their action potentials are triggered preferentially at the trough of theta cycles (top). Note a sequence of theta cycles during which the spikes of the pyramidal cell (LK14a) phase precess (asterisks). The rat was walking during this period. Two putative GABAergic interneurons fired theta-rhythmically (bottom) with different rates and coupled to the trough (LK25b) or after the peak (LK23e) of the oscillatory theta cycles, respectively. The high firing rate and preferential spiking just after the peak of theta is characteristic for axo-axonic cells. Note the differences in the autocorrelograms of spike-timing. pPC, putative pyramidal cell; pIN, putative GABAergic interneuron; SWRs, sharp wave associated ripples.

GABAergic interneurons

	Cell identifier	Cell type identified / hypothesised	Layer	Firing rate (Hz)
Labelled	LK01ab	O-LM	SO	13.5
	LK06ah	O-LM	SO	11.1
	LK08c	PV+ basket	SP	10.1
	LK12o	"unconventional"	SP/SR	3.6
	LK13k	O-LM	SO	18.8
	LK20p	bistratified	SP	27.0
	LK24g	axo-axonic	SO/SP	11.2
	LK27d	bistratified	SP	25.1
Non-labelled	LK01d	projection	SO	50.0
	LK04i	ivy	SP	6.5
	LK06o	bistratified	SP	43.6
	LK06r	unknown	SP	4.1
	LK06aa	perforant path associated	SR/SLM	4.2
	LK07e	unknown	SP/SR	3.9
	LK07f	unknown	SO/SP	20.7
	LK10c	unknown	SO	18.4
	LK10l	unknown	SR	14.0
	LK10p	CCK+ dendrite targeting	SR/SLM	3.7
	LK10x	O-LM/double projection	SO	17.9
	LK12g	unknown	SO	18.1
	LK13f	O-LM	SO	16.1
	LK13j	unknown	SO	7.9
	LK13l	unknown	SO	29.9
	LK14d	unknown	SO	4.9
	LK14e	PV+ basket	SO/SP	25.7
	LK14j	CCK+/ivy	SR	2.9
	LK14k	trilaminar	SO	2.5
	LK14l	trilaminar	SO	5.3
	LK14p	trilaminar	SO/SP	5.5
	LK14r	unknown	SO/SP	3.5
	LK14s	unknown	SP	7.6
	LK14t	CCK+/ivy	SP	4.7
	LK14u	CCK+/ivy	SP	5.5
	LK18d	unknown	SO/SP	5.8
	LK18h	O-LM	SO	12.0
	LK20g	bistratified	SO/SP	19.1
	LK20l	PV+ basket	SO/SP	33.5
	LK22b	unknown	SO	24.4
	LK23d	PV+ basket	SP	15.3
	LK23e	axo-axonic	SP	35.0
	LK24d	O-LM	SP	10.8
	LK25b	projection	SO	33.6
	LK25g	PV+ basket	SP	34.5
	LK25h	unknown	SP	10.5
	LK25n	PV+ basket/bistratified	SP	24.9
	LK26a	trilaminar	SO	9.3
	LK26b	projection	SO	9.1
	LK26g	CCK+/ivy	SP/SR	1.8
	LK27a	PV+ basket	SP	13.6
	LK27c	projection	SO	6.9

Pyramidal cells

	Cell identifier	Firing rate (Hz)
Labelled	LK01v	0.4
	LK08d	2.9
	LK14v	1.8
	LK18m	1.0
Non-labelled	LK01e	2.1
	LK01h	0.7
	LK01k	9.7
	LK01u	0.2
	LK01aa	0.1
	LK04g	5.5
	LK06m	3.4
	LK06ad	0.8
	LK06ae	6.2
	LK07d	0.2
	LK10e	0.2
	LK10k	0.1
	LK10n	3.6
	LK10o	0.6
	LK12m	0.1
	LK13c	1.3
	LK13e	5.1
	LK13g	6.5
	LK13h	6.6
	LK14a	0.5
	LK14b	3.1
	LK14c	1.7
	LK14g	2.7
	LK14i	0.2
	LK14o	2.9
	LK16a	4.3
	LK18b	0.4
	LK18e	0.2
	LK18i	0.7
	LK18k	0.4
	LK18l	1.1
	LK20h	1.9
	LK20n	3.3
	LK25c	0.6
	LK26c	0.5

Table 3.1 Experimental summary.

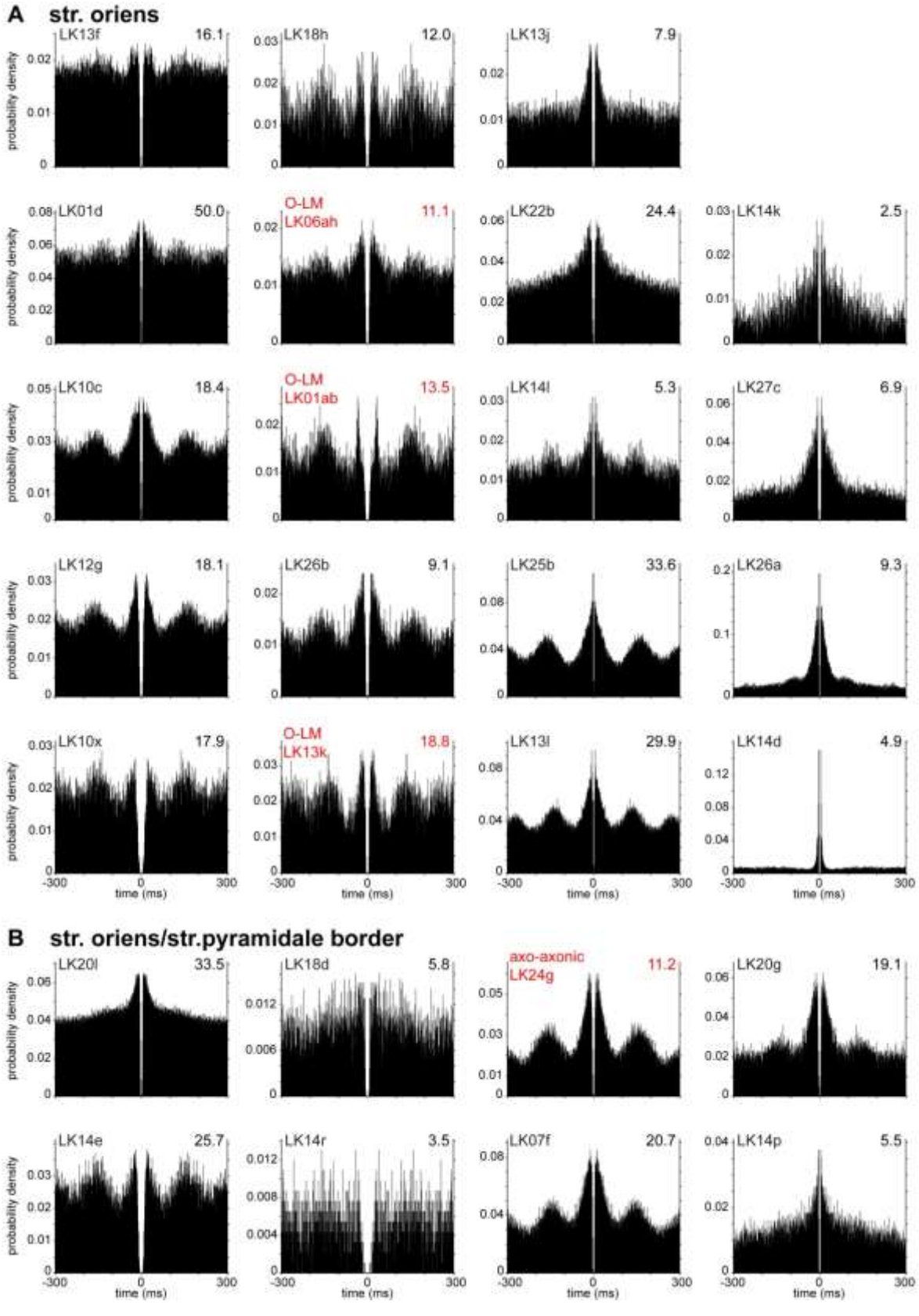
A str. oriens
LK13f 16.1
LK18h 12.0
LK13j 7.9
LK01d 50.0
O-LM
LK06ah 11.1
LK22b 24.4
LK14k 2.5
LK10c 18.4
O-LM
LK01ab 13.5
LK14l 5.3
LK27c 6.9
LK12g 18.1
LK26b 9.1
LK25b 33.6
LK26a 9.3
LK10x 17.9
O-LM
LK13k 18.8
LK13l 29.9
LK14d 4.9
probability density
time (ms)
B str. oriens/str.pyramidale border
LK20l 33.5
LK18d 5.8
axo-axonic
LK24g 11.2
LK20g 19.1
LK14e 25.7
LK14r 3.5
LK07f 20.7
LK14p 5.5

Figure 3-2 Action potential autocorrelograms of identified and putative GABAergic cells recorded in the hippocampal CA1 area of freely moving rats.

A,B. Interneurons recorded in stratum oriens (A) or at the border of strata oriens and pyramidale (B) show varying mean firing rates and their autocorrelation patterns are different. The firing of some cells is rhythmic (e.g. LK10c, LK13l, LK07f, etc.) others fire more sparsely (e.g. LK26a, LK27c, etc.). Identified O-LM and axo-axonic cells are labelled in red. Note that mean firing rates are shown in Hz at the top right corner of autocorrelation plots. Time axis is limited to 300 ms, bin width was set to 1 ms.

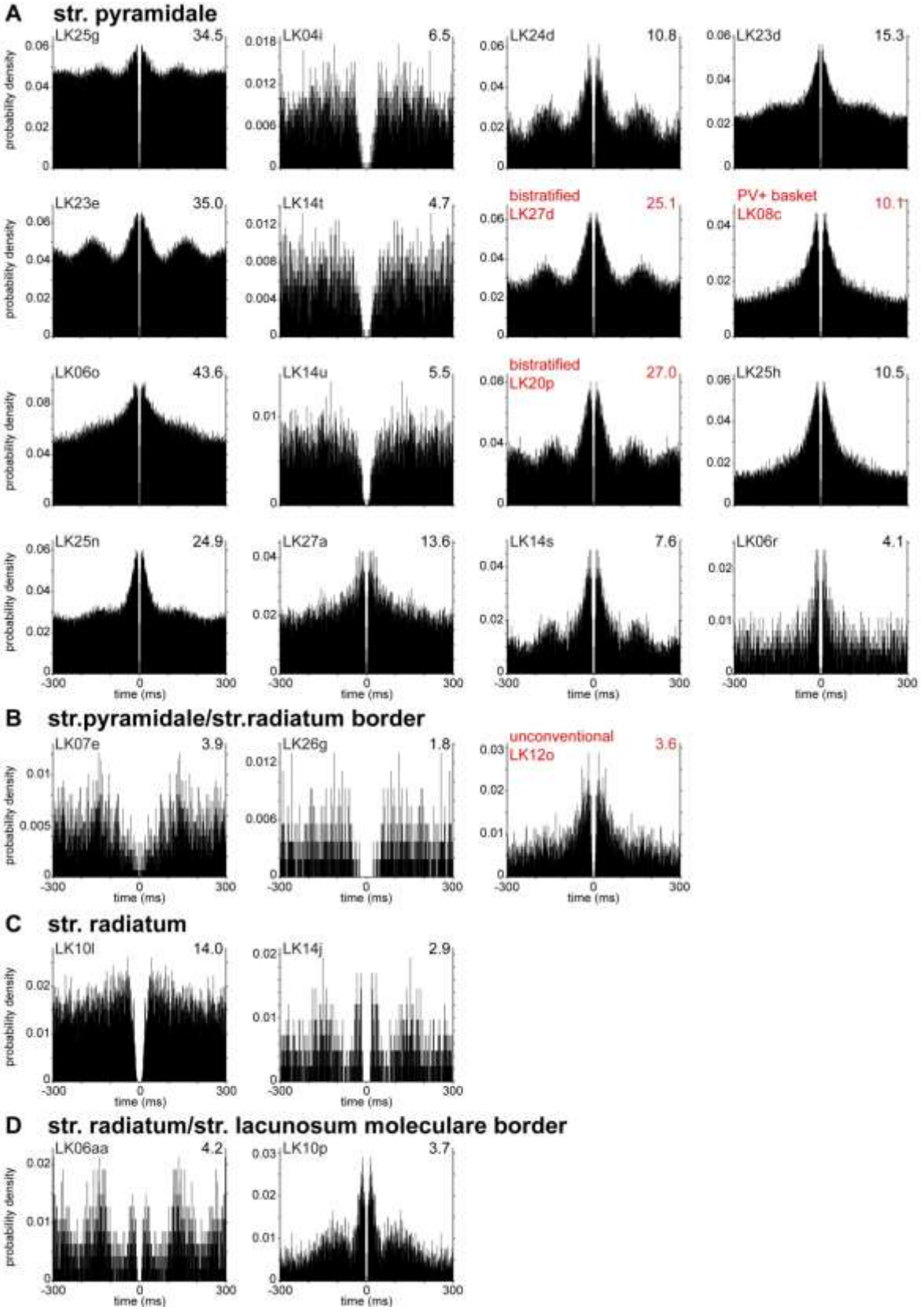
A str. pyramidale
LK25g 34.5
LK04i 6.5
LK24d 10.8
LK23d 15.3
LK23e 35.0
LK14t 4.7
bistratified LK27d 25.1
PV+ basket LK08c 10.1
LK06o 43.6
LK14u 5.5
bistratified LK20p 27.0
LK25h 10.5
LK25n 24.9
LK27a 13.6
LK14s 7.6
LK06r 4.1
B str.pyramidale/str.radiatum border
LK07e 3.9
LK26g 1.8
unconventional LK12o 3.6
C str. radiatum
LK10l 14.0
LK14j 2.9
D str. radiatum/str. lacunosum moleculare border
LK06aa 4.2
LK10p 3.7
probability density
time (ms)

Figure 3-3 Action potential autocorrelograms of identified and putative GABAergic cells recorded in the hippocampal CA1 area of freely moving rats.

Interneurons recorded between stratum pyramidale and the border of strata radiatum and lacunosum moleculare **(A-D)** show varying mean firing rates and their autocorrelation patterns are different. The firing of some cells is rhythmic (e.g. LK24d, LK14s, LK06aa etc.) others fire more sparsely (e.g. LK25h, LK10p, etc.). Identified bistratified and basket cells and an "unconventional interneuron" are labelled in red. Note that mean firing rates are shown in Hz at the top right corner of autocorrelation plots. Time axis is limited to 300 ms, bin width was set to 1 ms.

3.3 Discussion

I demonstrate behavioural and network oscillatory state dependent transitions in the activity patterns of different types of hippocampal neuron in freely moving rats. Much of our current knowledge including my explorations is built on previous work performed under anaesthetised conditions which outlined the spatio-temporal principles of hippocampal network operations (Klausberger and Somogyi, 2008; Somogyi et al., 2014). In chapters 4 and 5, I will specify what rules I managed to confirm in the drug-free brain and what are the changes induced by urethane anaesthesia.

The sparse firing of pyramidal cells is a result of their GABA-mediated inhibition as suggested by the cell-type specific spike trains. GABAergic synapses of distinct types of interneuron are associated with different postsynaptic compartments innervating overall the entire membrane surface of pyramidal cells (Bezaire and Soltesz, 2013; Somogyi, 2010). The site of action of GABA oscillates leading to a cyclic redistribution of inhibition from the axon initial segment via the cell body to distal dendritic tuft and back during rhythmic network events (Somogyi et al., 2014). This temporal redistribution of inhibition regulates the output of pyramidal cells, which, at the population level, formulates the code being transferred to downstream regions completing the mnemonic processing. Oscillatory network states of different frequencies (e.g., theta-, gamma- and ripple oscillations) create the optimal temporal windows for the encoding, retrieval and consolidation of information during the separate stages of learning, respectively (Buzsáki, 1989). What the specific roles of different types of interneuron in this refined output tuning is remains to be discussed thoroughly in the following chapters.

Significance

The outcome of my challenging experiments is a handful of behaviour-related spike trains of single identified neurons in the hippocampal CA1 area of freely moving rats. Complemented by another handful of such recordings accomplished by colleagues in the laboratory, this very original data set establishes a unique interface towards the understanding of the roles of distinct GABAergic interneuron types in the regulation of pyramidal cell firing during mnemonic processing. By calculating autocorrelograms and quantifying behaviour and network-state-dependent firing patterns, theta modulated spike-timing and SWR-related responses, I determined cell- type specific stereotypes of juxtacellularly labelled and identified single cells in the drug-free brain. Matching these parameters with those of isolated units recorded using tetrodes, allows the "quasi-identification" of the latter as cell types. It is now possible to make novel observations about the interactions between pyramidal cells and the "quasi-identified" GABAergic interneurons recorded during memory related task performance lasting for several days up to weeks.

During learning, old information encoded by one group of pyramidal cell assemblies is gradually overwritten by the new representation provided by other groups of pyramidal cells. During this change, interneuron associations get reconfigured as well (Dupret et al., 2013). Their monosynaptic connections from pyramidal cells representing the new association get strengthened while those associated with the old get lost. Which types of interneuron are involved in the reconfiguration of circuit dynamics during learning? Are all pyramidal-cell-interneuron pairs affected to the same extent? Do axo-axonic, PV+ basket or bistratified cells phase precess? What are the changes required for such action? Are certain types of interneuron more important during slow wave sleep/consolidation and others

during exploration/encoding or retrieval? There is now an opportunity to investigate such and similar stimulating questions.

It was exciting to find that novel axonal patterns that we discover are associated with novel network-related spike timing. Unpublished single examples of recorded cells which do not fit any know types (LK12o in Chapter 4, ZsB49b, recorded by Dr Zs. Borhegyi in Vienna) illustrate the need for continued investigation and analysis of GABAergic cell types.

Moreover, the firing patterns of the majority of the known GABAergic cell types in the hippocampus are still unknown in the drug free brain. Regarding str. oriens, in addition to O-LM cells and horizontal bistratified cells many other GABAergic cell types have been reported based on molecular expression profiles (Ferraguti et al., 2005; Ganter et al., 2004; Maccaferri et al., 2000; Somogyi et al., 2003). Their recording during behaviour and labelling will allow the recognition of neurons of the same type using cluster analyses and pattern matching algorithms across the existing large data sets provided by tetrode and/or silicone probe recordings.

4 Perisomatic-targeting and axon initial segment-innervating GABAergic interneurons

4.1 Introduction

The activity of hippocampal glutamatergic principal cells is partly regulated by the effects of GABA released onto their somatic and proximal dendritic membranes as well as their axon initial segments from distinct sources. GABA is delivered selectively to these pyramidal cell compartments by a diverse population of GABAergic interneurons (Somogyi, 2010). In the CA1 area, at least five distinct such cell types have been reported identified by their target-domain specific axonal distribution patterns and their unique molecular expression profiles: three types of basket cell innervating pyramidal cell somata and proximal dendrites (Buhl et al., 1994a; Freund and Katona, 2007; Gulyás et al., 1993; Halasy et al., 1996; Klausberger et al., 2003; Klausberger et al., 2005 ; Takács et al., 2014); axo-axonic cells, initially identified as chandelier cells in the neocortex (Somogyi, 1977; Szentagothai and Arbib, 1974), targeting exclusively the axon initial segment of pyramidal cells (Buhl et al., 1994b; Klausberger et al., 2003; Li et al., 1992; Somogyi et al., 1985; Somogyi et al., 1983; Takács et al., 2014) and trilaminar neurons forming synapses, beside interneuron dendrites, with cell bodies and dendrites of principal neurons in CA1 and subiculum (Ferraguti et al., 2005; Jinno et al., 2007; Sik et al., 1995). Basket cells, named after their terminals wrapping around the somata of pyramidal cells (Lorente De No, 1934; Ramon y Cajal, 1893), were

differentiated into two non-overlapping populations (Armstrong and Soltesz, 2012; Freund and Katona, 2007; Klausberger et al., 2005) based on their immunopositivity for either the calcium binding protein parvalbumin (PV) (Katsumaru et al., 1988b; Kosaka et al., 1987) or the peptide cholecystokinin (CCK) jointly with the cannabinoid receptor type 1 (CB1) (Harris et al., 1985; Nunzi et al., 1985). The latter population was further subdivided into two types: one expressing the vesicular glutamate transporter type 3 and the other expressing the neuropeptide vasoactive intestinal polypepetide (VIP) but immunonegative for the vesicular transporter (Acsády et al., 1996a; Klausberger et al., 2005; Kosaka et al., 1985).

The anatomically established rich diversity of hippocampal GABAergic cell types likely underlies a functional polychotomy. It is hypothesised that distinct GABAergic cell types have evolved to provide specialised spatio-temporal control over information processing within cortical networks (Klausberger and Somogyi, 2008; Soltesz, 2005; Somogyi, 2010; Somogyi et al., 2014). Indeed, evidence from developmental studies supports this idea, showing that, similar to the cortex (Butt et al., 2005; Miyoshi et al., 2007; Butt et al., 2008), hippocampal interneurons immunopositive for PV, including axo-axonic and one type of basket cell arise from the medial ganglionic eminence (MGE) and show a fast spiking phenotype, whereas their CCK-expressing counterparts and trilaminar neurons originate from the caudal ganglionic eminence (CGE) and exhibit regular spiking activity (Butt et al., 2005; Butt et al., 2008; Miyoshi et al., 2007; Tricoire et al., 2011). These differences in spike-timing, dependent on intrinsic cellular properties and input synaptic organisation, correlate with the differential spatial and temporal origin of the interneuron precursors and are determined by cell fate regulating genetic programs within each lineage together with local environmental factors (Fishell, 2007).

Assuming that firing patterns are predictors of GABA release, fast- and regular-spiking GABAergic interneurons were suggested to have distinct effects on the postsynaptic neurons. GABA release by PV+ basket and axo-axonic cells onto the cell body and axon initial segment of pyramidal cells, respectively, is thought to have the strongest control over the temporal precision of the output and is well suited to generate oscillatory activity in the network. In contrast, regular firing interneurons act on a longer time scale which allows temporally distant influences to synergistically shape the behavioural-dependent network activity (Armstrong and Soltesz, 2012; Freund and Katona, 2007; Glickfeld and Scanziani, 2006; Klausberger and Somogyi, 2008; Somogyi et al., 2014). Indeed CCK+ cells are under multiple neuromodulatory influences (e.g., serotonergic, cholinergic, etc.) from subcortical derived inputs that carry emotional and motivational information (Férézou et al., 2002; Morales and Bloom, 1997; Porter et al., 1999). Parvalbumin-expressing basket and axo-axonic cells receive overlapping glutamatergic inputs but they innervate distinct domains of pyramidal cells. This well-differentiated synaptic output organisation suggests that interneurons have specialised roles in the modulation of information flow and in the coordination of network events. Specifically, basket cells and axo-axonic cells are ideally placed to synchronise pyramidal cell firing. Do distinct cell types have specific roles in shaping different network activities *in vivo* and, if so, what are the mechanisms of such regulation? In order to gain insights into the processes of hippocampal information transfer it is necessary to define the temporal contribution of distinct cell types to behaviourally relevant network states.

The postsynaptic response properties and somatic action potential firing of basket cells and axo-axonic cells has been investigated *in vitro* (Buhl et al., 1994a; Buhl et al., 1994b; Buhl et al., 1996; Halasy et al., 1996). Independent of the targeted

subcellular domain, GABA was reported to hyperpolarise the entire surface of pyramidal cells (Glickfeld et al., 2009) contrasting previous findings about its depolarising effect on the axon initial segment (Szabadics et al., 2006). In the CA1 area, Cobb et. al (1995) showed that due to $GABA_A$ receptor-mediated perisomatic hyperpolarisation, PV+ basket and axo-axonic cells entrain pyramidal cells to sub- and suprathreshold theta frequency oscillations *in vitro* (4-7 Hz) and synchronise their output. *In vivo*, intra- and extracellular electrophysiological experiments in anaesthetised rodents revealed variable firing patterns of recorded single cells in the hippocampal CA1. Under urethane anaesthesia, during theta oscillations (4-8 Hz) PV+ basket and axo-axonic cells fired preferentially either along the descending phase or around the peak of the oscillatory cycles, respectively. During ripple frequency oscillations (120-200 Hz), axo-axonic cells were silent in marked contrast to PV+ basket cells which discharged spikes at high frequencies (Klausberger et al., 2003). Basket cells expressing CCK, complementing their PV+ partners, fired action potentials on the ascending phases of theta cycles and their activity during ripples was variable, being activated during some and becoming silent during other events (Klausberger et al., 2005). Trilaminar cells fired only occasionally during theta epochs spiking in bursts of action potentials preferentially at the trough of the oscillatory cycles. During SWRs, these neurons increased strongly their firing rates (Ferraguti et al., 2005). With the exception of the latter, the cell types were also identified and recorded in the CA3 area, where some neurons had activity patterns shifted in time compared to their CA1 counterparts (Lasztoczi et al., 2011; Papp et al., 2013; Tukker et al., 2013; Viney et al., 2013). Furthermore, the *in vivo* firing dynamics of unidentified interneurons were shown to be network state-dependent as evidenced from large scale multiunit recordings. Theta oscillations during movement or large-amplitude irregular activity

during sleep influenced the spike-timing of the neurons (Buzsaki, 2006; Csicsvari et al., 2000; Ego-Stengel and Wilson, 2007; O'Keefe and Dostrovsky, 1971; O'Keefe and Nadel, 1978; Ranck, 1973; Vanderwolf, 1969). Unidentified interneurons recorded in the pyramidal layer, some of which were likely basket or axo-axonic cells, either increased or decreased their firing rates during SWRs (Csicsvari et al., 1999b; Csicsvari et al., 2000). These studies however could not address the *in vivo* activity of identified basket cells, axo-axonic cells or trilaminar neurons during behaviour, which is largely unknown in the drug-free brain. Moreover, there are several types of anatomically identified GABAergic interneuron (e.g., interneurons selectively innervating only interneurons) the activity of which hitherto has not been recorded *in vivo.* Finally, the existence of yet unidentified neuron types cannot be excluded.

What are the *in vivo* temporal dynamics of the perisomatic targeting hippocampal neurons during behaviour? Are there differences in the behavioural and network state related spike-timing of GABAergic interneurons that would suggest selective spatio-temporal mechanisms of pyramidal cell output regulation? Does the behavioural and network state dependent action potential firing of the interneurons correlate with the differences in their axonal distribution pattern? How do the activity patterns determine the involvement of pyramidal cell assemblies in encoding and/or retrieval of episodic memories?

By performing *in vivo* electrophysiological recordings and juxtacellular neurobiotin-labelling of single GABAergic cells in freely moving rats (Lapray et al., 2012; Pinault, 1996), I set out to test whether distinct identified cell types innervating either the cell body or the dendrites or the axon initial segment of pyramidal cells would release GABA and act on their postsynaptic targets with different temporal dynamics. After identifying one PV+ basket cell, one axo-axonic cell and one

"unconventional interneuron", I studied their behavioural- and oscillatory network-state-related spike-timing, together with cells of the same type recorded by others in the laboratory. I also developed new analysis techniques, as required.

4.2 Spike-timing of PV-expressing basket and axo-axonic cells and an "unconventional interneuron" in freely moving rats

From a population of fifty putative non-pyramidal cells (Table 3.1) recorded using a glass electrode in the hippocampus of freely moving rats I have labelled and identified three as perisomatic-targeting or axon initial segment-innervating interneurons. Based on the axonal arborisations and molecular expression profiles these were one PV-expressing (PV+) basket cell (LK08c), one axo-axonic cell (LK24g) and one "unconventional interneuron" (LK12o; Table 3.1, Table 4.1). Two cells were recorded and labelled in the CA1 area (LK08c and LK12o) and one in the CA2 area (LK24g) over a region of 1.1 x 0.6 mm along the rostro-caudal and medio-lateral axes of the hippocampus (Figure 4-1). In addition, I have also analysed the SWR related firing during sleep and wakefulness of four PV+ basket cells (Lapray et al., 2012) and another axo-axonic cell (Viney et al., 2013) recorded by colleagues in the group in order to gain insight into the variability of firing within the same cell type. In this section I report the cell-type specific firing patterns of these neurons during different behavioural and oscillatory network states.

4.2.1 Anatomical analysis and identification of cell types

From one cell, I recovered only the axon, which was branching in and around the pyramidal layer (Figure 4-2A). Because of weak labelling the complete axonal arbour could not be studied, but I examined all visible axon collaterals in consecutive sections by light microscopy. Large PV-expressing (Figure 4-2B) boutons of the axon

were in apparent contact with putative pyramidal cell somata and proximal dendrites, which led me to identify the neuron as a PV+ basket cell (LK08c, Figure 4-1, Figure 4-2 and Table 4.1).

Another GABAergic interneuron (LK24g, Figure 4-1, Figure 4-3 and Table 4.1) was labelled in the pyramidal layer with radially oriented dendritic tree and axon at the border between strata pyramidale and oriens. Using the distribution of CB immunoreactivity I determined that the labelled dendrites overlapped with CB-immunopositive pyramidal cells in the CA2 area outside the region of immunopositive mossy fibres in stratum lucidum and immunonegative pyramidal cells of area CA3 (Figure 4-3C). The cell body was immunonegative for the transcription factor Satb1 (Figure 4-3A) and the dendrites were immunopositive for PV and lacked CB immunoreactivity (Figure 4-3B). Due to weak labelling, only short segments of axon could be visualised using HRP reaction to reveal neurobiotin. To investigate the postsynaptic targets and to assess cell type identity the HRP-DAB reacted axon was re-embedded in resin and processed for electron microscopic analysis. I found axon terminals forming type II synapses (Figure 4-3D) selectively with pyramidal cell axon initial segments (AIS, n=14/14 boutons), thus, I identified the cell as an axo-axonic interneuron.

The soma location and the axo-dendritic distribution of the third labelled GABAergic cell (LK12o, Figure 4-1, Figure 4-4 and Table 4.1) was similar to those of the previous interneurons and this cell was located in the CA1 area. The neuron had atypical thin dendrites ending in elaborate tufts extending over only two 70 μm-thick sections on each side of the soma. The axon collaterals running in parallel with the pyramidal layer had sparse and very small boutons concentrated on the layer (Figure 4-3A). These features were consistent with those of a basket cell, therefore, to test this

hypothesis, electron microscopic target identification was performed (Figure 4-3G,H). Together with two colleagues we have sampled two distinct axonal segments. Indeed, the majority of synapses were found in the pyramidal layer, however, the postsynaptic profiles were either AISs (n=8/26 synapses), or dendrites (n=13/26 synapses), or somata (n=4/26) or one spine (Figure 4-4I). When the identity of the postsynaptic target neuron could be determined (n=15/26 synapses) we have found the majority of boutons making synapses with pyramidal cells (n=13/15 synapses) and much fewer with interneurons (n=2/15 synapses), the rest of targets being classified as unidentified neurons (n=11/26 synapses). Based on these findings I rejected the initial hypothesis and concluded that the interneuron is not a basket cell. To further question the identity of this cell I investigated its molecular expression profile by testing it for the expression of calcium binding proteins, neuropeptides and transcription factors that are known to differentiate between cell types (Table 4.1). After multiple series of immunoreactions, most performed on the cell body, I have only found one positive molecular marker chicken ovalbumin upstream promoter type II (COUP-TFII, Figure 4-4B) for which a weak signal could be detected in the nucleus. Interestingly, the cell body and proximal dendrites were densely surrounded by strongly CR-expressing boutons (Figure 4-4C) however the neuron was immunonegative for CR (Figure 4-4C), PV (Figure 4-4E), VIP (Figure 4-4D) and mGluR1a (Figure 4-4F). I am unaware of a known GABAergic cell type in the hippocampal CA1 area that would be compatible with the features of LK12o therefore I will refer to it as the "unconventional interneuron".

4.2.2 Behaviour-related activity patterns of GABAergic cells

Next I studied the firing dynamics of the perisomatic-targeting and AIS-innervating interneurons during sleep, movement and quiet wakefulness. I first

segmented the recorded action potential time series according to behavioural states to compare the three cell types (Figure 4-2C, Figure 4-3E, Figure 4-4J and Table 4.2, Table 4.3). This needed the extraction of behaviourally relevant time windows based on motion tracking and quantitative analysis (Lapray et al., 2012) of hippocampal and cortical local field potential (LFP) measurements.

Firing rates and spiking patterns

PV+ basket (n=5) and axo-axonic cells (n=2) (Lapray et al., 2012; Viney et al., 2013), but not the "unconventional interneuron", fired with behaviour-dependent rates (Figure 4-5A and Table 4.2). These differences (Lapray et al., 2012; Viney et al., 2013) were confirmed by the ISI distributions and autocorrelograms (Figure 4-5B-D and Table 4.3).

During movement, the firing rate of PV+ basket and axo-axonic cells was higher (by 126%, LK08c; by 242%, LK24g) than that of the "unconventional interneuron" (Table 4.2). Indeed, the largest proportion of ISIs of both former corresponded to the gamma frequency range of firing (5-12 Hz, 18.3% and 14.1%; 12-30 Hz, 29.8% and 10.9%; 30-100 Hz, 42.4% and 46.3%; 100-250 Hz, 3.9% and 23%, respectively), in contrast, the "unconventional interneuron" fired most frequently with low instantaneous frequency (IF) in the theta and beta ranges (5-12 Hz, 46.5%; 12-30 Hz, 30.3%; 30-100 Hz, 10.7%; 100-250 Hz, 0.0%). Note that the axo-axonic cell, but not the PV+ basket cell, often fired with ISIs shorter than 10 ms (IF>100 Hz).

During slow wave sleep, PV+ basket cells increased further their firing rate (by 27%, LK08c) whereas axo-axonic cells and the "unconventional interneuron" became less active (by 52%, LK24g; by 22%, LK12o; Table 4.2). The spike rate distribution of the axo-axonic cell remained comparable to that during movement, whereas, the PV+

basket cell fired more frequently in the fast frequency range (5-12 Hz, 8.4%; 12-30 Hz, 14.6%; 30-100 Hz, 43.1%; 100-250 Hz, 23.5%) and the "unconventional interneuron" switched to trigger action potentials more frequently in the gamma range (5-12 Hz, 13.3%; 12-30 Hz, 17.2%; 30-100 Hz, 32.7%; 100-250 Hz, 7.7%). All three cell types dropped in their firing rates during quiet wakefulness as compared to movement (by 11%, LK08c; by 58%, LK24g and by 44%, LK12o; Table 4.2). This was demonstrated by a proportionate rightward shift in the ISI distribution peaks for PV+ basket and axo-axonic cells to the gamma frequency range (5-12 Hz, 13.5% and 12.3%; 12-30 Hz, 16.5% and 8.3%; 30-100 Hz, 35.6% and 37.6%; 100-250 Hz, 14.6% and 24.8%, respectively) and for the "unconventional interneuron" to the theta range (5-12 Hz, 39.5%; 12-30 Hz, 13.6%; 30-100 Hz, 7.4%; 100-250 Hz, 0.7%).

4.2.3 Firing patterns during oscillatory network states

Similarly to segregating the spike trains according to behavioural-specific time windows (Lapray et al., 2012), I detected for each labelled interneuron theta oscillatory epochs (5-12 Hz, Figure 4-2D, Figure 4-3F, Figure 4-4K), SWRs (130-230Hz, Fig. Figure 4-2E, Figure 4-3G, Fig. Figure 4-4L) and LOSC periods from the hippocampal LFP. In order to test whether the spike-timing of different GABAergic interneurons is influenced by such rhythmic network states, I have calculated and compared the mean firing rates and ISI distributions of the labelled neurons.

Firing rates and spiking patterns

The firing rates, ISI distributions and autocorrelograms of all three cell types (Figure 4-6A,D-F and Table 4.2, Table 4.3) were network oscillatory-state-dependent. During theta oscillations PV+ basket cells (n=5) and axo-axonic cells (n=2) fired at higher rates (Lapray et al., 2012; Viney et al., 2013) than the "unconventional

interneuron" (by 455%, LK08c and by 437%, LK24g; Table 4.2). Indeed, the largest proportion of ISIs of both former corresponded to the gamma frequency range of firing (5-12 Hz, 12.7% and 14.2%; 12-30 Hz, 31.6% and 11.2%; 30-100 Hz, 48.3% and 47.7%; 100-250 Hz, 5.5% and 23.0%, respectively). Note that the axo-axonic cell, but not the PV+ basket cell, often fired with ISIs shorter than 10 ms (IF>100 Hz). In contrast, the "unconventional interneuron" fired most frequently with low instantaneous frequency (IF) in the theta and beta ranges (5-12 Hz, 50.5%; 12-30 Hz, 19.2%; 30-100 Hz, 5.3%; 100-250 Hz, 0.0%). During SWRs, PV+ basket cells and the "unconventional interneuron" strongly increased their firing rate (by 286%, LK08c and by 461%, LK12o), in contrast to axo-axonic cells which very rarely fired, even then only one spike per event (drop by 97%, Table 4.2). The PV+ basket cell mostly discharged with ISIs of 4 to 10 ms (5-12 Hz, 0.0%; 12-30 Hz, 6.1%; 30-100 Hz, 34.3%; 100-250 Hz, 57.7%), whereas the largest proportion of the ISIs measured for the "unconventional interneuron" corresponded to the gamma frequency range (5-12 Hz, 0.0%; 12-30 Hz, 7.7%; 30-100 Hz, 59.7%; 100-250 Hz, 32.2%). During LOSC, the firing rates of the three cell types were significantly lower (by 91%, LK08c; by 56%, LK24g and by 45%, LK12o) as compared to theta epochs (Table 4.2) as confirmed by proportionate right-shifted ISI distributions for PV+ basket and axo-axonic cells to the gamma frequency range (5-12 Hz, 18.3% and 12.5%; 12-30 Hz, 15.9% and 16.9%; 30-100 Hz, 25.3% and 47.6%; 100-250 Hz, 0.0% and 7.5%, respectively) and for the "unconventional interneuron" to the theta range (5-12 Hz, 36.4%; 12-30 Hz, 11.8%; 30-100 Hz, 10.9%; 100-250 Hz, 0.0%).

Spike-timing during theta and ripple oscillations

The theta phase of interneuron firing informs about the time of GABA release relative to the activity of extrinsic glutamatergic inputs. Therefore, I have tested the preferential discharge of the three distinct interneuron types relative to the phase of the theta oscillatory cycles (Figure 4-6C and Table 4.2). PV+ basket cells fired preferentially along the descending phase of the pyramidal layer LFP theta cycles (Lapray et al., 2012), with LK08c being very close to the trough (331.9°±67.5°, mean angle ± angular deviation). In contrast, the two axo-axonic cells (Viney et al., 2013) and the "unconventional interneuron" triggered spikes around the peak of the oscillatory cycles (190.6°±58.6° for LK24g; 214.7°±66.3° for LK12o). The axo-axonic cell was most strongly phase coupled to LFP theta compared to the PV+ basket cell and the "unconventional interneuron" (Table 4.2).

During slow wave sleep and quiet wakefulness SWRs emerge in the hippocampal LFP. GABAergic interneuron types have diverse relationships to the occurrence of these events. First I calculated the mean spike count of PV+ basket (n=5) and axo-axonic cells (n=2) and the "unconventional interneuron" during individual SWRs during either sleep or wakefulness (Figure 4-6B and Table 4.2). The mean number of spikes of PV+ basket as well as axo-axonic cells was similar during SWRs recorded during sleep or wakefulness (One-way ANOVA, F=0.025, p=0.877, for *PV+ basket cells*). PV+ basket cells were very active during individual SWRs, unlike axo-axonic cells which very rarely fired. In contrast, the "unconventional interneuron" fired more during sleep-SWRs than during awake-SWRs. Another measure of SWR responses is the firing probability of distinct cells during and around the rhythmic events. The PV+ basket cell fired with higher probability during SWRs (Figure 4-2F) compared to the ± 0.5 s surrounding the peak of SWR events. The axo-axonic cell was

silenced during SWRs (Figure 4-3H) and stayed supressed even after the events. The "unconventional interneuron" gradually started increasing its firing probability around 100 ms before SWRs and fired with higher probability during SWRs (Figure 4-4M). Finally to test if there was a change in the firing rate during SWRs as compared to outside SWR time periods, I have calculated cumulative distribution functions (CDFs) of mean firing rates per measured SWRs and compared these with mean rates per 'surrogate' SWRs. The latter were randomly placed time windows during periods outside SWRs. The firing rate of the PV+ basket cells (n=5) was 4 to 12 times higher (surrogate CDFs, $p<0.05$ during *sleep*; $p<0.05$ during *wakefulness*; LK08c on Figure 4-2G *insets* and Table 4.2) than expected from the activity outside SWRs, hence the cells were considered as activated during SWRs. Axo-axonic cells (n=2) were either silent or strongly inhibited during SWRs (surrogate CDFs, $p<0.0001$ for *sleep* and *wakefulness*; LK24g on Figure 4-3I *insets* and Table 4.2). The "unconventional interneuron", during sleep, increased its firing rate by 2 to 9 fold over the full range of firing frequencies (surrogate CDFs, $p<0.0001$; LK12o on Figure 4-4N and Table 4.2). In contrast, it did not change its rate during awake-SWRs (surrogate CDFs, $p=0.039$; LK12o on Figure 4-4N and Table 4.2).

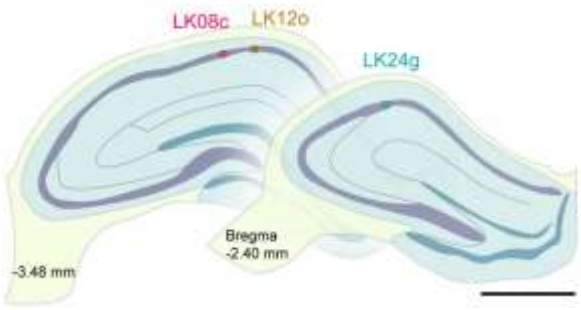

Figure 4-1 Recording and labelling locations of one PV+ basket cell (red, LK08c) and one "unconventional interneuron" (orange, LK12o) in CA1 and one axo-axonic cell (blue, LK24g) in CA2.

Individual cell body locations in stratum pyramidale are shown in two schematic coronal sections from rostral to caudal direction, from left to right of the right hemisphere. Dark shaded areas delineate the pyramidal cell layer and the granule cell layer (blue) in the dentate gyrus. Scale bar, 1 mm.

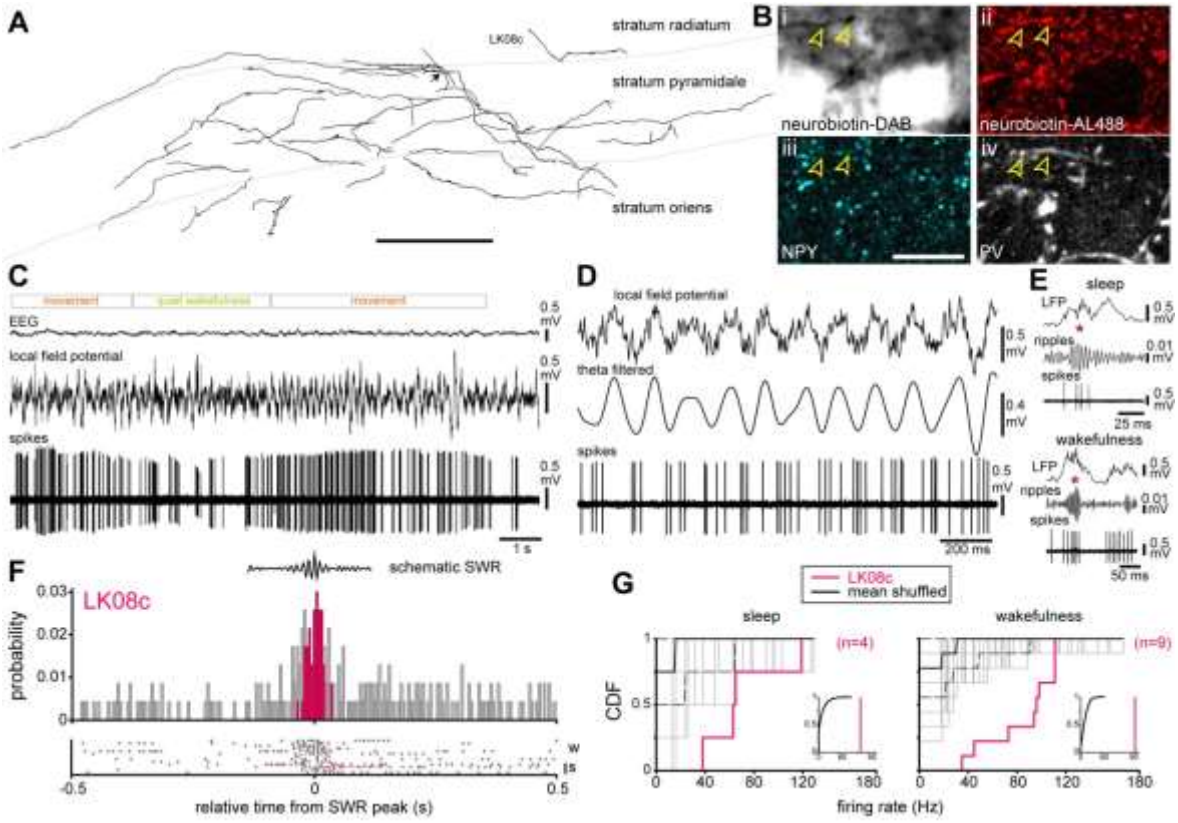

Figure 4-2 Behaviour-related activity patterns of one identified PV+ basket cell.

A. Reconstruction of the axon collaterals in and around stratum pyramidale (three 70-μm-thick sections; axonal origin, black arrow). Note that I have only recovered the axon of this cell. **B.** The axon (arrowheads) was immunopositive for PV and lacked NPY immunoreactivity. (i) HRP reaction using DAB as chromogen. The weak fluorescence signal for neurobiotin was confirmed by DAB visualisation imaged using conventional transmitted light microscopy. (ii-iv) Confocal microscopic images (single optical section, 0.7 μm). Scale bars: A, 100 μm; B, 10 μm. See also Figure 4-1. **C.** Increased firing rate and more rhythmic spike train of the PV+ basket cell associated with transition from quiet wakefulness to movement. **D.** PV+ basket cell activity during theta oscillations (filtered, 5-12 Hz). The cell discharged multiple action potentials on every theta cycle near the trough. **E.** During both rest and slow wave sleep, the cell increased its firing rate during SWRs (asterisks). **F.** Raster plot and average firing probability relative to SWR events (w, wakefulness; s, sleep). The basket cell fired with higher probability during SWRs (red bars in histogram) compared to the ± 0.5 s (grey) surrounding the peak of SWR events. For this cell only fifteen SWRs were recorded. **G.** Firing rates of the PV+ basket cell relative to SWRs during sleep (left) and wakefulness (right). The distribution of measured firing rates per individual SWR are displayed as cumulative distribution functions (CDF). The distribution of PV+ basket cell firing rates (red) was significantly different from the median (black) of the surrogate sets (2-sample Kolmogorov-Smirnov tests, $p<0.001$, for sleep; $p<0.0001$ for wakefulness), and the right shift demonstrates an increase over the full range of firing rates. Surrogate sets of 1000 firing rate-distributions (grey; median, solid black line; 95% confidence intervals, broken lines). *Insets*, comparison of mean SWR-related firing rate (red lines) with the distribution of surrogate mean SWR-related rates (black lines). The PV+ basket cell (red) was always strongly activated during SWRs ($p<0.0001$ for sleep and wakefulness, relative to the surrogate CDF).

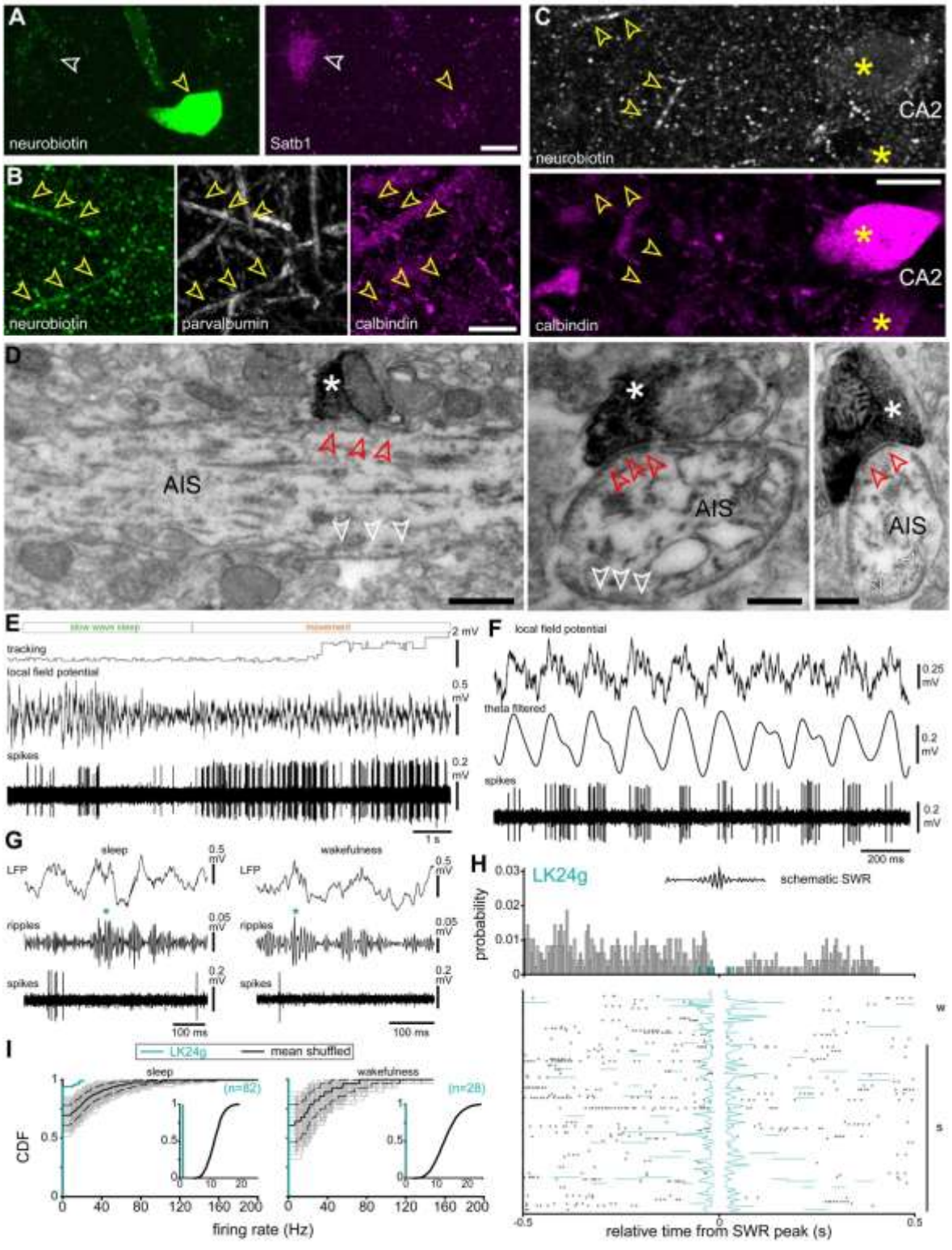
A
neurobiotin
Satb1
C
CA2
neurobiotin
B
neurobiotin
parvalbumin
calbindin
CA2
calbindin
D
AIS
AIS
AIS
E
slow wave sleep
movement
2 mV
tracking
local field potential
0.5 mV
spikes
0.2 mV
1 s
F
local field potential
0.25 mV
theta filtered
0.2 mV
spikes
0.2 mV
200 ms
G
sleep
wakefulness
LFP
0.5 mV
ripples
0.05 mV
spikes
0.2 mV
100 ms
H
LK24g
schematic SWR
probability
0.03
0.02
0.01
0
w
s
-0.5
0
0.5
relative time from SWR peak (s)
I
LK24g
mean shuffled
sleep
wakefulness
(n=82)
(n=28)
CDF
1
0.5
0
0
40
80
120
160
200
firing rate (Hz)

Figure 4-3 Behaviour-related activity patterns of one identified axo-axonic cell.

A. The labelled cell body (yellow arrowhead) was immunonegative for Satb1. Note a neighbouring Satb1-expressing neuron (white arrowhead). Confocal microscopic images (maximum intensity projection, z-stack, height 4.2 μm). **B, C.** Dendrites (arrowheads) were immunopositive for PV and lacked CB expression. Confocal microscopic images (maximum intensity projection, z-stack, height 7.1 μm, *B*; height 3.4 μm, *C*). Dendritic location (arrowheads) overlap with that of CB immunoreactive pyramidal cell dendrites in area CA2. Note that CA2 pyramidal cells (yellow asterisks) express CB, unlike those in CA3. **D.** Electron micrographs of boutons (asterisk) of the labelled axo-axonic cell making type II synapses (red arrowheads) with AISs identified by membrane undercoating (white arrowheads). Scale bars, A-C 10 μm; D *left,* 0.5 μm; *middle, right,* 0.25 μm. **E.** The axo-axonic cell increased its firing rate during movement. The spiking pattern became more regular than during the quiet wakefulness period. **F.** During theta oscillations (filtered, 5-12 Hz) the cell fired rhythmically with up to 10 spikes/cycle. **G.** During SWRs (asterisk), the axo-axonic cell was silent both during sleep and rest. **H.** Raster plot and average firing probability relative to SWR events (w, wakefulness; s, sleep). The cell was silent during SWRs (blue bars in histogram represent 5 action potentials which happened to occur within the detected events) and appeared suppressed even after the events. Note higher firing probabilities during the ± 0.5 s (grey) surrounding the peak of SWRs than during the events (see also raster plot). **I.** Firing rates of the axo-axonic cell relative to SWRs during sleep (left) and wakefulness (right). The distribution of measured firing rates per individual SWR are displayed as cumulative distribution functions (CDF). The distribution of axo-axonic cell firing rates (blue) was significantly different from the median (black) of the surrogate sets (2-sample Kolmogorov-Smirnov tests, $p<0.0001$, for sleep and wakefulness), and the left shift demonstrates a decrease over the full range of firing rates. Surrogate sets of 1000 firing rate-distributions (grey; median, solid black line; 95% confidence intervals, broken lines). *Insets*, comparison of mean SWR-related firing rate (coloured lines) with the distribution of surrogate mean SWR-related rates (black lines). The axo-axonic cell (blue) was always strongly inhibited during SWRs ($p<0.0001$ for sleep and wakefulness, relative to the surrogate CDF).

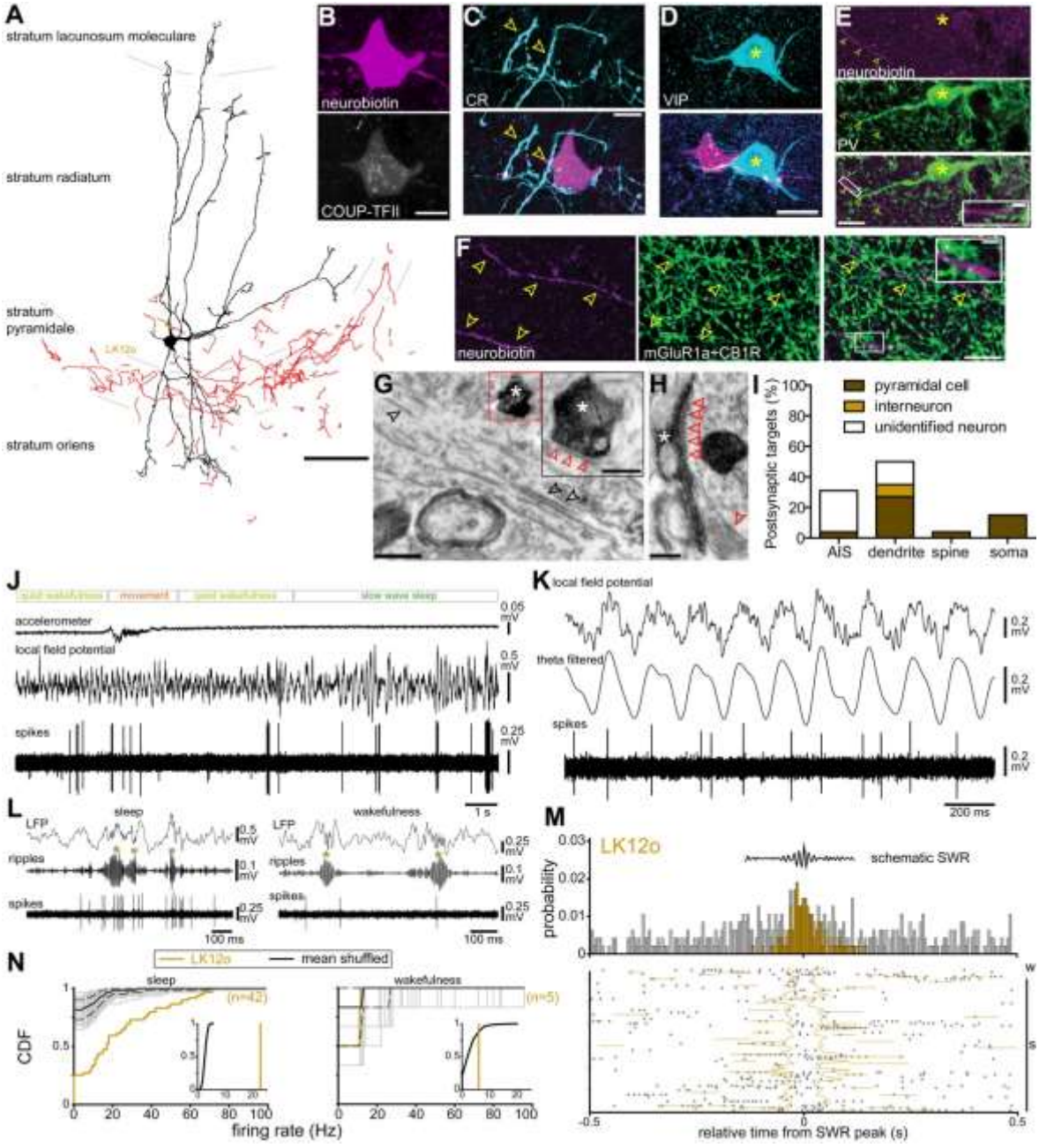
A
stratum lacunosum moleculare
stratum radiatum
stratum pyramidale
stratum oriens
LK12o
B
neurobiotin
COUP-TFII
C
CR
D
VIP
E
neurobiotin
PV
F
neurobiotin
mGluR1a+CB1R
G
H
I
pyramidal cell
interneuron
unidentified neuron
Postsynaptic targets (%)
AIS
dendrite
spine
soma
J
accelerometer
local field potential
spikes
K
local field potential
theta filtered
spikes
200 ms
L
sleep
wakefulness
LFP
ripples
spikes
100 ms
1 s
M
LK12o
schematic SWR
probability
relative time from SWR peak (s)
N
LK12o
mean shuffled
sleep
wakefulness
(n=42)
(n=5)
CDF
firing rate (Hz)

Figure 4-4 Behaviour-related activity patterns of an "unconventional interneuron".

A. Partial reconstruction of the cell body, dendrites and axon of LK12o (three 70-μm-thick sections; axonal origin, arrow). **B, C, D.** The labelled cell body was weakly immunopositive for COUP-TFII (white dots, B) and lacked CR and VIP immunoreactivity (C, D). The cell body was innervated by CR-expressing afferents. Note the characteristic dendro-dendritic and axo-dendritic contacts formed by the CR positive interneurons (C, arrowheads). Note the close apposition of a VIP-expressing unlabelled interneuron (D, asterisk) to the "unconventional interneuron". Confocal microscopic images (maximum intensity projection, z-stack, height 17 μm, 19.5 μm and 27.5 μm, respectively). **E, F.** The dendrites in stratum radiatum (arrowheads) were immunonegative for PV (E) and mGluR1a (F). Note a PV-expressing cell (asterisk) in proximity in stratum pyramidale (E). Note the dense CB1R positive axonal plexus, which was previously also tested in this section for potential axonal expression in the cell (F). Confocal microscopic images (maximum intensity projection, z-stack, height 1.6 μm and 14.7 μm, respectively). See also Figure 4-1. **G, H.** Electron micrographs of boutons of the labelled neuron (asterisks) forming synapses (arrowheads) on a postsynaptic AIS (G) and on a dendrite with a thick postsynaptic membrane specialisation (H). Scale bars, A, 100 μm; B, C, E, F, 10 μm; D, 20 μm; E, F *inset*, 2 μm; G, 0.5 μm; H, G *inset*, 0.25 μm. **I.** Distribution of twenty-six postsynaptic targets innervated by the "unconventional interneuron". Synapses were formed mostly on dendrites and on axon initial segments (AIS) but some were also found on spines and cell bodies. **J.** This neuron fired irregularly during different behavioural states. **K.** The spike train of the "unconventional interneuron" was irregular during theta episodes (filtered, 5-12 Hz), occasionally being silent for 2-3 s during the oscillatory epoch. **L.** During sleep, the cell increased its firing rate during SWRs (left*,* asterisks). During wakefulness, the cell was either silent or it fired 1-2 spikes during SWRs (right*,* asterisks). **M.** Raster plot and average firing probability relative to SWR events (w, wakefulness; s, sleep). The "unconventional interneuron" fired with higher probability during SWRs (orange bars in histogram) compared to the ± 0.5 s (grey) surrounding the peak of SWR events. Note the gradual increase in firing probability starting 100 ms before SWRs (see also raster plot). **N.** Firing rates of the "unconventional interneuron" relative to SWRs during sleep (left) and wakefulness (right). The distribution of measured firing rates per individual SWR are displayed as cumulative distribution functions (CDF). During sleep, the distribution of the cell firing rates (orange) was significantly different from the median (black) of the surrogate sets (2-sample Kolmogorov-Smirnov test, $p<0.0001$), and the right shift demonstrates an increase over the full range of firing rates. During wakefulness, the distribution of the cell firing rates (orange) was similar to the median (black) of the surrogate sets (2-sample Kolmogorov-Smirnov test, $p=0.078$) as it was within the confidence intervals over the full range of firing rates, but note the low number of recorded events. Surrogate sets of 1000 firing rate-distributions (grey; median, solid black line; 95% confidence intervals, broken lines). *Insets*, comparison of mean SWR-related firing rate (coloured lines) with the distribution of surrogate mean SWR-related rates (black lines). The "unconventional interneuron" (orange) was strongly activated by the SWRs during sleep ($p<0.0001$, relative to the surrogate CDF), but it did not change its rate during awake-SWRs ($p=0.039$, relative to the surrogate CDF).

Table 4.1 Molecular expression profiles of interneurons.

		Immunohistochemical test											
Cell type	**Cell**	PV	Satb1	COUP-TFII	CR	CB	mGluR1a	VIP	CCK	SOM	NPY	PPE	CB1R
PV+ basket cell	LK08c	+ a	nt	nt	nt	nt	nt	nt	nc a	nc a	nc a	nt	nt
Axo-axonic cell	LK24g	+ d	- s	nt	nt	- d	nt	nt	nt	nt	nt	nt	nt
"Unconventional interneuron"	LK12o	- d	nt	+ s	- s	- d	- d	- s	- s	nt	nt	- s	nc a

+, immunopositive; -, no immunoreactivity detected in the cell, while other immunopositive cells were documented nearby; nc, not conclusive; nt, not tested; s,d,a, tested on soma, dendrite or axon.

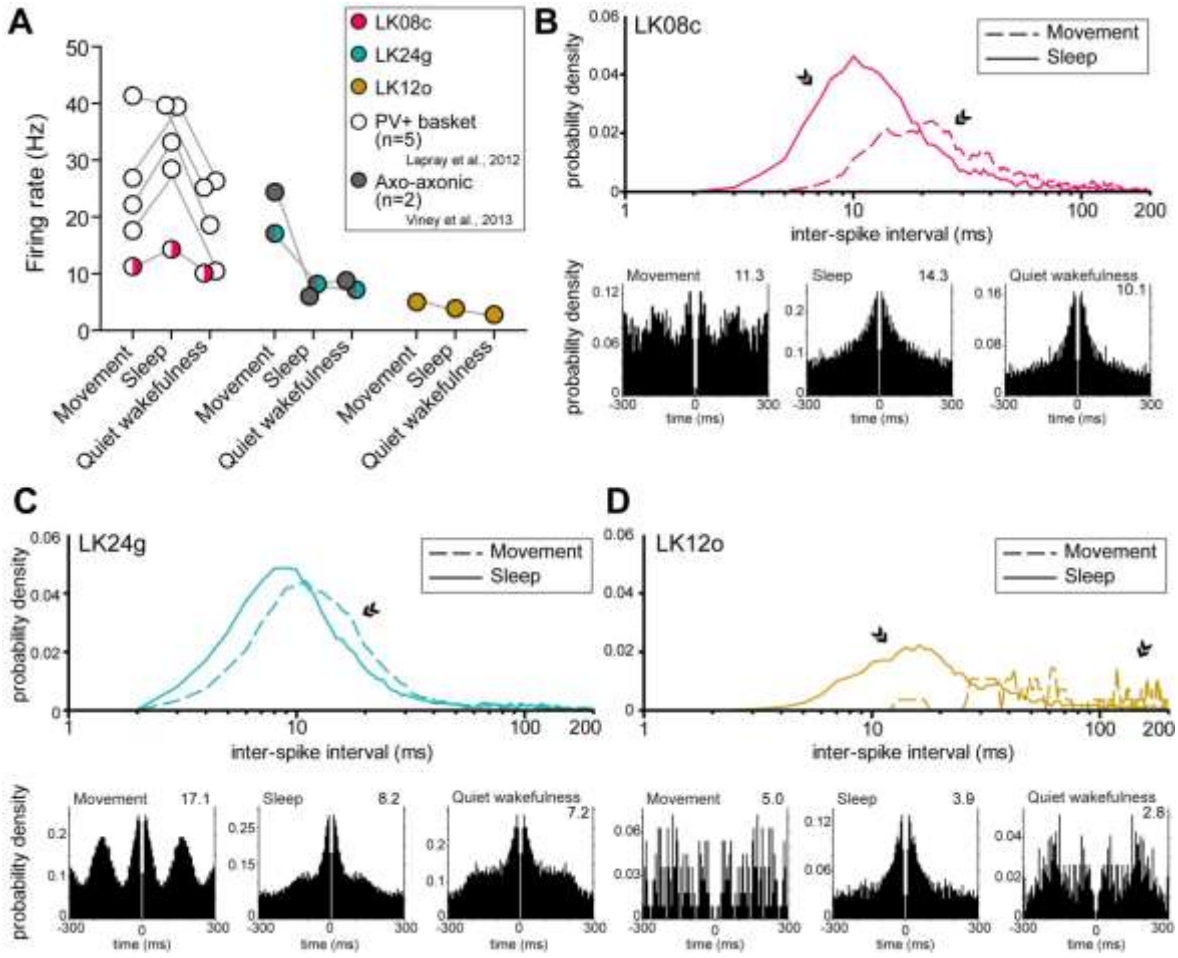

Figure 4-5 Behavioural-state-dependent firing patterns of PV+ basket cells (n=5), axo-axonic cells (n=2) and an "unconventional interneuron" (LK12o).

A. Cell-type specific and behaviour-dependent comparison of firing rates. Colour-coded dots represent individual labelled interneurons; the cell type appears different. **B, C, D.** Inter-spike interval distributions (ISI, top) and autocorrelograms (bottom) of a PV+ basket cell (LK08c, red), an axo-axonic cell (LK24g, blue) and an "unconventional interneuron" (LK12o, orange) during movement and sleep. During movement, the largest proportion of ISIs of the PV+ basket and axo-axonic cells correspond to the gamma frequency range of firing (30-100 Hz, 42.4% and 46.3%, arrowheads respectively) and these cells discharge rhythmically (bottom), in contrast, the "unconventional interneuron" fires most frequently in the lower theta and beta ranges (5-12 Hz, 46.5%, arrowheads; 12-30 Hz, 30.3%). During slow-wave sleep, the spike rate distribution of the axo-axonic cell is comparable to that during movement however the respective autocorrelograms differ significantly, as theta modulation of the cell is shown exclusively during movement. In comparison, the ISIs of the PV+ basket cell are mostly in the fast frequency ranges (30-100 Hz, 43.1%; 100-250 Hz, 23.5%, arrowheads) and the "unconventional interneuron" triggers action potentials more frequently in the gamma range (30-100 Hz, 32.7%, arrowheads). Note logarithmic time scales on ISI plots limited to 200 ms (top). Note that mean firing rates are shown in Hz at the top right corner of autocorrelation plots. Time axis is limited to 300 ms, bin width was set to 5 ms.

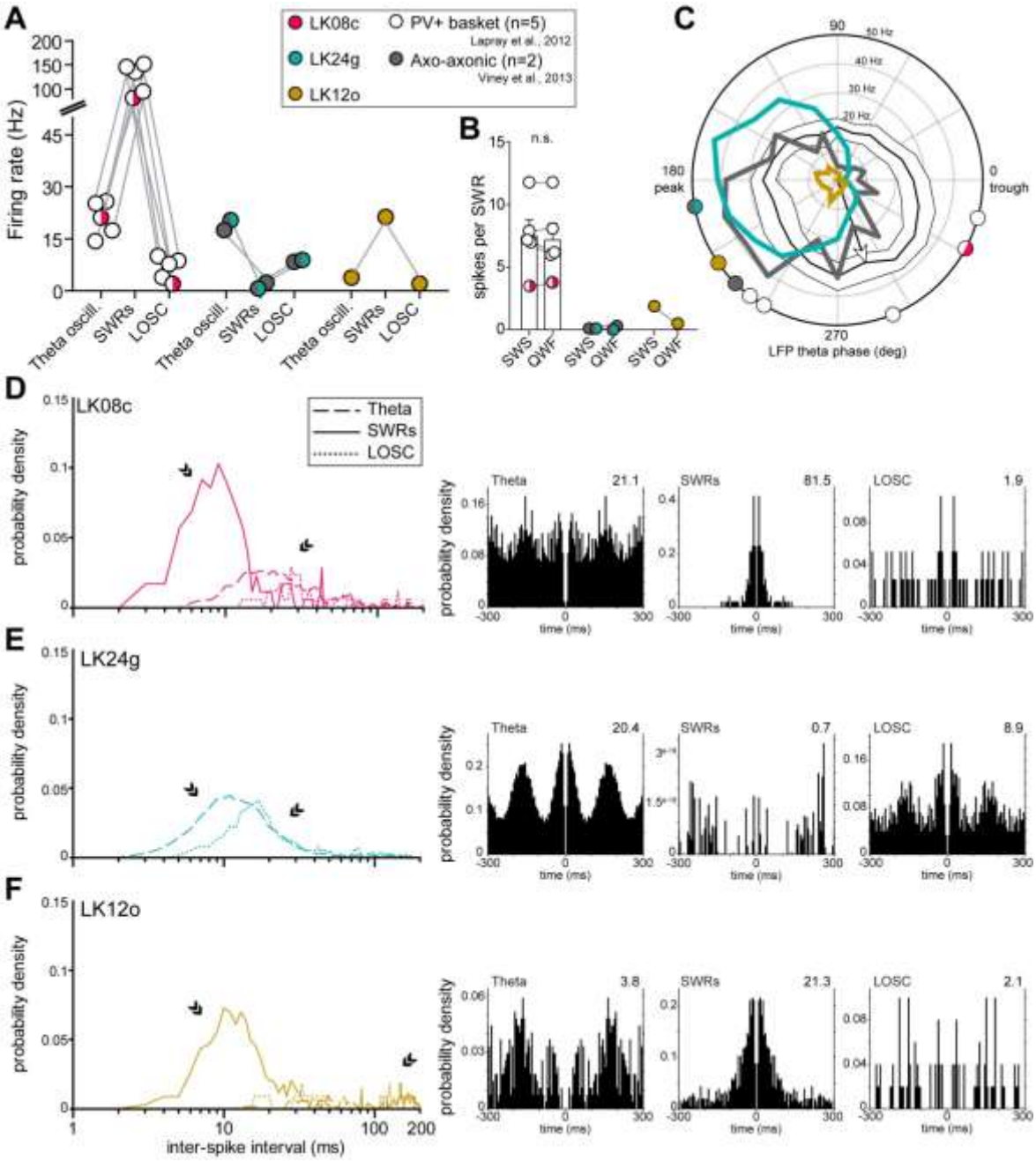
A
LK08c
LK24g
LK12o
PV+ basket (n=5)
Lapray et al., 2012
Axo-axonic (n=2)
Viney et al., 2013
Firing rate (Hz)
Theta oscill.
SWRs
LOSC
B
n.s.
spikes per SWR
SWS
QWF
C
90
180
peak
0
trough
270
LFP theta phase (deg)
D
LK08c
Theta
SWRs
LOSC
probability density
E
LK24g
F
LK12o
inter-spike interval (ms)
time (ms)

Figure 4-6 Activity of PV+ basket (n=5) and axo-axonic (n=2) cells and an "unconventional interneuron" during hippocampal network oscillations.

A. Cell-type specific and oscillatory-state-dependent comparison of firing rates. Colour-coded dots represent individual labelled interneurons; the cell type appears different. **B.** Comparison of mean spike count per SWR of PV+ basket cells (n=5) and axo-axonic cells (n=2) and an "unconventional interneuron" recorded during sleep and wakefulness. **C.** Preferred firing phases of PV+ basket (mean frequency, black line; white area and circles, ± s.e.m., n=5) and axo-axonic cells (grey and blue lines and circles) and an "unconventional interneuron" (orange line and circles) during theta oscillations. **D, E, F.** The ISIs (left) and autocorrelograms (right) of a PV+ basket cell (LK08c, red), an axo-axonic cell (LK24g, blue) and an "unconventional interneuron" (LK12g, orange) during theta oscillations, SWRs and LOSC. During theta oscillations, PV+ basket and axo-axonic cells fire mostly with instantaneous frequencies in the gamma frequency range (30-100 Hz, 48.3% and 47.7%, arrowheads respectively). Note that the axo-axonic cell, but not the PV+ basket cell, often fired with ISIs shorter than 10 ms (IF>100 Hz, arrowheads). In contrast, the largest proportions of ISIs of the "unconventional interneuron" are in the lower frequency theta and beta ranges (5-12 Hz, 50.5%; 12-30 Hz, 19.2%, arrowheads). During SWRs, PV+ basket cells and the "unconventional interneuron" strongly increase their firing rate by mostly discharging with ISIs of 4 to 10 ms (100-250 Hz, 57.7%, arrowheads) and of 10 to 33 ms (30-100 Hz, 59.7%, arrowheads), respectively. Note that the axo-axonic cell is very rarely active during SWRs and it only fires non-consecutive spikes. During LOSC, right-shifted ISI distributions demonstrate lower firing rates. Note logarithmic time scales limited to 200 ms (left) and 250 Hz (right). Autocorrelograms demonstrate theta-rhythmic firing pattern for all three interneurons and burst-like firing during SWRs with the exception of the axo-axonic cell. Note that mean firing rates are shown in Hz at the top right corner of autocorrelation plots. Time axis is limited to 300 ms, bin width was set to 5 ms.

Table 4.2 Firing rates and patterns of interneurons.

Cell type		PV+ basket cell	Axo-axonic cell	"Unconventional interneuron"
Cell		LK08c	LK24g	LK12o
Mean firing rate (Hz)	**Movement**	11.3	17.1	5.0
	Sleep	14.3	8.2	3.9
	Quiet wakefulness	10.1	7.2	2.8
	Theta	21.1	20.4	3.8
	SWRs	81.5	0.7	21.3
	LOSC	1.9	8.9	2.1
Mean theta phase of firing (°)		331.9 ± 67.5	190.6 ± 58.6	214.7 ± 66.3
Mean theta vector length of firing[a]		0.32	0.48	0.33
Mean number of spikes per SWR	**Slow wave sleep**	3.5	0.1	1.9
	Quiet wakefulness	3.8	0.0	0.5
SWR-activity index[b]	**Slow wave sleep**	11.1	0.1	8.5
	Quiet wakefulness	11.7	0.0	1.8

[a]theta modulation of firing [0,1], maximally correlated=1; see Experimental procedures in chapter 2.

[b]ratio of the mean firing rate during detected SWRs to the mean firing rate during the surrogate 'SWR' population.

Table 4.3 Point estimates of ISI distributions.

		Median ± interquartile range of ISI (ms)								
Cell type	**Cell**	**Movement**			**Sleep**			**Quiet wakefulness**		
PV+ basket cell	LK08c	36.3	±	58.7	18.3	±	37.8	32.8	±	122.9
Axo-axonic cell	LK24g	17.7	±	35.6	16.5	±	74.0	18.2	±	88.9
"Unconventional interneuron"	LK12o	116.0	±	119.6	49.3	±	233.8	169.1	±	229.0

Cell type	**Cell**	**Theta**			**SWRs**			**LOSC**		
PV+ basket cell	LK08c	30.9	±	41.3	9.2	±	6.3	135.3	±	386.9
Axo-axonic cell	LK24g	17.2	±	31.0	NA	±	NA	28.2	±	87.3
"Unconventional interneuron"	LK12o	157.8	±	112.0	13.1	±	10.3	149.1	±	325.8

4.3 Discussion

Perisomatic targeting PV+ basket cells and axon initial segment-innervating axo-axonic cells have contrasting *in vivo* spike-timing in the drug-free hippocampal network. An "unconventional interneuron", not reported before in the hippocampus, shows differences in its action potential firing compared to both of former cell types. Differences in firing patterns changed with transitory behavioural states and rhythmic network events suggesting that distinct interneuron types have specific roles in the regulation of pyramidal cell output at different times during behaviour.

The strong modulation of axo-axonic cells by the theta rhythm is suggestive of their role in synchronising pyramidal cells to theta frequencies. Both, axo-axonic and PV+ basket cells fired with high frequency bursts during movement but on complementary segments of the descending slope of theta cycles, with the former discharging trains of action potentials just after the peak followed by the latter [see also (Lapray et al., 2012) and (Viney et al., 2013)]. Interestingly, in our rats, the mean firing phase of individual PV+ basket cells positively correlated with the distance of their cell bodies relative to bregma along the septotemporal hippocampal axis (Lapray et al., 2012), indicative of a travelling theta rhythm (Hartwich et al., 2009; Lubenov and Siapas, 2009; Patel et al., 2012). Hence, in awake head-fixed mice, the slight shift of PV+ basket cell firing to the late descending phase of theta cycles (Varga et al., 2012), beside possible species differences, might be due to relatively posterior and lateral electrode placement. In contrast to the PV-immunopositive cell types, the "unconventional interneuron" fired only occasionally during movement.

The movement-related high frequency burst discharges of axo-axonic and PV+ basket cells but not of the "unconventional interneuron" were in the gamma range, as indicated by their inter-spike interval distributions. Indeed, gamma- (25-90 Hz) and

epsilon-frequency (90-130 Hz) modulation of PV+ basket cell firing has been reported *in vitro* (Hájos et al., 2004; Oren et al., 2006) and *in vivo* under urethane anaesthesia (Tukker et al., 2007) and in drug-free mice, where the strength of coupling increased with the oscillatory frequency (Varga et al., 2012). Given the axonal distribution surrounding the cell bodies of pyramidal cells and the strongly oscillatory-phase coupled spike-timing of PV+ basket cells it was suggested that this interneuron type is important in the gamma entrainment of pyramidal cell somatic membranes (Bartos et al., 2007; Mann et al., 2005; Oren et al., 2010; Tukker et al., 2007). As shown recently in urethane anaesthetised rats and awake head-fixed mice, PV+ basket cells in the CA1 area are key participants in the generation of "$\text{gamma}_{\text{perisomatic}}$" oscillations (60-100 Hz) at the trough of theta oscillatory cycles (Lasztoczi and Klausberger, 2014). Whether any relationship exists between the spike-timing of axo-axonic cells and these hippocampal fast rhythms during behaviour have not been explored. I could not define a relationship between the spike-timing of the recorded interneurons and the phase of ongoing gamma or ripple oscillations in the LFP because of the spike contribution of the recorded cell to the LFP signal. These high frequency oscillations are localised events and have phase-shifts depending on the hippocampal layer where they are measured. For the correlation analysis described above one has to obtain spike-artefact-free LFP measurements from the close proximity of the recorded neuron. Moreover, in order to produce a good reference for comparison between experiments, these LFP measurements have to be made repeatedly from within the same target location i.e. the middle of the dorsal CA1 pyramidal layer. With the use of anaesthesia or stereotaxic head fixation during the experiments such reproducibility is achievable. However, under our protocol in the freely moving rats (Figure 2-2) given the very restricted space on the skull due to the head mounted stage, the exact placement of an

external electrode for recording reference LFP signal proved to be very challenging. Having the electrode tips at various depths, either above or below the pyramidal layer, the signals I measured were not applicable for this kind of analysis. In nine experiments I tried implementing a single movable tetrode within the head stage but I did not succeed in obtaining consistent location for recordings. Signals originating from the glass electrode, even when band-pass filtered for LFP (0.3-500 Hz), will contain the spectral components of the action potentials fired by the recorded neuron over a broad frequency range (>50 Hz). For correlation studies involving gamma oscillations (30-130 Hz) and SWRs (130-230 Hz), processing the spike-contaminated LFP measurements is not optimal because of the overlap between the frequencies of the network rhythms and that of the spike resulting in spurious correlations [see Fig. 5 in (Belluscio et al., 2012; Manning et al., 2009; Zanos et al., 2011)]. None of the different kinds of spike artefact removal algorithms (David et al., 2010; Galindo-Leon and Liu, 2010; Jacobs et al., 2007; Okun et al., 2010; Pesaran et al., 2002; Zanos et al., 2011) can eliminate the problem completely, therefore their application and the resulting conclusions leave significant uncertainties. Accordingly, when analysing LFP and spike data provided by the same electrode, reliable conclusions can only be drawn with respect to low frequency bands within delta (<3Hz) and theta (5-12 Hz) ranges where the influence of spike contamination is minimal.

The most striking differences in spiking pattern between the perisomatic-targeting and axon initial segment-innervating interneuron types was observed during ripple frequency oscillations. Axo-axonic cells were inhibited, whereas PV+ basket cells and the “unconventional interneuron” showed activation during SWRs in comparison to time periods outside such events by increasing their mean firing rates several fold. What are the consequences and hypothesised roles of this divergent SWR-related

silencing versus increased activity of distinct interneuron types? I have addressed this question in section 4.3.3 and in chapter 6. Overall, these data indicate a compartment-specific regulation of pyramidal cell output mediated by a temporal redistribution of GABA from the cell body and proximal dendrites to the axon initial segment and back according to ongoing behavioural-dependent hippocampal network events.

4.3.1 The "unconventional interneuron"

My observations regarding the "unconventional interneuron" appear to differ from previously published rules of GABAergic neuronal innervation in the CA1 area of the rat hippocampus. The substantially tufted dendritic tree, the unique postsynaptic target distribution selectivity together with unexpected spike-timing during behaviour and the lack of immunoreactivity for major cell type markers raise the possibility of a novel cell type that has not been reported previously. As I only found one such neuron, I am not able to conclude how these features contribute to hippocampal activity therefore I discuss my findings in comparison with previously reported cell types.

The only molecular marker I found for this neuron was a weak reactivity for the chicken ovalbumin upstream promoter transcription factor type II (COUP-TFII) a nuclear receptor involved in developmental control. It is expressed in interneuron types derived almost exclusively from the caudal ganglionic eminence (CGE) (Batista-Brito and Fishell, 2009; Kanatani et al., 2008 ; Marín, 2013; Marin and Rubenstein, 2001; Marín and Rubenstein, 2003), however its role in adult hippocampal neurons is unknown. In general, CGE-derived cells, in contrast to their fast-spiking MGE-derived counterparts, are regular-spiking neurons *in vitro* (Butt et al., 2005). The "unconventional interneuron" recorded *in vivo* had low spike rate and rarely fired rhythmically. In the hippocampal CA1, COUP-TFII expression is present exclusively in

GABAergic cells at varying intensities. The majority of such cells are located in the pyramidal cell layer (Fuentealba et al., 2010) where the "unconventional interneuron" was. Co-expression of COUP-TFII and parvalbumin within the same cell was not found (Fuentealba et al., 2010) excluding the possibility of the "unconventional interneuron" being a subtype within PV+ axo-axonic cells. Some parvalbumin immunonegative axo-axonic synapses were reported on pyramidal cell axon initial segments in the visual cortex of rats and monkeys (Gonchar et al., 2002), but the possibility of false negative reaction were not excluded. There are five largely non-overlapping identified types of COUP-TFII immunopositive neuron recorded in different layers possessing distinct input-output connectivity: interneuron specific interneurons (ISI) (Acsády et al., 1996b), ivy cells (Fuentealba et al., 2008a), some basket cells (Freund and Katona, 2007; Klausberger et al., 2005), neurogliaform cells (Price et al., 2005) and retrohippocampally projecting neurons (Fuentealba et al., 2010). Based on the axonal innervation pattern of the recorded interneuron concentrated along the pyramidal cell layer a resemblance to some basket cell or ISI cell type could be hypothesised. Indeed, one of the published COUP-TFII+ basket cells (Fuentealba et al., 2010) had similarly tufted dendritic tree and it was immunonegative for parvalbumin and cholecystokinin, however it was recorded in upper stratum radiatum in close proximity to stratum lacunosum moleculare and its postsynaptic targets, contrary to the "unconventional interneuron", were mainly pyramidal cell somata. Moreover, despite the similarity of the preferential theta phase firing of the two neurons at the peak of the oscillatory cycles (during exploration and under anaesthesia, respectively), their SWR-related spiking patterns differed. The "unconventional interneuron" mostly increased its firing rate, whereas the neuron recorded under urethane anaesthesia was inactive during the

majority of SWR events. These discrepancies between the two neurons make it very unlikely that they are the same cell type.

Tufted dendrites have been reported for another subpopulation of COUP-TFII+ GABAergic interneuron in the CA1 with CGE origin (Kanatani et al., 2008). These neurons are immunopositive for the calcium binding protein calretinin (CR) (Gulyás et al., 1992; Kanatani et al., 2008; Miettinen et al., 1992) and target selectively other interneurons (Acsády et al., 1996b; Gulyás et al., 1996). However, the activity of these cells has not been reported *in vivo*. The members of this subpopulation are strongly interconnected via specialised dendro-dendritic and axo-dendritic attachement junctions in addition to conventional synapses. Their axon is thin bearing small boutons (Gulyás et al., 1992) very similar to what I observed for the "unconventional interneuron", which together with its densely surrounded cell body by CR+ immunopositive boutons, was suggestive of the interneuron being a representative of ISI cell type. When tested however, I could not observe CR immunoreactivity in the cell body of the "unconventional interneuron". After examining some control hippocampal sections in which CR immunoreactivity was visualised using HRP-reaction product, I found that the level of CR-expression in CA1 interneurons showed large variability. Therefore, there is a possibility that the method I used (anti-CR primary antibody combined with fluorophore conjugated secondary antibody) was not sensitive enough to detect a low level of CR. Thus, under our conditions the "unconventional interneuron" lacked CR immunoreactivity and as its postsynaptic targets were mostly pyramidal cells together with some interneurons, I concluded that its features do not fit the reported ISI cells. Interestingly, such basket-like innervation pattern as observed around the soma of the interneuron formed by axon collaterals of ISI cells has also been shown around CR immunonegative somata (Gulyás et al., 1996). Therefore I

persevered with the identification process by testing for calbindin (CB) or vasoactive intestinal polypeptide expression, as demonstrated in postsynaptic targets of CR+ interneurons. I could not detect any of these molecules in the recorded neuron. Positive matches were unlikely, because the only known such cells with axon in stratum pyramidale were recorded either in different layers or co-expressed other molecules not present in the "unconventional interneuron". A possible source for the CR+ terminals wrapping around the "unconventional interneuron" is from extrahippocampal sources (e.g., supramammillary nucleus or nucleus reuniens of thalamus). In the CA1 area, such CR-expressing long-range projecting axons, some glutamatergic (Kiss et al., 2000; Krzywkowski et al., 1995; Leranth et al., 1999; Nitsch and Leranth, 1993; Nitsch and Leranth, 1996) were shown to give rise to short collaterals with large boutons forming synapses mostly with CR+ cells in strata radiatum and/or oriens (Gulyás et al., 1992). It is intriguing that these terminals also group into small basket-like clusters in stratum pyramidale (Gulyás et al., 1992), where the soma of the "unconventional interneuron" was labelled. The postsynaptic target preference of such projecting axons remains to be identified.

The many irregularities making the classification of the interneuron challenging might be due to abnormal cellular development resulting in possible displacement during migration and altered connectivity. Alternatively, the cell could be newly born and not yet integrated in its environment or, in contrast, it could be undergoing atrophy. For example, the majority of Cajal-Retzius neurons, a subpopulation of cells instrumental for corticogenesis and expressing COUP-TFII (Hevner et al., 2003; Marín-Padilla, 1998; Mienville, 1999; Radnikow et al., 2002; Soda et al., 2003; Soriano and del Río, 2005; Tripodi et al., 2004) disappear in the adult brain (del Río et al., 1995; Derer and Derer, 1990; Mienville and Pesold, 1999; Pesold et al., 1998) but those surviving

become synaptically coupled to other cells in the network (Quattrocolo and Maccaferri, 2013; Radnikow et al., 2002). They have been hypothesised to direct synapse formation between the entorhinal cortex and CA1 in stratum lacunosum moleculare (del Rio et al., 1997; Marchionni et al., 2010). Given the specific input and output synaptic organisation of the "unconventional interneuron" in the CA1 area, absence of immature characteristics and the robust firing dynamics recorded during behaviour, it is improbable that the cell is a surviving and modified Cajal-Retzius neuron.

Through its elaborate dendritic tree the "unconventional interneuron" samples all hippocampal layers and can integrate the temporally segregated glutamatergic inputs arriving from the entorhinal cortex and the hippocampal CA1 and CA3 areas. By targeting mainly axon initial segments and dendrites of pyramidal cells, it likely regulates action potential generation and dendritic integration. Is there a need for another cell type, besides the PV+ axo-axonic cells, for the control of pyramidal cell output? A modifiable GABAergic input to the axon initial segment could complement the clock-like activity of PV+ axo-axonic cells and provide plasticity to regulating pyramidal cell firing on longer time scales. There is such a domain specific synaptic organisation, the dual GABAergic innervation of the pyramidal cell soma by PV+ vs CCK+ basket cells (Armstrong et al., 2013; Freund and Katona, 2007; Takács et al., 2014). However, the low frequency spiking and the lack of change in the activity of the "unconventional interneuron" during different behavioural states are suggestive of a minimal contribution of the neuron to network state adjustments. Only the strong excitatory drive during sleep-SWRs indicated that the "unconventional interneuron" contributed to modulating the firing of CA1 pyramidal cells. Considering the frequent silent periods in the spike train of this neuron during behaviour it is not surprising that

it has not been recorded earlier especially under urethane anaesthesia, when firing rates drop significantly.

The frequent synapses on axon initial segments made by the “unconventional interneuron”, and also known for PV+ axo-axonic cells, have not been reported for any other interneuron type. Furthermore, the spike-timing is unique amongst all other recovered cells in the laboratory. Taking into account the molecules which could not be detected in the cell, I am unaware of a cell type with the reported characteristics. At present, the only way to obtain a larger sample is by electrophysiological recording and juxtacellular neurobiotin-labelling of single cells *in vivo*, which even in anaesthetised rats, is a very challenging technique and low yield method. As urethane changes hippocampal network and neuronal activity, the recognition of the same type of cell might be impossible in anaesthetised rats. A possible approach for testing the presence of such cells on a larger scale is to record and label neurons in the pyramidal cell layer visualised in slice preparations *in vitro,* from rodents with genetically pre-labelled caudal ganglionic eminence derived interneurons. The recorded neurons could be labelled and those with axons mainly in the pyramidal cell layer could be tested for postsynaptic targets using electron microscopy. In conclusion, determining the place and role of the "unconventional interneuron" in the hippocampal network will require further large scale studies.

4.3.2 Intrinsic cellular properties and synaptic afferents

Modalities of action potential discharge in neurons are determined by a combination of cell autonomous and network factors. The fast spiking phenotype in the cortex and hippocampus is mostly associated with GABAergic interneuron types (McCormick et al., 1985), such as basket and axo-axonic cells (Buhl et al., 1994b; Buhl

et al., 1996; Kawaguchi et al., 1987; Kosaka et al., 1987) expressing the calcium-binding protein parvalbumin. Parvalbumin was shown to block spike adaptation and to regulate neuronal excitability (Celio, 1986). Interestingly, the machinery generating firing at high rates in these neurons is induced postnatally by changes in their receptor expression and in their input-output connectivity (Butt et al., 2005; Doischer et al., 2008). Increased firing rates of PV+ basket and axo-axonic cells, like recorded in my rats, require rapid action potential repolarisation which is achieved by these neurons via voltage-gated $Na_v1.1$ and $Na_v1.6$ channels (Lorincz and Nusser, 2008a, 2010; Martina and Jonas, 1997; Ogiwara et al., 2007); high voltage-activating K_v3, $K_v1.1$ and $K_v1.2$ channels (Du et al., 1996; Erisir et al., 1999; Goldberg et al., 2008; Hu et al., 2010; Jonas et al., 2004; Lau et al., 2000; Lorincz and Nusser, 2008a; Martina et al., 1998; Rudy and McBain, 2001; Weiser et al., 1995; Zhang and McBain, 1995); extrasynaptic $\alpha1$ subunit containing $GABA_A$ receptors (Baude et al., 2007; Gao and Fritschy, 1994; Kasugai et al., 2010; Nusser et al., 1995); and P/Q-type Ca^{2+} channels (Aponte et al., 2008; Bucurenciu et al., 2010; Hefft and Jonas, 2005). Due to the fast inactivating Na^+ channels the rapid repolarisation often leads to doublets in the spike trains of axo-axonic cells recorded *in vitro* or *in vivo* under anaesthesia (Buhl et al., 1994b; Klausberger et al., 2003) and likely contributes to the observed bursts of spikes recorded *in vivo* during behaviour [see also (Viney et al., 2013)]. The somato-dendritic (Hughes et al., 2013) and axonal expression [see Fig. 1c in Nusser et al. (2009) (Notomi and Shigemoto, 2004; Santoro et al., 1997)] of hyperpolarization-activated cyclic nucleotide-gated (HCN) channels by PV+ basket and axo-axonic cells contributes greatly to their fast signalling affecting active dendritic cable properties and lowering the threshold for spike initiation (Aponte et al., 2006; Nörenberg et al., 2010; Nusser, 2009). These mechanisms result in precise input transduction and allow action

potentials to follow faithfully high frequency repetitive inputs like those received from glutamatergic afferents active at gamma and/or ripple frequencies. Cell autonomous mechanisms involving HCN channels entrain (Marcelin et al., 2009; Nusser, 2009) the spike-timing of PV+ basket and axo-axonic cells to gamma and theta frequency oscillations *in vitro* and *in vivo* (Bartos et al., 2007; Gulyás et al., 2010; Lapray et al., 2012; Varga et al., 2012; Vida et al., 2006; Viney et al., 2013; Ylinen et al., 1995b). The high temporal precision of PV+ basket and axo-axonic cell spikes (Bartos et al., 2007; Hefft and Jonas, 2005; Kraushaar and Jonas, 2000) is additionally regulated by tonic inhibition (Brickley et al., 1996; Farrant and Nusser, 2005; Semyanov et al., 2003) via extrasynaptic and synaptic $GABA_A$ receptors. The membranes of PV+ basket, but not axo-axonic, cells are highly enriched in these receptors (Baude et al., 2007; Gao and Fritschy, 1994; Kasugai et al., 2010; Nusser et al., 1995), which likely determines their millisecond-precision coupling to high-frequency SWRs (Klausberger et al., 2003; Lapray et al., 2012; Varga et al., 2012). The latter, expressing low levels of the receptor cease firing during SWRs (Klausberger et al., 2003; Viney et al., 2013) possibly due to SWR-related strengthened GABAergic inputs. Moreover, frequent gap junctions between members of the PV+ cell population contribute to the presumed synchronous discharge during network oscillations (Baude et al., 2007; Fukuda and Kosaka, 2003; Fukuda et al., 2006; Hormuzdi et al., 2001; Katsumaru et al., 1988a; Tamas et al., 2000). Gap junction coupling between axo-axonic cells might be of particular importance because of the lack of synapses between members of this cell type (Baude et al., 2007).

In the hippocampal CA1 area, PV+ basket cells sample the same range of glutamatergic afferents as axo-axonic cells originating from the hippocampal CA1 and CA3 areas (Ali et al., 1998; Andersen et al., 1963; Buhl et al., 1994b; Buhl et al., 1996; Debanne et al., 1995; Frotscher et al., 1984; Glickfeld and Scanziani, 2006; Gulyas et al.,

1993; Schwartzkroin and Kunkel, 1985) and the entorhinal cortical layer 3 (Kiss et al., 1996; Li et al., 1992; Witter and Amaral, 1991). However, axo-axonic cells are probably under stronger extrahippocampal influence having their large tufted dendrites overlapping with the entorhinal cortical termination zone (Li et al., 1992). In contrast, PV+ basket cells are most likely dominated by the commissural/Schaffer collateral pathway and the local CA1 recurrent fibres. Because of the small proportion of dendritic surface reaching into stratum lacunosum moleculare (Halasy et al., 1996) the entorhinal cortical influence on them is probably minimal. Both neuron types exhibit NMDA-independent long-term potentiation (Alle et al., 2001l; Kullmann and Lamsa, 2007; Nissen et al., 2010; Perez et al., 2001) that likely supports changes in strength of pyramidal-cell–interneuron connections reported during learning (Dupret et al., 2013; Hangya et al., 2010). Differences in the timing and proportion of the glutamatergic inputs of PV+ basket and axo-axonic cells cannot completely explain the striking divergence in their SWR-related firing activity and their out-of-phase coupling to oscillatory theta cycles. What phases the spike-timing of the two cell types if not these inputs?

Inhibitory postsynaptic potentials elicited in axo-axonic and PV+ basket cells (Buhl et al., 1994b; Buhl et al., 1996; Lacaille, 1991; Ylinen et al., 1995b) are indicative of GABAergic inputs to the two cell types. Indeed, parvalbumin-expressing interneurons in the CA1 area receive GABAergic synapses from extrahippocampal afferents (Freund, 1992; Freund and Antal, 1988; Fukuda et al., 1996; Melzer et al., 2012; Viney et al., 2013) and from other local interneurons (Cobb et al., 1997; Fukuda et al., 1996; Gulyás et al., 1999; Katsumaru et al., 1988b; Sik et al., 1995). Around 30% of the GABAergic presynaptic terminals targeting dendrites and 70% of the terminals innervating somata are also immunopositive for parvalbumin (Gulyás et al., 1999). It

remains to be determined if these rules are uniform among the distinct PV+ interneuron types. To define their synaptic input organisation, first basket and axo-axonic cells have to be unequivocally identified which usually required electron microscopic investigation of their postsynaptic targets. Recently, a subpopulation of hippocampal PV+ interneurons were reported to lack the transcription factor Satb1 and these were identified as axo-axonic cells (Viney et al., 2013). Furthermore, it was observed that, in the CA1 area, some septal GABAergic boutons strongly innervate those PV-expressing neurons which are immunonegative for Satb1, hence axo-axonic cells, and not those which are immunopositive for Satb1, hence basket or bistratified cells. Whether the latter are targeted by other subpopulations of medial septal neurons is unknown (Freund and Antal, 1988; Hangya et al., 2009), but if so, this may explain why PV+ basket cells are relatively weakly theta-modulated (Lapray et al., 2012; Varga et al., 2012), in contrast to axo-axonic cells. Furthermore, under anaesthesia, one population of medial septal neurons fired rhythmically around the trough and another one around the peak of theta oscillations (Borhegyi et al., 2004). These different groups of neuron, if targeting hippocampal interneurons may restrict postsynaptic action potential discharge to the peak, or around the trough of theta cycles, like observed for axo-axonic and basket cells, respectively. Taken together, existing evidences suggest a cell-type selective GABAergic innervation of distinct PV+ interneurons without excluding the possibility of some proportion of shared inputs.

Based on my observations the spike-timing of these two cell types during theta oscillations was predicted correctly from tetrode recordings of unidentified pyramidal layer interneurons (Czurkó et al., 2011; Zhang et al., 2012). Because I only recorded short periods of movement, I could not detect theta phase precession in the spike trains of the reported cells. However, it has been suggested that some unidentified

interneurons recorded using tetrodes advance their preferential phase of firing during short bouts of theta cycles (Ego-Stengel and Wilson, 2007; Maurer et al., 2006).

The coupling of basket cells to gamma oscillations (Varga et al., 2012) and SWRs, is likely due to their simultaneous activation by CA1 and CA3 pyramidal cells. In contrast, axo-axonic cells receive substantially stronger inhibitory inputs (Hájos et al., 2013) during SWRs *in vitro*, which might supress their action potential discharge especially after the peak of these events. As well as septal inputs, PV+ basket, bistratified and trilaminar cells could also contribute to the silencing of axo-axonic cells.

4.3.3 The effects of anaesthesia on neurons and network dynamics

Until recently, the *in vivo* investigation of action potential firing of identified interneuron types in the hippocampus was performed using urethane and ketamine–xylazine anaesthesia (Klausberger and Somogyi, 2008; Somogyi, 2010). Having now recorded and analysed interneuron types in the drug-free brain, similarities and differences can be established between the two conditions that should reveal which features of neuronal activity remain valid when studied under physiological conditions. Under anaesthesia, in the rodent hippocampus, theta, gamma and ripple frequency network oscillations persist but at reduced frequencies of 3-6 Hz, 30-80 Hz and 90-130 Hz, respectively (Klausberger et al., 2003; Soltesz and Deschenes, 1993; Tukker et al., 2007; Ylinen et al., 1995a; Ylinen et al., 1995b). Furthermore, it has been shown that urethane potentiates $GABA_A$ and nicotinic acetylcholine receptors and inhibits NMDA and AMPA receptors (Hara and Harris, 2002; Lawrence, 2008), therefore probably induces changes in the action potential firing of neurons. Indeed, in the CA1 area, PV+ basket cells recorded under urethane anaesthesia (Klausberger et

al., 2003) fired with greatly reduced (repeated-measures ANOVA, $F_{1,8}$=25.41, p=0.001 for the interaction factor) rates (mean ± s.e.m., 32.7 ± 8.9 Hz during SWRs; 7.3 ± 2.7 Hz during theta periods) compared to those recorded in the drug-free brain [121.8 ± 14.2 Hz during SWRs; 20.8 ± 2.2 Hz during theta periods; see also (Lapray et al., 2012; Varga et al., 2012)]. In contrast, axo-axonic cells had variable spike rates under anaesthesia (Klausberger et al., 2003), either higher or lower by ~40% than the axo-axonic cells recorded during behaviour in areas CA1 and CA2 [see also (Viney et al., 2013); cell LK24g was recorded in the CA2 area but had comparable firing rates and spike-timing to that in CA1]. The sensitivity of PV+ basket cell firing rates to urethane might be partly explained by the strong expression of synaptic and extrasynaptic $GABA_A$ receptors on their membranes (Baude et al., 2007) involved in the regulation of neuronal excitability via tonic inhibition (Brickley et al., 1996). The expression of these receptors was much weaker in axo-axonic cells.

However, the preferential phase of theta-oscillations-related spike-timing of both interneuron types under anaesthesia (Klausberger et al., 2003) corresponds well to that recorded in freely moving rats or awake head-fixed mice (Lapray et al., 2012; Varga et al., 2012; Viney et al., 2013). Parvalbumin-expressing basket cells discharged preferentially on the descending slope of theta cycles, whereas axo-axonic cells were maximally active just after the peak of the oscillations during both conditions. This preservation of spike-timing in the absence of inputs from place cells and grid cells is suggestive of an external regulatory input source, e.g., from the medial septum controlling interneuron activity. Moreover, the 30-100 Hz gamma-frequency instantaneous firing rate of PV+ basket and axo-axonic cells recorded during movement in our rats (Figure 4-5B,C) is preserved within theta cycles under urethane

anaesthesia (Klausberger et al., 2003) although at lower rates as reflected by inter-spike intervals of 45 ± 25 ms for basket cells and 20 ± 17 ms for axo-axonic cells (mean $\pm$ s.d.). Because of lack of data from freely moving animals, it is not known if the discharge of either cell types is entrained by gamma oscillations in the drug-free rat hippocampus. Under anaesthesia, PV+ basket and axo-axonic cells in the CA1 area are moderately or weakly coupled to oscillatory gamma cycles (30-80 Hz) with mean vector lengths between 0.064 and 0.117 [(Tukker et al., 2007); see also Tukker thesis]. These values however might be influenced by urethane as suggested by the report, in awake mice, of stronger PV+ basket cell modulation by both gamma- (r=0.18) and high frequency epsilon oscillations (r=0.39) (Varga et al., 2012). Whether this higher strength in gamma-coupling is true for other interneuron types and is consistent between species remains to be investigated. During SWRs, PV+ basket cells increase their firing rate in contrast to axo-axonic cells which are silent, both with and without anaesthesia (Klausberger et al., 2003; Lapray et al., 2012; Varga et al., 2012; Viney et al., 2013).

4.3.4 Rhythmic entrainment of pyramidal cell assemblies and generation of networks oscillations

The influence of different interneuron types on hippocampal network activity may be assisted by diversified $GABA_A$ receptor varieties with different kinetics (Banks et al., 1998; Buhl et al., 1994a; Pearce, 1993) and by differential susceptibility to neuromodulators (Armstrong and Soltesz, 2012; Cea-del Rio et al., 2010; Frotscher and Léránth, 1985; Gulyás et al., 2010; Hájos et al., 1997; Lawrence, 2008; Morales et al., 2008; Szabó et al., 2010). In the hippocampal CA1 area, we recognise five distinct types of parvalbumin-expressing interneuron: basket cells, axo-axonic cells, bistratified cells,

O-LM cells and certain double-projection neurons (Somogyi, 2010). My results demonstrate that the output of PV+ basket and axo-axonic cells, as well as that of bistratified and O-LM cells (see chapter 5), changes dependent on the ongoing behaviour hence supporting these suggestions. The activity of double-projection neurons in freely moving rats remains to be defined.

The activation of $GABA_A$ receptors (Buhl et al., 1994a) in and around the pyramidal cell layer induces inhibitory mechanisms which regulate the action potential output of pyramidal cells and/or stop the phase-precession of their spikes (Harris et al., 2002). The preferential theta-phase related increases in firing rates of axo-axonic and PV+ basket cells during exploration reflect enhanced GABA release onto the axon-initial segment as well as the cell body and proximal dendrites of pyramidal cells on the peak and descending slope of theta cycles, respectively. This action restricts the pyramidal cell spike discharge to a short time window during theta cycles, and indeed, pyramidal cells, on average, fire with the highest probability at the trough [see chapter 3; (Buzsaki, 2006; Dragoi and Buzsáki, 2006)]. Optogenetic silencing of unknown types of PV+ cells increased the firing rates of pyramidal cells selectively in the rising parts of their place fields corresponding to the descending phases of theta oscillations and delayed their spiking to the trough (Royer et al., 2012).

As dicussed earlier, the gamma frequency spiking of PV+ basket cells during theta episodes (Bragin et al., 1995; Buzsaki et al., 1983; Klausberger et al., 2003; Varga et al., 2012) has led to suggestions that these interneurons contribute to rhythmogenesis (Csicsvari et al., 2003; Gulyás et al., 2010; Hájos et al., 2004; Mann et al., 2005; Penttonen et al., 1998). Moreover, inhibition of unidentified PV+ cells supressed *in vivo* gamma oscillations in cortex (Sohal et al., 2009) and depletion of their excitatory drive reduced the power of kainite-induced gamma oscillations leading to

memory impairment (Fuchs et al., 2007). Indeed, recently, PV+ basket cells were proven to perform gamma phasing of active CA3 inputs onto pyramidal cell membranes critical for the generation of "$gamma_{perisomatic}$" (60-100 Hz) field potential oscillations at the trough of theta oscillatory cycles (Lasztoczi and Klausberger, 2014).

Axo-axonic cells, by gatekeeping the action potential initiation site, select and time-restrict the firing of pyramidal cell assemblies. The periodic activation of axo-axonic cells at 120 ms intervals phases pyramidal cell membranes to the theta rhythm. *In vivo*, rhythmic photoactivation of unknown types of PV+ cells elicited postinhibitory rebound spiking in pyramidal cells restricted to the theta (4-11 Hz) frequency band (Stark et al., 2013). During SWRs, temporally compressed learnt sequences of cell assemblies are replayed and transferred to the neocortex (Carr et al., 2011; Csicsvari and Dupret, 2014; Davidson et al., 2009; Diba and Buzsaki, 2007; Foster and Wilson, 2006; Karlsson and Frank, 2009; Nádasdy et al., 1999; O'Neill et al., 2010; Skaggs and McNaughton, 1996). The silencing of axo-axonic cells (Hájos et al., 2013; Klausberger et al., 2003; Viney et al., 2013) results in the withdrawal of inhibition from the axon initial segment of pyramidal cells allowing them to fire spikes. Via highly synchronous discharges of CA1 pyramidal cells, initiated by SWR-entrained inputs from the CA3 area, information is relayed from the hippocampus to downstream cortical areas.

Because GABA can be depolarising dependent on the intracellular Cl^- levels, a controversy emerged about the postsynaptic effects of axo-axonic cells. It has been shown that axo-axonic cells depolarise pyramidal cells *in vitro* and can trigger action potentials in rat and human cortical pyramidal cells mainly recorded under whole cell conditions (Khirug et al., 2008; Szabadics et al., 2006; Woodruff et al., 2009; Woodruff et al., 2011). However, the firing of pyramidal cell axons and the resultant recorded excitatory postsynaptic potentials in brain slices may be an artefact due to the

preparation; many pyramidal cells are truncated, axons may be separated from cell bodies and still bearing intact axo-axonic cell innervation which may fire the axons in the absence of a chloride pump located on the dendrites and soma (Szabadics et al., 2006). Also, GABA was reported to be hyperpolarising along the entire membrane surface of pyramidal cells (Glickfeld et al., 2009) and intact pyramidal cells have not been demonstrated to fire action potentials *in vivo* upon axo-axonic cell input. I found that, during behaviour, identified axo-axonic cells discharge at high frequencies with a temporal pattern inversely related to pyramidal cells [see also (Viney et al., 2013)] which supports the original suggestion of pyramidal cells being inhibited rather than excited by axo-axonic cell spikes (Somogyi, 1977).

The SWR-coupled rhythmic innervation of somatic and dendritic membranes of pyramidal cells provided by PV+ basket cells and bistratified cells (Csicsvari et al., 1999b; Lapray et al., 2012; Varga et al., 2012; Ylinen et al., 1995a) contributes to setting rhythmic changes in excitability of pyramidal cells and their discharge as assemblies (Cobb et al., 1995; Csicsvari et al., 1999b; Klausberger et al., 2003; Varga et al., 2012). Furthermore it demonstrates how these interneurons by generating network oscillations at ripple frequencies (Ellender et al., 2010; Hájos et al., 2013; Klausberger et al., 2003; Maier et al., 2003) may contribute to memory consolidation. The involvement of PV+ basket and axo-axonic cells, together with several other GABAergic interneuron types, in the regulation of pyramidal cell firing during exploration and slow wave sleep will be discussed in the concluding chapter.

5 GABAergic interneurons innervating pyramidal cell dendrites

5.1 Introduction

The majority of GABAergic synapses innervating pyramidal cells are formed on dendritic membranes across all hippocampal layers (Megias et al., 2001) and originate from a diverse population of distinct GABAergic cell types (Somogyi, 2010). Grouped as *dendrite-targeting interneurons*, the cells have been most extensively studied in the CA1 region of the hippocampus, in rodents (Klausberger, 2009). At present, at least fifteen distinct types of such interneuron can be identified, seven of which are long-range projecting cells, known to target, beside local pyramidal cells, neurons in extra-hippocampal areas (Gulyás et al., 2003; Jinno et al., 2007), including the entorhinal cortex as reported in the mouse (Melzer et al., 2012). Some of their postsynaptic targets are exclusively GABAergic interneurons (Gulyás et al., 2003; Jinno et al., 2007; Katona et al., 1999a). The cell types were categorised based on the differences found in the layer-specific input and output synaptic organisations of the neurons and the different combinatorial expression of neuropeptides (e.g., somatostatin, SOM; cholecystokinin, CCK; neuropeptide tyrosine, NPY), calcium binding proteins (e.g., parvalbumin, PV; calbindin, CB) and enzymes (nitric oxide synthase, NOS) (Somogyi, 2010). Furthermore, findings about the *in vitro* and anaesthetised *in vivo* spike-timings of these cells point towards cell-type specific differences between neurons. Taken together, we predict that distinct dendrite-targeting GABAergic interneurons have

evolved to provide temporally diversified inhibition of pyramidal cells at specific domains along their dendrites. This fine-tuned inhibition may control action potential generation via regulating dendritic excitability and integration and it may govern learning-related synaptic plasticity (Dupret et al., 2010; Spruston, 2008).

Bistratified, oriens-lacunosum moleculare (O-LM), double projection, oriens-retrohippocampal and large NOS+ cells are five such types of dendrite-targeting GABAergic interneuron in CA1 (Baude et al., 1993; Jinno et al., 2007; Klausberger et al., 2004; Somogyi, 2010) expressing somatostatin (Brazeau et al., 1973), a fourteen amino acid neuropeptide that might have an overall inhibitory effect on cortex (Tallent, 2008). Somatostatin is often co-expressed with other neuropeptides and co-released with amino acid neurotransmitters and acts on sst1-sst5 G protein-coupled receptors distributed pre- (Boehm and Betz, 1997; Cammalleri et al., 2009; Tallent and Siggins, 1997) and/or postsynaptically (Moore et al., 1988; Schweitzer et al., 1998) on the membranes of pyramidal cells and interneurons. This suggests that the primary role of somatostatin-expressing interneurons is the regulation of dendritic inputs and ultimately, signal integration. It is not known when GABA and/or somatostatin are released by the distinct cell types and what would be their synergistic effects. Peptide release is most likely predicted by high frequency firing needed for the exocytosis of large dense core vesicles from the axon terminals (Takagi et al., 1983) and dendrites (Ludwig and Leng, 2006). Therefore it is expected that the firing patterns of somatostatin-expressing GABAergic interneurons are predictors of GABA/somatostatin co-release and of their synergistic effects in the modulation of postsynaptic neurons. What are the *in vivo* temporal dynamics of the hippocampal dendrite-targeting neurons during different behavioural states in naïve animals? How

do these activity patterns determine the involvement of pyramidal cell assemblies in encoding and/or retrieval of episodic memories?

The *in vivo* activity of somatostatin-expressing GABAergic interneurons is largely unknown in the drug-free brain. Two such types of neuron are bistratified and O-LM cells innervating non-overlapping dendritic zones of pyramidal cells associated with the two major glutamatergic inputs to the CA1 network. The axons of bistratified cells parallel the CA3 Schaffer collaterals targeting small and oblique dendrites in strata radiatum and oriens (Buhl et al., 1994a; Klausberger et al., 2004), whereas O-LM cells innervate the distal apical tuft which is the entorhinal cortical input zone (McBain et al., 1994). This well-differentiated synaptic output organisation suggests that interneurons have distinct cell-type specific roles in the modulation of information flow and in the coordination of network events. Specifically, bistratified cells are in key position to modulate the retrieval of internal hippocampal representations, whereas O-LM cells are likely to gate the encoding of sensory information.

To date, only the spike-timing of O-LM cells has been reported *in vivo* from awake head-fixed mice during distinct hippocampal oscillations (Varga et al., 2012), which however did not include sleep. Recently bistratified cells (Colmers et al., 1985) were reported to control pyramidal cell output *in vitro* (Lovett-Barron et al., 2012). Furthermore, the spike-timing of non-identified interneurons, was shown to be network-state-dependent (Buzsaki, 2006; Ego-Stengel and Wilson, 2007; O'Keefe and Dostrovsky, 1971; O'Keefe and Nadel, 1978; Ranck, 1973; Vanderwolf, 1969) being influenced by theta oscillations during movement or large-amplitude irregular activity during sleep. Under urethane anaesthesia, bistratified and O-LM cells had different firing rates during “behaviourally relevant network oscillations”; the spikes of both cell type were phase coupled to the trough of theta oscillations (3-6 Hz) and during SWRs

(90-130 Hz) bistratified cells strongly increased their firing rates whereas O-LM cells stopped firing (Klausberger et al., 2003; Klausberger et al., 2004). Taken together, these reports suggest differences in the behavioural and network state-related temporal dynamics of somatostatin-expressing bistratified and O-LM cells, and point towards complex and selective spatio-temporal mechanisms of dendritic regulation. Do the behavioural- and network-state-dependent discharges of these interneurons correlate with the differences in their axonal termination fields? Also, are the observed spike-timings consistent with the conditions necessary for the co-release of GABA and somatostatin? I proposed the hypothesis that the diversification of somatostatin-expressing interneuron types and the selective spatial distribution of their axons predict that GABA and somatostatin are released with different temporal dynamics from different GABAergic cells acting at distinct subcellular sites.

To test this, I recorded the *in vivo* spike-timing of single GABAergic cells extracellularly in freely moving rats (Lapray et al., 2012) and labelled the cells by the juxtacellular labelling technique (Pinault, 1996). I have identified five dendrite-targeting interneurons expressing somatostatin: two bistratified and three O-LM cells. Using existing methods and also developing new analysis, I investigated the activity patterns of these interneurons, together with similar cells recorded by others in the laboratory, during different behaviours.

5.2 Spike-timing of bistratified and O-LM cells in freely moving rats

The recording and labelling of single cells was performed using a glass electrode in the dorsal CA1 of drug-free rats during sleep, movement and quiet wakefulness, as described in previous chapters. I revealed the dendritic and axonal arborisations of the labelled interneurons and tested them for the expression of cell-type specific

combinations of molecules using immunohistochemistry. From a population of fifty putative GABAergic cells (Table 3.1) I have identified five as somatostatin- and/or NPY-expressing dendrite-targeting interneurons, which, based on the axonal arborisations, were either bistratified (n=2, Table 3.1, Table 5.1; LK20p and LK27d) or O-LM cells (n=3, Table 3.1, Table 5.1; LK01ab, LK06ah and LK13k). In order to facilitate the generalisation of my results over a larger dataset, I have analysed additional three bistratified cells (Table 5.1, Table 5.2; K202j, TV21f, TV30d) and one O-LM cell (Table 5.1, Table 5.2; ZsB43d) recorded by colleagues in the group. In this chapter I present data obtained from a total of five bistratified and four O-LM cells, recorded over an area of 1.7 x 1.4 mm along the rostro-caudal and medio-lateral axes of the hippocampal CA1 area (Figure 5-1). These data were also reported in Katona et al. (2014).

5.2.1 Input and output synaptic organisation of bistratified and O-LM cells in the CA1 area

Bistratified cell somata (n=4/5 recovered) located in stratum pyramidale or at the border with stratum oriens (Figure 5-1, Figure 5-2A,G) gave rise to mainly radially branching dendritic trees (n=3/5 recovered; note exception Figure 5-2G) and the axon collaterals invaded strata oriens and radiatum (n=3/5 recovered). When measured, the axonal extent of a well-labelled cell (Figure 5-2A) was 2.4 mm medio-laterally and 1.7 mm rostro-caudally, confirming previous results obtained *in vivo* (Klausberger et al., 2004). Cell bodies (n=4/4 tested) were immunopositive for NPY (Figure 5-2B,I and Table 5.1) and dendrites and the axon expressed parvalbumin (PV, Figure 5-2C,H). Only axon and some dendrites were recovered from the fifth interneuron (TV30d). The latter were immunopositive for parvalbumin (Table 5.1), which together with the axonal distribution let me identify the neuron as a bistratified cell. When tested, somata

were immunopositive for somatostatin (n=3/4 tested, Figure 5-2B) (Klausberger et al., 2004), for the metabotropic glutamate receptor type 1 alpha (mGluR1a ; n=1/2 tested) and one expressed the transcription factor Satb1 (Huang et al., 2011) (n=1/3 tested, Table 5.1). The somatic and dendritic membranes of all three tested bistratified cells were enriched in tyrosine-protein kinase receptor ErbB4 (Fazzari et al., 2010) (Figure 5-2D).

O-LM cells (n=4) with horizontal spiny dendrites (n=4/4 recovered) were recorded in stratum oriens (Figure 5-1, Figure 5-4A), and had main axons running into stratum lacunosum moleculare (n=3/4 recovered) arborizing densely within the layer (Figure 5-4A). The axon of a well labelled O-LM cell (Figure 5-4A) measured 0.6 mm medio-laterally and 1.1 mm rostro-caudally. Because of weak labelling, for one O-LM cell (LK01ab) I only recovered the cell body and some dendrites. When tested, all somata (n=4/4 tested) were immunopositive for somatostatin (Figure 5-4B) and, together with the dendrites, their membranes were enriched in mGluR1a (Figure 5-4D) and decorated by the metabotropic glutamate receptor type 7 alpha (mGluR7a) immunopositive boutons (4/4 tested, Table 5.1). O-LM cells were immunopositive for parvalbumin (n=3/4 tested) (Figure 5-4C), for the zinc finger protein transcription factor Fog-2 (Zfpm2, n=3/3 tested) (Figure 5-4E) and for the extracellular leucine-rich repeat fibronectin containing protein type 1 (Elfn1, n= 2/2 tested) (Sylwestrak and Ghosh, 2012) (Figure 5-4F). I have not found calbindin or NPY expression in any of the tested O-LM cells (Table 5.1).

In contrast to their similar horizontal axonal length, the transmitter releasing terminals of bistratified and O-LM cells are nearly completely separated in different layers, paralleling different glutamatergic inputs to pyramidal cells on segregated dendritic membrane domains. In order to test the hypothesis that spatial segregation

correlates with differences in spike-timing, I first segmented the recorded action potential time series according to sleep, movement and quiet wakefulness, and then I compared the cell types in terms of their firing dynamics during these different behavioural states (Table 5.2-Table 5.5). For the extraction of behaviourally relevant time windows I performed quantitative analyses (Lapray et al., 2012) of motion tracking and of local field potential (LFP) measurements in the cortex and in the hippocampus (Figure 5-2E,F, Figure 5-4G,H).

5.2.2 Behavioural-dependent firing rates and spiking patterns of GABAergic interneurons

Seeking for novel *in vivo* functional relationships between hippocampal interneurons, I compared the firing rates of the dendrite-targeting PV+ and somatostatin-expressing bistratified and O-LM cells with the recently reported firing rates of PV+ basket cells (Lapray et al., 2012). The latter is a type of interneuron that targets cell bodies and proximal dendrites and does not express any known neuropeptides. One of the five published PV+ basket cells (LK08c) was recorded and analysed by me and presented in the previous chapter (Figure 4-1, Figure 4-2 and Table 4.1-Table 4.3). Specifically, I aimed to reveal the effects movement and sleep may have on the activity of the three cell types (Table 5.3-Table 5.5).

Behavioural states, such as movement and sleep, influence the firing rates of bistratified (n=5), O-LM (n=4) and PV+ basket cells (n=5) (Lapray et al., 2012) differently (repeated-measures ANOVA, $F_{2,10}=4.81$, $p=0.0343$ for the interaction between the factors cell type and behavioural state; Figure 5-5A and Table 5.2, Table 5.3). During sleep, the mean firing rates of both bistratified and PV+ basket cells were significantly higher by 16.9 and 19.2 Hz, respectively, than that of O-LM cells

(t(10)=2.35, p=0.0407, for bistratified cells; t(10)=2.75, p=0.0204, for PV+ basket cells). As expected, most ISIs (Figure 5-5B, Figure 5-6) of bistratified cells corresponded to high instantaneous firing frequencies (IFs) (5-12 Hz, 7.5%; 12-30 Hz, 11.9%; 30-100 Hz, 36.4%; 100-250 Hz, 35.1%; Figure 5-3B) as further evidenced by a peak in close proximity to zero in the autocorrelograms (Figure 5-5B and Figure 5-6). In contrast, ISIs of O-LM cells were more often in the theta and beta frequency ranges (5-12 Hz, 25.5%; 12-30 Hz, 25.3%; 30-100 Hz, 29.9%; 100-250 Hz, 8.8%).

During movement, the autocorrelograms of both bistratified and O-LM cells presented repetitive peaks every 150 ms (Figure 5-5B, Figure 5-6), demonstrating theta-rhythmic firing. During these time periods the instantaneous firing rate of the neurons was frequently in the gamma range (30-100 Hz, 42.2% and 50.4%, respectively). Bistratified cells (29.2%), but not O-LM cells (5.2%), discharged repeatedly with ISIs shorter than 10 ms (IF>100 Hz; Figure 5-3A). Moreover, the mean firing rate of bistratified and O-LM cells was higher during movement than that during sleep, by 25.1% and 75.6%, respectively. Conversely, PV+ basket cells decreased their mean firing rates during movement by 22.9% as compared to sleep.

Despite these observations, *post hoc* pairwise comparisons showed no significant difference (Table 5.3, p>0.05) between the movement-related mean firing rates (Figure 5-5A) or between the quiet wakefulness-related mean firing rates (Table 5.4) of the different interneuron types. Nor did the evident difference between the mean firing rate of cell types during movement as compared to their firing rates during sleep reach statistical significance levels (Table 5.3, p>0.05), which could be due to the large cell to cell variability. Thus, the changes in firing rates of bistratified, O-LM and basket cells were cell-type specific and behaviour-dependent.

5.2.3 Differential recruitment of bistratified, O-LM and PV+ basket cells during hippocampal network oscillations

At specific times during behaviour, in the hippocampus, distinct rhythmic network activities emerge from the cooperative activity of specialised neuronal assemblies. Using quantitative detection criteria (Lapray et al., 2012), each behavioural state can be segmented into epochs of such rhythmic network events. In our LFP measurements, I have detected theta oscillations (5-12 Hz, Figure 5-2E, Figure 5-4G) during movement, sharp wave associated ripples (SWRs, 130-230 Hz, Figure 5-2F, Figure 5-4H, Figure 5-8A,B) during sleep and wakefulness, and low oscillatory periods (LOSC) which are often associated with state transitions (Lapray et al., 2012). The participation of GABAergic interneurons in oscillatory network events might be reflected in their firing rates.

Firing rates and spiking patterns

The mean firing rates of bistratified (n=5), O-LM (n=4) and PV+ basket cells (n=5) (Lapray et al., 2012) were different during theta oscillations, SWRs and LOSC (repeated-measures ANOVA, $F_{4,21}=22.27$, $p<0.0001$ for the interaction between the factors cell type and network-oscillatory state; Figure 5-7A and Table 5.2, Table 5.3). During SWRs, the mean firing rates of bistratified and PV+ basket cells were significantly higher by 94.6 Hz and 109.6 Hz, respectively, than that of O-LM cells ($t(21)=8.75$, $p<0.0001$, for bistratified cells; $t(21)=10.14$, $p<0.0001$, for PV+ basket cells). As confirmed by the ISI distributions and the autocorrelograms (Figure 5-7C), the discharge of bistratified cells corresponded to IFs above 100 Hz (ISI 4 to 10 ms, 67% of n=1486), in contrast, O-LM cells fired much less in this high frequency range (33.8% of n=86).

During theta oscillations (Figure 5-7C), the cells were spiking rhythmically and the largest proportions of ISIs for both bistratified and O-LM cells were within 10 to 33 ms corresponding to the gamma frequency range (41.4% and 44.2%, respectively). Consequently, the mean firing rate of bistratified cells was significantly (by 73.3%) decreased ($t(21)=7.45$, $p<0.0001$), whereas the mean firing rate of O-LM cells was strongly (by 55.7%) increased, as compared to mean firing rates during SWRs. During LOSC, the two cell types had similar spiking patterns to those during theta oscillations (Figure 5-7C). Furthermore, the mean firing rates between cell types during theta oscillations or during LOSC (Table 5.3, repeated-measures ANOVA, *post hoc* pairwise comparisons) were not significantly different. Thus, the mean firing rates of these GABAergic neurons were influenced differentially by distinct network oscillatory states.

Firing during theta- and ripple oscillations

The specialised spike-timing of GABAergic interneurons can also be analysed relative to the phase of theta oscillatory cycles, reflecting on their postsynaptic effects on pyramidal cells, which fire strongest, on average, at the trough of theta oscillations (Buzsaki, 2006). I determined that the two somatostatin-expressing interneurons also fired mostly around the trough of theta oscillations recorded in strata pyramidale or oriens (Figure 5-7B and Table 5.2). The mean theta phases of bistratified (2.4°±19.4°, mean angle ± angular deviation; n=5) and O-LM cells (341.6°±10.1°; n=4) did not differ significantly [permutation test (Tukker et al., 2007)], difference 20.8°, $p=0.1508$). Furthermore, the mean strength of phase coupling ($r=0.33$, for both) was also similarly high (permutation test, difference 0.0009, $p=1$) for the two cell types (Figure 5-7B and Table 5.2). Next, I have compared these parameters to those reported for PV+ basket

cells (mean angle=288.5°±44.4, mean r=0.15; n=5; Figure 5-7B) (Lapray et al., 2012). The pooled phase angle and coupling strength of the neuropeptide-expressing interneurons differed from those of PV+ basket cells (permutation tests, mean phase difference, 64.4°, p=0.005; mean strength of phase coupling difference 0.1685, p=0.0315).

Alternatively, I studied the firing dynamics of bistratified and O-LM cells during SWRs, recorded either during sleep or wakefulness. Bistratified cells increased their firing rate strongly during SWRs (Figure 5-8A,D). In contrast O-LM cells were mostly silent during SWR events (Figure 5-8B,E). Using repeated-measures ANOVA ($F_{1,5}$=7.64, p=0.0396 for the interaction between the factors cell type and behavioural state), I showed that bistratified cells (n=5) fired significantly more spikes per SWR than O-LM cells (n=4) (Figure 5-8C and Table 5.2-Table 5.4) during both sleep (t(5)=7.0, p=0.0009, mean difference 4.6) and wakefulness (t(5)=5.62, p=0.0025, mean difference 3.4). O-LM, but not bistratified cells, had higher SWR-related spike count during wakefulness compared to sleep (t(5)=3.62, p=0.0152, mean difference 1.3, for O-LM cells; t(5)=-0.5, p=0.6410, mean difference 0.9, for bistratified cells).

The firing probability of bistratified cells was higher during SWRs than during periods of ±0.5s before and after SWRs (Figure 5-8D). The firing rate during SWRs was 2 to 6 times higher (cumulative distribution functions, CDFs, p<0.05 for n=4 cells during *sleep*; p<0.05 for n=4 cells during *wakefulness*; Figure 5-8F, Figure 5-9A and Table 5.2) than expected from the activity outside SWR time periods. In contrast, on average, O-LM cells did not change their overall firing probability during SWRs (Figure 5-8E). However, I have observed decreased or rarely increased firing rates during individual SWRs, and individual O-LM cells also slightly but significantly changed firing rates during SWRs in either directions (e.g., LK13k). During wakefulness, the firing rate

during SWRs was significantly lower for one O-LM cell and higher for the other three cells than during sleep-SWRs (cumulative distribution functions, $p<0.05$ for n=4 cells; Figure 5-8G, Figure 5-9B and Table 5.2). During sleep-SWRs, the mean rates were significantly decreased for two cells and increased for one cell (cumulative distribution functions, $p<0.05$ for n=3 cells; Figure 5-8G, Figure 5-9B and Table 5.2).

High frequency firing and potential peptide release

High frequency action potential bursts are potential predictors of neuropeptide release. Next I investigated when could GABA/somatostatin be co-released by bistratified (n=5) and O-LM cells (n=4) based on their "burst-firing" during SWRs or theta oscillatory cycles. I detected action potential burst patterns in the spike trains of each cell, consisting of at least *three* consecutive action potentials of ISIs, each ≤12 ms during individual oscillatory network events. Bistratified cells fired such bursts (Figure 5-2E,F, Figure 5-8A) during 55.2 ± 4.7% of events (mean ± s.e.m.) overall, significantly more (repeated-measures ANOVA, $F_{1,7}=56.24$, $p=0.0001$, for the factor cell type) than O-LM cells (Figure 5-4G,H, Figure 5-8B), which rarely emitted such bursts (2.7 ± 5.2%). This difference in the probability of bursting between bistratified and O-LM cells was independent of the network oscillatory event (Table 5.3, Table 5.4). I found similar differences also when testing for the occurrence of *four* consecutive action potentials having each ISI ≤12 ms. Furthermore, bistratified cells fired bursts of three action potentials more frequently (2.8 ± 0.7 Hz; mean ± s.e.m.) than O-LM cells (0.4 ± 0.7 Hz), independent of behaviour (repeated-measures ANOVA, $F_{1,7}=5.90$, $p=0.0455$ for the factor cell type), suggesting that bistratified, but not O-LM cells, may release neuropeptides during both movement and sleep. Thus, O-LM cells may be more

selective in their release of somatostatin compared to bistratified cells during different behaviours.

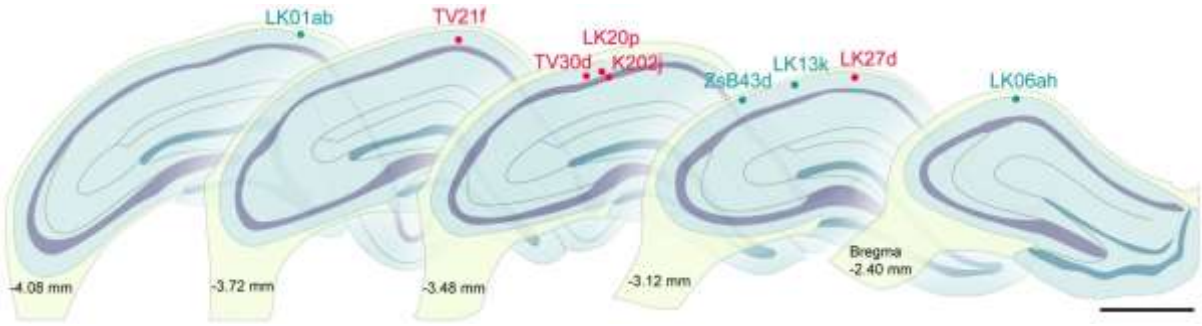

Figure 5-1 Recording locations of labelled bistratified (red, n=5) and O-LM (blue, n=4) cells in the CA1 area.

Location of individual somata in strata oriens and pyramidale are shown in schematic coronal sections from rostral to caudal direction, from left to right of the right hemisphere. Dark shaded areas delineate the pyramidal cell layer and the granule cell layer (blue) in the dentate gyrus. Scale bar, 1 mm.

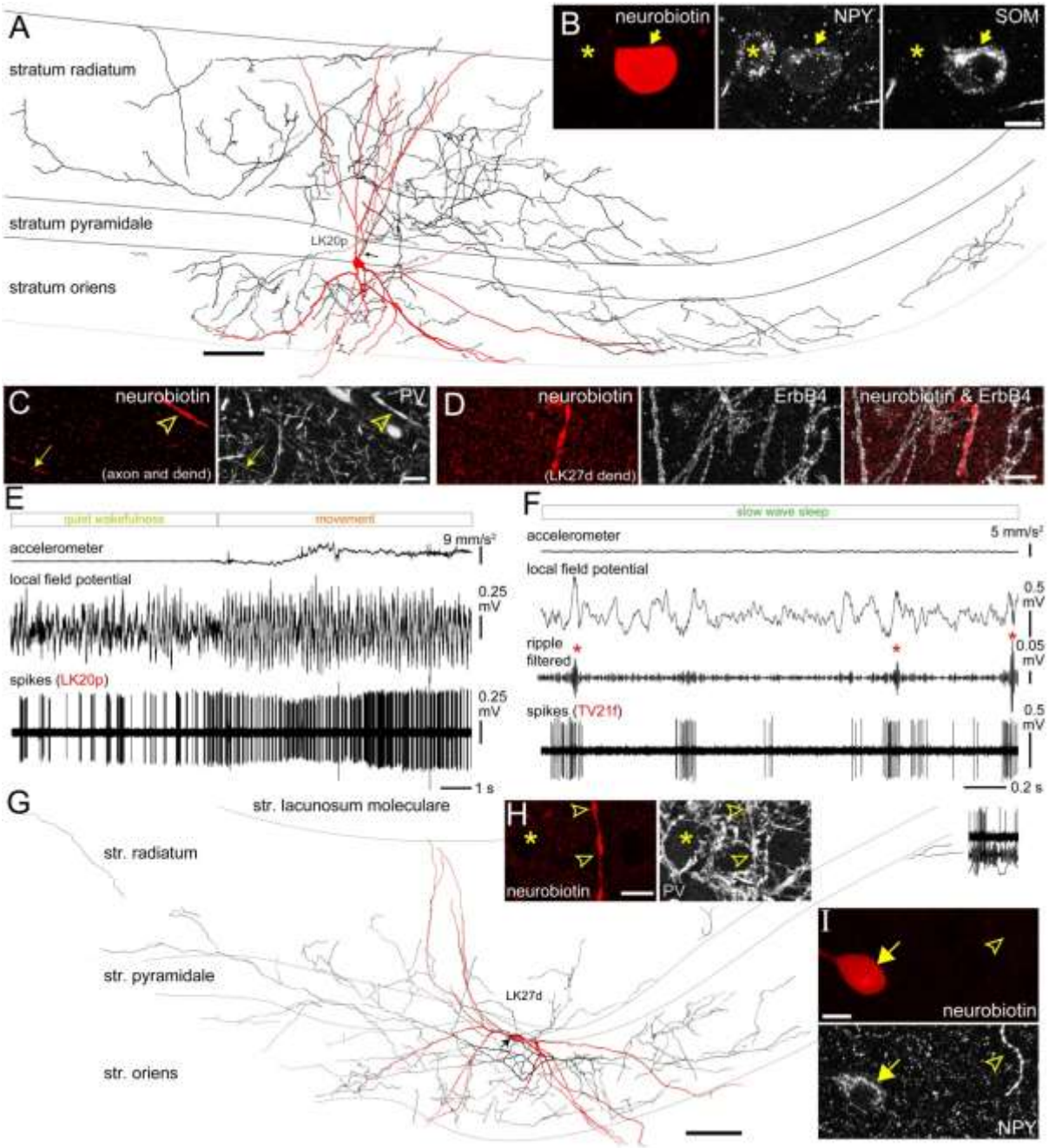
A
stratum radiatum
stratum pyramidale
stratum oriens
LK20p
B
neurobiotin
NPY
SOM
C
neurobiotin
(axon and dend)
PV
D
neurobiotin
(LK27d dend)
ErbB4
neurobiotin & ErbB4
E
quiet wakefulness
movement
accelerometer
9 mm/s²
local field potential
0.25 mV
spikes (LK20p)
0.25 mV
1 s
F
slow wave sleep
accelerometer
5 mm/s²
local field potential
0.5 mV
ripple filtered
0.05 mV
spikes (TV21f)
0.5 mV
0.2 s
G
str. lacunosum moleculare
str. radiatum
str. pyramidale
str. oriens
LK27d
H
neurobiotin
PV
I
neurobiotin
NPY

Figure 5-2 Behaviour-related activity patterns of identified bistratified cells.

A. Reconstruction of the soma, complete dendritic tree (red, n=11 sections) and representative part of the axon (black, 3 out of 24 70-μm-thick sections; axonal origin, arrow). Note the selective axonal arborisation in strata oriens and radiatum, avoiding strata pyramidale and lacunosum-moleculare. **B.** The cell body (arrow) was immunopositive for NPY and somatostatin; a neighbouring neuron (asterisk) was immunopositive only for NPY (confocal microscopy; single optical section, 0.7 μm). **C.** The dendrite (arrowhead) and axon (arrow) were immunopositive for parvalbumin (maximum intensity projection, z-stack, height 5.2 μm). **D.** The dendritic membrane of another labelled bistratified cell (LK27d, G) contained high levels of ErbB4 receptor (maximum intensity projection, z-stack, height 15.0 μm). **E.** The bistratified cell increased its firing rate and changed to a more regular rhythmic pattern at behavioural transition from quiet wakefulness to movement. **F.** Action potentials of another identified bistratified cell (TV21f) during slow wave sleep. Note the SWRs-related (asterisks) strong increases in the firing rate. **G.** Reconstruction of the soma, complete dendritic tree (red, n=9 70-μm-thick sections) and representative part of the axon (black, 3 out of 20 70-μm-thick sections; axonal origin, arrow) of a horizontal bistratified cell. Note the preference in the axonal innervation towards stratum oriens. Collaterals also entered stratum radiatum but to a much lower extent. **H.** The dendrite (arrowheads) was immunopositive for parvalbumin (maximum intensity projection, z-stack, height 3.1 μm). **I.** The cell body (arrow) and a neighbouring non-labelled axon (arrowhead) were immunopositive for NPY. (maximum intensity projection, z-stack, height 3.9 μm). Scale bars, A,G 100 μm; B,C,D,H,I 10 μm. See also Figure 5-1.

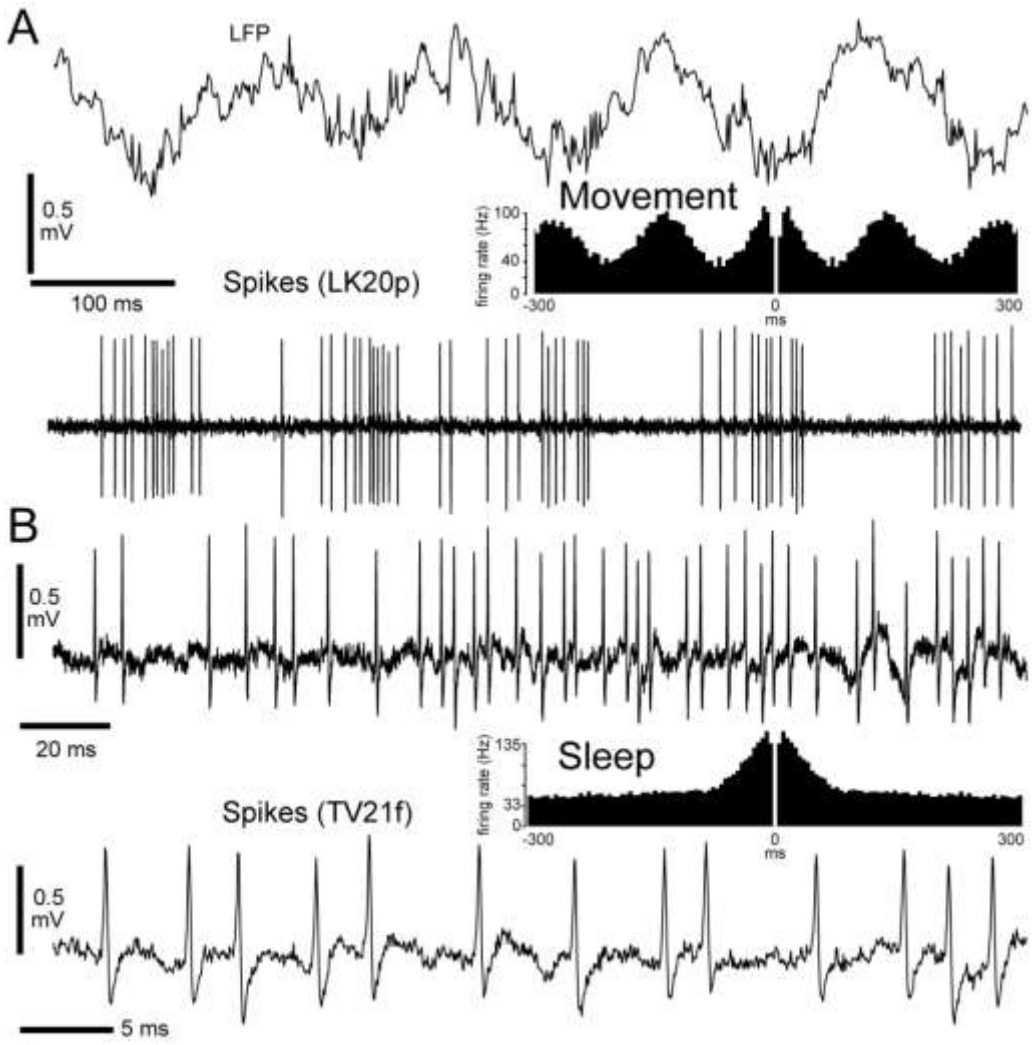

Figure 5-3 Firing patterns of bistratified cells during movement and sleep demonstrating short inter-spike intervals.

A. Spike train of a bistratified cell during movement. Note preferential timing of most spikes around the trough of the theta-oscillatory LFP (band-pass filtered 0.3-500 Hz). Inset, autocorrelogram of the interneuron. Note refractory period (5 ms time bins). **B.** Top, spike train of a bistratified cell during sleep (band-pass filtered 0.8-8 kHz). Bottom, spike train at higher temporal resolution revealing uniform spike shapes. Inset, autocorrelogram of the interneuron. Note refractory period (5 ms time bins).

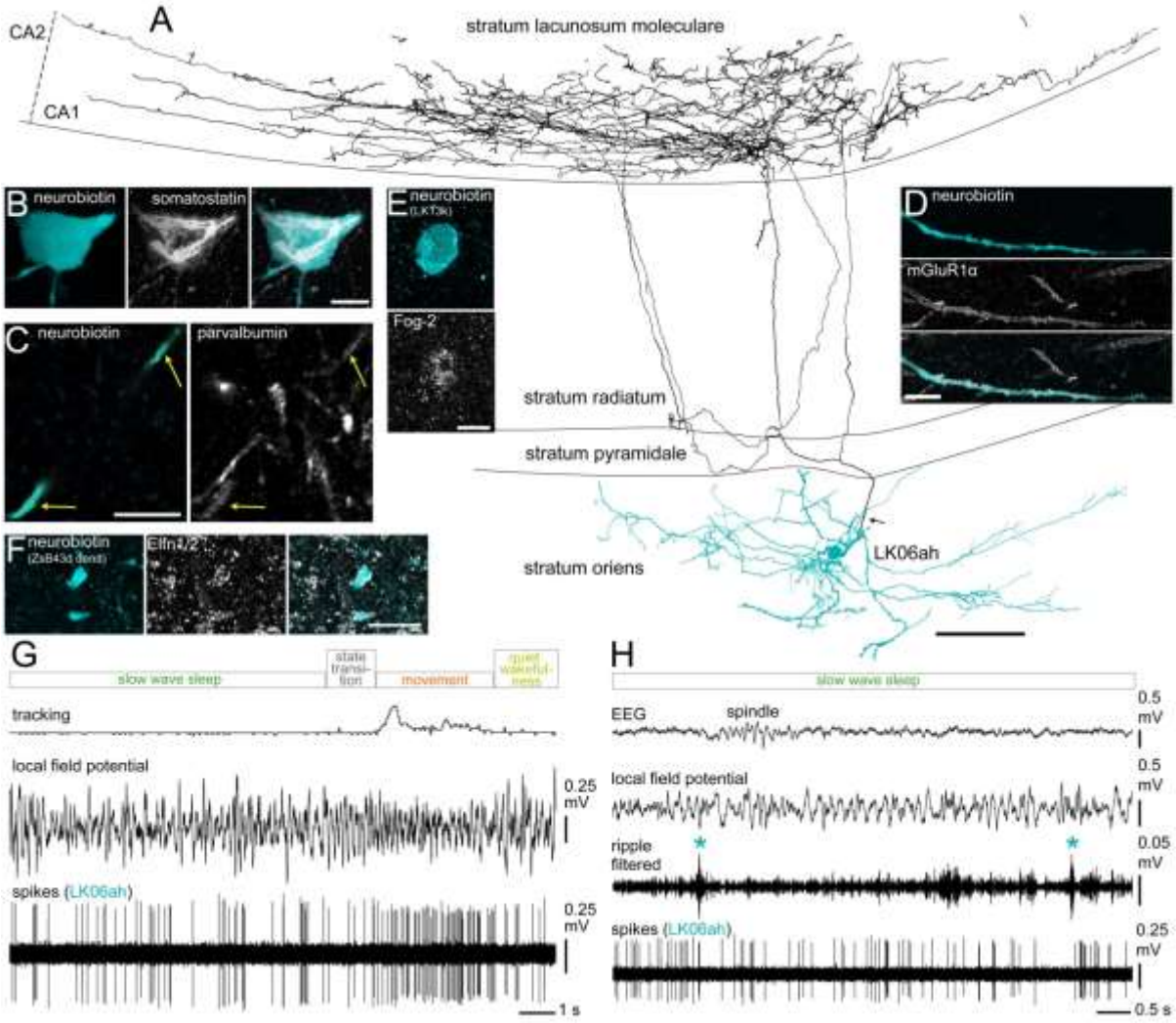

Figure 5-4 Behaviour-related activity patterns of identified O-LM cells.

A. Reconstruction of the soma, complete dendritic tree (blue, n=11 sections) and representative axon collaterals (black, 3 out of 15 70-μm-thick sections; the main axon originated from a dendrite, arrow). Note the dense axonal plexus in stratum lacunosum moleculare, and the lack of innervation of other layers. **B.** The cell body was immunopositive for somatostatin (depth-cued projection z-stack, height 28.7 μm). **C.** Dendrites (arrows) contained low levels of parvalbumin immunoreactivity (projection of two non-consecutive optical sections, 0.7 μm each). **D.** The dendritic membrane was enriched in mGluR1a (maximum intensity projection z-stack, height 2.0 μm). **E.** Fog-2 was detected in the cell body of another identified O-LM cell (single optical section, 0.7 μm). **F.** The dendrites of another recorded O-LM cell (ZsB43d) were immunopositive for Elfn1 (single optical section, 0.7 μm). Scale bars, A, 100 μm; B-F 10 μm. **G, H.** The rhythmic firing of the O-LM cell during movement (G) became irregular during slow wave sleep (H). The cell did not appear to change its activity in relation to SWRs (asterisks). See also Figure 5-1.

Table 5.1 Molecular expression profiles of interneurons.

		Immunohistochemical test									
Cell type	**Cell**	SOM	NPY	PV	CB	mGluR1a	mGluR7a	Elfn1/2	ErbB4	Fog-2	Satb1
Bistratified cells	K202j	+ s	+ s	+ s	nt	nt	nt	nt	nt	nt	nt
	LK20p	+ s, d	+ s	+ s, d	- d	- s,d	nt	- d	+ d	nt	+ s
	LK27d	nc s	+ s	+ s, d	nc s	- d	- d	- d	+ d	- s	nc s
	TV21f	+ s	+ s	+ s	nc s	+ s	nt	nt	nt	- s	nc s
	TV30d	nc a	nc a	+ d	nt	nc d	nt	nt	+ d	nt	nt
O-LM cells	LK01ab	+ s,d	- s	+ d	nc s	+ s,d	+ d	nt	nt	nc s	nt
	LK06ah	+ s,d	- s	+ d	- s,d	+ d	+ d	nt	nt	+ s	nt
	LK13k	+ s	- s	+ d	- s,d	+ s,d	+ d	+ d	nt	+ s	nt
	ZsB43d	+ s	- s	- s,d	- s	+ d	+ d	+ d	nt	+ s	nt

+, immunopositive; -, no immunoreactivity detected in the cell, while other immunopositive cells were documented nearby; nc, not conclusive; nt, not tested; s,d,a, tested on soma, dendrite or axon.

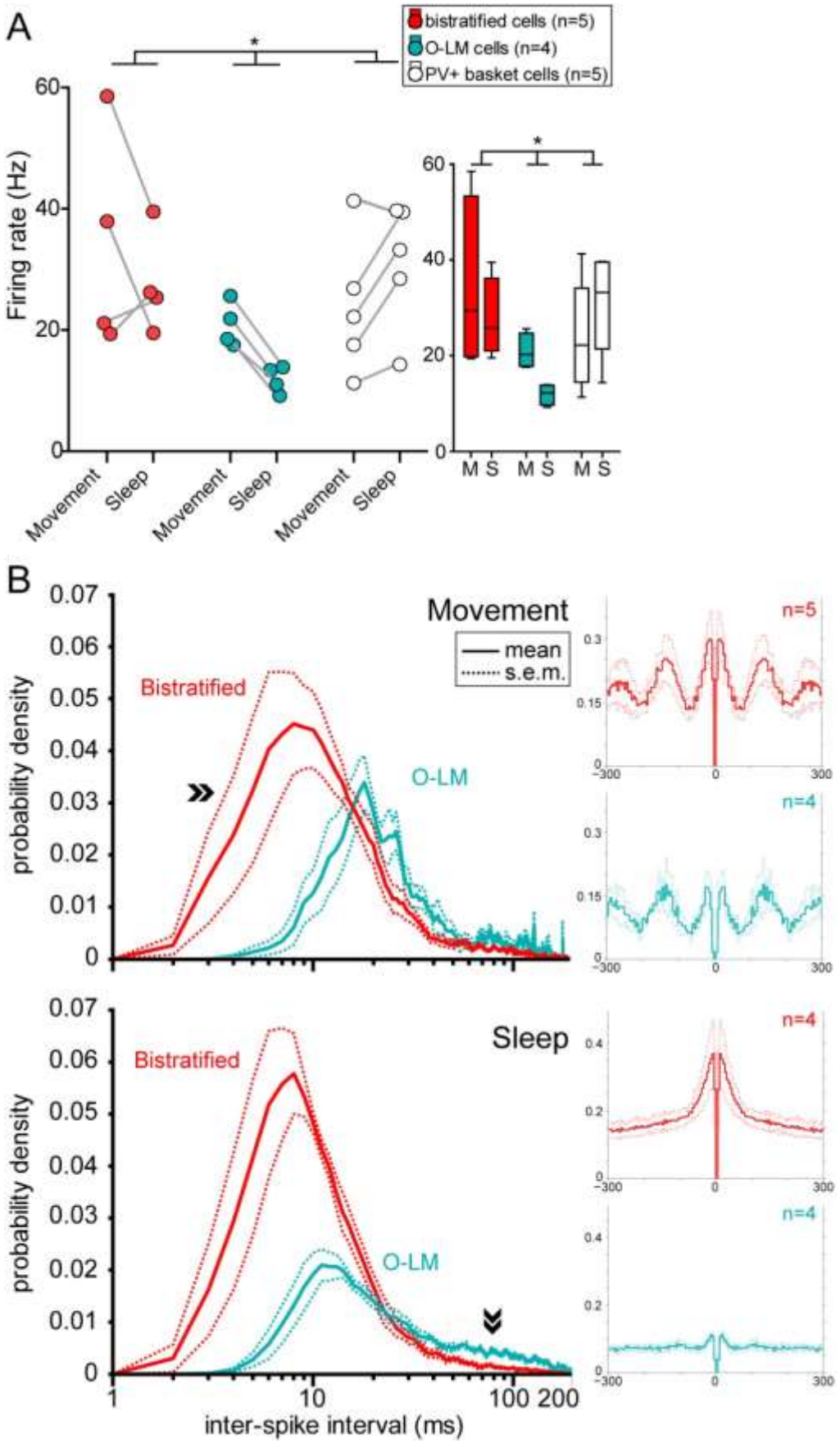
A
bistratified cells (n=5)
O-LM cells (n=4)
PV+ basket cells (n=5)
Firing rate (Hz)
Movement
Sleep
M S
B
Movement
Sleep
mean
s.e.m.
Bistratified
O-LM
probability density
inter-spike interval (ms)
n=5
n=4

Figure 5-5 Behavioural-state-dependent firing patterns of bistratified, O-LM and PV+ basket cells.

A. *Left*, The differences in firing rates between cell types changed with behavioural states (repeated-measures ANOVA, $F_{2,10}$=4.81, p=0.0343 for the interaction between the factors cell type and behavioural state). *Right*, box plot of cell-type and behavioural-state-dependent firing rates (horizontal line, median); M, movement; S, sleep. **B.** Inter-spike interval distributions and autocorrelograms (mean ± s.e.m.) of bistratified (red) and O-LM (blue) cells during movement (top) and sleep (bottom). *Top*, during movement, the largest proportion of inter-spike intervals of bistratified (42.2%) and O-LM cells (50.4%) were between 10 to 33 ms corresponding to gamma frequency firing (30-100 Hz). Bistratified cells, but not O-LM cells, fired frequently (29.2%) with <10 ms intervals (>100 Hz, arrowheads). Note repetitive peaks in the autocorrelograms at every 150 ms. *Bottom*, during sleep, bistratified cells fired most frequently within fast frequency ranges (30-100 Hz and 100-250 Hz) discharging action potentials at intervals as short as 4 to 33 ms. In contrast, O-LM cells, fired proportionally mostly at lower instantaneous frequencies with 10 to 200 ms intervals (arrowheads). Note logarithmic time scales for ISI plots limited to 200 ms and time axis on the autocorrelograms limited to 300 ms, bin width was set to 5 ms. See also Figure 5-6 and Table 5.5.

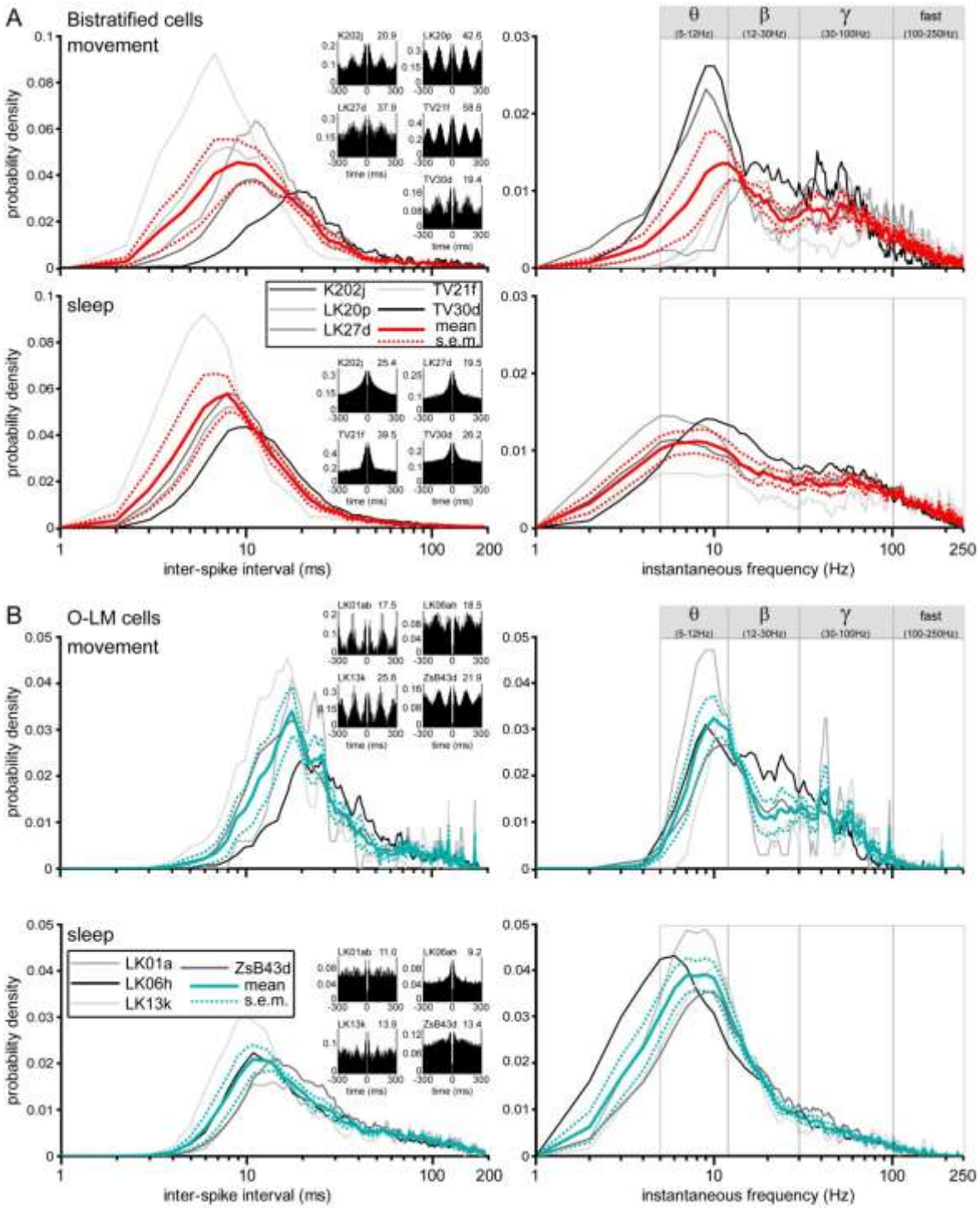
A
Bistratified cells
movement
sleep
probability density
K202j
LK20p
LK27d
TV21f
TV30d
mean
s.e.m.
θ
β
γ
fast
(5-12Hz)
(12-30Hz)
(30-100Hz)
(100-250Hz)
inter-spike interval (ms)
instantaneous frequency (Hz)
B
O-LM cells
movement
sleep
LK01a
LK06h
LK13k
ZsB43d
mean
s.e.m.
inter-spike interval (ms)
instantaneous frequency (Hz)

Figure 5-6 Individual inter-spike interval (ISI) and instantaneous frequency (IF) distributions and autocorrelograms of bistratified and O-LM cells.

A. *Left*, ISI distributions and inset autocorrelograms (mean ± s.e.m., solid and dashed lines) from all bistratified cells (individual cells, shades of grey; mean red) were calculated during sleep (top, n=4 cells) and movement (bottom, n=5 cells). Individual ISI distributions were more similar during sleep than during movement; TV21f had shorter ISIs than the other bistratified cells. *Right*, corresponding IF distributions across frequency ranges. **B.** *Left*, ISI distributions and inset autocorrelograms (mean ± s.e.m., solid and dashed lines) from all O-LM cells (individual cells, shades of grey; mean blue) were calculated during sleep (top, n=4 cells) and movement (bottom, n=4 cells). Distributions were more similar during sleep than movement. *Right*, corresponding IF distributions. Note logarithmic time and frequency scales limited to 200 ms and 250 Hz, respectively and time axis on the autocorrelograms limited to 300 ms, bin width was set to 5 ms.

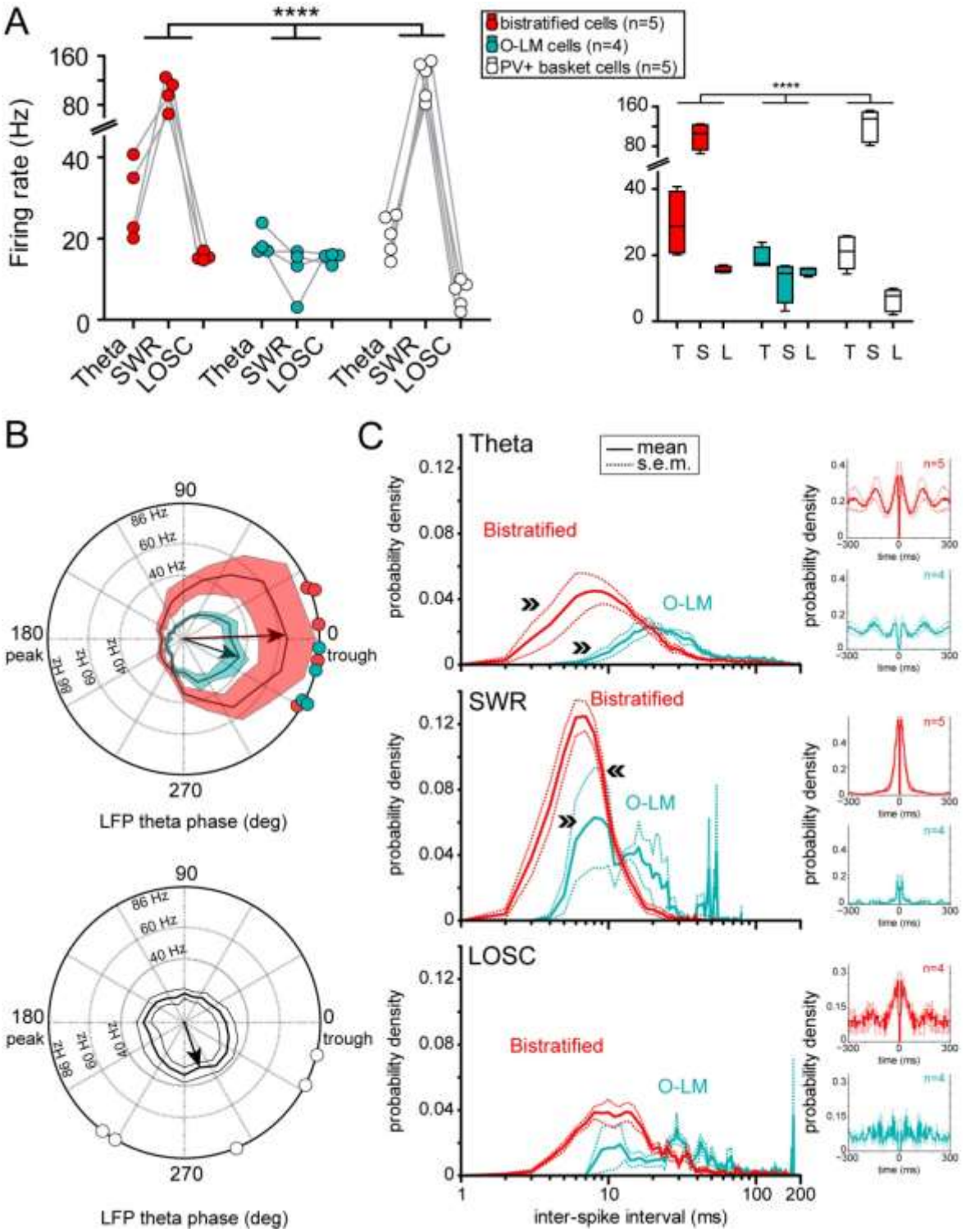
A
****
bistratified cells (n=5)
O-LM cells (n=4)
PV+ basket cells (n=5)
Firing rate (Hz)
160
80
40
20
0
Theta
SWR
LOSC
T S L
B
90
180
peak
0
trough
270
86 Hz
60 Hz
40 Hz
LFP theta phase (deg)
C
Theta
mean
s.e.m.
Bistratified
O-LM
SWR
LOSC
probability density
0.12
0.08
0.04
n=5
n=4
time (ms)
1
10
100
200
inter-spike interval (ms)

Figure 5-7 Activity of bistratified, O-LM and PV+ basket cells during hippocampal network oscillations.

A. *Left*, Different network-oscillatory states had different effects on the mean firing rates (repeated-measures ANOVA, $F_{4,21}=22.27$, $p<0.0001$ for the interaction between the factors cell type and network-oscillatory state). *Right*, box plot of cell-type-specific and oscillatory-state-dependent firing rates; T, theta oscillations; S, SWRs; L, LOSC. **B.** Preferred firing phases of bistratified, O-LM (top) and PV+ basket cells (bottom) during theta oscillations. *Top*, bistratified (red circles, individual cells; dark coloured line, mean frequency; red area, s.e.m.) and O-LM cells (blue circles and area) increased their firing probability around the trough of the theta cycle. The mean phase difference (20°) between the cell types (arrows) was not significant (permutation test, p=0.1508). The mean strength of phase coupling (r=0.33, for both) was similarly strong for both cell types. *Bottom*, conversely, PV+ basket cells (white circles and area) fired at significantly earlier phases of the theta cycle (permutation test, p=0.005) and showed weaker phase coupling (r=0.15). **C.** Inter-spike interval distributions and autocorrelograms of bistratified (red) and O-LM (blue) cells during theta oscillations (top), SWRs (middle) and LOSC (bottom). *Top*, during theta oscillations, bistratified cells fired spikes mostly (70.6%) at intervals between 4 to 33 ms corresponding to fast instantaneous firing frequencies (30-250 Hz, arrowheads); O-LM cells rarely fired within the 100-250 Hz range (4-10 ms, arrowheads, 3.3%). Note repetitive peaks in the autocorrelograms at every 150 ms. *Middle*, during SWRs, both cell types increased their instantaneous rates, although O-LM cells fired rarely. Bistratified cells fired mostly above 100 Hz (arrowheads, 67.0%), whereas a smaller proportion (33.8%) of O-LM cell inter-spike intervals were within 4 to 10 ms (100-250 Hz, arrowheads). *Bottom*, the distributions during LOSC were similar to those during theta oscillations. Note logarithmic time scales limited to 200 ms and time axis on the autocorrelograms limited to 300 ms, bin width was set to 5 ms. See also Table 5.5.

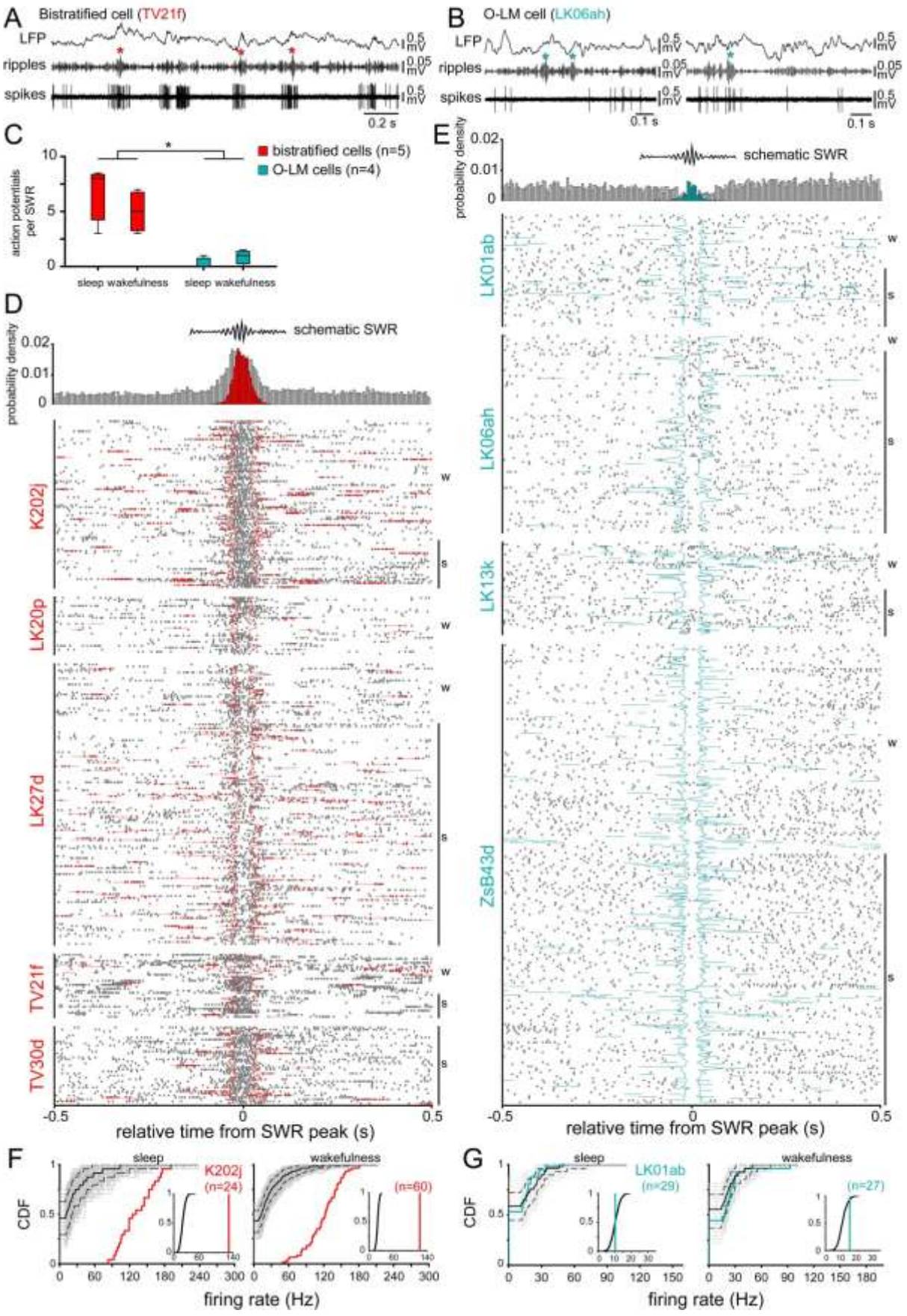
A
Bistratified cell (TV21f)
LFP
ripples
spikes
0.5 mV
0.05 mV
0.2 s
B
O-LM cell (LK06ah)
0.1 s
C
bistratified cells (n=5)
O-LM cells (n=4)
action potentials per SWR
sleep wakefulness
sleep wakefulness
D
schematic SWR
probability density
K202j
LK20p
LK27d
TV21f
TV30d
w
s
relative time from SWR peak (s)
E
LK01ab
LK06ah
LK13k
ZsB43d
F
sleep
wakefulness
K202j
(n=24)
(n=60)
CDF
firing rate (Hz)
G
LK01ab
(n=29)
(n=27)

Figure 5-8 Firing activity of bistratified and O-LM cells during SWRs.

A. Bistratified cells increased their firing rate strongly around and during SWRs (red asterisks). *Top*, LFP measured by the extracellular glass electrode in stratum pyramidale; *middle*, LFP band pass filtered (130-230 Hz); *bottom*, action potentials of the recorded and labelled bistratified cell. **B.** O-LM cells were silent during the majority (left), but not all (right) SWR events (blue asterisks, both periods during sleep). **C.** Comparison of mean spike count per SWR of bistratified (n=5) and O-LM cells (n=4) recorded during sleep and wakefulness. The difference in spike counts between cell types depended on the behavioural state during which the SWRs occurred (repeated-measures ANOVA, $F_{1,5}$=7.64, p=0.0396 for the interaction between the factors cell type and behavioural state). **D, E.** Raster plots and average firing probability (top) of bistratified (D) and O-LM (E) cells relative to SWR events (w, wakefulness; s, sleep). Bistratified, but not O-LM cells, fired with higher probability during SWRs (coloured bars in histogram) compared to the ± 0.5 s (grey) surrounding the peak of SWR events. Note that the increase in firing of bistratified cells during SWRs was often apparent before and continued after the events (see also raster plots). Overall, the firing probability of O-LM cells did not change during SWRs (blue bars in histogram); they decreased or rarely increased their firing probability. Spike raster plots were aligned to the peak SWR power. Coloured lines delineate the beginnings and ends of aligned SWRs and surrounding SWR episodes. **F, G.** Examples of SWR-related firing rates of bistratified and O-LM cells, during sleep (left) and wakefulness (right). The distribution of measured firing rates per individual SWR are displayed as cumulative distribution functions (CDF). The distribution of bistratified cell firing rates (red) was significantly different from the median (black) of the surrogate sets (2-sample Kolmogorov-Smirnov test , $p<0.05$), and the right shift demonstrates an increase over the full range of firing rates. Surrogate sets of 1000 firing rate-distributions (grey; median, solid black line; 95% confidence intervals, broken lines). *Insets*, comparison of mean SWR-related firing rate (coloured lines) with the distribution of surrogate mean SWR-related rates (black lines). The bistratified cell (red) was always strongly activated by the SWRs (relative to the surrogate CDF, $p<0.05$ for sleep; $p<0.05$ for wakefulness). The measured distribution of the O-LM cell was also significantly different from the median (black) of the surrogate set (2-sample Kolmogorov-Smirnov test, $p<0.05$). The shift to the left or right of the measured CDF over part of the surrogate firing rate range indicates decreased or increased firing of the O-LM cell, respectively. *Insets*, during sleep, the mean firing rate of the O-LM cell (blue) was not different from the surrogate distribution (black). In contrast, during the awake condition, the measured mean firing rate of the O-LM cell was significantly increased during SWRs (relative to the surrogate CDF, p=0.035). See also Figure 5-9.

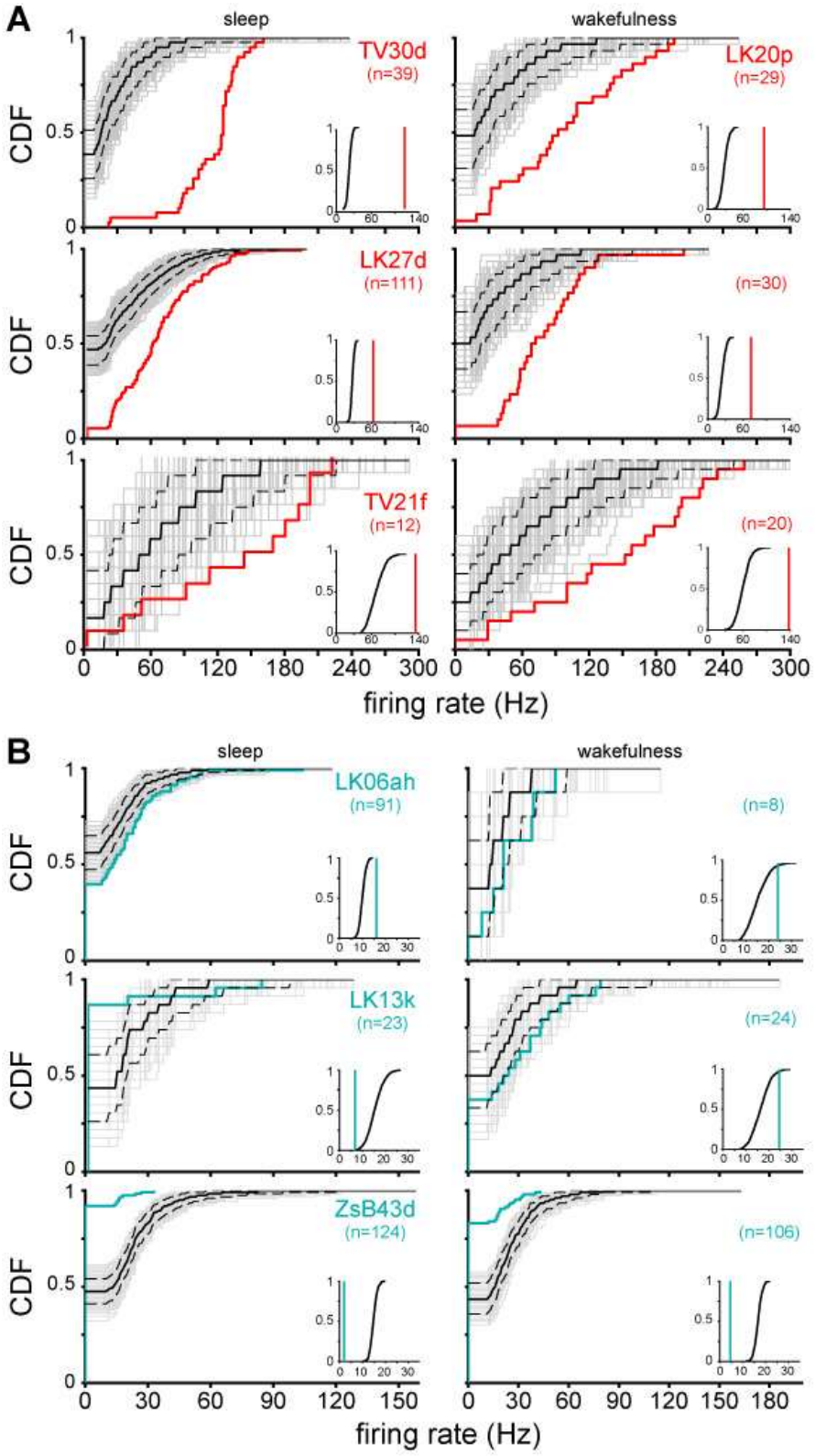
A
sleep
wakefulness
TV30d
(n=39)
LK20p
(n=29)
LK27d
(n=111)
(n=30)
TV21f
(n=12)
(n=20)
CDF
firing rate (Hz)
B
sleep
wakefulness
LK06ah
(n=91)
(n=8)
LK13k
(n=23)
(n=24)
ZsB43d
(n=124)
(n=106)
CDF
firing rate (Hz)

Figure 5-9 SWR-related firing rate distributions of bistratified and O-LM cells, during sleep and wakefulness.

A. Bistratified cells were activated by SWRs in all behavioural states (LK20p, no sleep period and TV30d no wakefulness recorded). The distribution of measured firing rates per individual SWR are displayed as CDFs. For bistratified cells, the measured distributions (red) were significantly different from the medians (black) of the surrogate sets (2-sample Kolmogorov-Smirnov tests, n=4 cells in total, $p<0.05$ for all cells), and the right shift demonstrates an increase over the full range of firing rates. *Insets*, comparison of mean SWR-related firing rate (red lines), for each cell, with the distribution of surrogate mean rates (black lines). Bistratified cells (red) were strongly activated by the SWRs, their measured mean rates were between 2 to 6 times higher than the means resulting from the surrogate distributions (relative to the CDFs for all four cells, $p<0.05$ for sleep; $p<0.05$ for wakefulness). **B.** O-LM cells changed significantly their firing rates during SWRs (2-sample Kolmogorov-Smirnov tests, n=3 cells in total, $p<0.05$, for all cells). The shift to the left or right of the measured CDFs (blue) relative to the median of the surrogate CDFs (grey) over the full or part of the surrogate firing rate range indicates decreased or increased firing of O-LM cells, respectively. Surrogate sets of 1000 firing rate-distributions (grey; median, solid black line; 95% confidence intervals, broken lines). *Insets*, comparison of mean SWR-related firing rate (blue lines), for each cell with the distribution of surrogate mean SWR-related rates (black lines). During *sleep*, the mean rates of LK13k and ZsB43d were decreased (probabilities given by CDFs, $p=0.004$ for LK13k, $p=0$ for ZsB43d) and the rate of LK06ah was increased (probability given by CDF, $p=0$). For cells LK06ah and LK13k in the *awake* condition, the measured rates were higher than those expected from the surrogate sets. *Insets*, comparison of mean SWR-related firing rates (blue lines) with the distribution of surrogate mean SWR-related rates (black lines). The rate of ZsB43d was decreased (relative to the CDF, $p=0$) and the rates of LK06ah and LK13k were increased (probabilities given by CDFs, $p=0.01$ for LK06ah; $p=0.009$ for LK13k) during SWRs. Note the differences in the dimensions of x axis between bistratified and O-LM cells in the insets.

Table 5.2 Firing rates and patterns of interneurons.

	Mean firing rate (Hz)								Mean number of spikes per SWR		SWR-activity index[b]	
Cell	**Movement**	**Sleep**	**Quiet wakefulness**	**Theta**	**SWRs**	**LOSC**	**Mean theta phase of firing (°)**	**Mean theta vector length of firing[a]**	**Slow wave sleep**	**Quiet wakefulness**	**Slow wave sleep**	**Quiet wakefulness**
Bistratified cells												
K202j	20.9	25.4	20.9	22.7	125.1	15.4	22.1±71.4	0.22	8.0	7.0	6.1	5.8
LK20p	42.6	NA	23.6	40.7	95.7	15.1	6.2±59.9	0.45	NA	4.0	NA	3.4
LK27d	37.9	19.5	32.2	34.9	65.2	17.0	350.9±66.3	0.33	3.0	3.0	2.3	3
TV21f	58.6	39.5	56.7	60.7	132.2	NA	21.3±60.8	0.44	8.5	6.0	2.1	2.3
TV30d	19.4	26.2	18.7	20.1	115.8	14.7	330.6±68.9	0.28	8.0	NA	5.2	NA
O-LM cells												
LK01ab	17.5	11.0	15.6	17.0	13.3	16.1	356.2±68.2	0.29	0.0	1.0	1	1.3
LK06ah	18.5	9.2	15.3	16.9	16.8	15.9	333.1±67.4	0.31	1.0	1.5	1.6	1.6
LK13k	25.6	13.9	22.3	23.9	15.5	13.4	346.1±59.4	0.46	0.0	1.0	0.4	1.5
ZsB43d	21.9	13.4	16.0	18.0	3.1	15.7	331.3±69.6	0.26	0.0	0.0	0.1	0.3

[a]theta modulation of firing [0,1], maximally correlated=1; see Experimental procedures in chapter 2.

[b]ratio of the mean firing rate during detected SWRs to the mean firing rate during the surrogate 'SWR' population.

Table 5.3 Statistical analyses.

Repeated-measures ANOVA of mean firing rates of bistratified (BIC), O-LM and PV+ basket (PVBC) cells during movement and sleep

Type 3 test of fixed effects

Effect	df	F	p
cell type	2,11	3.22	0.08
behavioural state	1,10	1.55	0.24
interaction	2,10	4.81	0.03

***Post hoc* pairwise comparisons**

	bistratified			O-LM			PV+ basket			movement vs sleep		
	df	t	p	df	t	p	df	t	p	df	t	P
BIC				10	2.35	0.04	10	-0.34	0.74	10	1.68	0.12
O-LM	10	-2.16	0.06				10	-2.75	0.02	10	2.07	0.06
PVBC	10	-1.84	0.10	10	0.43	0.68	movement		sleep	10	-1.85	0.09

Repeated-measures ANOVA of mean firing rates of bistratified (BIC), O-LM and PV+ basket (PVBC) cells during theta oscillations, SWRs and LOSC

Type 3 test of fixed effects

Effect	df	F	p
cell type	2,11	16.97	0.0004
oscillatory state	2,21	76.69	<0.0001
interaction	4,21	22.27	<0.0001

***Post hoc* pairwise comparisons**

	Theta			SWRs			LOSC		
	df	t	p	df	t	p	df	t	p
BIC vs O-LM	21	1.56	0.13	21	8.75	<0.0001	21	0.15	0.88
BIC vs PVBC	21	1.48	0.15	21	-1.47	0.16	21	0.97	0.34
O-LM vs PVBC	21	-0.17	0.87	21	-10.14	<0.0001	21	0.82	0.42

	bistratified			O-LM			PV+ basket		
	df	t	p	df	t	p	df	t	p
Theta vs SWRs	21	-7.45	<0.0001	21	0.64	0.53	21	-10.60	<0.0001
Theta vs LOSC	21	1.85	0.08	21	0.34	0.73	21	1.50	0.15
SWRs vs LOSC	21	8.83	<0.0001	21	-0.29	0.77	21	12.1	<0.0001

Repeated-measures ANOVA of frequency of burst firing of bistratified (BIC) and O-LM cells during movement and sleep

Type 3 test of fixed effects

Effect	df	F	p
cell type	1,7	5.9	0.0455
behavioural state	1,6	0.66	0.4467
interaction	1,6	0.25	0.6327

***Post hoc* pairwise comparisons**

	BIC vs O-LM			movement vs sleep		
	df	t	p	df	t	p
movement	6	2.39	0.05	6	0.94	0.38
sleep	6	1.79	0.12	6	0.22	0.84

Repeated-measures ANOVA of bursting probability of bistratified (BIC) and O-LM cells during theta cycles and SWRs

Type 3 test of fixed effects

Effect	df	F	p
cell type	1,7	56.24	0.0001
oscillatory state	1,7	1.79	0.2222
interaction	1,7	1.3	0.2921

***Post hoc* pairwise comparisons**

	BIC vs O-LM			Theta vs SWRs		
	df	t	p	df	t	p
Theta	7	2.91	0.023	7	-1.86	0.11
SWRs	7	4.86	0.002	7	-0.13	0.90

Repeated-measures ANOVA of mean spike count of bistratified (BIC) and O-LM cells during awake- and sleep-SWRs

Type 3 test of fixed effects

Effect	df	F	p
cell type	1,7	42.49	0.0003
behavioural state	1,5	4.08	0.0994
interaction	1,5	7.64	0.0396

***Post hoc* pairwise comparisons**

	BIC vs O-LM			awake vs sleep		
	df	t	p	df	t	p
awake	5	5.62	0.003	5	-0.5	0.64
sleep	5	7.00	0.0009	5	3.62	0.02

Table 5.4 Complementary statistical comparisons of firing rates, bursting probability and spike counts of bistratified, O-LM and PV+ basket cells.

			One-way ANOVA		Kruskal Wallis test	
Measure	**Comparison between**	**Condition**	**F**	**p**	**χ^2**	**p**
Firing rates	bistratified, O-LM and PV+ basket cells	movement	2.02 (2,11)	0.1788	2.5657	0.2772
		sleep	6.68 (2,10)	0.0144	7.9813	0.0185
		quiet wakefulness	2.28 (2,11)	0.1485	3.9057	0.1419
		theta oscillations	3.75 (2,11)	0.0572	4.7057	0.0951
		SWRs	23.73 (2,11)	0.0001	8.4629	0.0145
		LOSC	23.09 (2,10)	0.0002	8.6044	0.0135
Bursting probability	bistratified and O-LM cells	theta cycles	7.41 (1,7)	0.0297	6	0.0143
		SWRs	27.38 (1,7)	0.0012	6	0.0143
Mean number of spikes	bistratified and O-LM cells	sleep-SWRs	49.59 (1,6)	0.0004	5.3333	0.0209
		awake-SWRs	23.76 (1,6)	0.0028	5.3333	0.0209
	sleep-SWRs and awake-SWRs	bistratified cells	0.33 (1,6)	0.5864	0.3333	0.5637
		O-LM cells	1.36 (1,6)	0.2884	1.3333	0.2482

Table 5.5 Point estimates of ISI distributions of bistratified and O-LM cells.

		Median ± interquartile range of ISI (ms)		
Cell type	**Cell**	**Movement**	**Sleep**	**Quiet wakefulness**
Bistratified cells	K202j	20.4 ± 37.3	13.2 ± 22.3	15.9 ± 31.1
	LK20p	12.6 ± 17.3	NA ± NA	12.9 ± 21.1
	LK27d	13.3 ± 14.3	15.0 ± 26.9	13.5 ± 16.8
	TV21f	7.7 ± 10.2	7.7 ± 10.9	7.3 ± 9.1
	TV30d	25.8 ± 43.4	17.4 ± 29.8	22.8 ± 42.5
O-LM cells	LK01ab	26.0 ± 66.4	65.6 ± 101.5	42.7 ± 66.3
	LK06ah	39.2 ± 44.6	54.8 ± 119.6	41.8 ± 60.2
	LK13k	22.5 ± 38.3	45.5 ± 87.8	26.2 ± 45.1
	ZsB43d	27.6 ± 43.7	44.4 ± 76.5	42.1 ± 57.5

Cell type	**Cell**	**Theta**	**SWRs**	**LOSC**
Bistratified cells	K202j	22.4 ± 36.3	6.4 ± 3.7	24.1 ± 73.2
	LK20p	13.2 ± 19.4	6.2 ± 4.3	20.9 ± 21.9
	LK27d	13.4 ± 15.4	8.9 ± 8.2	14.1 ± 19.8
	TV21f	7.6 ± 9.9	4.9 ± 2.9	NA ± NA
	TV30d	23.1 ± 46.7	6.7 ± 3.4	20.4 ± 46.4
O-LM cells	LK01ab	36.2 ± 66.2	15.0 ± 19.7	44.5 ± 54.5
	LK06ah	38.9 ± 54.3	14.9 ± 19.3	45.8 ± 53.0
	LK13k	23.3 ± 47.6	7.1 ± 4.1	30.0 ± 45.7
	ZsB43d	38.2 ± 53.8	20.1 ± 5.4	43.5 ± 60.1

5.3 Discussion

The *in vivo* action potential firing of two types of identified somatostatin-expressing dendrite-targeting GABAergic interneuron during natural behaviour in freely moving rats shows similarities and striking differences. As suggested by the divergence observed in their axonal terminal fields, the activity of bistratified cells differed from that of O-LM cells and the differences changed according to behavioural and oscillatory network states. During movement, both cell types fired high frequency rhythmic bursts around the trough of theta cycles releasing GABA on segregated dendritic domains of pyramidal cells. However, the theta time scale cooperation of the two cell types contrasted with their differential firing relative to the simultaneously occurring gamma oscillations (Tukker et al., 2007) or SWRs occurring during rest and sleep. In our awake rats, bistratified cells fired with intra-burst frequencies in the gamma range; in contrast, only a small proportion of spikes from O-LM cells showed such instantaneous frequencies. Interestingly, in awake head-fixed mice O-LM cell firing was phase-modulated by the gamma (25–90 Hz) and epsilon oscillatory (90–130) frequencies (Varga et al., 2012). During SWRs, bistratified cells fired strongly in bursts, but O-LM cells fired only infrequently. Different frequencies of burst occurrence of these cells suggest cell-type specific mechanisms and conditions underlying peptide release. The results demonstrate that GABA and somatostatin are released to distinct dendritic zones of CA1 pyramidal cells differentially coordinating inputs from entorhinal cortex and CA3 both during sleep and wakefulness.

5.3.1 Intrinsic cellular properties and synaptic afferents

Cell-type specific intrinsic cellular properties together with the activity of distinct afferent synapses could explain the spike-timing of bistratified and O-LM cells.

Recurrent collaterals of CA1 pyramidal cells are a common source of glutamate for the two interneuron types, but their postsynaptic action is differentiated. Synapses formed on bistratified cells show short-term depression (Ali et al., 1998), whereas the terminals recruiting O-LM cells have low release probability and show strong frequency facilitation (Ali and Thomson, 1998; Losonczy et al., 2002). Furthermore, these axons are the main glutamatergic drive of O-LM cells (Blasco-Ibanez and Freund, 1995). Another glutamatergic input is provided by the pyramidal cells in CA3 via their Schaffer collaterals. The termination zone of these axons overlaps completely with the dendrites of bistratified cells suggesting the relevance of this input to this cell type. Interestingly, Schaffer collaterals do not appear to target O-LM cells (Kim et al., 2012). The strength of pyramidal cell–interneuron connections changes during learning as cell assemblies form (Dupret et al., 2013), and the firing of such pairs of neuron can be either positively or negatively correlated (Dupret et al., 2013; Hangya et al., 2010). Somata and/or dendrites of both somatostatin-expressing interneurons may be innervated by entorhinal cortical afferents in the alveus, but the strength of such connectivity is unknown. It is likely that this input, if it exists, is substantially smaller than those from CA1 and CA3 pyramidal cells. Furthermore, bistratified and O-LM cells receive inhibitory synapses originating from other local GABAergic interneurons and possibly from the medial septum. Indeed, medial septal GABAergic afferents were shown to target somatostatin-expressing interneurons in CA1 (Gulyás et al., 1990). Cholinergic inputs, arriving from the septum activate O-LM cells via nicotinic acetylcholine receptors (Leao et al., 2012; Lovett-Barron et al., 2014) and contribute to the increased firing of the interneurons during arousal.

According to their mean firing rates, bistratified, O-LM and parvalbumin-expressing basket cells (Lapray et al., 2012) are similarly active during theta

oscillations. However, the cell types differentiate in their preferential spike-timing during individual theta cycles. The dendrite-targeting interneurons are maximally active around the theta troughs measured in the pyramidal layer. This preferential theta phase firing of bistratified and O-LM cells is partly suggested by their shared inputs from pyramidal cells, which, on average, also fire at highest probability around the troughs of theta cycles (Buzsaki, 2006). This was also predicted from tetrode recorded interneurons in the pyramidal layer (Czurkó et al., 2011) but cell type identities could not be assessed. The repetitive pyramidal cell firing over several theta cycles can activate both O-LM (Losonczy et al., 2002) and bistratified cells, however this excitatory effect is unlikely to explain the sharp phase tuning of the somatostatin-expressing cell types because the phase-modulation of pyramidal cells as a population is shallow. The spike-timing of these interneurons is more likely to be coordinated by counter-phased inhibition around the peak of pyramidal layer theta.

The medial septal GABAergic input, if shared by O-LM and bistratified cells, might explain the relatively strong theta modulation and precise phase coupling of the interneurons to theta troughs. One population of parvalbumin positive septal GABAergic neurons, with a discharge that was temporally leading hippocampal theta (Hangya et al., 2009), produced rhythmic firing around the peak of theta oscillations under anaesthesia (Borhegyi et al., 2004). But, whether such neurons project to the hippocampus and innervate bistratified and O-LM cells has not been established. The possible phase-modulation of O-LM cells by medial septal neurons is further suggested by the *in vitro* recorded large-amplitude perisomatic input to these cells during theta-like activity (Chamberland et al., 2010). As parvalbumin positive basket cells are relatively weakly theta-modulated [see chapter 4; (Lapray et al., 2012; Varga et al., 2012)] and fire earlier during the theta cycle, their inhibition probably is not provided

by the same medial septal GABAergic cells. Hippocampal interneurons firing at the peak of the LFP theta cycles may provide the local GABA out of phase with O-LM and bistratified cell firing, thus contributing to their theta modulation. In the mouse, bistratified cells are strongly targeted by other parvalbumin positive interneurons (Lovett-Barron et al., 2012). However, neither axo-axonic cells (Klausberger et al., 2003; Viney et al., 2013) nor parvalbumin-expressing basket cells are likely to provide this input, since these interneurons either exclusively innervate pyramidal cells (Somogyi et al., 1983), or their spikes significantly overlap with those of bistratified cells, respectively. Bistratified cells were suggested (Ego-Stengel and Wilson, 2007) to be some of the unidentified interneurons that show phase precession (Maurer et al., 2006). Under our conditions, these cells do not significantly phase precessed in their firing as evidenced by the sharp theta phase locking to the LFP theta. However, it cannot be excluded that the relatively little phase precession in our sample of interneurons is due to the animals' slow and limited movement (Ego-Stengel and Wilson, 2007).

During SWRs, the strong activation of bistratified cells is likely to be due to the higher release probability of their input synapses and their simultaneous activation by CA1 and CA3 pyramidal cells, in contrast to O-LM cells, which are only weakly affected by the average 1–2 action potentials fired by single local pyramidal cells. Overall, O-LM cells decreased their firing rates during SWRs, and were silent during at least some such events. Their silencing may be determined by their weak glutamatergic drive and some inhibitory input activated during SWRs. Beside the population of parvalbumin positive theta-inhibiting medial septal neurons, O-LM cells are also known to be targeted by a population of VIP-expressing, interneuron-specific GABAergic IS-III cells (Acsády et al., 1996b; Chamberland et al., 2010; Gulyás et al., 1990). Unfortunately, the

activity patterns of neither of these GABAergic inputs are known *in vivo*. Interestingly, in the mouse, O-LM cells fired at higher rates during SWRs *in vitro* in the CA1 (Pangalos et al., 2013) and the CA3 areas (Hájos et al., 2013) and *in vivo* (Varga et al., 2012). This is different from the lack of change in the firing relative to peri-SWR periods, or the inhibition of O-LM cells during SWRs reported here. These discrepancies may be due to species differences, loss of some inhibitory connectivity *in vitro* and a relatively higher firing rate during quiet wakefulness compared to sleep. I have found that O-LM cells reported here fired significantly more during awake-SWRs than during sleep-SWRs.

5.3.2 Anaesthesia influences neuronal firing and network dynamics

The comparison of *in vivo* spike-timing of bistratified and O-LM cells recorded from freely moving rats with that recorded under anaesthesia provides novel insights into the influence of anaesthetics on the hippocampal circuitry. Urethane and ketamine–xylazine reduced the frequency of theta- and gamma oscillations and SWRs (Soltesz and Deschenes, 1993; Tukker et al., 2007; Ylinen et al., 1995a; Ylinen et al., 1995b) and attenuated the effects of extra- and intrahippocampal excitatory inputs (Kamondi et al., 1988). Furthermore, urethane may affect the excitability of individual neuron types through the potentiation of $GABA_A$ and nicotinic acetylcholine receptors and the inhibition of NMDA and AMPA receptors (Hara and Harris, 2002; Lawrence, 2008). Low doses of ketamine–xylazine have similar effects to those of urethane, but the precise network mechanisms remain unknown.

Some of these mechanisms may contribute to the reduced firing rates of bistratified (by 64.0 $\pm$ 9.3 Hz, mean $\pm$ s.e.m. during SWRs; by 29.9 $\pm$ 9.3 Hz during theta oscillations) and O-LM cells (by 11.9 $\pm$ 3.0 Hz during SWRs; by 14.1 $\pm$ 3.0 Hz

during theta oscillations) recorded under anaesthesia compared to their rates recorded during behaviour (repeated-measures ANOVA, $F_{1,10}$=7.40, p=0.0215, for the interaction between the factors recording condition and oscillatory state for *bistratified cells*; $F_{1,5}$=31.02, p=0.0026, for the factor recording condition for *O-LM cells*). More importantly, the complete silencing of O-LM cells during SWRs under anaesthesia may be a consequence of the urethane-activation of their alpha 7 nicotinic acetylcholine receptors (Griguoli et al., 2009).

Nicotinic acetylcholine receptor activation, in GIN mice, strongly reduced the firing frequency of green fluorescent protein (GFP)- and somatostatin-expressing neurons in stratum oriens of the hippocampus. In this transgenic mouse line, the expression of GFP is restricted to a subpopulation of somatostatin-expressing interneurons, the majority of which, in stratum oriens of the hippocampus, are likely O-LM cells (Griguoli et al., 2009). In contrast, as my results show, during awake- and sleep-SWRs, O-LM cells occasionally fire action potentials, some even show increases in firing rate.

5.3.3 Neuropeptide and GABA co-release

Pyramidal cell dendrites have non-linear integrative properties mediated by voltage dependent active conductances (Losonczy and Magee, 2006; Spruston, 2008; Takahashi and Magee, 2009). Through the modulation of dendrites, neuropeptides acting synergistically with GABA, have an overall inhibitory effect on the activation of pyramidal cells. The pre- and postsynaptic action of somatostatin released by O-LM and bistratified cells and NPY released by bistratified cells is likely to regulate dendritic electrogenesis at a slower time scale than GABA. Neuropeptide release requires high frequency firing (van den Pol, 2012) therefore the identification of such spiking within

the activity of recorded interneurons may predict peptidergic effects of these cells during behaviour.

I have observed a cell-type dependent pattern of occurrence of high frequency bursting in the spike trains of bistratified and O-LM cells. During movement and sleep bistratified cells have much higher frequency of bursts than O-LM cells. This suggests that the glutamatergic input from CA3 is under stronger peptidergic inhibition than the entorhinal input. Indeed, somatostatin (Tallent and Siggins, 1997) and NPY (Colmers et al., 1985) were shown to inhibit the excitatory effects of CA3 pyramidal cells (Boehm and Betz, 1997; Stanic et al., 2006; Tallent and Siggins, 1997). As O-LM cells burst less frequently, these may require fewer spikes and at lower frequencies compared to bistratified cells for peptide release.

Hippocampal and entorhinal glutamatergic neurons express the somatostatin receptors sst2R, sst3R and sst4R (Breder et al., 1992) (Dournaud et al., 1996; Schreff et al., 2000; Schulz et al., 2000). Entorhinal terminals in stratum lacunosum moleculare were shown to be immunopositive for sst2R (Dournaud et al., 1996), and probably are modulated by O-LM cells. Bistratified cells are in key position to activate sst3Rs (Einstein et al., 2010) and sst4Rs (Schreff et al., 2000) localised on pyramidal cell dendrites. In mice, knocking out the sst3R impaired their object-recognition memories (Einstein et al., 2010). The sst4R mediates (Qiu et al., 2008) somatostatin-mediated augmentation of the voltage sensitive non-inactivating K+ M-current (I-M) (Moore et al., 1988) and a K+ leak current (Schweitzer et al., 1998). During theta oscillations, when cholinergic tone is increased, the M-current is likely dominated by ACh-mediated suppression mediated by the activation of the m1 muscarinic ACh receptor (Dasari and Gulledge, 2011; Halliwell and Adams, 1982). In this state, due to the voltage sensitivity of this current, augmentation by somatostatin may differ between active and inactive

pyramidal cells. During SWRs, when cholinergic tone is low and somatostatin release from bistratified cells increases, the augmentation of I-M may dominate and contribute synergistically with NPY to the termination of SWRs. Overall, neuropeptide- and $GABA_B$ receptor-mediated presynaptic inhibitory effects (Breder et al., 1992; Schulz et al., 2000) reduce release probability of glutamate, thereby preserving presynaptic potency over periods of high firing rates.

5.3.4 Regulation of firing and synaptic plasticity of pyramidal cells via dendritic inhibition

The differential timing of the two glutamatergic inputs to CA1 explain why a single type of interneuron cannot deliver the modulation of both inputs and along the whole pyramidal cell dendritic domain. But what are the possible roles of bistratified and O-LM cells during behaviour?

During SWRs, the firing of bistratified cells (Klausberger et al., 2004) rarely dropped below 80 Hz, hence these cells provide high frequency rhythmic entrainment of the thin pyramidal cell dendrites, together with PV-expressing basket cells that innervate the cell body and proximal dendrites (Lapray et al., 2012; Varga et al., 2012). The silencing of O-LM cells and the withdrawal of their inhibition from the most distal dendrites in CA1 may be required to allow a reverberation between CA1 and the entorhinal cortex during closely timed repeated ripples (Davidson et al., 2009). Alternatively, the firing dynamics of bistratified and O-LM cells during SWRs, recorded either during sleep or wakefulness, can be informative of their role in the time-compressed encoding of memories (<100 ms).

Both cell types fired high frequency rhythmic bursts around the trough of theta cycles releasing GABA on segregated dendritic domains of pyramidal cells. At each

location, postsynaptic $GABA_A$ receptors are activated, in strata radiatum and oriens by bistratified cells and in stratum lacunosum moleculare by O-LM cells (Buhl et al., 1994a; Maccaferri et al., 2000). This activation may increase dendritic input conductance and contributes to the scaling and rhythmic control of EPSPs received from both entorhinal as well as CA3 afferents. Furthermore, this cooperative $GABA_A$ receptor mediated input onto pyramidal cells during theta trough, at the time of their relative highest somatic depolarisation, maintains the theta phase reversal along the soma-to-apical-dendritic-tuft axis. Around the theta peak, when the firing probability of both bistratified and O-LM cells is the lowest, long-term potentiation (LTP) may occur in pyramidal cell dendrites at both CA3 and entorhinal synapses. Indeed this is when LTP is most easily evoked (Hölscher et al., 1997). What would be the mechanisms required for LTP? In CA1, pyramidal cells can fire complex spike bursts, a series of action potentials of decreasing amplitude riding on a slower dendritic calcium spike, often followed by a plateau potential (Epsztein et al., 2011; Kandel and Spencer, 1961; Pissadaki et al., 2010; Takahashi and Magee, 2009; Wong and Prince, 1978). In neocortical pyramidal cells, inhibition of dendrite-innervating somatostatin-expressing GABAergic neurons is necessary for such burst firing and the occurrence of calcium spikes evoked by sensory stimuli (Gentet et al., 2012). In the hippocampus, inhibition of somatostatin-expressing interneurons *in vivo* promotes burst firing (Royer et al., 2012), whereas their activation *in vitro* greatly diminishes the generation of calcium plateau potentials in pyramidal cells (Lovett-Barron et al., 2012). These findings point towards the contribution of dendrite-targeting bistratified and O-LM interneurons to the reduction of calcium spike generation and gating of LTP in CA1.

Hippocampal circuit-level dynamics regulated by bistratified and O-LM cells during behaviour will be discussed in detail in the final chapter of the thesis. I will

consider the contribution of several types of GABAergic neuron controlling pyramidal place cell activity during the stages of learning during exploration, rest and slow wave sleep. Possible mechanisms of memory encoding and retrieval during theta oscillations and memory consolidation during SWRs will be reviewed.

6 General discussion

6.1 Outline

During learning, structural and functional changes are induced in the hippocampal neuronal network to enable the encoding of new information and removal or updating of stored knowledge. Information, contained in the firing of pyramidal cell assemblies is regulated by a diverse population of GABAergic interneurons temporally coordinated by transient network oscillations. I attempted to dissect the contribution of distinct GABAergic interneuron types to network oscillations during exploration and natural slow wave sleep in freely moving rats. Using a combination of techniques detailed in chapter 2, I examined the timing of action potential discharge of hippocampal interneurons during theta- and sharp wave associated ripple oscillations (SWRs), indicative of GABA released onto functionally different postsynaptic domains of pyramidal cells. As reported in chapters 3-5, the firing patterns of identified PV+ basket, axo-axonic, dendrite-targeting bistratified and O-LM cells and one "unconventional interneuron", together with further non-labelled putative GABAergic cells are behavioural- and oscillatory network-state-dependent.

My main findings are:

- During sleep, PV+ basket and bistratified cells fire at higher rates than axo-axonic and O-LM cells, and unlike axo-axonic and O-LM cells, strongly increase spiking during SWRs.
- Axo-axonic and O-LM cells decrease firing during sleep relative to awake states and are inhibited during all or most of SWRs, respectively.
- During movement, axo-axonic and PV+ basket cells fire with similarly high frequencies but on complementary segments of the descending slope of theta cycles.
- Bistratified and O-LM cells fire cooperatively during movement at the troughs of theta oscillations but with different frequencies.
- The "unconventional interneuron" in contrast to the other identified cell types has a low spike rate and becomes highly activated during SWRs.
- My results predict that behaviour and rhythmic network events differentiate GABA and peptide release to distinct membrane domains of pyramidal cells.

My results have also established those features of the spike-timing of distinct GABAergic interneuron types that remain valid under drug-free conditions and were reported originally under urethane anaesthesia (Klausberger and Somogyi, 2008; Somogyi, 2010). Although the firing rates are reduced by the anaesthesia, the preferential theta phase of firing of PV+ basket, axo-axonic, bistratified and O-LM cells (Klausberger et al., 2003; Klausberger et al., 2004) corresponds to that recorded in freely moving rats or mice [see chapters 4 and 5 and (Katona et al., 2014; Lapray et al., 2012; Varga et al., 2012; Viney et al., 2013)]. The preservation of theta phase preference in the absence of spatially modulated inputs, e.g., from place cells, is

suggestive of an extrinsic controller of interneuron activity, e.g., from the medial septum. The SWR-related responses of PV+ basket, axo-axonic and bistratified interneurons are also similar with and without anaesthesia [see chapters 4 and 5 and (Katona et al., 2014; Klausberger et al., 2003; Klausberger et al., 2004; Lapray et al., 2012; Varga et al., 2012; Viney et al., 2013)]. However, O-LM cells are often completely silent during SWRs in urethane anaesthetised rats, whereas these interneurons occasionally fire action potentials during awake- and sleep-SWRs, sometimes leading to firing rate increases. The reduction in the firing frequency of O-LM interneurons under anaesthesia is likely to be a consequence of the combined effects urethane on the activation of their nicotinic acetylcholine receptors (Griguoli et al., 2009; Hara and Harris, 2002) and/or on the suppression of acetylcholine release (Leao et al., 2012).

Overall, the data indicate functional specialisation of distinct types of GABAergic interneuron. These GABAergic interneurons contribute to the cyclic redistribution of inhibition from the axon initial segment through the cell body down to the distal apical tuft and back providing a compartment-specific regulation of pyramidal cell output during behaviour.

6.2 Rhythmic neuronal network activity in the dorsal hippocampal CA1 area

6.2.1 Hippocampal neuronal operations during theta frequency oscillations

Distant cortical areas are synchronised during certain behaviours as evident by coherent theta frequency (5-12 Hz) oscillations (Buzsáki, 2002; Jones and Wilson, 2005; Mizuseki and Buzsaki, 2014; O'Neill et al., 2013; Siapas et al., 2005; Young and McNaughton, 2009). The emergence of this co-operation is governed by a network of subcortical regions (Freund and Antal, 1988; Hangya et al., 2009; Lawrence, 2008; Pan

and McNaughton, 2004; Rawlins et al., 1979; Vertes, 1982; Vertes et al., 2001) and was suggested to support mnemonic processing (Buzsáki, 1989; Buzsáki, 2002; Buzsaki and Moser, 2013; Hasselmo, 1999; O'Keefe, 1993; Sutherland and McNaughton, 2000). Furthermore, in the hippocampus, the theta rhythm modulates the amplitude of gamma oscillations (Belluscio et al., 2012; Bragin et al., 1995), which are involved in cognitive processes. Theta oscillations are prominent during spatial navigation (Brandon et al., 2011; Burgess and O'Keefe, 2011; Buzsáki, 2002, 2005; Geisler et al., 2007). The amplitude and frequency of hippocampal theta oscillations are modulated by the speed of movement (Rivas et al., 1996; Wells et al., 2013) and the phase shifts with distance along the septo-temporal axis resulting in a topographic travelling wave (Hartwich et al., 2009; Lubenov and Siapas, 2009; Patel et al., 2012). According to a model, different stages of learning are regulated by different phases of theta oscillations in the hippocampal CA1 area (Hasselmo et al., 2002; Manns et al., 2007). Information encoding, inducing synaptic plasticity at CA1 pyramidal cell inputs, happens at the peak of theta oscillatory cycles and the retrieval of existing associations, dependent on the CA3 area, occurs at the trough.

Pyramidal place cells

Pyramidal cells in the CA1 area are entrained by theta oscillations (Fox, 1989; Kamondi et al., 1998; Lapray et al., 2012; Soltesz and Deschenes, 1993; Ylinen et al., 1995b). Although, the majority of pyramidal cells are silent during exploration, there are some which fire action potentials. The firing rate of the active pyramidal cells is highest at the trough of theta oscillations, recorded in the pyramidal layer, but spikes can occur at any phase of the oscillatory cycles (Buzsaki, 2006). At place field traversal, pyramidal place cells [see Fig. 3 in (Lapray et al., 2012)] associated with the current

location increase their firing rates and trigger spikes around the peak of the theta oscillations (O'Keefe and Recce, 1993), when their membrane potential is most depolarized (Epsztein et al., 2011; Harvey et al., 2009). During the subsequent few theta cycles the timing of the action potentials shift to earlier phases showing phase precession (Harris et al., 2002; O'Keefe and Recce, 1993; Skaggs et al., 1996) due to faster intracellular oscillation, within the place field, than the extracellular LFP theta oscillation (Geisler et al., 2010; Harvey et al., 2009).

GABAergic interneurons

The theta modulation of the activity of pyramidal cells is influenced by the inhibition arriving via presynaptic GABAergic interneurons (Kamondi et al., 1998; Ylinen et al., 1995b). How do GABAergic interneurons regulate the encoding and retrieval of information in the hippocampus? In freely moving rats, identified hippocampal GABAergic cells fire on average at higher rates than pyramidal cells and distinct types of interneuron release GABA at specific times during theta oscillations, supporting previous results (Czurkó et al., 2011; Klausberger and Somogyi, 2008; Ranck, 1973; Somogyi et al., 2014; Zhang et al., 2012). Theta phase precession of spiking has been demonstrated for some unidentified interneurons during short bouts of theta cycles recorded using tetrodes (Ego-Stengel and Wilson, 2007; Maurer et al., 2006). Under our conditions, most interneurons do not significantly phase-advance their spiking as revealed by their sharp theta phase locking to the LFP theta. I have not tested phase precession in interneurons formally, but visual inspection rarely revealed precession and only over few theta cycles. It cannot be excluded that the relatively little or no phase precession in my sample of GABAergic cells was caused by the relatively little movement of the animals (Ego-Stengel and Wilson, 2007) and remained

unrecognisable due to the short recording periods. Axo-axonic cells and the "unconventional interneuron" fire around the peak, followed by PV+ basket cells on the descending slope of theta cycles. The preferential spike-timing of O-LM, bistratified and putative long-range projection cells is at the theta trough. Some non-labelled putative GABAergic cells fired on the ascending part of theta cycles similar to CCK-expressing or ivy cells identified under urethane anaesthesia (Fuentealba et al., 2008a; Klausberger et al., 2005). What is the importance of the temporal co-operation of some interneuron types and the divergence of theta phase selectivity of others during theta oscillations?

The firing of axo-axonic cells is strongly phase coupled to the peak of theta oscillatory cycles [chapter 4 and (Klausberger et al., 2003; Viney et al., 2013)] and reflects enhanced GABA release onto the axon initial segments of pyramidal cells. It is likely that axo-axonic cells exert the strongest influence on the firing probability of pyramidal cells during theta oscillations given that these cells innervate exclusively the site of action potential initiation. Indeed, pyramidal cells fire least around the peak of theta oscillations, suggesting that axo-axonic cells - as "gatekeepers" - select and temporally restrict the firing of pyramidal cell assemblies. The rhythmic increases in axo-axonic cell activity tune pyramidal cell action potential generation probability to theta frequencies. How the "unconventional interneuron" contributes to the gating of pyramidal cell output at the peak of theta oscillations by innervating to some extent also axon initial segments remains to be discovered. Coincidental with the GABAergic innervation of the axon initial segment, the opposite pole of pyramidal cells, the distal apical tuft in stratum lacunosum moleculare receives a slow inhibitory input from neurogliaform cells (Fuentealba et al., 2010). This input is driven by the entorhinal/thalamic inputs and provides feed-forward modulation of synaptic

plasticity of glutamatergic inputs arriving from the entorhinal cortex on the theta peak (Buzsaki, 2006; Capogna and Pearce, 2011; Mizuseki et al., 2009).

During the descending slope of theta cycles, GABA is released by PV+ basket cells innervating the cell bodies and proximal dendrites of pyramidal cells [chapter4 and (Klausberger et al., 2003; Lapray et al., 2012; Varga et al., 2012)]. The $GABA_A$ receptor-mediated and gamma rhythmic inhibitory mechanisms provided by PV+ basket cells regulate the timing of action potential output of their target neurons (Lasztoczi and Klausberger, 2014; Royer et al., 2012; Tukker et al., 2007; Varga et al., 2012). PV+ basket cells together with bistratified cells are responsible for the gamma frequency entrainment of pyramidal cells during exploration.

Somatostatin-expressing bistratified and O-LM cells fire with maximal probability around the trough of theta cycles and regulate the glutamatergic inputs of CA1 pyramidal cells received from both the CA3 area and the entorhinal cortex, in strata radiatum and oriens and in stratum lacunosum moleculare, respectively (Katona et al., 2014; Klausberger et al., 2003; Somogyi and Klausberger, 2005; Varga et al., 2012). Around the theta peak, when the firing probability of both bistratified and O-LM cells is the lowest, long-term potentiation (LTP) may occur in pyramidal cell dendrites at both CA3 and entorhinal synapses. Indeed, LTP is most easily evoked at the peak of theta oscillations (Hölscher et al., 1997). The collaboration at theta time scale of the two cell types predicts their involvement in the theta phase dependent encoding and retrieval of spatial memories.

What mechanisms may regulate LTP in pyramidal cell dendrites? In the CA1 area, pyramidal cells can fire complex spike bursts, a sequence of high frequency action potentials of decreasing amplitude riding on a slower dendritic calcium spike, often followed by a plateau potential (Epsztein et al., 2011; Kandel and Spencer, 1961;

Pissadaki et al., 2010; Takahashi and Magee, 2009; Wong and Prince, 1978). The generation of such calcium plateau potentials in pyramidal cells *in vitro* is attenuated by the activation of somatostatin-expressing GABAergic interneurons (Lovett-Barron et al., 2012). Inversely, burst firing and the occurrence of calcium spikes *in vivo,* in both, neocortical and hippocampal pyramidal cells, requires the inhibition of dendrite-innervating somatostatin-expressing GABAergic interneurons (Gentet et al., 2012; Royer et al., 2012). The lowest spiking probability of bistratified and O-LM cells is at the peak of theta oscillations, which would be expected to coincide with the highest probability of dendritic calcium spikes. However, the time during the theta cycle when active place cells fire complex bursts is controversial because of the lack of simultaneous local field potential recordings. Extracellular recordings demonstrated the occurrence of complex bursts in some place cells during entry or at the periphery of the place fields (Harris et al., 2001), which is likely to be around the peak of theta cycles. In contrast, *in vivo* whole cell recordings predicted maximal occurrence of calcium spikes and plateau potentials in the middle or throughout the place field, at the time of highest firing rate (Epsztein et al., 2011). Pyramidal cells in the CA1 area fire the highest number of action potentials per theta cycle at the trough (Mizuseki et al., 2009) which usually coincides with the middle of the place field. How can it be reconciled that at the trough of theta cycles, when bistratified and O-LM cells fire with the highest probability, active place cells also trigger calcium spikes with the highest probability? It is possible that active place cells can reduce the effectiveness of their GABAergic input by calcium dependent retrograde signalling whereas most silent pyramidal cells are under inhibitory control. Such mechanism is provided by the release of endocannabinoids and the suppression of GABA release from CB1 receptor expressing terminals. However, somatostatin positive interneurons are not known to

express CB1 receptors. Another candidate for the suppression of GABA release from terminals is the messenger nitric oxide (NO) (Kaplan et al., 2013; McBain and Kauer, 2009). Indeed, both calcium permeable NMDARs (Szabadits et al., 2011) and the calcium/calmodulin dependent enzyme nNOS (Szabadits et al., 2007) are present in the postsynaptic active zone of some GABAergic synapses on pyramidal cells. Moreover, GABAergic terminals of the majority of PV-expressing and one third of SOM-expressing interneurons express the NO-sensitive guanylyl cyclase (NOsGC) (Szabadits et al., 2007), which mediates the effect of NO in presynaptic terminals. Therefore it is possible that O-LM and bistratified cells may have the required molecular machinery for the retrograde NO mediated suppression of GABA release. Increases in local calcium concentrations via NMDARs and voltage gated calcium channels in the dendrites of active place cells activate nNOS. The same interneurons simultaneously inhibit the dendrites of silent pyramidal cells. This selective depolarisation induced suppression of inhibition may support the segregation of active versus silent pyramidal cells, which is consistent with the conversion of silent cells into place cells upon depolarization (Lee et al., 2012).

Similar to bistratified and O-LM cells, other types of dendrite-targeting GABAergic cell also fire action potentials mostly at the trough of theta oscillatory cycles, e.g., the local collaterals of the long-range projecting GABAergic neurons innervate dendrites in the CA1 area and form synapses mainly on dendrites of pyramidal cells in extrahippocampal areas. These GABAergic cells synchronise the activity of local pyramidal cells in the CA1 area with those is distant regions cells e.g., in septum and retrohippocampal areas promoting the coherence of theta oscillations.

The identity of putative non-labelled GABAergic interneurons (chapter 3) with spikes coupled to the ascending phases of theta cycles remains to be determined. One

likely candidate, the ivy cell, was identified recently in freely moving rats and its activity patterns confirmed those recorded under urethane anaesthesia (Fuentealba et al., 2008a; Lapray et al., 2012). The firing rates of ivy cells correlate with the frequency and amplitude of theta oscillations reflecting their participation in synchronous network activity. In the CA1 area, CCK-expressing basket cells and dendrite-targeting interneurons also fire on the ascending phase of theta oscillations under urethane anaesthesia (Klausberger et al., 2005). The joint inhibitory influence of CCK+ and PV+ basket cells is highest at the peak of theta cycles and lowest at the trough, which together with axo-axonic cell regulation restricts the maximal pyramidal cell firing to the trough of theta oscillations. Interestingly, pyramidal place cells start firing on the ascending part of theta cycles and the phase precession of their spikes continue up to 360°. It was suggested that a loss of effectiveness by CCK+ cells expressing cannabinoid type 1 receptors in their terminals may contribute to the phase precession of place cells. GABAergic cells expressing CB1 receptors mediate the depolarisation induced suppression of inhibition (Freund, 2003; Katona and Freund, 2008). Active place cells start firing on the ascending slope of theta cycles, and an increase in postsynaptic calcium may trigger endocannabinoid release and retrograde signalling (Freund and Hajos, 2003) which results in the selective suppression of their GABAergic input via presynaptic CB1 receptors.

What mechanisms might regulate the firing modulation of GABAergic interneurons by the theta rhythm? Distinct types of GABAergic interneuron can be activated by the repetitive firing of pyramidal cells (Losonczy et al., 2002), but their sharp phase tuning during theta oscillations is very unlikely to be determined by CA1 pyramidal cells. The latter, as a population is weakly theta-modulated (Mizuseki et al., 2009). Some interneurons also receive spatially tuned glutamatergic inputs from the

CA3 area in strata radiatum and oriens (Kim et al., 2012), which is strongest at the descending phase of theta cycles (Mizuseki et al., 2009), and/or from the entorhinal cortex, in stratum lacunosum moleculare (Kiss et al., 1996; Kitamura et al., 2014), at highest rate at the peak of theta oscillations. Furthermore, septal cholinergic input strongly activates O-LM cells via nicotinic acetylcholine receptors during wakefulness (Leao et al., 2012; Lovett-Barron et al., 2014) but it is not known at what theta phases. Complementary to the glutamatergic drive, the preferential spike-timing of GABAergic interneurons during theta cycles may well be coordinated by counter-phased inhibitory inputs. Inhibitory afferents to GABAergic interneurons originate from other local interneurons and from extrahippocampal GABAergic projections e.g., from the medial septum and entorhinal cortex. The activity of some medial septal neurons is rhythmic showing preferences either to the trough or the peak of theta oscillations recorded in the hippocampal CA1 area (Borhegyi et al., 2004; Dragoi et al., 1999; King et al., 1998; Viney et al., 2013) and some such neurons express parvalbumin (Pascale Simon et al., 2006). The different groups of parvalbumin-expressing neuron were suggested to target selectively certain types of GABAergic interneuron restricting the postsynaptic cells to discharge action potentials at the peak or around the trough of theta cycles, like observed for axo-axonic, PV+ basket, bistratified and O-LM cells, respectively. However, there are many septo-hippocampal projecting neurons and the medial septum also innervates other cortical and subcortical areas, therefore the contributing cellular and synaptic mechanisms have not been defined. Also, the axonal tracing of recorded septal neurons into the hippocampus and the identification of their GABAergic interneuron targets has not been reported so far.

Conclusion

Altogether, the observed great specificity in spike-timing paralleled by the synaptic target selectivity of GABAergic interneurons supports a rhythmic and sequential redistribution of inhibition over the different pyramidal cell compartments during a theta cycle. Orchestrated by theta frequency network oscillations, this compartmentalised redistribution of inhibition may achieve the proposed pyramidal cell synchronization during encoding of new sensory information, driven around the peak of the theta cycles, and during retrieval of stored associations, strongest around the theta trough (Hasselmo et al., 2002).

When an animal enters a place field, the cooperative inhibition provided by axo-axonic, PV+ and CCK+ basket cells sets a high firing threshold for most pyramidal cells at the theta peak in the pyramidal layer, selecting only the few most depolarised place cells. Both bistratified and O-LM cells are minimally active at this theta phase, which may enable encoding in the place cell dendrites via LTP at both CA3 and entorhinal synapses. As the animal traverses the field, the place cell initiates increasing numbers of action potentials starting around the peak and progressing to earlier phases of consecutive theta cycles. This may be partly due to the selective suppression of its inhibition via retrograde signalling mechanisms. On the descending theta phase and towards the trough, the increasing CA3 input activates PV+ basket, bistratified and projection cells, enabling the retrieval of stored associations undergoing updating. At the trough, the increased O-LM cell activity likely contributes to the elimination of spurious entorhinal cortical input interfering with the recalled CA3 contextual pattern. The simultaneous termination of axo-axonic cell firing creates a window of higher firing probability for the place cell. Discharging maximally and with gamma

frequencies, the place cell may synchronise its spikes with other members of the assembly in the CA1 and in other distal regions.

6.2.2 Hippocampal neuronal operations during sharp wave associated ripple oscillations

During sharp wave associated ripple oscillations (SWRs, 130-230 Hz) (O'Keefe and Nadel, 1978), the discharge of ~10–20% of all pyramidal cells in the CA1 area becomes highly synchronised (Csicsvari et al., 1999a, b). Assemblies representing newly acquired associations become reactivated (Lee and Wilson, 2002; Nádasdy et al., 1999; O'Neill et al., 2006; O'Neill et al., 2008; Pavlides and Winson, 1989; Skaggs and McNaughton, 1996; Wilson and McNaughton, 1994) and their output is transferred to neocortex for long-term storage (Buzsáki, 1989, 1996; Chrobak and Buzsáki, 1996; Chrobak and Buzsáki, 1998b; Hasselmo, 1999). The co-firing of pyramidal cells during ripple cycles of 4-10 ms may initiate long-term potentiation in their targets leading to memory consolidation (Bendor and Wilson, 2012; Buzsaki, 1998; Dupret et al., 2010; Ego-Stengel and Wilson, 2010; Girardeau et al., 2009; Jadhav et al., 2012). Generated in the CA3 area (Buzsaki, 2006), SWRs propagate to the CA1 area via the Schaffer collaterals and commissural axons of CA3 pyramidal cells. These rhythmically entrained axons activate their target pyramidal cells and GABAergic interneurons by innervating their dendrites in strata radiatum and oriens. Furthermore, it was recently demonstrated that SWRs can travel along the septo-temporal axis of the hippocampus and transfer integrated information from the dorsal and intermediate parts of the CA1 area to target regions (Patel et al., 2013).

GABAergic interneurons

How do GABAergic interneurons regulate the information transfer from the hippocampus to downstream cortical areas during SWRs? The combined action of GABA on the distinct pyramidal cell compartments will determine when pyramidal cells fire during SWRs. I observed that, identified types of hippocampal GABAergic interneuron have different SWR-related firing responses in drug-free rats, predicting temporally differentiated GABA release. Parvalbumin-expressing basket and bistratified cells and the "unconventional interneuron" become activated during SWRs in comparison to similar duration time periods outside of SWR events by increasing their mean firing rates several fold. In contrast, axo-axonic and O-LM cells are inhibited during all or most of SWR events, respectively. Some non-labelled putative GABAergic interneurons, on average, do not change their firing rates with respect to SWRs. What are the consequences and hypothesised roles of this divergent SWR-related increased activity versus silencing of distinct interneuron types?

The strong activation of PV+ basket and bistratified cells during SWRs [see chapters 4 and 5 (Hájos et al., 2013; Katona et al., 2014; Klausberger et al., 2003; Klausberger et al., 2004; Lapray et al., 2012; Varga et al., 2012)] is elicited by simultaneous rhythmic inputs from pyramidal cells in the CA1 and CA3 areas. By entraining the somatic and dendritic membrane conductance of CA1 pyramidal cells to ripple frequencies, these two cell types co-operate by setting windows of minimal excitability of their targets therefore timing the synchronised discharge of pyramidal cells as assemblies (Cobb et al., 1995; Csicsvari et al., 1999b; Ellender et al., 2010; Hájos et al., 2013; Klausberger et al., 2003; Lapray et al., 2012; Varga et al., 2012; Ylinen et al., 1995a). Moreover, bistratified cells may also contribute to the peptide-mediated termination of SWRs by releasing somatostatin and/or NPY as predicted by their SWR-

related high frequency burst firing (Boehm and Betz, 1997; Colmers et al., 1985; Moore et al., 1988; Tallent and Siggins, 1997).

Similar to the above, axo-axonic cells also receive rhythmic glutamatergic inputs from the CA1 and CA3 pyramidal cells, but unlike PV+ basket and bistratified cells, their firing is strongly inhibited during SWRs [see chapter 4 and (Hájos et al., 2013; Klausberger et al., 2003; Viney et al., 2013)]. The contrasting SWR responses are most likely due to some GABAergic input of axo-axonic cells being highly active during SWRs. Indeed, it was discovered recently that cell bodies of axo-axonic cells are the preferential targets of a medial septal inhibitory input (Viney et al., 2013), but ripple-active PV+ basket and bistratified cells may also contribute. The silencing of axo-axonic cells during SWRs results in the withdrawal of inhibition from the axon initial segment of targeted pyramidal cells allowing the action potential firing of assemblies during the reactivation of newly acquired associations.

Overall, O-LM cells decrease their firing rates during SWRs, as shown by my novel analysis, and are silent during at least some such events [see chapter 5 and (Katona et al., 2014)]. This activity pattern may be due to a weak glutamatergic drive provided by in average 1–2 action potentials fired by single pyramidal cells (Ali and Thomson, 1998) in combination with an inhibitory input activated during SWRs. GABAergic afferents innervating O-LM cells originate from a population of parvalbumin positive medial septal neurons and a population of VIP-expressing, interneuron-specific GABAergic IS-III cells in the CA1 area (Acsády et al., 1996b; Chamberland et al., 2010; Gulyás et al., 1990) but, unfortunately, the spike-timing of neither of these GABAergic inputs are known *in vivo*. The SWR-related inhibition of O-LM cells in rats under urethane anaesthesia (Klausberger et al., 2003) or their decreased firing relative to peri-SWR periods reported here is in contrast with the high

firing rates of these interneurons in the mouse hippocampus, both *in vitro* (Hájos et al., 2013; Pangalos et al., 2013) and *in vivo* (Varga et al., 2012). There might be multiple factors accounting for the observed discrepancies e.g., species differences, loss of some inhibitory connectivity *in vitro* and a relatively higher firing rate during quiet wakefulness of head-fixed mice compared to sleep. I have found that O-LM cells reported here fire significantly more during awake-SWRs than during sleep-SWRs. The reduction in firing of O-LM cells results in the withdrawal of GABA and possibly somatostatin from the distal apical tuft of CA1 pyramidal cells which may enable the input from the entorhinal cortex to return to CA1 and strengthen the connectivity between CA1 and the entorhinal cortex during repetitive ripples (Davidson et al., 2009).

Similarly to bistratified cells, trilaminar cells (Ferraguti et al., 2005) and double projection cells (Jinno et al., 2007), including those that project to the septum, also have strongly increased firing rates during SWRs (unpublished observations in drug-free rats by Dr. D. Lapray and some putative non-labelled interneurons reported in chapter 3). These dendrite-targeting, long-range projection cells coupled their spike-timing to ripple oscillations under urethane anaesthesia (Jinno et al., 2007). How this firing activity compares to that under normal physiological conditions is unknown but if maintained, this activity pattern may entrain dendritic membranes of local pyramidal cells in the CA1 area to ripple frequencies, in cooperation with bistratified cells. Furthermore, via their long-range projections, these cells provide the simultaneous rhythmic phasing of postsynaptic dendrites in distant extrahippocampal areas e.g., subiculum, septum and other retrohippocampal regions.

Ivy cells are the most abundant type of GABAergic interneuron in the CA1 area and have an exceptionally dense axonal cloud (Fuentealba et al., 2008a; Szabadics and

Soltesz, 2009). Recent recordings in freely moving rats demonstrated that these interneurons fire with similar mean frequencies during different network oscillations and do not change their spike rates during SWRs as compared to periods outside SWR events (Lapray et al., 2012). Such activity patterns indicate their role in regulating homeostasis by providing widespread synaptic and extrasynaptic slow GABAergic input, together with NPY and nitric oxide, to pyramidal cell dendrites and their afferents.

How the strong activation of the "unconventional interneuron" during sleep-SWRs contributes to the modulation of pyramidal cell firing remains to be established. The spike-timing of other identified GABAergic interneurons (e.g., CCK-expressing basket and dendrite-targeting cells) remains to be recorded in freely moving rats or awake head-fixed mice. Based on activity patterns recorded under anaesthesia (Klausberger et al., 2005; Lasztoczi et al., 2011), some may regulate pyramidal cell firing via SWR-related disinhibitory mechanisms (Freund, 2003; Katona and Freund, 2008). The cell bodies and dendrites of pyramidal cells are innervated by CCK+ interneuron types which express cannabinoid receptor type 1 (CB1) in their terminals. When activated by endocannabinoids released by the strongly depolarised postsynaptic pyramidal cells, CB1 receptors mediate the retrograde suppression of GABA release from interneuron terminals (Katona et al., 1999b).

Conclusion

The observed high specificity in spike-timing during SWRs paralleled by the synaptic target selectivity of GABAergic interneurons suggest that distinct cell types evolved to support a temporal redistribution of inhibition over the different pyramidal cell compartments as found during different frequency network oscillations. Rhythmic

inhibition provided by PV+ basket and bistratified cells, regulates the output of pyramidal cells by periodically decreasing their firing probability. At the time when rhythmic inhibition is increased on the somata and dendrites of pyramidal cells, GABA is withdrawn from their axon initial segments and distal apical tuft by the SWR-silencing of axo-axonic cells and O-LM cells, respectively, contributing to the selection of active pyramidal cells via disinhibition. The specialisation of distinct types of GABAergic interneuron also during SWRs supports the functional specialisation of subcellular pyramidal cell domains.

6.3 Technical limitations

My experiments were challenging and of low yield but, when successful, I obtained highly original results about the functional specificity of hippocampal GABAergic interneurons in the CA1 area. I have recorded the spike-timing of large numbers of neuron but because of the need for cell type identification the final counts of labelled cells are low. Labelling was always attempted only after recording the activity of the undisturbed cells, because current injection and potential damage to the membrane likely perturbs firing. I aimed the complete labelling of one neuron per experiment with its activity patterns recorded during different behavioural states. However, my labelling attempts were not always successful, mostly because of the instability of the position of the pipette relative to the cell, which was exacerbated by the grooming of the animal. Furthermore, some cell types might be more difficult to label than others due to differences in shape, and the surrounding tissue components. In some cases, the weak labelling or incomplete diffusion of the neurobiotin rendered the identification of labelled neurons impossible because of the lack of sufficient detail. The population of GABAergic interneurons is diverse therefore their recognition

requires a sufficient number of parameters to be measured for intra- and inter-group comparisons.

Problems with stability during recording and labelling originate from the fact that the rats are free to move. Head fixation or the use of anaesthesia may have reduced this risk, but my aim was to study hippocampal neuronal activity during undisturbed behaviour and under normal physiological conditions. These conditions are not satisfied by the alternative experimental configurations, e.g., restricted movements in head-fixed mice, anaesthetic drugs alter neuronal network oscillations and the firing of individual cells.

Sometimes the short recording periods contain only minimal movement and associated theta oscillations. As discussed in earlier chapters, this limited the possibilities of analysing the spatial preference of neuronal discharges and the phase precession of their spikes in my data. Because of the low probability of successful labelling, the rats were not trained to perform a behavioural task. In order to stimulate them to walk, I have introduced changes to their environment within and outside the recording arena during some of the experiments. I have changed the size of the box as well as its shape and I placed new objects some with aversive odours (e.g., cat fur, synthetic fox urine smell). This initiated locomotion for an initial period during which I tried finding a cell by advancing the glass pipette into the hippocampus.

The action potentials measured extracellularly with the glass electrode are most likely of somatic origin. The extracellular recording prevents the neuron from mechanical injuries and does not disturb the intracellular milieu like whole cell recording. However, it limits the readout to a spike-no spike information and subthreshold transient depolarisations and hyperpolarisations are not detectable (Epsztein et al., 2011; Lee et al., 2012; Quilichini et al., 2010). Also local dendritic events

instrumental in understanding action potential generation and synaptic plasticity mechanisms are not detected by the extracellular electrode. I use the output of spiking GABAergic cell types to predict postsynaptic GABA receptor activation whereas it is known that the effect of presynaptic spikes is strongly influenced by retrograde signalling mechanisms and short- and long-term plasticity (Gaiarsa et al., 2002; Katona et al., 1999b; Mody, 2005). The method I used could be strengthened if further information concerning the intracellular state of the neurons could be extrapolated from the extracellular signals (Henze et al., 2000) or if it was combined with multi-unit recordings (Hartwich et al., 2009; Isomura et al., 2009; Lasztoczi and Klausberger, 2014).

Bistratified cells showed surprising variability which could be due to different experimental conditions despite the efforts to minimise these (e.g., different rats, different experimental days, different experimenters, different recording laboratories). In order to assess whether bistratified cells constitute several groups of interneuron, more cells would need to be recorded for the duration of several hours or days, and further molecular characterisation is needed to establish if the embryonic origin correlates with response patterns in the adult. It is also possible that some of my short recordings captured only time periods when the recorded bistratified cell has changed its firing rate because it was reconfiguring its connectivity to active place cells (Dupret et al., 2013). In contrast, the spike-timing of another bistratified cell might have been measured during stabilised network conditions. Large scale simultaneous recordings of hundreds of interneurons of all types using optical methods would be optimal to answer questions about the participation and connectivity of distinct types of neuron in neuronal network activity given that all recorded neurons could be identified.

6.4 Outlook

In order to have better understanding of the mnemonic functions performed by the hippocampal formation, a systematic and high resolution investigation is required of the neuronal networks involved and their synaptic organisation. Improved anatomical and electrophysiological tools will help elucidate the spiking patterns of cell types not reported previously, as well as, the timing and the roles of intra- and extra-hippocampal long range projections e.g., the GABAergic input from the medial septum which may determine the different preferential firing phases of hippocampal interneuron types (Borhegyi et al., 2004).

As discussed in chapter 3, the significance of my results can be appreciated when considered as a step towards large scale recordings from the hippocampus of animals performing behavioural tasks. Using my results it is now possible to predict the identity of thousands of tetrode-recorded interneurons in rich behavioural situations. This "quasi-identification" of interneurons during well-defined behaviours might bring insights into their contribution to the regulation of pyramidal cell assemblies during learning, memory consolidation and retrieval.

In future, the selective control and recording of targeted populations of neurons during behaviour needs to be achieved to test hypotheses formulated about their roles in the generation and maintenance of distinct network oscillations (Lim et al., 2013; Luo et al., 2008; Tsuda et al., 2013). This requires genetic labelling strategies with better precision and the use of high performance light-gated ion channels (Arenkiel et al., 2007; Lórenz-Fonfría and Heberle, 2014; Schneider et al., 2013) and the development of fast time scale calcium- and/or voltage sensitive dye imaging *in vivo* during behaviour (Akerboom et al., 2013; Bradley et al., 2009; Canepari et al., 2013a; Canepari et al., 2008; Canepari et al., 2013b; Canepari et al., 2010; Canepari et al.,

2013c; Fisher et al., 2008; Flusberg et al., 2008; Greenberg et al., 2008; Kisfali et al., 2013; Mutoh et al., 2012). Several manipulations have been developed (Cardin et al., 2010; Kaifosh et al., 2013; Madisen et al., 2012; Magnus et al., 2011) which allow interference with the neuronal temporal dynamics over various time scales (Sidor and McClung, 2014), some selective to certain groups of interneurons based on the expression of a protein- or peptide in those cells (Asrican et al., 2013; Fuchs et al., 2007; Gentet et al., 2012; Kuhlman and Huang, 2008; Kvitsiani et al., 2013; Lovett-Barron et al., 2014; Pfeffer et al., 2013; Pi et al., 2013; Royer et al., 2012). However, some studies ignore the very different behaviour of distinct cell types expressing the same molecule, e.g., parvalbumin, as demonstrated also in this thesis; e.g., at least ten distinct interneuron types in the CA1 area of the rat hippocampus are immunopositive for either parvalbumin or somatostatin or both, yet their action is segregated in space and time. The existing strategies need improvements in order to provide cell-type specificity and greater temporal resolution for the investigation of physiological events of shorter duration than a theta cycle (Tada et al., 2014), as well as, the interpretations will need to take into account the established diversity of synaptic connections. When accomplished, the upgraded tools will permit the deciphering of the direct contribution of distinct GABAergic interneurons to "gatekeeping" and rhythmic organisation of pyramidal cell firing (Ramirez et al., 2014).

The merging of these novel techniques with experiments of specialised behavioural analyses, e.g., goal oriented learning (Dupret et al., 2013), navigation in virtual environment (Domnisoru et al., 2013; Harvey et al., 2009), is likely to answer exciting questions about hippocampal roles in spatial navigation and memory. Place fields are shared between positively, but not negatively, correlated pyramidal-cell–interneuron pairs (Hangya et al., 2010; Marshall et al., 2002; Maurer et al., 2006).

Synaptic plasticity of the input and output connectivity of GABAergic interneurons may contribute to the formation of such associations (Buzsáki and Eidelberg, 1982; Marshall et al., 2002). The connectivity of unidentified GABAergic interneurons recorded in and around the pyramidal cell layer in the CA1 area is reconfigured in the context of spatial learning (Dupret et al., 2013). It remains to be defined which of the possible ten distinct interneuron types in this location participate in this spatial learning.

Conclusion

My explorations of the hippocampal "chronocircuit" reveal certain roles of cell-type selective synaptic connectivity during theta- and ripple-frequency oscillations in freely moving rats. This work demonstrates the existence of a rhythmic redistribution of GABA acting on different pyramidal cell membrane domains, at slower and faster time scales, which is necessary for the separation of function during different stages of mnemonic processing. The precise dynamics of synaptic changes between neuron types and how this knowledge could be implemented for therapies of cortical disorders will be addressed in the future.

References

Acsády, L., Arabadzisz, D., and Freund, T.F. (1996a). Correlated morphological and neurochemical features identify different subsets of vasoactive intestinal polypeptide-immunoreactive interneurons in rat hippocampus. Neuroscience *73*, 299-315.

Acsády, L., Görcs, T.J., and Freund, T.F. (1996b). Different populations of vasoactive intestinal polypeptide-immunoreactive interneurons are specialized to control pyramidal cells or interneurons in the hippocampus. Neuroscience *73*, 317-334.

Aggleton, J.P. (2012). Multiple anatomical systems embedded within the primate medial temporal lobe: Implications for hippocampal function. Neurosci Biobehav Rev *36*, 1579-1596.

Aggleton, J.P., Wright, N.F., Vann, S.D., and Saunders, R.C. (2012). Medial temporal lobe projections to the retrosplenial cortex of the macaque monkey. Hippocampus *22*, 1883-1900.

Airaksinen, M.S., Eilers, J., Garaschuk, O., Thoenen, H., Konnerth, A., and Meyer, M. (1997). Ataxia and altered dendritic calcium signaling in mice carrying a targeted null mutation of the calbindin D28k gene. Proc Natl Acad Sci U S A *94*, 1488-1493.

Akerboom, J., Carreras Calderón, N., Tian, L., Wabnig, S., Prigge, M., Tolö, J., Gordus, A., Orger, M.B., Severi, K.E., Macklin, J.J.*, et al.* (2013). Genetically encoded calcium indicators for multi-color neural activity imaging and combination with optogenetics. Front Mol Neurosci *6*.

Ali, A.B., Deuchars, J., Pawelzik, H., and Thomson, A.M. (1998). CA1 pyramidal to basket and bistratified cell EPSPs: dual intracellular recordings in rat hippocampal slices. J Physiol *507*, 201-217.

Ali, A.B., and Thomson, A.M. (1998). Facilitating pyramid to horizontal oriens-alveus interneurone inputs: dual intracellular recordings in slices of rat hippocampus. J Physiol *507*, 185-199.

Alle, H., Jonas, P., and Geiger, J.R.P. (2001). PTP and LTP at a hippocampal mossy fiber-interneuron synapse. Proc Natl Acad Sci U S A *98*, 14708-14713.

Allen, Y.S., Adrian, T.E., Allen, J.M., Tatemoto, K., Crow, T.J., Bloom, S.R., and Polak, J.M. (1983). Neuropeptide Y distribution in the rat brain. Science *221*, 877-879.

Amaral, D.G., Dolorfo, C., and Alvarez-Royo, P. (1991). Organization of CA1 projections to the subiculum: A PHA-L analysis in the rat. Hippocampus *1*, 415-435.

Amaral, D.G., Scharfman, H.E., and Lavenex, P. (2007). The dentate gyrus: fundamental neuroanatomical organization (dentate gyrus for dummies). In Prog Brain Res, E.S. Helen, ed. (Elsevier), pp. 3-790.

Amaral, D.G., and Witter, M.P. (1989). The three-dimensional organization of the hippocampal formation: A review of anatomical data. Neuroscience *31*, 571-591.

Andersen, P., Eccles, J.C., and LoYning, Y. (1963). Hippocampus of the Brain: Recurrent Inhibition in the Hippocampus with Identification of the Inhibitory Cell and its Synapses. Nature *198*, 540-542.

Aponte, Y., Bischofberger, J., and Jonas, P. (2008). Efficient Ca2+ buffering in fast-spiking basket cells of rat hippocampus. J Physiol *586*, 2061-2075.

Aponte, Y., Lien, C.-C., Reisinger, E., and Jonas, P. (2006). Hyperpolarization-activated cation channels in fast-spiking interneurons of rat hippocampus. J Physiol *574*, 229-243.

Arenkiel, B.R., Peca, J., Davison, I.G., Feliciano, C., Deisseroth, K., Augustine, George J., Ehlers, M.D., and Feng, G. (2007). In vivo light-induced activation of neural circuitry in transgenic mice expressing channelrhodopsin-2. Neuron *54*, 205-218.

Armstrong, C., Krook-Magnuson, E., Oijala, M., and Soltesz, I. (2013). Closed-loop optogenetic intervention in mice. Nat Protoc *8*, 1475-1493.

Armstrong, C., and Soltesz, I. (2012). Basket cell dichotomy in microcircuit function. J Physiol *590*, 683-694.

Asrican, B., Augustine, G.J., Berglund, K., Chen, S., Chow, N., Deisseroth, K., Feng, G., Gloss, B., Hira, R., Hoffmann, C.*, et al.* (2013). Next-generation transgenic mice for optogenetic analysis of neural circuits. Front Neural Circuits *7*.

Balamotis, M.A., Tamberg, N., Woo, Y.J., Li, J., Davy, B., Kohwi-Shigematsu, T., and Kohwi, Y. (2012). Satb1 ablation alters temporal expression of immediate early genes and reduces dendritic spine density during postnatal brain development. Mol Cell Biol *32*, 333-347.

Banks, M.I., Li, T.-B., and Pearce, R.A. (1998). The synaptic basis of GABAA,slow. J Neurosci *18*, 1305-1317.

Bannerman, D.M., Grubb, M., Deacon, R.M.J., Yee, B.K., Feldon, J., and Rawlins, J.N.P. (2003). Ventral hippocampal lesions affect anxiety but not spatial learning. Behav Brain Res *139*, 197-213.

Bannerman, D.M., Rawlins, J.N.P., McHugh, S.B., Deacon, R.M.J., Yee, B.K., Bast, T., Zhang, W.N., Pothuizen, H.H.J., and Feldon, J. (2004). Regional dissociations within the hippocampus—memory and anxiety. Neurosci Biobehav Rev *28*, 273-283.

Bannerman, D.M., Sprengel, R., Sanderson, D.J., McHugh, S.B., Rawlins, J.N.P., Monyer, H., and Seeburg, P.H. (2014). Hippocampal synaptic plasticity, spatial memory and anxiety. Nat Rev Neurosci *15*, 181-192.

Bartos, M., Vida, I., and Jonas, P. (2007). Synaptic mechanisms of synchronized gamma oscillations in inhibitory interneuron networks. Nat Rev Neurosci *8*, 45-56.

Basar, E., and Guntekin, B. (2008). A review of brain oscillations in cognitive disorders and the role of neurotransmitters. Brain Res *1235*, 172-193.

Batista-Brito, R., and Fishell, G. (2009). Chapter 3 The Developmental Integration of Cortical Interneurons into a Functional Network. In Current Topics in Developmental Biology, H. Oliver, ed. (Academic Press), pp. 81-118.

Baude, A., Bleasdale, C., Dalezios, Y., Somogyi, P., and Klausberger, T. (2007). Immunoreactivity for the GABAA receptor alpha1 subunit, somatostatin and Connexin36 distinguishes axoaxonic, basket, and bistratified interneurons of the rat hippocampus. Cereb Cortex *17*, 2094-2107.

Baude, A., Nusser, Z., Roberts, J.D.B., Mulvihill, E., Jeffrey Mcllhinney, R.A., and Somogyi, P. (1993). The metabotropic glutamate receptor (mGluRlα) is concentrated at perisynaptic membrane of neuronal subpopulations as detected by immunogold reaction. Neuron *11*, 771-787.

Bazelot, M., Dinocourt, C., Cohen, I., and Miles, R. (2010). Unitary inhibitory field potentials in the CA3 region of rat hippocampus. J Physiol *588*, 2077-2090.

Bekinschtein, P., Katche, C., Slipczuk, L., Gonzalez, C., Dorman, G., Cammarota, M., Izquierdo, I., and Medina, J. (2010). Persistence of long-term memory storage: New insights into its molecular signatures in the hippocampus and related structures. Neurotox Res *18*, 377-385.

Belluscio, M.A., Mizuseki, K., Schmidt, R., Kempter, R., and Buzsáki, G. (2012). Cross-frequency phase–phase coupling between theta and gamma oscillations in the hippocampus. J Neurosci *32*, 423-435.

Benarroch, E.E. (2012). GABAB receptors: Structure, functions, and clinical implications. Neurology *78*, 578-584.

Bendor, D., and Wilson, M.A. (2012). Biasing the content of hippocampal replay during sleep. Nat Neurosci *15*, 1439-1444.

Berger, H. (1929). Uber das Elektroenkephalogramm des Menschen. Arch Psychiatr Nervenkrankh *87*, 527-570.

Bezaire, M.J., and Soltesz, I. (2013). Quantitative assessment of CA1 local circuits: Knowledge base for interneuron-pyramidal cell connectivity. Hippocampus *23*, 751-785.

Blasco-Ibanez, J.M., and Freund, T.F. (1995). Synaptic input of horizontal interneurons in stratum oriens of the hippocampal CA1 subfield: structural basis of feed-back activation. Eur J Neurosci *7*, 2170-2180.

Bliss, T.V.P., and Lømo, T. (1973). Long-lasting potentiation of synaptic transmission in the dentate area of the anaesthetized rabbit following stimulation of the perforant path. J Physiol *232*, 331-356.

Boehm, S., and Betz, H. (1997). Somatostatin inhibits excitatory transmission at rat hippocampal synapses via presynaptic receptors. J Neurosci *17*, 4066-4075.

Borhegyi, Z., Varga, V., Szilágyi, N., Fabo, D., and Freund, T.F. (2004). Phase segregation of medial septal GABAergic neurons during hippocampal theta activity. J Neurosci *24*, 8470-8479.

Bradley, J., Luo, R., Otis, T.S., and DiGregorio, D.A. (2009). Submillisecond optical reporting of membrane potential in situ using a neuronal tracer dye. J Neurosci *29*, 9197-9209.

Bragin, A., Engel, J., Wilson, C.L., Fried, I., and Buzsáki, G. (1999). High-frequency oscillations in human brain. Hippocampus *9*, 137-142.

Bragin, A., Jando, G., Nadasdy, Z., Hetke, J., Wise, K., and Buzsaki, G. (1995). Gamma (40-100 Hz) oscillation in the hippocampus of the behaving rat. J Neurosci *15*, 47-60.

Brandon, M.P., Bogaard, A.R., Libby, C.P., Connerney, M.A., Gupta, K., and Hasselmo, M.E. (2011). Reduction of Theta Rhythm Dissociates Grid Cell Spatial Periodicity from Directional Tuning. Science *332*, 595-599.

Brankačk, J., Stewart, M., and E. Fox, S. (1993). Current source density analysis of the hippocampal theta rhythm: associated sustained potentials and candidate synaptic generators. Brain Res *615*, 310-327.

Brazeau, P., Vale, W., Burgus, R., Ling, N., Butcher, M., Rivier, J., and Guillemin, R. (1973). Hypothalamic polypeptide that inhibits the secretion of immunoreactive pituitary growth hormone. Science *179*, 77-79.

Breder, C.D., Yamada, Y., Yasuda, K., Seino, S., Saper, C.B., and Bell, G.I. (1992). Differential expression of somatostatin receptor subtypes in brain. J Neurosci *12*, 3920-3934.

Brickley, S.G., Cull-Candy, S.G., and Farrant, M. (1996). Development of a tonic form of synaptic inhibition in rat cerebellar granule cells resulting from persistent activation of GABAA receptors. J Physiol *497*, 753-759.

Britanova, O., Akopov, S., Lukyanov, S., Gruss, P., and Tarabykin, V. (2005). Novel transcription factor Satb2 interacts with matrix attachment region DNA elements in a tissue-specific manner and demonstrates cell-type-dependent expression in the developing mouse CNS. Eur J Neurosci *21*, 658-668.

Britanova, O., Depew, M.J., Schwark, M., Thomas, B.L., Miletich, I., Sharpe, P., and Tarabykin, V. (2006). Satb2 haploinsufficiency phenocopies 2q32-q33 deletions, whereas loss suggests a fundamental role in the coordination of jaw development. Am J Hum Genet *79*, 668-678.

Buckmaster, P.S., and Jongen-Rêlo, A.L. (1999). Highly specific neuron loss preserves lateral inhibitory circuits in the dentate gyrus of kainate-induced epileptic rats. J Neurosci *19*, 9519-9529.

Bucurenciu, I., Bischofberger, J., and Jonas, P. (2010). A small number of open Ca2+ channels trigger transmitter release at a central GABAergic synapse. Nat Neurosci *13*, 19-21.

Buhl, E.H., Halasy, K., and Somogyi, P. (1994a). Diverse sources of hippocampal unitary inhibitory postsynaptic potentials and the number of synaptic release sites. Nature *368*, 823-828.

Buhl, E.H., Han, Z.S., Lorinczi, Z., Stezhka, V.V., Karnup, S.V., and Somogyi, P. (1994b). Physiological properties of anatomically identified axo-axonic cells in the rat hippocampus. J Neurophysiol *71*, 1289-1307.

Buhl, E.H., Szilágyi, T., Halasy, K., and Somogyi, P. (1996). Physiological properties of anatomically identified basket and bistratified cells in the CA1 area of the rat hippocampus in vitro. Hippocampus *6*, 294-305.

Burgess, N., Maguire, E.A., and O'Keefe, J. (2002). The human hippocampus and spatial and episodic memory. Neuron *35*, 625-641.

Burgess, N., and O'Keefe, J. (2011). Models of place and grid cell firing and theta rhythmicity. Curr Opin Neurobiol *21*, 734-744.

Burwell, R.D. (2000). The parahippocampal region: corticocortical connectivity. Ann N Y Acad Sci *911*, 25-42.

Butt, S.J.B., Fuccillo, M., Nery, S., Noctor, S., Kriegstein, A., Corbin, J.G., and Fishell, G. (2005). The Temporal and Spatial Origins of Cortical Interneurons Predict Their Physiological Subtype. Neuron *48*, 591-604.

Butt, S.J.B., Sousa, V.H., Fuccillo, M.V., Hjerling-Leffler, J., Miyoshi, G., Kimura, S., and Fishell, G. (2008). The Requirement of Nkx2-1 in the Temporal Specification of Cortical Interneuron Subtypes. Neuron *59*, 722-732.

Buzsaki, G. (1998). Memory consolidation during sleep: a neurophysiological perspective. J Sleep Res *7*, 17-23.

Buzsaki, G. (2006). Rhythms of the brain (New York: Oxford University Press).

Buzsáki, G. (1989). Two-stage model of memory trace formation: A role for "noisy" brain states. Neuroscience *31*, 551-570.

Buzsáki, G. (1996). The hippocampo-neocortical dialogue. Cereb Cortex *6*, 81-92.

Buzsáki, G. (2002). Theta oscillations in the hippocampus. Neuron *33*, 325-340.

Buzsáki, G. (2005). Theta rhythm of navigation: Link between path integration and landmark navigation, episodic and semantic memory. Hippocampus *15*, 827-840.

Buzsáki, G., and Chrobak, J.J. (1995). Temporal structure in spatially organized neuronal ensembles: a role for interneuronal networks. Curr Opin Neurobiol *5*, 504-510.

Buzsáki, G., and Draguhn, A. (2004). Neuronal oscillations in cortical networks. Science *304*, 1926-1929.

Buzsáki, G., and Eidelberg, E. (1982). Direct afferent excitation and long-term potentiation of hippocampal interneurons. J Neurophysiol *48*, 597-607.

Buzsaki, G., Horvath, Z., Urioste, R., Hetke, J., and Wise, K. (1992). High-frequency network oscillation in the hippocampus. Science *256*, 1025-1027.

Buzsaki, G., Leung, L.W., and Vanderwolf, C.H. (1983). Cellular bases of hippocampal EEG in the behaving rat. Brain Res *287*, 139-171.

Buzsaki, G., and Moser, E.I. (2013). Memory, navigation and theta rhythm in the hippocampal-entorhinal system. Nat Neurosci *16*, 130-138.

Buzsáki, G., and Wang, X.-J. (2012). Mechanisms of gamma oscillations. Annu Rev Neurosci *35*, 203-225.

Cammalleri, M., Martini, D., Timperio, A.M., and Bagnoli, P. (2009). Functional effects of somatostatin receptor 1 activation on synaptic transmission in the mouse hippocampus. J Neurochem *111*, 1466-1477.

Cammarota, M., Losi, G., Chiavegato, A., Zonta, M., and Carmignoto, G. (2013). Fast spiking interneuron control of seizure propagation in a cortical slice model of focal epilepsy. J Physiol *591*, 807-822.

Canepari, M., De Waard, M., and Ogden, D. (2013a). Combining Ca2+ imaging with L-glutamate photorelease. Cold Spring Harb Protoc *2013*, pdb.prot073122.

Canepari, M., Vogt, K., and Zecevic, D. (2008). Combining voltage and calcium imaging from neuronal dendrites. Cell Mol Neurobiol *28*, 1079-1093.

Canepari, M., Vogt, K.E., De Waard, M., and Zecevic, D. (2013b). Combining Ca2+ and membrane potential imaging in single neurons. Cold Spring Harb Protoc *2013*, pdb.prot073114.

Canepari, M., Willadt, S., Zecevic, D., and Vogt, K.E. (2010). Imaging inhibitory synaptic potentials using voltage sensitive dyes. Biophys J *98*, 2032-2040.

Canepari, M., Zecevic, D., Vogt, K.E., Ogden, D., and De Waard, M. (2013c). Combining calcium imaging with other optical techniques. Cold Spring Harb Protoc *2013*, pdb.top066167.

Canolty, R.T., Edwards, E., Dalal, S.S., Soltani, M., Nagarajan, S.S., Kirsch, H.E., Berger, M.S., Barbaro, N.M., and Knight, R.T. (2006). High gamma power is phase-locked to theta oscillations in human neocortex. Science *313*, 1626-1628.

Capogna, M., and Pearce, R.A. (2011). GABAA,slow: causes and consequences. Trends Neurosci *34*, 101-112.

Cardin, J.A., Carlen, M., Meletis, K., Knoblich, U., Zhang, F., Deisseroth, K., Tsai, L.-H., and Moore, C.I. (2010). Targeted optogenetic stimulation and recording of neurons in vivo using cell-type-specific expression of Channelrhodopsin-2. Nat Protoc *5*, 247-254.

Carr, M.F., Jadhav, S.P., and Frank, L.M. (2011). Hippocampal replay in the awake state: a potential substrate for memory consolidation and retrieval. Nat Neurosci *14*, 147-153.

Castellucci, V., Pinsker, H., Kupfermann, I., and Kandel, E.R. (1970). Neuronal Mechanisms of Habituation and Dishabituation of the Gill-Withdrawal Reflex in Aplysia. Science *167*, 1745-1748.

Cea-del Rio, C.A., Lawrence, J.J., Tricoire, L., Erdelyi, F., Szabo, G., and McBain, C.J. (2010). M3 Muscarinic Acetylcholine Receptor Expression Confers Differential Cholinergic Modulation to Neurochemically Distinct Hippocampal Basket Cell Subtypes. J Neurosci *30*, 6011-6024.

Celio, M.R. (1986). Parvalbumin in most gamma-aminobutyric acid-containing neurons of the rat cerebral cortex. Science *231*, 995-997.

Celio, M.R., Baier, W., Schärer, L., De Viragh, P.A., and Gerday, C. (1988). Monoclonal antibodies directed against the calcium binding protein parvalbumin. Cell Calcium *9*, 81-86.

Celio, M.R., and Heizmann, C.W. (1981). Calcium-binding protein parvalbumin as a neuronal marker. Nature *293*, 300-302.

Chamberland, S., Salesse, C., Topolnik, D., and Topolnik, L. (2010). Synapse-specific inhibitory control of hippocampal feedback inhibitory circuit. Front Cell Neurosci *4:130*, doi: 10.3389/fncel.2010.00130.

Chaudhuri, J.D., Hiltunen, M., Nykänen, M., Ylä-Herttuala, S., Soininen, H., and Miettinen, R. (2005). Localization of m2 muscarinic receptor protein in parvalbumin and calretinin containing cells of the adult rat entorhinal cortex using two complementary methods. Neuroscience *131*, 557-566.

Chen, X., Levkowitz, G., Tzahar, E., Karunagaran, D., Lavi, S., Ben-Baruch, N., Leitner, O., Ratzkin, B.J., Bacus, S.S., and Yarden, Y. (1996). An immunological approach reveals biological differences between the two NDF/Heregulin receptors, ErbB-3 and ErbB-4. J Biol Chem *271*, 7620-7629.

Chrobak, J.J., and Buzsáki, G. (1996). High-frequency oscillations in the output networks of the hippocampal–entorhinal axis of the freely behaving rat. J Neurosci *16*, 3056-3066.

Chrobak, J.J., and Buzsáki, G. (1998a). Gamma oscillations in the entorhinal cortex of the freely behaving rat. J Neurosci *18*, 388-398.

Chrobak, J.J., and Buzsáki, G. (1998b). Operational dynamics in the hippocampal-entorhinal axis. Neurosci Biobehav Rev *22*, 303-310.

Claiborne, B.J., Amaral, D.G., and Cowan, W.M. (1986). A light and electron microscopic analysis of the mossy fibers of the rat dentate gyrus. J Comp Neurol *246*, 435-458.

Clemens, Z., Mölle, M., Erőss, L., Barsi, P., Halász, P., and Born, J. (2007). Temporal coupling of parahippocampal ripples, sleep spindles and slow oscillations in humans. Brain *130*, 2868-2878.

Clemens, Z., Mölle, M., Erőss, L., Jakus, R., Rásonyi, G., Halász, P., and Born, J. (2011). Fine-tuned coupling between human parahippocampal ripples and sleep spindles. Eur J Neurosci *33*, 511-520.

Clemens, Z., Weiss, B., Szűcs, A., Erőss, L., Rásonyi, G., and Halász, P. (2009). Phase coupling between rhythmic slow activity and gamma characterizes mesiotemporal rapid-eye-movement sleep in humans. Neuroscience *163*, 388-396.

Cobb, S.R., Buhl, E.H., Halasy, K., Paulsen, O., and Somogyi, P. (1995). Synchronization of neuronal activity in hippocampus by individual GABAergic interneurons. Nature *378*, 75-78

Cobb, S.R., Halasy, K., Vida, I., Nyíri, G., Tamás, G., Buhl, E.H., and Somogyi, P. (1997). Synaptic effects of identified interneurons innervating both interneurons and pyramidal cells in the rat hippocampus. Neuroscience *79*, 629-648.

Colgin, L.L., Denninger, T., Fyhn, M., Hafting, T., Bonnevie, T., Jensen, O., Moser, M.-B., and Moser, E.I. (2009). Frequency of gamma oscillations routes flow of information in the hippocampus. Nature *462*, 353-357.

Colgin, L.L., and Moser, E.I. (2010). Gamma oscillations in the hippocampus. Physiology *25*, 319-329.

Colmers, W.F., Lukowiak, K., and Pittman, Q.J. (1985). Neuropeptide Y reduces orthodromically evoked population spike in rat hippocampal CA1 by a possibly presynaptic mechanism. Brain Res *346*, 404-408.

Constantinople, C.M., Disney, A.A., Maffie, J., Rudy, B., and Hawken, M.J. (2009). Quantitative analysis of neurons with Kv3 potassium channel subunits, Kv3.1b and Kv3.2, in macaque primary visual cortex. J Comp Neurol *516*, 291-311.

Corkin, S., Amaral, D.G., González, R.G., Johnson, K.A., and Hyman, B.T. (1997). H. M.'s medial temporal lobe lesion: Findings from Magnetic Resonance Imaging. J Neurosci *17*, 3964-3979.

Csicsvari, J., and Dupret, D. (2014). Sharp wave/ripple network oscillations and learning-associated hippocampal maps. Philos Trans R Soc Lond B Biol Sci *369*.

Csicsvari, J., Hirase, H., Czurkó, A., Mamiya, A., and Buzsáki, G. (1999a). Fast network oscillations in the hippocampal CA1 region of the behaving rat. J Neurosci *19*, RC20.

Csicsvari, J., Hirase, H., Czurkó, A., Mamiya, A., and Buzsáki, G. (1999b). Oscillatory coupling of hippocampal pyramidal cells and interneurons in the behaving rat. J Neurosci *19*, 274-287.

Csicsvari, J., Hirase, H., Mamiya, A., and Buzsáki, G. (2000). Ensemble patterns of hippocampal CA3-CA1 neurons during sharp wave–associated population events. Neuron *28*, 585-594.

Csicsvari, J., Jamieson, B., Wise, K.D., and Buzsáki, G. (2003). Mechanisms of gamma oscillations in the hippocampus of the behaving rat. Neuron *37*, 311-322.

Csicsvari, J., O'Neill, J., Allen, K., and Senior, T. (2007). Place-selective firing contributes to the reverse-order reactivation of CA1 pyramidal cells during sharp waves in open-field exploration. Eur J Neurosci *26*, 704-716.

Cunningham, M.O., Hunt, J., Middleton, S., LeBeau, F.E.N., Gillies, M.G., Davies, C.H., Maycox, P.R., Whittington, M.A., and Racca, C. (2006). Region-specific reduction in entorhinal gamma oscillations and parvalbumin-immunoreactive neurons in animal models of psychiatric illness. J Neurosci *26*, 2767-2776.

Czurkó, A., Huxter, J., Li, Y., Hangya, B., and Muller, R.U. (2011). Theta phase classification of interneurons in the hippocampal formation of freely moving rats. J Neurosci *31*, 2938-2947.

Dale, R.M., Remo, B.F., and Svensson, E.C. (2007). An alternative transcript of the FOG-2 gene encodes a FOG-2 isoform lacking the FOG repression motif. Biochem Biophys Res Commun *357*, 683-687.

Dasari, S., and Gulledge, A.T. (2011). M1 and M4 receptors modulate hippocampal pyramidal neurons. J Neurophysiol *105*, 779-792.

David, S.V., Malaval, N., and Shamma, S.A. (2010). Decoupling action potential bias from cortical local field potentials. Comp Intell Neurosci *2010*.

Davidson, T.J., Kloosterman, F., and Wilson, M.A. (2009). Hippocampal replay of extended experience. Neuron *63*, 497-507.

de Bergeyck, V., Naerhuyzen, B., Goffinet, A.M., and Lambert de Rouvroit, C. (1998). A panel of monoclonal antibodies against reelin, the extracellular matrix protein defective in reeler mutant mice. J Neurosci Methods *82*, 17-24.

Deacon, R.M.J., and Rawlins, J.N.P. (2006). T-maze alternation in the rodent. Nat Protoc *1*, 7-12.

Debanne, D., Guerineau, N.C., Gahwiler, B.H., and Thompson, S.M. (1995). Physiology and pharmacology of unitary synaptic connections between pairs of cells in areas CA3 and CA1 of rat hippocampal slice cultures. J Neurophysiol *73*, 1282-1294.

Debanne, D., and Thompson, S.M. (1996). Associative long-term depression in the hippocampus in vitro. Hippocampus *6*, 9-16.

del Rio, J.A., Heimrich, B., Borrell, V., Forster, E., Drakew, A., Alcantara, S., Nakajima, K., Miyata, T., Ogawa, M., Mikoshiba, K.*, et al.* (1997). A role for Cajal-Retzius cells and reelin in the development of hippocampal connections. Nature *385*, 70-74.

del Río, J.A., Martinez, A., Fonseca, M., Auladell, C., and Soriano, E. (1995). Glutamate-like Immunoreactivity and Fate of Cajal-Retzius Cells in the Murine Cortex as Identified with Calretinin Antibody. Cereb Cortex *5*, 13-21.

del Pino, I., García-Frigola, C., Dehorter, N., Brotons-Mas, Jorge R., Alvarez-Salvado, E., Martínez de Lagrán, M., Ciceri, G., Gabaldón, María V., Moratal, D., Dierssen, M.*, et al.* (2013). Erbb4 deletion from fast-spiking interneurons causes schizophrenia-like phenotypes. Neuron *79*, 1152-1168.

Derer, P., and Derer, M. (1990). Cajal-retzius cell ontogenesis and death in mouse brain visualized with horseradish peroxidase and electron microscopy. Neuroscience *36*, 839-856.

Destexhe, A., and Paré, D. (1999). Impact of network activity on the integrative properties of neocortical pyramidal neurons in vivo. J Neurophysiol *81*, 1531-1547.

Deuchars, J., and Thomson, A.M. (1996). CA1 pyramid-pyramid connections in rat hippocampus in vitro: Dual intracellular recordings with biocytin filling. Neuroscience *74*, 1009-1018.

Diba, K., and Buzsaki, G. (2007). Forward and reverse hippocampal place-cell sequences during ripples. Nat Neurosci *10*, 1241-1242.

Dickinson, L.A., Joh, T., Kohwi, Y., and Kohwi-Shigematsu, T. (1992). A tissue-specific MARSAR DNA-binding protein with unusual binding site recognition. Cell *70*, 631-645.

Dobreva, G., Chahrour, M., Dautzenberg, M., Chirivella, L., Kanzler, B., Fariñas, I., Karsenty, G., and Grosschedl, R. (2006). SATB2 is a multifunctional determinant of craniofacial patterning and osteoblast differentiation. Cell *125*, 971-986.

Doischer, D., Aurel Hosp, J., Yanagawa, Y., Obata, K., Jonas, P., Vida, I., and Bartos, M. (2008). Postnatal Differentiation of Basket Cells from Slow to Fast Signaling Devices. J Neurosci *28*, 12956-12968.

Dolleman-Van der Weel, M.J., and Witter, M.P. (2000). Nucleus reuniens thalami innervates γ aminobutyric acid positive cells in hippocampal field CA1 of the rat. Neurosci Lett *278*, 145-148.

Domnisoru, C., Kinkhabwala, A.A., and Tank, D.W. (2013). Membrane potential dynamics of grid cells. Nature *495*, 199-204.

Douchamps, V., Jeewajee, A., Blundell, P., Burgess, N., and Lever, C. (2013). Evidence for encoding versus retrieval scheduling in the hippocampus by theta phase and acetylcholine. J Neurosci *33*, 8689-8704.

Dournaud, P., Gu, Y.Z., Schonbrunn, A., Mazella, J., Tannenbaum, G.S., and Beaudet, A. (1996). Localization of the somatostatin receptor SST2A in rat brain using a specific anti-peptide antibody. J Neurosci *16*, 4468-4478.

Dragoi, G., and Buzsáki, G. (2006). Temporal encoding of place sequences by hippocampal cell assemblies. Neuron *50*, 145-157.

Dragoi, G., Carpi, D., Recce, M., Csicsvari, J., and Buzsáki, G. (1999). Interactions between hippocampus and medial septum during sharp waves and theta oscillation in the behaving rat. J Neurosci *19*, 6191-6199.

Du, J., Zhang, L., Weiser, M., Rudy, B., and McBain, C.J. (1996). Developmental expression and functional characterization of the potassium-channel subunit Kv3.1b in parvalbumin-containing interneurons of the rat hippocampus. J Neurosci *16*, 506-518.

Dudek, S.M., and Bear, M.F. (1992). Homosynaptic long-term depression in area CA1 of hippocampus and effects of N-methyl-D-aspartate receptor blockade. Proc Natl Acad Sci U S A *89*, 4363-4367.

Dupret, D., O'Neill, J., Pleydell-Bouverie, B., and Csicsvari, J. (2010). The reorganization and reactivation of hippocampal maps predict spatial memory performance. Nat Neurosci *13*, 995-1002.

Dupret, D., O Neill, J., and Csicsvari, J. (2013). Dynamic reconfiguration of hippocampal interneuron circuits during spatial learning. Neuron *78*, 166-180.

Ego-Stengel, V., and Wilson, M.A. (2007). Spatial selectivity and theta phase precession in CA1 interneurons. Hippocampus *17*, 161-174.

Ego-Stengel, V., and Wilson, M.A. (2010). Disruption of ripple-associated hippocampal activity during rest impairs spatial learning in the rat. Hippocampus *20*, 1-10.

Eichenbaum, H., and Lipton, P.A. (2008). Towards a functional organization of the medial temporal lobe memory system: Role of the parahippocampal and medial entorhinal cortical areas. Hippocampus *18*, 1314-1324.

Eichenbaum, H., Sauvage, M., Fortin, N., Komorowski, R., and Lipton, P. (2012). Towards a functional organization of episodic memory in the medial temporal lobe. Neurosci Biobehav Reviews *36*, 1597-1608.

Einstein, E.B., Patterson, C.A., Hon, B.J., Regan, K.A., Reddi, J., Melnikoff, D.E., Mateer, M.J., Schulz, S., Johnson, B.N., and Tallent, M.K. (2010). Somatostatin signaling in neuronal cilia is critical for object recognition memory. J Neurosci *30*, 4306-4314.

Ellender, T.J., Nissen, W., Colgin, L.L., Mann, E.O., and Paulsen, O. (2010). Priming of hippocampal population bursts by individual perisomatic-targeting interneurons. J Neurosci *30*, 5979-5991.

Elvander-Tottie, E., Eriksson, T.M., Sandin, J., and Ogren, S.O. (2009). 5-HT(1A) and NMDA receptors interact in the rat medial septum and modulate hippocampal-dependent spatial learning. Hippocampus.

Engel, A.K., and Singer, W. (2001). Temporal binding and the neural correlates of sensory awareness. Trends Cogn Sci *5*, 16-25.

Epsztein, J., Brecht, M., and Lee, A.K. (2011). Intracellular determinants of hippocampal CA1 place and silent cell activity in a novel environment. Neuron *70*, 109-120.

Erisir, A., Lau, D., Rudy, B., and Leonard, C.S. (1999). Function of specific K+ channels in sustained high-frequency firing of fast-spiking neocortical interneurons. J Neurophysiol *82*, 2476-2489.

Fanselow, M.S., and Dong, H.-W. (2010). Are the dorsal and ventral hippocampus functionally distinct structures? Neuron *65*, 7-19.

Farrant, M., and Nusser, Z. (2005). Variations on an inhibitory theme: phasic and tonic activation of GABAA receptors. Nat Rev Neurosci *6*, 215-229.

Fazzari, P., Paternain, A.V., Valiente, M., Pla, R., Lujan, R., Lloyd, K., Lerma, J., Marin, O., and Rico, B. (2010). Control of cortical GABA circuitry development by Nrg1 and ErbB4 signalling. Nature *464*, 1376-1380.

Feldt Muldoon, S., Soltesz, I., and Cossart, R. (2013). Spatially clustered neuronal assemblies comprise the microstructure of synchrony in chronically epileptic networks. Proc Natl Acad Sci U S A *110*, 3567-3572.

Férézou, I., Cauli, B., Hill, E.L., Rossier, J., Hamel, E., and Lambolez, B. (2002). 5-HT3 Receptors Mediate Serotonergic Fast Synaptic Excitation of Neocortical Vasoactive Intestinal Peptide/Cholecystokinin Interneurons. J Neurosci *22*, 7389-7397.

Ferraguti, F., Klausberger, T., Cobden, P., Baude, A., Roberts, J.D.B., Szucs, P., Kinoshita, A., Shigemoto, R., Somogyi, P., and Dalezios, Y. (2005). Metabotropic glutamate receptor 8-expressing nerve terminals target subsets of GABAergic neurons in the hippocampus. J Neurosci *25*, 10520-10536.

Fisahn, A., Neddens, J., Yan, L., and Buonanno, A. (2009). Neuregulin-1 modulates hippocampal gamma oscillations: Implications for schizophrenia. Cereb Cortex *19*, 612-618.

Fisahn, A., Pike, F.G., Buhl, E.H., and Paulsen, O. (1998). Cholinergic induction of network oscillations at 40Hz in the hippocampus in vitro. Nature *394*, 186-189.

Fishell, G. (2007). Perspectives on the developmental origins of cortical interneuron diversity. Novartis Found Symp *288*, 21-35.

Fisher, J.A.N., Barchi, J.R., Welle, C.G., Kim, G.-H., Kosterin, P., Obaid, A.L., Yodh, A.G., Contreras, D., and Salzberg, B.M. (2008). Two-photon excitation of potentiometric probes enables optical recording of action potentials from mammalian nerve terminals in situ. J Neurophysiol *99*, 1545-1553.

Flusberg, B.A., Nimmerjahn, A., Cocker, E.D., Mukamel, E.A., Barretto, R.P.J., Ko, T.H., Burns, L.D., Jung, J.C., and Schnitzer, M.J. (2008). High-speed, miniaturized fluorescence microscopy in freely moving mice. Nat Methods *5*, 935-938.

Fortin, N.J., Agster, K.L., and Eichenbaum, H.B. (2002). Critical role of the hippocampus in memory for sequences of events. Nat Neurosci *5*, 458-462.

Foster, D.J., and Wilson, M.A. (2006). Reverse replay of behavioural sequences in hippocampal place cells during the awake state. Nature *440*, 680-683.

Fox, S.E. (1989). Membrane potential and impedance changes in hippocampal pyramidal cells during theta rhythm. Exp Brain Res *77*, 283-294.

Freund, T.F. (1989). GABAergic septohippocampal neurons contain parvalbumin. Brain Res *478*, 375-381.

Freund, T.F. (1992). GABAergic septal and serotonergic median raphe afferents preferentially innervate inhibitory interneurons in the hippocampus and dentate gyrus. Epilepsy Res Suppl *7*, 79-91.

Freund, T.F. (2003). Interneuron diversity series: Rhythm and mood in perisomatic inhibition. Trends Neurosci *26*, 489-495.

Freund, T.F., and Antal, M. (1988). GABA-containing neurons in the septum control inhibitory interneurons in the hippocampus. Nature *336*, 170-173.

Freund, T.F., and Buzsáki, G. (1996). Interneurons of the hippocampus. Hippocampus *6*, 347-470.

Freund, T.F., and Hajos, N. (2003). Excitement reduces inhibition via endocannabinoids. Neuron *38*, 362-365.

Freund, T.F., and Katona, I. (2007). Perisomatic inhibition. Neuron *56*, 33-42.

Fries, P. (2009). Neuronal gamma-band synchronization as a fundamental process in cortical computation. Annu Rev Neurosci *32*, 209-224.

Fries, P., Nikolić, D., and Singer, W. (2007). The gamma cycle. Trends Neurosci *30*, 309-316.

Fries, P., Reynolds, J.H., Rorie, A.E., and Desimone, R. (2001). Modulation of oscillatory neuronal synchronization by selective visual attention. Science *291*, 1560-1563.

Fritschy, J.-M., and Panzanelli, P. (2014). GABAA receptors and plasticity of inhibitory neurotransmission in the central nervous system. Eur J Neurosci, 10.1111/ejn.12534.

Frotscher, M., and Léránth, C. (1985). Cholinergic innervation of the rat hippocampus as revealed by choline acetyltransferase immunocytochemistry: A combined light and electron microscopic study. J Comp Neurol *239*, 237-246.

Frotscher, M., Léránth, C., Lübbers, K., and Oertel, W.H. (1984). Commissural afferents innervate glutamate decarboxylase immunoreactive non-pyramidal neurons in the guinea pig hippocampus. Neurosci Lett *46*, 137-143.

Fuchs, E.C., Zivkovic, A.R., Cunningham, M.O., Middleton, S., LeBeau, F.E.N., Bannerman, David M., Rozov, A., Whittington, M.A., Traub, R.D., Rawlins, J.N.P.*, et al.* (2007). Recruitment of parvalbumin-positive interneurons determines hippocampal function and associated behavior. Neuron *53*, 591-604.

Fuentealba, P., Begum, R., Capogna, M., Jinno, S., Marton, L.F., Csicsvari, J., Thomson, A., Somogyi, P., and Klausberger, T. (2008a). Ivy cells: a population of nitric-oxide-producing, slow-spiking GABAergic neurons and their involvement in hippocampal network activity. Neuron *57*, 917-929.

Fuentealba, P., Klausberger, T., Karayannis, T., Suen, W.Y., Huck, J., Tomioka, R., Rockland, K., Capogna, M., Studer, M., Morales, M.*, et al.* (2010). Expression of COUP-TFII nuclear receptor in restricted GABAergic neuronal populations in the adult rat hippocampus. J Neurosci *30*, 1595-1609.

Fuentealba, P., Tomioka, R., Dalezios, Y., Márton, L.F., Studer, M., Rockland, K., Klausberger, T., and Somogyi, P. (2008b). Rhythmically active enkephalin-expressing GABAergic cells in the CA1 area of the hippocampus project to the subiculum and preferentially innervate interneurons. J Neurosci *28*, 10017-10022.

Fujisawa, S., and Buzsáki, G. (2011). A 4 Hz oscillation adaptively synchronizes prefrontal, VTA, and hippocampal activities. Neuron *72*, 153-165.

Fukuda, T., Aika, Y., Heizmann, C.W., and Kosaka, T. (1996). Dense GABAergic input on somata of parvalbumin-immunoreactive GABAergic neurons in the hippocampus of the mouse. Neurosci Res *26*, 181-194.

Fukuda, T., and Kosaka, T. (2003). Ultrastructural study of gap junctions between dendrites of parvalbumin-containing GABAergic neurons in various neocortical areas of the adult rat. Neuroscience *120*, 5-20.

Fukuda, T., Kosaka, T., Singer, W., and Galuske, R.A.W. (2006). Gap Junctions among Dendrites of Cortical GABAergic Neurons Establish a Dense and Widespread Intercolumnar Network. J Neurosci *26*, 3434-3443.

Fukudome, Y., Ohno-Shosaku, T., Matsui, M., Omori, Y., Fukaya, M., Tsubokawa, H., Taketo, M.M., Watanabe, M., Manabe, T., and Kano, M. (2004). Two distinct classes of muscarinic action on hippocampal inhibitory synapses: M2-mediated direct suppression and M1/M3-mediated indirect suppression through endocannabinoid signalling. Eur J Neurosci *19*, 2682-2692.

Gaiarsa, J.-L., Caillard, O., and Ben-Ari, Y. (2002). Long-term plasticity at GABAergic and glycinergic synapses: mechanisms and functional significance. Trends Neurosci *25*, 564-570.

Galindo-Leon, E., and Liu, R. (2010). Predicting stimulus-locked single unit spiking from cortical local field potentials. J Comput Neurosci *29*, 581-597.

Gao, B., and Fritschy, J.M. (1994). Selective Allocation of GABAA Receptors Containing the α1 Subunit to Neurochemically Distinct Subpopulations of Rat Hippocampal Interneurons. Eur J Neurosci *6*, 837-853.

Geisler, C., Diba, K., Pastalkova, E., Mizuseki, K., Royer, S., and Buzsáki, G. (2010). Temporal delays among place cells determine the frequency of population theta oscillations in the hippocampus. Proc Natl Acad Sci U S A *107*, 7957-7962.

Geisler, C., Robbe, D., Zugaro, M., Sirota, A., and Buzsáki, G. (2007). Hippocampal place cell assemblies are speed-controlled oscillators. Proc Natl Acad Sci U S A *104*, 8149-8154.

Gentet, L.J., Kremer, Y., Taniguchi, H., Huang, Z.J., Staiger, J.F., and Petersen, C.C.H. (2012). Unique functional properties of somatostatin-expressing GABAergic neurons in mouse barrel cortex. Nat Neurosci *15*, 607-612.

Girardeau, G., Benchenane, K., Wiener, S.I., Buzsaki, G., and Zugaro, M.B. (2009). Selective suppression of hippocampal ripples impairs spatial memory. Nat Neurosci *12*, 1222-1223.

Glickfeld, L.L., Roberts, J.D., Somogyi, P., and Scanziani, M. (2009). Interneurons hyperpolarize pyramidal cells along their entire somatodendritic axis. Nat Neurosci *12*, 21-23.

Glickfeld, L.L., and Scanziani, M. (2006). Distinct timing in the activity of cannabinoid-sensitive and cannabinoid-insensitive basket cells. Nat Neurosci *9*, 807-815.

Goldberg, E.M., Clark, B.D., Zagha, E., Nahmani, M., Erisir, A., and Rudy, B. (2008). K+ channels at the axon initial segment dampen near-threshold excitability of neocortical fast-spiking GABAergic interneurons. Neuron *58*, 387-400.

Gonchar, Y., Turney, S., Price, J.L., and Burkhalter, A. (2002). Axo-axonic synapses formed by somatostatin-expressing GABAergic neurons in rat and monkey visual cortex. J Comp Neurol *443*, 1-14.

Good, P. (2000). Permutation tests : a practical guide to resampling methods for testing hypotheses (New York: Springer).

Green, J.R., and Scheetz, D.G. (1964). Surgery of epileptogenic lesions of the temporal lobe. Arch Neurol *10*, 135-148.

Greenberg, D.S., Houweling, A.R., and Kerr, J.N.D. (2008). Population imaging of ongoing neuronal activity in the visual cortex of awake rats. Nat Neurosci *11*, 749-751.

Griguoli, M., Scuri, R., Ragozzino, D., and Cherubini, E. (2009). Activation of nicotinic acetylcholine receptors enhances a slow calcium-dependent potassium conductance and reduces the firing of stratum oriens interneurons. Eur J Neurosci *30*, 1011-1022.

Grosmark, Andres D., Mizuseki, K., Pastalkova, E., Diba, K., and Buzsáki, G. (2012). REM sleep reorganizes hippocampal excitability. Neuron *75*, 1001-1007.

Gulyás, A.I., Görcs, T.J., and Freund, T.F. (1990). Innervation of different peptide-containing neurons in the hippocampus by GABAergic septal afferents. Neuroscience *37*, 31-44.

Gulyás, A.I., Hájos, N., and Freund, T.F. (1996). Interneurons containing calretinin are specialized to control other interneurons in the rat hippocampus. J Neurosci *16*, 3397-3411.

Gulyás, A.I., Hájos, N., Katona, I., and Freund, T.F. (2003). Interneurons are the local targets of hippocampal inhibitory cells which project to the medial septum. Eur J Neurosci *17*, 1861-1872.

Gulyás, A.I., Megías, M., Emri, Z., and Freund, T.F. (1999). Total number and ratio of excitatory and Inhibitory synapses converging onto single interneurons of different types in the CA1 area of the rat hippocampus. J Neurosci *19*, 10082-10097.

Gulyás, A.I., Miettinen, R., Jacobowitz, D.M., and Freund, T.F. (1992). Calretinin is present in non-pyramidal cells of the rat hippocampus—I. A new type of neuron specifically associated with the mossy fibre system. Neuroscience *48*, 1-27.

Gulyás, A.I., Miles, R., Hájos, N., and Freund, T.F. (1993). Precision and variability in postsynaptic target selection of inhibitory cells in the hippocampal CA3 region. Eur J Neurosci *5*, 1729-1751.

Gulyas, A.I., Miles, R., Sik, A., Toth, K., Tamamaki, N., and Freund, T.F. (1993). Hippocampal pyramidal cells excite inhibitory neurons through a single release site. Nature *366*, 683-687.

Gulyás, A.I., Szabó, G.G., Ulbert, I., Holderith, N., Monyer, H., Erdélyi, F., Szabó, G., Freund, T.F., and Hájos, N. (2010). Parvalbumin-containing fast-spiking basket cells generate the field potential oscillations induced by cholinergic receptor activation in the hippocampus. J Neurosci *30*, 15134-15145.

Haiss, F., Butovas, S., and Schwarz, C. (2010). A miniaturized chronic microelectrode drive for awake behaving head restrained mice and rats. J Neurosci Methods *187*, 67-72.

Hajós, M., Hoffmann, W.E., and Weaver, R.J. (2003). Regulation of septo-hippocampal activity by 5-Hydroxytryptamine2C receptors. J Pharmacol Exp Ther *306*, 605-615.

Hájos, N., Karlócai, M.R., Németh, B., Ulbert, I., Monyer, H., Szabó, G., Erdélyi, F., Freund, T.F., and Gulyás, A.I. (2013). Input-output features of anatomically identified CA3 neurons during hippocampal sharp wave/ripple oscillation in vitro. J Neurosci *33*, 11677-11691.

Hájos, N., Pálhalmi, J., Mann, E.O., Németh, B., Paulsen, O., and Freund, T.F. (2004). Spike timing of distinct types of GABAergic interneuron during hippocampal gamma oscillations in vitro. J Neurosci *24*, 9127-9137.

Hájos, N., Papp, E.C., Acsády, L., Levey, A.I., and Freund, T.F. (1997). Distinct interneuron types express m2 muscarinic receptor immunoreactivity on their dendrites or axon terminals in the hippocampus. Neuroscience *82*, 355-376.

Hájos, N., and Paulsen, O. (2009). Network mechanisms of gamma oscillations in the CA3 region of the hippocampus. Neural Netw *22*, 1113-1119.

Halasy, K., Buhl, E.H., Lörinczi, Z., Tamás, G., and Somogyi, P. (1996). Synaptic target selectivity and input of GABAergic basket and bistratified interneurons in the CA1 area of the rat hippocampus. Hippocampus *6*, 306-329.

Halliwell, J.V., and Adams, P.R. (1982). Voltage-clamp analysis of muscarinic excitation in hippocampal neurons. Brain Res *250*, 71-92.

Hangya, B., Borhegyi, Z., Szilágyi, N., Freund, T.F., and Varga, V. (2009). GABAergic neurons of the medial septum lead the hippocampal network during theta activity. J Neurosci *29*, 8094-8102.

Hangya, B., Li, Y., Muller, R.U., and Czurkó, A. (2010). Complementary spatial firing in place cell–interneuron pairs. J Physiol *588*, 4165-4175.

Hara, K., and Harris, R.A. (2002). The anesthetic mechanism of urethane: The effects on neurotransmitter-gated ion channels. Anesth Analg *94*.

Harris, K.D. (2005). Neural signatures of cell assembly organization. Nat Rev Neurosci *6*, 399-407.

Harris, K.D., Csicsvari, J., Hirase, H., Dragoi, G., and Buzsaki, G. (2003). Organization of cell assemblies in the hippocampus. Nature *424*, 552-556.

Harris, K.D., Henze, D.A., Hirase, H., Leinekugel, X., Dragoi, G., Czurko, A., and Buzsaki, G. (2002). Spike train dynamics predicts theta-related phase precession in hippocampal pyramidal cells. Nature *417*, 738-741.

Harris, K.D., Hirase, H., Leinekugel, X., Henze, D.A., and Buzsaki, G. (2001). Temporal interaction between single spikes and complex spike bursts in hippocampal pyramidal cells. Neuron *32*, 141-149.

Harris, K.M., Marshall, P.E., and Landis, D.M.D. (1985). Ultrastructural study of cholecystokinin-immunoreactive cells and processes in area CA1 of the rat hippocampus. J Comp Neurol *233*, 147-158.

Hartwich, K., Pollak, T., and Klausberger, T. (2009). Distinct firing patterns of identified basket and dendrite-targeting interneurons in the prefrontal cortex during hippocampal theta and local spindle oscillations. J Neurosci *29*, 9563-9574.

Harvey, C.D., Collman, F., Dombeck, D.A., and Tank, D.W. (2009). Intracellular dynamics of hippocampal place cells during virtual navigation. Nature *461*, 941-946.

Hasselmo, M.E. (1999). Neuromodulation: acetylcholine and memory consolidation. Trends Cogn Sci *3*, 351-359.

Hasselmo, M.E., Bodelón, C., and Wyble, B.P. (2002). A proposed function for hippocampal theta rhythm: separate phases of encoding and retrieval enhance reversal of prior learning. Neural Comput *14*, 793-817.

Hebb, D.O. (1949). The organization of behaviour: A neuropsychological approach (New York: Wiley).

Hefft, S., and Jonas, P. (2005). Asynchronous GABA release generates long-lasting inhibition at a hippocampal interneuron-principal neuron synapse. Nat Neurosci *8*, 1319-1328.

Henriksen, E.J., Colgin, L.L., Barnes, C.A., Witter, M.P., Moser, M.-B., and Moser, E.I. (2010). Spatial representation along the proximodistal axis of CA1. Neuron *68*, 127-137.

Henze, D.A., Borhegyi, Z., Csicsvari, J., Mamiya, A., Harris, K.D., and Buzsáki, G. (2000). Intracellular features predicted by extracellular recordings in the hippocampus in vivo. J Neurophysiol *84*, 390-400.

Hevner, R.F., Neogi, T., Englund, C., Daza, R.A.M., and Fink, A. (2003). Cajal–Retzius cells in the mouse: transcription factors, neurotransmitters, and birthdays suggest a pallial origin. Dev Brain Res *141*, 39-53.

Hölscher, C., Anwyl, R., and Rowan, M.J. (1997). Stimulation on the positive phase of hippocampal theta rhythm induces long-term potentiation that can be depotentiated by stimulation on the negative phase in area CA1 in vivo. J Neurosci *17*, 6470-6477.

Hormuzdi, S.G., Pais, I., LeBeau, F.E.N., Towers, S.K., Rozov, A., Buhl, E.H., Whittington, M.A., and Monyer, H. (2001). Impaired electrical signaling disrupts gamma frequency oscillations in connexin 36-deficient mice. Neuron *31*, 487-495.

Howard, M.W., Rizzuto, D.S., Caplan, J.B., Madsen, J.R., Lisman, J., Aschenbrenner-Scheibe, R., Schulze-Bonhage, A., and Kahana, M.J. (2003). Gamma oscillations correlate with working memory load in humans. Cereb Cortex *13*, 1369-1374.

Hu, H., Martina, M., and Jonas, P. (2010). Dendritic mechanisms underlying rapid synaptic activation of fast-spiking hippocampal interneurons. Science *327*, 52-58.

Huang, Y., Zhang, L., Song, N.-N., Hu, Z.-L., Chen, J.-Y., and Ding, Y.-Q. (2011). Distribution of Satb1 in the central nervous system of adult mice. Neurosci Res *71*, 12-21.

Hughes, D.I., Boyle, K.A., Kinnon, C.M., Bilsland, C., Quayle, J.A., Callister, R.J., and Graham, B.A. (2013). HCN4 subunit expression in fast-spiking interneurons of the rat spinal cord and hippocampus. Neuroscience *237*, 7-18.

Huusko, N., Römer, C., Ndode-Ekane, X., Lukasiuk, K., and Pitkänen, A. (2013). Loss of hippocampal interneurons and epileptogenesis: a comparison of two animal models of acquired epilepsy. Brain Struct Funct, 1-39.

Hyman, B.T., Van Hoesen, G.W., Damasio, A.R., and Barnes, C.L. (1984). Alzheimer's disease: cell-specific pathology isolates the hippocampal formation. Science *225*, 1168-1170.

Ishizuka, N. (2001). Laminar organization of the pyramidal cell layer of the subiculum in the rat. J Comp Neurol *435*, 89-110.

Ishizuka, N., Cowan, W.M., and Amaral, D.G. (1995). A quantitative analysis of the dendritic organization of pyramidal cells in the rat hippocampus. J Comp Neurol *362*, 17-45.

Ishizuka, N., Weber, J., and Amaral, D.G. (1990). Organization of intrahippocampal projections originating from CA3 pyramidal cells in the rat. J Comp Neurol *295*, 580-623.

Isomura, Y., Harukuni, R., Takekawa, T., Aizawa, H., and Fukai, T. (2009). Microcircuitry coordination of cortical motor information in self-initiation of voluntary movements. Nat Neurosci *12*, 1586-1593.

Isomura, Y., Sirota, A., Özen, S., Montgomery, S., Mizuseki, K., Henze, D.A., and Buzsáki, G. (2006). Integration and segregation of activity in entorhinal-hippocampal subregions by neocortical slow oscillations. Neuron *52*, 871-882.

Jacobs, J., Kahana, M.J., Ekstrom, A.D., and Fried, I. (2007). Brain oscillations control timing of single-neuron activity in humans. J Neurosci *27*, 3839-3844.

Jadhav, S.P., Kemere, C., German, P.W., and Frank, L.M. (2012). Awake hippocampal sharp-wave ripples support spatial memory. Science *336*, 1454-1458.

Jeong, J. (2004). EEG dynamics in patients with Alzheimer's disease. Clin Neurophysiol *115*, 1490-1505.

Jinno, S. (2009). Structural organization of long-range GABAergic projection system of the hippocampus. Front Neuroanat *3*.

Jinno, S., Klausberger, T., Marton, L.F., Dalezios, Y., Roberts, J.D., Fuentealba, P., Bushong, E.A., Henze, D., Buzsaki, G., and Somogyi, P. (2007). Neuronal diversity in GABAergic long-range projections from the hippocampus. J Neurosci *27*, 8790-8804.

Jinno, S., and Kosaka, T. (2000). Colocalization of parvalbumin and somatostatin-like immunoreactivity in the mouse hippocampus: Quantitative analysis with optical disector. J Comp Neurol *428*, 377-388.

Johnston, D., and Brown, T.H. (1986). Control theory applied to neural networks illuminates synaptic basis of interictal epileptiform activity. Adv Neurol *44*, 263-274.

Jonas, P., Bischofberger, J., Fricker, D., and Miles, R. (2004). Interneuron Diversity series: Fast in, fast out – temporal and spatial signal processing in hippocampal interneurons. Trends Neurosci *27*, 30-40.

Jones, M.W., and Wilson, M.A. (2005). Theta rhythms coordinate hippocampal–prefrontal interactions in a spatial memory task. PLoS Biol *3*, e402.

Kägi, U., Berchtold, M.W., and Heizmann, C.W. (1987). Ca2+-binding parvalbumin in rat testis. Characterization, localization, and expression during development. J Biol Chem *262*, 7314-7320.

Kaifosh, P., Lovett-Barron, M., Turi, G.F., Reardon, T.R., and Losonczy, A. (2013). Septo-hippocampal GABAergic signaling across multiple modalities in awake mice. Nat Neurosci *16*, 1182-1184.

Kamondi, A., Acsády, L., Wang, X.-J., and Buzsáki, G. (1998). Theta oscillations in somata and dendrites of hippocampal pyramidal cells in vivo: Activity-dependent phase-precession of action potentials. Hippocampus *8*, 244-261.

Kamondi, A., Horvath, Z., Bors, L., and Buzsaki, G. (1988). Perforant path activation of the hippocampus: spatial distribution, effects of urethane and atropine. Acta Physiol Hung *71*, 19-29.

Kanatani, S., Yozu, M., Tabata, H., and Nakajima, K. (2008). COUP-TFII Is Preferentially Expressed in the Caudal Ganglionic Eminence and Is Involved in the Caudal Migratory Stream. J Neurosci *28*, 13582-13591.

Kandel, E.R., and Spencer, W.A. (1961). Electrophysiology of hippocampal neurons: II. After-potentials and repetitive firing. J Neurophysiol *24*, 243-259.

Kaplan, J.S., Mohr, C., and Rossi, D.J. (2013). Opposite actions of alcohol on tonic GABAA receptor currents mediated by nNOS and PKC activity. Nat Neurosci *16*, 1783-1793.

Karlsson, M.P., and Frank, L.M. (2009). Awake replay of remote experiences in the hippocampus. Nat Neurosci *12*, 913-918.

Kasugai, Y., Swinny, J.D., Roberts, J.D.B., Dalezios, Y., Fukazawa, Y., Sieghart, W., Shigemoto, R., and Somogyi, P. (2010). Quantitative localisation of synaptic and extrasynaptic GABAA receptor subunits on hippocampal pyramidal cells by freeze-fracture replica immunolabelling. Eur J Neurosci *32*, 1868-1888.

Katona, I., Acsády, L., and Freund, T.F. (1999a). Postsynaptic targets of somatostatin-immunoreactive interneurons in the rat hippocampus. Neuroscience *88*, 37-55.

Katona, I., and Freund, T.F. (2008). Endocannabinoid signaling as a synaptic circuit breaker in neurological disease. Nat Med *14*, 923-930.

Katona, I., Sperlágh, B., Sík, A., Käfalvi, A., Vizi, E.S., Mackie, K., and Freund, T.F. (1999b). Presynaptically located CB1 cannabinoid receptors regulate GABA release from axon terminals of specific hippocampal interneurons. J Neurosci *19*, 4544-4558.

Katona, L., Lapray, D., Viney, Tim J., Oulhaj, A., Borhegyi, Z., Micklem, Benjamin R., Klausberger, T., and Somogyi, P. (2014). Sleep and movement differentiates actions of two types of somatostatin-expressing GABAergic interneuron in rat hippocampus. Neuron, *advance online publication*.

Katsumaru, H., Kosaka, T., Heizmann, C.W., and Hama, K. (1988a). Gap junctions on GABAergic neurons containing the calcium-binding protein parvalbumin in the rat hippocampus (CA1 region). Exp Brain Res *72*, 363-370.

Katsumaru, H., Kosaka, T., Heizmann, C.W., and Hama, K. (1988b). Immunocytochemical study of GABAergic neurons containing the calcium-binding protein parvalbumin in the rat hippocampus. Exp Brain Res *72*, 347-362.

Kawaguchi, Y., Katsumaru, H., Kosaka, T., Heizmann, C.W., and Hama, K. (1987). Fast spiking cells in rat hippocampus (CA1 region) contain the calcium-binding protein parvalbumin. Brain Res *416*, 369-374.

Kenward, M.G., and Roger, J.H. (1997). Small sample inference for fixed effects from restricted maximum likelihood. Biometrics *53*, 983-997.

Kerr, K.M., Agster, K.L., Furtak, S.C., and Burwell, R.D. (2007). Functional neuroanatomy of the parahippocampal region: The lateral and medial entorhinal areas. Hippocampus *17*, 697-708.

Khirug, S., Yamada, J., Afzalov, R., Voipio, J., Khiroug, L., and Kaila, K. (2008). GABAergic Depolarization of the Axon Initial Segment in Cortical Principal Neurons Is Caused by the Na–K–2Cl Cotransporter NKCC1. J Neurosci *28*, 4635-4639.

Kim, J., Zhao, T., Petralia, R.S., Yu, Y., Peng, H., Myers, E., and Magee, J.C. (2012). mGRASP enables mapping mammalian synaptic connectivity with light microscopy. Nat Methods *9*, 96-102.

King, C., Recce, M., and O'Keefe, J. (1998). The rhythmicity of cells of the medial septum/diagonal band of Broca in the awake freely moving rat: relationships with behaviour and hippocampal theta. Eur J Neurosci *10*, 464-477.

Kirby, B.P., and Rawlins, J.N.P. (2003). The role of the septo-hippocampal cholinergic projection in T-maze rewarded alternation. Behav Brain Res *143*, 41-48.

Kisfali, M., Lőrincz, T., and Vizi, E.S. (2013). Comparison of Ca2+ transients and [Ca2+]i in the dendrites and boutons of non-fast-spiking GABAergic hippocampal interneurons using two-photon laser microscopy and high- and low-affinity dyes. J Physiol *591*, 5541-5553.

Kiss, J., Buzsaki, G., Morrow, J.S., Glantz, S.B., and Leranth, C. (1996). Entorhinal cortical innervation of parvalbumin-containing neurons (basket and chandelier cells) in the rat ammon's horn. Hippocampus *6*, 239-246.

Kiss, J., Csáki, Á., Bokor, H., Shanabrough, M., and Leranth, C. (2000). The supramammillo-hippocampal and supramammillo-septal glutamatergic/aspartatergic projections in the rat: a combined [3H]d-aspartate autoradiographic and immunohistochemical study. Neuroscience *97*, 657-669.

Kitamura, T., Pignatelli, M., Suh, J., Kohara, K., Yoshiki, A., Abe, K., and Tonegawa, S. (2014). Island cells control temporal association memory. Science *343*, 896-901.

Kitchigina, V., Popova, I., Sinelnikova, V., Malkov, A., Astasheva, E., Shubina, L., and Aliev, R. (2013). Disturbances of septohippocampal theta oscillations in the epileptic brain: Reasons and consequences. Exp Neurol *247*, 314-327.

Klausberger, T. (2009). GABAergic interneurons targeting dendrites of pyramidal cells in the CA1 area of the hippocampus. Eur J Neurosci *30*, 947-957.

Klausberger, T., Magill, P.J., Marton, L.F., Roberts, J.D.B., Cobden, P.M., Buzsaki, G., and Somogyi, P. (2003). Brain-state- and cell-type-specific firing of hippocampal interneurons in vivo. Nature *421*, 844-848.

Klausberger, T., Marton, L.F., Baude, A., Roberts, J.D.B., Magill, P.J., and Somogyi, P. (2004). Spike timing of dendrite-targeting bistratified cells during hippocampal network oscillations in vivo. Nat Neurosci *7*, 41-47.

Klausberger, T., Marton, L.F., O'Neill, J., Huck, J.H.J., Dalezios, Y., Fuentealba, P., Suen, W.Y., Papp, E., Kaneko, T., Watanabe, M.*, et al.* (2005). Complementary roles of cholecystokinin- and parvalbumin-expressing GABAergic neurons in hippocampal network oscillations. J Neurosci *25*, 9782-9793.

Klausberger, T., and Somogyi, P. (2008). Neuronal diversity and temporal dynamics: The unity of hippocampal circuit operations. Science *321*, 53-57.

Knierim, J.J., Neunuebel, J.P., and Deshmukh, S.S. (2014). Functional correlates of the lateral and medial entorhinal cortex: objects, path integration and local–global reference frames. Philos Trans R Soc Lond B Biol Sci *369*.

Kohara, K., Pignatelli, M., Rivest, A.J., Jung, H.-Y., Kitamura, T., Suh, J., Frank, D., Kajikawa, K., Mise, N., Obata, Y.*, et al.* (2014). Cell type-specific genetic and optogenetic tools reveal hippocampal CA2 circuits. Nat Neurosci *17*, 269-279.

Kosaka, T., Katsumaru, H., Hama, K., Wu, J.-Y., and Heizmann, C.W. (1987). GABAergic neurons containing the Ca2+-binding protein parvalbumin in the rat hippocampus and dentate gyrus. Brain Res *419*, 119-130.

Kosaka, T., Kosaka, K., Tateishi, K., Hamaoka, Y., Yanaihara, N., Wu, J.-Y., and Hama, K. (1985). GABAergic neurons containing CCK-8-like and/or VIP-like immunoreactivities in the rat hippocampus and dentate gyrus. J Comp Neurol *239*, 420-430.

Koutsoukos, E., Angelopoulos, E., Maillis, A., Papadimitriou, G.N., and Stefanis, C. (2013). Indication of increased phase coupling between theta and gamma EEG rhythms associated with the experience of auditory verbal hallucinations. Neurosci Lett *534*, 242-245.

Kovac, S., and Walker, M.C. (2013). Neuropeptides in epilepsy. Neuropeptides *47*, 467-475.

Kramis, R., Vanderwolf, C.H., and Bland, B.H. (1975). Two types of hippocampal rhythmical slow activity in both the rabbit and the rat: Relations to behavior and effects of atropine, diethyl ether, urethane, and pentobarbital. Exp Neurol *49*, 58-85.

Kraushaar, U., and Jonas, P. (2000). Efficacy and Stability of Quantal GABA Release at a Hippocampal Interneuron–Principal Neuron Synapse. J Neurosci *20*, 5594-5607.

Krook-Magnuson, E., Varga, C., Lee, S.-H., and Soltesz, I. (2012). New dimensions of interneuronal specialization unmasked by principal cell heterogeneity. Trends Neurosci *35*, 175-184.

Krug, M., Müller-Welde, P., Wagner, M., Ott, T., and Matthies, H. (1985). Functional plasticity in two afferent systems of the granule cells in the rat dentate area: Frequency-related changes, long-term potentiation and heterosynaptic depression. Brain Res *360*, 264-272.

Krzywkowski, P., Jacobowitz, D.M., and Lamour, Y. (1995). Calretinin-containing pathways in the rat forebrain. Brain Res *705*, 273-294.

Kubota, Y., Shigematsu, N., Karube, F., Sekigawa, A., Kato, S., Yamaguchi, N., Hirai, Y., Morishima, M., and Kawaguchi, Y. (2011). Selective coexpression of multiple chemical markers defines discrete populations of neocortical GABAergic neurons. Cereb Cortex *21*, 1803-1817.

Kuhlman, S.J., and Huang, Z.J. (2008). High-resolution labeling and functional manipulation of specific neuron types in mouse brain by Cre-activated viral gene expression. PLoS ONE *3*, e2005.

Kullmann, D.M., and Lamsa, K.P. (2007). Long-term synaptic plasticity in hippocampal interneurons. Nat Rev Neurosci *8*, 687-699.

Kvitsiani, D., Ranade, S., Hangya, B., Taniguchi, H., Huang, J.Z., and Kepecs, A. (2013). Distinct behavioural and network correlates of two interneuron types in prefrontal cortex. Nature *498*, 363-366.

Lacaille, J.C. (1991). Postsynaptic potentials mediated by excitatory and inhibitory amino acids in interneurons of stratum pyramidale of the CA1 region of rat hippocampal slices in vitro. J Neurophysiol *66*, 1441-1454.

Lapray, D., Lasztoczi, B., Lagler, M., Viney, T.J., Katona, L., Valenti, O., Hartwich, K., Borhegyi, Z., Somogyi, P., and Klausberger, T. (2012). Behavior-dependent specialization of identified hippocampal interneurons. Nat Neurosci *15*, 1265-1271.

Lasztoczi, B., and Klausberger, T. (2014). Layer-specific GABAergic control of distinct gamma oscillations in the CA1 hippocampus. Neuron *81*, 1126-1139.

Lasztoczi, B., Tukker, J.J., Somogyi, P., and Klausberger, T. (2011). Terminal field and firing selectivity of cholecystokinin-expressing interneurons in the hippocampal CA3 area. J Neurosci *31*, 18073-18093.

Lau, D., de Miera, E.V.-S., Contreras, D., Ozaita, A., Harvey, M., Chow, A., Noebels, J.L., Paylor, R., Morgan, J.I., Leonard, C.S.*, et al.* (2000). Impaired fast-spiking, suppressed cortical inhibition, and increased susceptibility to seizures in mice lacking Kv3.2 K+ channel proteins. J Neurosci *20*, 9071-9085.

Lawrence, J.J. (2008). Cholinergic control of GABA release: emerging parallels between neocortex and hippocampus. Trends Neurosci *31*, 317-327.

Lawson, V.H., and Bland, B.H. (1993). The role of the septohippocampal pathway in the regulation of hippocampal field activity and behavior: Analysis by the intraseptal microinfusion of carbachol, atropine, and procaine. Exp Neurol *120*, 132-144.

Le Van Quyen, M., Staba, R., Bragin, A., Dickson, C., Valderrama, M., Fried, I., and Engel, J. (2010). Large-scale microelectrode recordings of high-frequency gamma oscillations in human cortex during sleep. J Neurosci *30*, 7770-7782.

Leao, R.N., Mikulovic, S., Leao, K.E., Munguba, H., Gezelius, H., Enjin, A., Patra, K., Eriksson, A., Loew, L.M., Tort, A.B.L.*, et al.* (2012). OLM interneurons differentially modulate CA3 and entorhinal inputs to hippocampal CA1 neurons. Nat Neurosci *15*, 1524-1530.

Lee, A.K., Manns, I.D., Sakmann, B., and Brecht, M. (2006). Whole-cell recordings in freely moving rats. Neuron *51*, 399-407.

Lee, A.K., and Wilson, M.A. (2002). Memory of sequential experience in the hippocampus during slow wave sleep. Neuron *36*, 1183-1194.

Lee, D., Lin, B.-J., and Lee, A.K. (2012). Hippocampal place fields emerge upon single-cell manipulation of excitability during behavior. Science *337*, 849-853.

Lee, T., Kaneko, T., Taki, K., and Mizuno, N. (1997). Preprodynorphin-, preproenkephalin-, and preprotachykinin-expressing neurons in the rat neostriatum: An analysis by immunocytochemistry and retrograde tracing. J Comp Neurol *386*, 229-244.

Léger, J.-F., Stern, E.A., Aertsen, A., and Heck, D. (2004). Synaptic integration in rat frontal cortex shaped by network activity. J Neurophysiol *93*, 281-293.

Leranth, C., Carpi, D., Buzsaki, G., and Kiss, J. (1999). The entorhino-septo-supramammillary nucleus connection in the rat: morphological basis of a feedback mechanism regulating hippocampal theta rhythm. Neuroscience *88*, 701-718.

Léránth, C., and Frotscher, M. (1987). Cholinergic innervation of hippocampal GAD- and somatostatin-immunoreactive commissural neurons. J Comp Neurol *261*, 33-47.

Leung, L.W. (1984). Model of gradual phase shift of theta rhythm in the rat. J Neurophysiol *52*, 1051-1065.

Levey, A.I., Edmunds, S.M., Hersch, S.M., Wiley, R.G., and Heilman, C.J. (1995). Light and electron microscopic study of m2 muscarinic acetylcholine receptor in the basal forebrain of the rat. J Comp Neurol *351*, 339-356.

Lewis, D.A., Hashimoto, T., and Volk, D.W. (2005). Cortical inhibitory neurons and schizophrenia. Nat Rev Neurosci *6*, 312-324.

Lewis, S. (2010). Synaptic transmission: A closer look at presynaptic GABAB receptors. Nat Rev Neurosci *11*, 664-665.

Li, X.G., Somogyi, P., Tepper, J.M., and Buzsáki, G. (1992). Axonal and dendritic arborization of an intracellularly labeled chandelier cell in the CA1 region of rat hippocampus. Exp Brain Res *90*, 519-525.

Li, X.G., Somogyi, P., Ylinen, A., and Buzsaki, G. (1994). The hippocampal CA3 network: an in vivo intracellular labeling study. J Comp Neurol *339*, 181-208.

Lim, D.H., LeDue, J., Mohajerani, M.H., Vanni, M.P., and Murphy, T.H. (2013). Optogenetic approaches for functional mouse brain mapping. Front Neurosci *7*.

Lisman, J., and Buzsáki, G. (2008). A neural coding scheme formed by the combined function of gamma and theta oscillations. Schizophr Bull *34*, 974-980.

Lisman, J.E. (1999). Relating hippocampal circuitry to function: recall of memory sequences by reciprocal dentate–CA3 interactions. Neuron *22*, 233-242.

Lisman, J.E., and Idiart, M.A. (1995). Storage of 7 +/- 2 short-term memories in oscillatory subcycles. Science *267*, 1512-1515.

Lisman, John E., and Jensen, O. (2013). The theta-gamma neural code. Neuron *77*, 1002-1016.

Lorente De No, R. (1934). Studies on the structure of the cerebral cortex. II. Continuation of the study of the ammonic system. J Psychol Neurol *46*, 113-177.

Lórenz-Fonfría, V.A., and Heberle, J. (2014). Channelrhodopsin unchained: Structure and mechanism of a light-gated cation channel. Biochim Biophys Acta *1837*, 626-642.

Lorincz, A., and Nusser, Z. (2008a). Cell-type-dependent molecular composition of the axon initial segment. J Neurosci *28*, 14329-14340.

Lorincz, A., and Nusser, Z. (2008b). Specificity of Immunoreactions: The Importance of Testing Specificity in Each Method. J Neurosci *28*, 9083-9086.

Lorincz, A., and Nusser, Z. (2010). Molecular identity of dendritic voltage-gated sodium channels. Science *328*, 906-909.

Losonczy, A., and Magee, J.C. (2006). Integrative properties of radial oblique dendrites in hippocampal CA1 pyramidal neurons. Neuron *50*, 291-307.

Losonczy, A., Zhang, L., Shigemoto, R., Somogyi, P., and Nusser, Z. (2002). Cell type dependence and variability in the short-term plasticity of EPSCs in identified mouse hippocampal interneurones. J Physiol *542*, 193-210.

Lovett-Barron, M., Kaifosh, P., Kheirbek, M.A., Danielson, N., Zaremba, J.D., Reardon, T.R., Turi, G.F., Hen, R., Zemelman, B.V., and Losonczy, A. (2014). Dendritic inhibition in the hippocampus supports fear learning. Science *343*, 857-863.

Lovett-Barron, M., Turi, G.F., Kaifosh, P., Lee, P.H., Bolze, F., Sun, X.H., Nicoud, J.F., Zemelman, B.V., Sternson, S.M., and Losonczy, A. (2012). Regulation of neuronal input transformations by tunable dendritic inhibition. Nat Neurosci *15*, 423-430.

Lubenov, E.V., and Siapas, A.G. (2009). Hippocampal theta oscillations are travelling waves. Nature *459*, 534-539.

Ludwig, M., and Leng, G. (2006). Dendritic peptide release and peptide-dependent behaviours. Nat Rev Neurosci *7*, 126-136.

Luo, L., Callaway, E.M., and Svoboda, K. (2008). Genetic dissection of neural circuits. Neuron *57*, 634-660.

Maccaferri, G., David, J., Roberts, B., Szucs, P., Cottingham, C.A., and Somogyi, P. (2000). Cell surface domain specific postsynaptic currents evoked by identified GABAergic neurones in rat hippocampus in vitro. J Physiol *524*, 91-116.

Madisen, L., Mao, T., Koch, H., Zhuo, J.-m., Berenyi, A., Fujisawa, S., Hsu, Y.-W.A., Garcia, A.J., Gu, X., Zanella, S.*, et al.* (2012). A toolbox of Cre-dependent optogenetic

transgenic mice for light-induced activation and silencing. Nat Neurosci *15*, 793-802.

Magee, J.C., and Johnston, D. (1997). A synaptically controlled, associative signal for hebbian plasticity in hippocampal neurons. Science *275*, 209-213.

Magnus, C.J., Lee, P.H., Atasoy, D., Su, H.H., Looger, L.L., and Sternson, S.M. (2011). Chemical and genetic engineering of selective ion channel–ligand interactions. Science *333*, 1292-1296.

Maier, N., Nimmrich, V., and Draguhn, A. (2003). Cellular and network mechanisms underlying spontaneous sharp wave–ripple complexes in mouse hippocampal slices. J Physiol *550*, 873-887.

Mann, E.O., Radcliffe, C.A., and Paulsen, O. (2005). Hippocampal gamma-frequency oscillations: from interneurones to pyramidal cells, and back. J Physiol *562*, 55-63.

Manning, J.R., Jacobs, J., Fried, I., and Kahana, M.J. (2009). Broadband shifts in local field potential power spectra are correlated with single-neuron spiking in humans. J Neurosci *29*, 13613-13620.

Manns, J.R., and Eichenbaum, H. (2006). Evolution of declarative memory. Hippocampus *16*, 795-808.

Manns, J.R., Zilli, E.A., Ong, K.C., Hasselmo, M.E., and Eichenbaum, H. (2007). Hippocampal CA1 spiking during encoding and retrieval: Relation to theta phase. Neurobiol Learn Mem *87*, 9-20.

Marcelin, B., Chauvière, L., Becker, A., Migliore, M., Esclapez, M., and Bernard, C. (2009). h channel-dependent deficit of theta oscillation resonance and phase shift in temporal lobe epilepsy. Neurobiol Dis *33*, 436-447.

Marchionni, I., Takács, V.T., Nunzi, M.G., Mugnaini, E., Miller, R.J., and Maccaferri, G. (2010). Distinctive properties of CXC chemokine receptor 4-expressing Cajal–Retzius cells versus GABAergic interneurons of the postnatal hippocampus. J Physiol *588*, 2859-2878.

Marín-Padilla, M. (1998). Cajal–Retzius cells and the development of the neocortex. Trends Neurosci *21*, 64-71.

Marín, O. (2013). Cellular and molecular mechanisms controlling the migration of neocortical interneurons. Eur J Neurosci *38*, 2019-2029.

Marin, O., and Rubenstein, J.L.R. (2001). A long, remarkable journey: Tangential migration in the telencephalon. Nat Rev Neurosci *2*, 780-790.

Marín, O., and Rubenstein, J.L.R. (2003). Cell migration in the forebrain. Annu Rev Neurosci *26*, 441-483.

Markram, H., Lübke, J., Frotscher, M., and Sakmann, B. (1997). Regulation of synaptic efficacy by coincidence of postsynaptic APs and EPSPs. Science *275*, 213-215.

Marshall, L., Henze, D.A., Hirase, H., Leinekugel, X., Dragoi, G., and Buzsáki, G. (2002). Hippocampal pyramidal cell-interneuron spike transmission is frequency dependent and responsible for place modulation of interneuron discharge. J Neurosci *22*, RC197-RC197.

Martina, M., and Jonas, P. (1997). Functional differences in Na+ channel gating between fast-spiking interneurones and principal neurones of rat hippocampus. J Physiol *505*, 593-603.

Martina, M., Schultz, J.H., Ehmke, H., Monyer, H., and Jonas, P. (1998). Functional and molecular differences between voltage-gated K+ channels of fast-spiking interneurons and pyramidal neurons of rat hippocampus. J Neurosci *18*, 8111-8125.

Maurer, A.P., Cowen, S.L., Burke, S.N., Barnes, C.A., and McNaughton, B.L. (2006). Phase precession in hippocampal interneurons showing strong functional coupling to individual pyramidal cells. J Neurosci *26*, 13485-13492.

McBain, C.J., DiChiara, T.J., and Kauer, J.A. (1994). Activation of metabotropic glutamate receptors differentially affects two classes of hippocampal interneurons and potentiates excitatory synaptic transmission. J Neurosci *14*, 4433-4445.

McBain, C.J., and Kauer, J.A. (2009). Presynaptic plasticity: targeted control of inhibitory networks. Curr Opin Neurobiol *19*, 254-262.

McCormick, D.A., Connors, B.W., Lighthall, J.W., and Prince, D.A. (1985). Comparative electrophysiology of pyramidal and sparsely spiny stellate neurons of the neocortex. J Neurophysiol *54*, 782-806.

McHugh, T.J., Blum, K.I., Tsien, J.Z., Tonegawa, S., and Wilson, M.A. (1996). Impaired hippocampal representation of space in CA1-specific NMDAR1 knockout mice. Cell *87*, 1339-1349.

Megias, M., Emri, Z., Freund, T.F., and Gulyás, A.I. (2001). Total number and distribution of inhibitory and excitatory synapses on hippocampal CA1 pyramidal cells. Neuroscience *102*, 527-540.

Melzer, S., Michael, M., Caputi, A., Eliava, M., Fuchs, E.C., Whittington, M.A., and Monyer, H. (2012). Long-range–projecting GABAergic neurons modulate inhibition in hippocampus and entorhinal cortex. Science *335*, 1506-1510.

Mienville, J.-M. (1999). Feature Article: Cajal–Retzius Cell Physiology: Just in Time to Bridge the 20th Century. Cereb Cortex *9*, 776-782.

Mienville, J.-M., and Pesold, C. (1999). Low Resting Potential and Postnatal Upregulation of NMDA Receptors May Cause Cajal–Retzius Cell Death. J Neurosci *19*, 1636-1646.

Miettinen, R., Gulyás, A.I., Baimbridge, K.G., Jacobowitz, D.M., and Freund, T.F. (1992). Calretinin is present in non-pyramidal cells of the rat hippocampus—II. Co-existence with other calcium binding proteins and gaba. Neuroscience *48*, 29-43.

Miles, R., Tóth, K., Gulyás, A.I., Hájos, N., and Freund, T.F. (1996). Differences between somatic and dendritic inhibition in the hippocampus. Neuron *16*, 815-823.

Milner, B., Squire, L.R., and Kandel, E.R. (1998). Cognitive neuroscience and the study of memory. Neuron *20*, 445-468.

Miyoshi, G., Butt, S.J.B., Takebayashi, H., and Fishell, G. (2007). Physiologically Distinct Temporal Cohorts of Cortical Interneurons Arise from Telencephalic Olig2-Expressing Precursors. J Neurosci *27*, 7786-7798.

Mizuseki, K., and Buzsaki, G. (2014). Theta oscillations decrease spike synchrony in the hippocampus and entorhinal cortex. Philos Trans R Soc Lond B Biol Sci *369*.

Mizuseki, K., Diba, K., Pastalkova, E., and Buzsaki, G. (2011). Hippocampal CA1 pyramidal cells form functionally distinct sublayers. Nat Neurosci *14*, 1174-1181.

Mizuseki, K., Sirota, A., Pastalkova, E., and Buzsáki, G. (2009). Theta oscillations provide temporal windows for local circuit computation in the entorhinal-hippocampal loop. Neuron *64*, 267-280.

Mody, I. (2005). Aspects of the homeostaic plasticity of GABAA receptor-mediated inhibition. J Physiol *562*, 37-46.

Montgomery, S.M., Betancur, M.I., and Buzsáki, G. (2009). Behavior-dependent coordination of multiple theta dipoles in the hippocampus. J Neurosci *29*, 1381-1394.

Montgomery, S.M., and Buzsáki, G. (2007). Gamma oscillations dynamically couple hippocampal CA3 and CA1 regions during memory task performance. Proc Natl Acad Sci U S A *104*, 14495-14500.

Moore, S.D., Madamba, S.G., Joels, M., and Siggins, G.R. (1988). Somatostatin augments the M-current in hippocampal neurons. Science *239*, 278-280.

Morales, M., and Bloom, F.E. (1997). The 5-HT3 Receptor Is Present in Different Subpopulations of GABAergic Neurons in the Rat Telencephalon. J Neurosci *17*, 3157-3167.

Morales, M., Hein, K., and Vogel, Z. (2008). Hippocampal interneurons co-express transcripts encoding the α7 nicotinic receptor subunit and the cannabinoid receptor 1. Neuroscience *152*, 70-81.

Moretti, d.v., Frisoni, g.b., Binetti, g., and Zanetti, o. (2011). Anatomical substrate and scalp EEG markers are correlated in subjects with cognitive impairment and Alzheimer's disease. Front Psychiatry *1*.

Morris, R.G.M. (2013). NMDA receptors and memory encoding. Neuropharmacology *74*, 32-40.

Morris, R.G.M., Garrud, P., Rawlins, J.N.P., and O'Keefe, J. (1982). Place navigation impaired in rats with hippocampal lesions. Nature *297*, 681-683.

Morris, R.G.M., Steele, R.J., Bell, J.E., and Martin, S.J. (2013). N-methyl-d-aspartate receptors, learning and memory: chronic intraventricular infusion of the NMDA receptor antagonist d-AP5 interacts directly with the neural mechanisms of spatial learning. Eur J Neurosci *37*, 700-717.

Mulkey, R.M., and Malenka, R.C. (1992). Mechanisms underlying induction of homosynaptic long-term depression in area CA1 of the hippocampus. Neuron *9*, 967-975.

Mutoh, H., Akemann, W., and Knöpfel, T. (2012). Genetically engineered fluorescent voltage reporters. ACS Chem Neurosci *3*, 585-592.

Naber, P.A., Lopes da Silva, F.H., and Witter, M.P. (2001a). Reciprocal connections between the entorhinal cortex and hippocampal fields CA1 and the subiculum are in register with the projections from CA1 to the subiculum. Hippocampus *11*, 99-104.

Naber, P.A., and Witter, M.P. (1998). Subicular efferents are organized mostly as parallel projections: A double-labeling, retrograde-tracing study in the rat. J Comp Neurol *393*, 284-297.

Naber, P.A., Witter, M.P., and Lopes da Silva, F.H. (2001b). Evidence for a direct projection from the postrhinal cortex to the subiculum in the rat. Hippocampus *11*, 105-117.

Nádasdy, Z., Hirase, H., Czurkó, A., Csicsvari, J., and Buzsáki, G. (1999). Replay and time compression of recurring spike sequences in the hippocampus. J Neurosci *19*, 9497-9507.

Nakamura, M., Sato, K., Fukaya, M., Araishi, K., Aiba, A., Kano, M., and Watanabe, M. (2004). Signaling complex formation of phospholipase Cβ4 with metabotropic glutamate receptor type 1α and 1,4,5-trisphosphate receptor at the perisynapse and endoplasmic reticulum in the mouse brain. Eur J Neurosci *20*, 2929-2944.

Nakashiba, T., Buhl, D.L., McHugh, T.J., and Tonegawa, S. (2009). Hippocampal CA3 output is crucial for ripple-associated reactivation and consolidation of memory. Neuron *62*, 781-787.

Nakazawa, K., Quirk, M.C., Chitwood, R.A., Watanabe, M., Yeckel, M.F., Sun, L.D., Kato, A., Carr, C.A., Johnston, D., Wilson, M.A., *et al.* (2002). Requirement for hippocampal CA3 NMDA receptors in associative memory recall. Science *297*, 211-218.

Nakazawa, K., Sun, L.D., Quirk, M.C., Rondi-Reig, L., Wilson, M.A., and Tonegawa, S. (2003). Hippocampal CA3 NMDA receptors are crucial for memory acquisition of one-time experience. Neuron *38*, 305-315.

Nakazawa, K., Zsiros, V., Jiang, Z., Nakao, K., Kolata, S., Zhang, S., and Belforte, J.E. (2012). GABAergic interneuron origin of schizophrenia pathophysiology. Neuropharmacology *62*, 1574-1583.

Neddens, J., Fish, K.N., Tricoire, L., Vullhorst, D., Shamir, A., Chung, W., Lewis, D.A., McBain, C.J., and Buonanno, A. (2011). Conserved interneuron-specific ErbB4 expression in frontal cortex of rodents, monkeys, and humans: Implications for schizophrenia. Biol Psychiatry *70*, 636-645.

Nissen, W., Szabo, A., Somogyi, J., Somogyi, P., and Lamsa, K.P. (2010). Cell type-specific long-term plasticity at glutamatergic synapses onto hippocampal interneurons expressing either parvalbumin or CB1 cannabinoid receptor. J Neurosci *30*, 1337-1347.

Nitsch, R., and Leranth, C. (1993). Calretinin immunoreactivity in the monkey hippocampal formation—II. Intrinsic gabaergic and hypothalamic non-gabaergic systems: An experimental tracing and co-existence study. Neuroscience *55*, 797-812.

Nitsch, R., and Leranth, C. (1996). GABAergic neurons in the rat dentate gyrus are innervated by subcortical calretinin-containing afferents. J Comp Neurol *364*, 425-438.

Nörenberg, A., Hu, H., Vida, I., Bartos, M., and Jonas, P. (2010). Distinct nonuniform cable properties optimize rapid and efficient activation of fast-spiking GABAergic interneurons. Proc Natl Acad Sci U S A *107*, 894-899.

Notomi, T., and Shigemoto, R. (2004). Immunohistochemical localization of Ih channel subunits, HCN1–4, in the rat brain. J Comp Neurol *471*, 241-276.

Nunzi, M.G., Gorio, A., Milan, F., Freund, T.F., Somogyi, P., and Smith, A.D. (1985). Cholecystokinin-immunoreactive cells form symmetrical synaptic contacts with pyramidal and nonpyramidal neurons in the hippocampus. J Comp Neurol *237*, 485-505.

Nusser, Z. (2009). Variability in the subcellular distribution of ion channels increases neuronal diversity. Trends Neurosci *32*, 267-274.

Nusser, Z., Roberts, J.D.B., Baude, A., Richards, J.G., Sieghart, W., and Somogyi, P. (1995). Immunocytochemical Localization of the α1 and β2/3 Subunits of the GABAA Receptor in Relation to Specific GABAergic Synapses in the Dentate Gyrus. Eur J Neurosci *7*, 630-646.

Nyakas, C., Luiten, P.G.M., Spencer, D.G., and Traber, J. (1987). Detailed projection patterns of septal and diagonal band efferents to the hippocampus in the rat with emphasis on innervation of CA1 and dentate gyrus. Brain Res Bull *18*, 533-545.

O'Keefe, J. (1993). Hippocampus, theta, and spatial memory. Curr Opin Neurobiol *3*, 917-924.

O'Keefe, J., and Conway, D.H. (1978). Hippocampal place units in the freely moving rat: why they fire where they fire. Exp Brain Res *31*, 573-590.

O'Keefe, J., and Dostrovsky, J. (1971). The hippocampus as a spatial map. Preliminary evidence from unit activity in the freely-moving rat. Brain Res *34*, 171-175.

O'Keefe, J., and Nadel, L. (1978). The hippocampus as a cognitive map (Oxford University Press).

O'Keefe, J., and Recce, M.L. (1993). Phase relationship between hippocampal place units and the EEG theta rhythm. Hippocampus *3*, 317-330.

O'Neill, J., Senior, T., and Csicsvari, J. (2006). Place-selective firing of CA1 pyramidal cells during sharp wave/ripple network patterns in exploratory behavior. Neuron *49*, 143-155.

O'Neill, J., Senior, T.J., Allen, K., Huxter, J.R., and Csicsvari, J. (2008). Reactivation of experience-dependent cell assembly patterns in the hippocampus. Nat Neurosci *11*, 209-215.

O'Neill, P.-K., Gordon, J.A., and Sigurdsson, T. (2013). Theta oscillations in the medial prefrontal cortex are modulated by spatial working memory and synchronize with the hippocampus through its ventral subregion. J Neurosci *33*, 14211-14224.

O'Neill, J., Pleydell-Bouverie, B., Dupret, D., and Csicsvari, J. (2010). Play it again: reactivation of waking experience and memory. Trends Neurosci *33*, 220-229.

Ogiwara, I., Miyamoto, H., Morita, N., Atapour, N., Mazaki, E., Inoue, I., Takeuchi, T., Itohara, S., Yanagawa, Y., Obata, K.*, et al.* (2007). Nav1.1 localizes to axons of parvalbumin-positive inhibitory interneurons: a circuit basis for epileptic seizures in mice carrying an Scn1a gene mutation. J Neurosci *27*, 5903-5914.

Okun, M., Naim, A., and Lampl, I. (2010). The subthreshold relation between cortical local field potential and neuronal firing unveiled by intracellular recordings in awake rats. J Neurosci *30*, 4440-4448.

Olsen, R.W., and Sieghart, W. (2009). GABAA receptors: Subtypes provide diversity of function and pharmacology. Neuropharmacology *56*, 141-148.

Olton, D.S. (1977). Spatial memory. Sci Am *236*, 82-84, 89-94, 96, 98.

Olton, D.S., Wible, C.G., and Shapiro, M.L. (1986). Mnemonic theories of hippocampal function. Behav Neurosci *100*, 852-855.

Oren, I., Hájos, N., and Paulsen, O. (2010). Identification of the current generator underlying cholinergically induced gamma frequency field potential oscillations in the hippocampal CA3 region. J Physiol *588*, 785-797.

Oren, I., Mann, E.O., Paulsen, O., and Hájos, N. (2006). Synaptic currents in anatomically identified CA3 neurons during hippocampal gamma oscillations in vitro. J Neurosci *26*, 9923-9934.

Pan, W.-X., and McNaughton, N. (2004). The supramammillary area: its organization, functions and relationship to the hippocampus. Prog Neurobiol *74*, 127-166.

Pangalos, M., Donoso, J.R., Winterer, J., Zivkovic, A.R., Kempter, R., Maier, N., and Schmitz, D. (2013). Recruitment of oriens-lacunosum-moleculare interneurons during hippocampal ripples. Proc Natl Acad Sci U S A *110*, 4398-4403.

Papp, E., Leinekugel, X., Henze, D.A., Lee, J., and Buzsaki, G. (2001). The apical shaft of CA1 pyramidal cells is under GABAergic interneuronal control. Neuroscience *102*, 715-721.

Papp, O.I., Karlócai, M.R., Tóth, I.E., Freund, T.F., and Hájos, N. (2013). Different input and output properties characterize parvalbumin-positive basket and Axo-axonic cells in the hippocampal CA3 subfield. Hippocampus *23*, 903-918.

Pascale Simon, A., Poindessous-Jazat, F., Dutar, P., Epelbaum, J., and Bassant, M.-H. (2006). Firing Properties of Anatomically Identified Neurons in the Medial Septum of Anesthetized and Unanesthetized Restrained Rats. J Neurosci *26*, 9038-9046.

Patel, J., Fujisawa, S., Berényi, A., Royer, S., and Buzsáki, G. (2012). Traveling theta waves along the entire septotemporal axis of the hippocampus. Neuron *75*, 410-417.

Patel, J., Schomburg, E.W., Berényi, A., Fujisawa, S., and Buzsáki, G. (2013). Local generation and propagation of ripples along the septotemporal axis of the hippocampus. J Neurosci *33*, 17029-17041.

Pavlides, C., and Winson, J. (1989). Influences of hippocampal place cell firing in the awake state on the activity of these cells during subsequent sleep episodes. J Neurosci *9*, 2907-2918.

Pearce, R.A. (1993). Physiological evidence for two distinct GABAA responses in rat hippocampus. Neuron *10*, 189-200.

Peng, Z., Zhang, N., Wei, W., Huang, C.S., Cetina, Y., Otis, T.S., and Houser, C.R. (2013). A reorganized GABAergic circuit in a model of epilepsy: Evidence from optogenetic labeling and stimulation of somatostatin interneurons. J Neurosci *33*, 14392-14405.

Penttonen, M., Kamondi, A., Acsády, L., and Buzsáki, G. (1998). Gamma frequency oscillation in the hippocampus of the rat: intracellular analysis in vivo. Eur J Neurosci *10*, 718-728.

Perez, Y., Morin, F., and Lacaille, J.-C. (2001). A hebbian form of long-term potentiation dependent on mGluR1a in hippocampal inhibitory interneurons. Proc Natl Acad Sci U S A *98*, 9401-9406.

Pesaran, B., Pezaris, J.S., Sahani, M., Mitra, P.P., and Andersen, R.A. (2002). Temporal structure in neuronal activity during working memory in macaque parietal cortex. Nat Neurosci *5*, 805-811.

Pesold, C., Impagnatiello, F., Pisu, M.G., Uzunov, D.P., Costa, E., Guidotti, A., and Caruncho, H.J. (1998). Reelin is preferentially expressed in neurons synthesizing γ-aminobutyric acid in cortex and hippocampus of adult rats. Proc Natl Acad Sci U S A *95*, 3221-3226.

Pfeffer, C.K., Xue, M., He, M., Huang, Z.J., and Scanziani, M. (2013). Inhibition of inhibition in visual cortex: the logic of connections between molecularly distinct interneurons. Nat Neurosci *16*, 1068-1076.

Pi, H.-J., Hangya, B., Kvitsiani, D., Sanders, J.I., Huang, Z.J., and Kepecs, A. (2013). Cortical interneurons that specialize in disinhibitory control. Nature *503*, 521-524.

Pinault, D. (1996). A novel single-cell staining procedure performed in vivo under electrophysiological control: morpho-functional features of juxtacellularly labeled thalamic cells and other central neurons with biocytin or Neurobiotin. J Neurosci Methods *65*, 113-136.

Pissadaki, E.K., Sidiropoulou, K., Reczko, M., and Poirazi, P. (2010). Encoding of spatio-temporal input characteristics by a CA1 pyramidal neuron model. PLoS Comput Biol *6*, e1001038.

Pitkanen, A., Pikkarainen, M., Nurminen, N., and Ylinen, A. (2000). Reciprocal connections between the amygdala and the hippocampal formation, perirhinal cortex, and postrhinal cortex in rat: A review. Ann N Y Acad Sci *911*, 369-391.

Poch, C., Fuentemilla, L., Barnes, G.R., and Düzel, E. (2011). Hippocampal theta-phase modulation of replay correlates with configural-relational short-term memory performance. J Neurosci *31*, 7038-7042.

Porter, J.T., Cauli, B., Tsuzuki, K., Lambolez, B., Rossier, J., and Audinat, E. (1999). Selective Excitation of Subtypes of Neocortical Interneurons by Nicotinic Receptors. J Neurosci *19*, 5228-5235.

Pouille, F., and Scanziani, M. (2004). Routing of spike series by dynamic circuits in the hippocampus. Nature *429*, 717-723.

Price, C.J., Cauli, B., Kovacs, E.R., Kulik, A., Lambolez, B., Shigemoto, R., and Capogna, M. (2005). Neurogliaform Neurons Form a Novel Inhibitory Network in the Hippocampal CA1 Area. J Neurosci *25*, 6775-6786.

Qin, J., Suh, J.M., Kim, B.-J., Yu, C.-T., Tanaka, T., Kodama, T., Tsai, M.-J., and Tsai, S.Y. (2007). The expression pattern of nuclear receptors during cerebellar development. Dev Dyn *236*, 810-820.

Qiu, C., Zeyda, T., Johnson, B., Hochgeschwender, U., de Lecea, L., and Tallent, M.K. (2008). Somatostatin receptor subtype 4 couples to the M-current to regulate seizures. J Neurosci *28*, 3567-3576.

Quattrocolo, G., and Maccaferri, G. (2013). Novel GABAergic Circuits Mediating Excitation/Inhibition of Cajal-Retzius Cells in the Developing Hippocampus. J Neurosci *33*, 5486-5498.

Quilichini, P., Sirota, A., and Buzsáki, G. (2010). Intrinsic circuit organization and theta–gamma oscillation dynamics in the entorhinal cortex of the rat. J Neurosci *30*, 11128-11142.

Radnikow, G., Feldmeyer, D., and Lübke, J. (2002). Axonal Projection, Input and Output Synapses, and Synaptic Physiology of Cajal–Retzius Cells in the Developing Rat Neocortex. J Neurosci *22*, 6908-6919.

Ramirez, S., Tonegawa, S., and Liu, X. (2014). Identification and optogenetic manipulation of memory engrams in the hippocampus. Front Behav Neurosci *7*.

Ramon y Cajal, S. (1893). Estructura del asta de Ammon y fascia dentata. Anal Soc Espan Hist Nat, 53-114.

Ramon y Cajal, S. (1911). Histologie du systeme nerveux de l'homme & des vertebres, Vol 2 (Paris: Maloine).

Ranck, J.B. (1973). Studies on single neurons in dorsal hippocampal formation and septum in unrestrained rats: Part I. Behavioral correlates and firing repertoires. Exp Neurol *41*, 462-531.

Rawlins, J.N.P., Feldon, J., and Gray, J.A. (1979). Septo-hippocampal connections and the hippocampal theta rhythm. Exp Brain Res *37*, 49-63.

Rawlins, J.N.P., and Green, K.F. (1977). Lamellar organisation in the rat hippocampus. Exp Brain Res *28*, 335-344.

Rivas, J., Gaztelu, J.M., and García-Austt, E. (1996). Changes in hippocampal cell discharge patterns and theta rhythm spectral properties as a function of walking velocity in the guinea pig. Exp Brain Res *108*, 113-118.

Roche, A.E., Bassett, B.J., Samant, S.A., Hong, W., Blobel, G.A., and Svensson, E.C. (2008). The zinc finger and C-terminal domains of MTA proteins are required for FOG-2-mediated transcriptional repression via the NuRD complex. J Mol Cell Cardiol *44*, 352-360.

Royer, S., Zemelman, B.V., Losonczy, A., Kim, J., Chance, F., Magee, J.C., and Buzsaki, G. (2012). Control of timing, rate and bursts of hippocampal place cells by dendritic and somatic inhibition. Nat Neurosci *15*, 769-775.

Rudy, B., and McBain, C.J. (2001). Kv3 channels: voltage-gated K+ channels designed for high-frequency repetitive firing. Trends Neurosci *24*, 517-526.

Ruth, R.E., Collier, T.J., and Routtenberg, A. (1982). Topography between the entorhinal cortex and the dentate septotemporal axis in rats: I. Medial and intermediate entorhinal projecting cells. J Comp Neurol *209*, 69-78.

Ruth, R.E., Collier, T.J., and Routtenberg, A. (1988). Topographical relationship between the entorhinal cortex and the septotemporal axis of the dentate gyrus in rats: II. Cells projecting from lateral entorhinal subdivision. J Comp Neurol *270*, 506-516.

Santoro, B., Grant, S.G.N., Bartsch, D., and Kandel, E.R. (1997). Interactive cloning with the SH3 domain of N-src identifies a new brain specific ion channel protein, with homology to Eag and cyclic nucleotide-gated channels. Proc Natl Acad Sci U S A *94*, 14815-14820.

Sato, M., Tabata, T., Hashimoto, K., Nakamura, K., Nakao, K., Katsuki, M., Kitano, J., Moriyoshi, K., Kano, M., and Nakanishi, S. (2004). Altered agonist sensitivity and desensitization of neuronal mGluR1 responses in knock-in mice by a single amino acid substitution at the PKC phosphorylation site. Eur J Neurosci *20*, 947-955.

Schaffer, K. (1892). Beitrag zur Histologie der Ammonshornformation. Arch Mikrosk Anat *39*, 611-632.

Schiffmann, S.N., Cheron, G., Lohof, A., d'Alcantara, P., Meyer, M., Parmentier, M., and Schurmans, S. (1999). Impaired motor coordination and Purkinje cell excitability in mice lacking calretinin. Proc Natl Acad Sci U S A *96*, 5257-5262.

Schneider, F., Gradmann, D., and Hegemann, P. (2013). Ion selectivity and competition in channelrhodopsins. Biophys J *105*, 91-100.

Schreff, M., Schulz, S., Händel, M., Keilhoff, G., Braun, H., Pereira, G., Klutzny, M., Schmidt, H., Wolf, G., and Höllt, V. (2000). Distribution, targeting, and internalization of the sst4 somatostatin receptor in rat brain. J Neurosci *20*, 3785-3797.

Schulz, S., Händel, M., Schreff, M., Schmidt, H., and Höllt, V. (2000). Localization of five somatostatin receptors in the rat central nervous system using subtype-specific antibodies. J Physiol Paris *94*, 259-264.

Schwaller, B., Brückner, G., Celio, M.R., and Härtig, W. (1999a). A polyclonal goat antiserum against the calcium-binding protein calretinin is a versatile tool for various immunochemical techniques. J Neurosci Methods *92*, 137-144.

Schwaller, B., Dick, J., Dhoot, G., Carroll, S., Vrbova, G., Nicotera, P., Pette, D., Wyss, A., Bluethmann, H., Hunziker, W.*, et al.* (1999b). Prolonged contraction-relaxation cycle of fast-twitch muscles in parvalbumin knockout mice. Am J Physiol Cell Physiol *276*, C395-C403.

Schwartzkroin, P.A., and Kunkel, D.D. (1985). Morphology of identified interneurons in the CA1 regions of guinea pig hippocampus. J Comp Neurol *232*, 205-218.

Schweitzer, P., Madamba, S.G., and Siggins, G.R. (1998). Somatostatin increases a voltage-insensitive K+ conductance in rat CA1 hippocampal neurons. J Neurophysiol *79*, 1230-1238.

Scoville, W., and Milner, B. (1957). Loss of recent memory after bilateral hippocampal lesions. J Neurol Neurosurg Psychiatry *20*, 11-21.

Sederberg, P.B., Schulze-Bonhage, A., Madsen, J.R., Bromfield, E.B., McCarthy, D.C., Brandt, A., Tully, M.S., and Kahana, M.J. (2007). Hippocampal and neocortical gamma oscillations predict memory formation in humans. Cereb Cortex *17*, 1190-1196.

Semyanov, A., Walker, M.C., and Kullmann, D.M. (2003). GABA uptake regulates cortical excitability via cell type-specific tonic inhibition. Nat Neurosci *6*, 484-490.

Shigemoto, R., Kinoshita, A., Wada, E., Nomura, S., Ohishi, H., Takada, M., Flor, P.J., Neki, A., Abe, T., Nakanishi, S.*, et al.* (1997). Differential presynaptic localization of metabotropic glutamate receptor subtypes in the rat hippocampus. J Neurosci *17*, 7503-7522.

Shigemoto, R., Kulik, A., Roberts, J.D.B., Ohishi, H., Nusser, Z., Kaneko, T., and Somogyi, P. (1996). Target-cell-specific concentration of a metabotropic glutamate receptor in the presynaptic active zone. Nature *381*, 523-525.

Shinohara, Y., Hosoya, A., Yahagi, K., Ferecskó, A.S., Yaguchi, K., Sík, A., Itakura, M., Takahashi, M., and Hirase, H. (2012). Hippocampal CA3 and CA2 have distinct bilateral innervation patterns to CA1 in rodents. Eur J Neurosci *35*, 702-710.

Siapas, A.G., Lubenov, E.V., and Wilson, M.A. (2005). Prefrontal phase locking to hippocampal theta oscillations. Neuron *46*, 141-151.

Siapas, A.G., and Wilson, M.A. (1998). Coordinated interactions between hippocampal ripples and cortical spindles during slow-wave sleep. Neuron *21*, 1123-1128.

Sidor, M.M., and McClung, C.A. (2014). Timing matters: Using optogenetics to chronically manipulate neural circuits and rhythms. Front Behav Neurosci *8*.

Sik, A., Penttonen, M., Ylinen, A., and Buzsaki, G. (1995). Hippocampal CA1 interneurons: an in vivo intracellular labeling study. J Neurosci *15*, 6651-6665.

Sik, A., Tamamaki, N., and Freund, T.F. (1993). Complete axon arborization of a single CA3 pyramidal cell in the rat hippocampus, and its relationship with postsynaptic parvalbumin-containing interneurons. Eur J Neurosci *5*, 1719-1728.

Silva, A.J., Paylor, R., Wehner, J.M., and Tonegawa, S. (1992a). Impaired spatial learning in alpha-calcium-calmodulin kinase II mutant mice. Science *257*, 206-211.

Silva, A.J., Stevens, C.F., Tonegawa, S., and Wang, Y. (1992b). Deficient hippocampal long-term potentiation in alpha-calcium-calmodulin kinase II mutant mice. Science *257*, 201-206.

Sirota, A., Montgomery, S., Fujisawa, S., Isomura, Y., Zugaro, M., and Buzsáki, G. (2008). Entrainment of neocortical neurons and gamma oscillations by the hippocampal theta rhythm. Neuron *60*, 683-697.

Skaggs, W.E., and McNaughton, B.L. (1996). Replay of neuronal firing sequences in rat hippocampus during sleep following spatial experience. Science *271*, 1870-1873.

Skaggs, W.E., McNaughton, B.L., Wilson, M.A., and Barnes, C.A. (1996). Theta phase precession in hippocampal neuronal populations and the compression of temporal sequences. Hippocampus *6*, 149-172.

Sloviter, R.S. (1989). Calcium-binding protein (calbindin-D28k) and parvalbumin immunocytochemistry: Localization in the rat hippocampus with specific reference to the selective vulnerability of hippocampal neurons to seizure activity. J Comp Neurol *280*, 183-196.

Soda, T., Nakashima, R., Watanabe, D., Nakajima, K., Pastan, I., and Nakanishi, S. (2003). Segregation and Coactivation of Developing Neocortical Layer 1 Neurons. J Neurosci *23*, 6272-6279.

Sohal, V.S., Zhang, F., Yizhar, O., and Deisseroth, K. (2009). Parvalbumin neurons and gamma rhythms enhance cortical circuit performance. Nature *459*, 698-702.

Soltesz, I. (2005). Diversity in the neuronal machine (New York: Oxford University Press).

Soltesz, I., and Deschenes, M. (1993). Low- and high-frequency membrane potential oscillations during theta activity in CA1 and CA3 pyramidal neurons of the rat hippocampus under ketamine-xylazine anesthesia. J Neurophysiol *70*, 97-116.

Somogyi, P. (1977). A specific 'axo-axonal' interneuron in the visual cortex of the rat. Brain Res *136*, 345-350.

Somogyi, P. (2010). Hippocampus: Intrinsic organization. In Handbook of Brain Microcircuits (New York: Oxford University Press), pp. 148-164.

Somogyi, P., Freund, T.F., Hodgson, A.J., Somogyi, J., Beroukas, D., and Chubb, I.W. (1985). Identified axo-axonic cells are immunoreactive for GABA in the hippocampus visual cortex of the cat. Brain Res *332*, 143-149.

Somogyi, P., Katona, L., Klausberger, T., Lasztóczi, B., and Viney, T.J. (2014). Temporal redistribution of inhibition over neuronal subcellular domains underlies state-dependent rhythmic change of excitability in the hippocampus. Philos Trans R Soc Lond B Biol Sci *369*.

Somogyi, P., and Klausberger, T. (2005). Defined types of cortical interneurone structure space and spike timing in the hippocampus. J Physiol *562*, 9-26.

Somogyi, P., Nunzi, M.G., Gorio, A., and Smith, A.D. (1983). A new type of specific interneuron in the monkey hippocampus forming synapses exclusively with the axon initial segments of pyramidal cells. Brain Res *259*, 137-142.

Soriano, E., and del Río, J.A. (2005). The cells of Cajal-Retzius: still a mystery one century after. Neuron *46*, 389-394.

Spruston, N. (2008). Pyramidal neurons: dendritic structure and synaptic integration. Nat Rev Neurosci *9*, 206-221.

Squire, L.R. (2004). Memory systems of the brain: A brief history and current perspective. Neurobiol Learn Mem *82*, 171-177.

Squire, L.R. (2009a). The legacy of patient H.M. for neuroscience. Neuron *61*, 6-9.

Squire, L.R. (2009b). Memory and brain systems: 1969–2009. J Neurosci *29*, 12711-12716.

Squire, L.R., Stark, C.E.L., and Clark, R.E. (2004). The medial temporal lobe. Annu Rev Neurosci *27*, 279-306.

Stanic, D., Brumovsky, P., Fetissov, S., Shuster, S., Herzog, H., and Hökfelt, T. (2006). Characterization of neuropeptide Y2 receptor protein expression in the mouse brain. I. Distribution in cell bodies and nerve terminals. J Comp Neurol *499*, 357-390.

Stark, E., Eichler, R., Roux, L., Fujisawa, S., Rotstein, Horacio G., and Buzsáki, G. (2013). Inhibition-induced theta resonance in cortical circuits. Neuron *80*, 1263-1276.

Staudigl, T., and Hanslmayr, S. (2013). Theta oscillations at encoding mediate the context-dependent nature of human episodic memory. Curr Biol *23*, 1101-1106.

Steward, O. (1976). Topographic organization of the projections from the entorhinal area to the hippocampal formation of the rat. J Comp Neurol *167*, 285-314.

Steward, O., and Scoville, S.A. (1976). Cells of origin of entorhinal cortical afferents to the hippocampus and fascia dentata of the rat. J Comp Neurol *169*, 347-370.

Stumpf, C. (1965). The fast component in the electrical activity of rabbit's hippocampus. Electroencephalogr Clin Neurophysiol *18*, 477-486.

Sun, C., Sun, J., Erisir, A., and Kapur, J. (2014). Loss of cholecystokinin-containing terminals in temporal lobe epilepsy. Neurobiol Dis *62*, 44-55.

Sutherland, G.R., and McNaughton, B. (2000). Memory trace reactivation in hippocampal and neocortical neuronal ensembles. Curr Opin Neurobiol *10*, 180-186.

Swanson, L.W., and Cowan, W.M. (1977). An autoradiographic study of the organization of the efferet connections of the hippocampal formation in the rat. J Comp Neurol *172*, 49-84.

Sylwestrak, E.L., and Ghosh, A. (2012). Elfn1 regulates target-specific release probability at CA1-interneuron synapses. Science *338*, 536-540.

Szabadics, J., and Soltesz, I. (2009). Functional specificity of mossy fiber innervation of GABAergic cells in the hippocampus. J Neurosci *29*, 4239-4251.

Szabadics, J., Varga, C., Molnar, G., Olah, S., Barzo, P., and Tamas, G. (2006). Excitatory effect of GABAergic axo-axonic cells in cortical microcircuits. Science *311*, 233-235.

Szabadits, E., Cserép, C., Ludányi, A., Katona, I., Gracia-Llanes, J., Freund, T.F., and Nyíri, G. (2007). Hippocampal GABAergic synapses possess the molecular machinery for retrograde nitric oxide signaling. J Neurosci *27*, 8101-8111.

Szabadits, E., Cserép, C., Szőnyi, A., Fukazawa, Y., Shigemoto, R., Watanabe, M., Itohara, S., Freund, T.F., and Nyiri, G. (2011). NMDA receptors in hippocampal GABAergic synapses and their role in nitric oxide signaling. J Neurosci *31*, 5893-5904.

Szabó, G.G., Holderith, N., Gulyás, A.I., Freund, T.F., and Hájos, N. (2010). Distinct synaptic properties of perisomatic inhibitory cell types and their different modulation by cholinergic receptor activation in the CA3 region of the mouse hippocampus. Eur J Neurosci *31*, 2234-2246.

Szentagothai, J., and Arbib, M.A. (1974). Conceptual models of neural organization. Neurosci Res Program Bull *12*, 305-510.

Tada, M., Takeuchi, A., Hashizume, M., Kitamura, K., and Kano, M. (2014). A highly sensitive fluorescent indicator dye for calcium imaging of neural activity in vitro and in vivo. Eur J Neurosci, n/a-n/a.

Takács, V., Szőnyi, A., Freund, T., Nyiri, G., and Gulyás, A. (2014). Quantitative ultrastructural analysis of basket and axo-axonic cell terminals in the mouse hippocampus. Brain Struct Funct, 1-22.

Takács, V.T., Klausberger, T., Somogyi, P., Freund, T.F., and Gulyás, A.I. (2012). Extrinsic and local glutamatergic inputs of the rat hippocampal CA1 area differentially innervate pyramidal cells and interneurons. Hippocampus *22*, 1379-1391.

Takagi, H., Somogyi, P., Somogyi, J., and Smith, A.D. (1983). Fine structural studies on a type of somatostatin-immunoreactive neuron and its synaptic connections in the rat neostriatum: a correlated light and electron microscopic study. J Comp Neurol *214*, 1-16.

Takahashi, H., and Magee, J.C. (2009). Pathway interactions and synaptic plasticity in the dendritic tuft regions of CA1 pyramidal neurons. Neuron *62*, 102-111.

Tallent, M.K. (2008). Presynaptic inhibition of glutamate release by neuropeptides: use-dependent synaptic modification. In Inhibitory Regulation of Excitatory Neurotransmission (Germany: Springer Berlin Heidelberg), pp. 177-200.

Tallent, M.K., and Siggins, G.R. (1997). Somatostatin depresses excitatory but not inhibitory neurotransmission in rat CA1 hippocampus. J Neurophysiol *78*, 3008-3018.

Tallon-Baudry, C., Bertrand, O., Delpuech, C., and Pernier, J. (1996). Stimulus specificity of phase-locked and non-phase-locked 40 Hz visual responses in human. J Neurosci *16*, 4240-4249.

Tamas, G., Buhl, E.H., Lorincz, A., and Somogyi, P. (2000). Proximally targeted GABAergic synapses and gap junctions synchronize cortical interneurons. Nat Neurosci *3*, 366-371.

Terunuma, M., Revilla-Sanchez, R., Quadros, I.M., Deng, Q., Deeb, T.Z., Lumb, M., Sicinski, P., Haydon, P.G., Pangalos, M.N., and Moss, S.J. (2014). Postsynaptic GABAB receptor activity regulates excitatory neuronal architecture and spatial memory. J Neurosci *34*, 804-816.

Thomas, M.J., Watabe, A.M., Moody, T.D., Makhinson, M., and O'Dell, T.J. (1998). Postsynaptic complex spike bursting enables the induction of LTP by theta frequency synaptic stimulation. J Neurosci *18*, 7118-7126.

Thompson, C.L., Pathak, S.D., Jeromin, A., Ng, L.L., MacPherson, C.R., Mortrud, M.T., Cusick, A., Riley, Z.L., Sunkin, S.M., Bernard, A.*, et al.* (2008). Genomic anatomy of the hippocampus. Neuron *60*, 1010-1021.

Thompson, L.T., and Best, P.J. (1989). Place cells and silent cells in the hippocampus of freely-behaving rats. J Neurosci *9*, 2382-2390.

Tort, A.B.L., Komorowski, R.W., Manns, J.R., Kopell, N.J., and Eichenbaum, H. (2009). Theta–gamma coupling increases during the learning of item–context associations. Proc Natl Acad Sci U S A *106*, 20942-20947.

Tóth, K., Freund, T.F., and Miles, R. (1997). Disinhibition of rat hippocampal pyramidal cells by GABAergic afferents from the septum. J Physiol *500*, 463-474.

Tricoire, L., Pelkey, K.A., Erkkila, B.E., Jeffries, B.W., Yuan, X., and McBain, C.J. (2011). A blueprint for the spatiotemporal origins of mouse hippocampal interneuron diversity. J Neurosci *31*, 10948-10970.

Tripodi, M., Filosa, A., Armentano, M., and Studer, M. (2004). The COUP-TF nuclear receptors regulate cell migration in the mammalian basal forebrain. Development *131*, 6119-6129.

Tsuda, S., Kee, M.Z.L., Cunha, C., Kim, J., Yan, P., Loew, L.M., and Augustine, G.J. (2013). Probing the function of neuronal populations: Combining micromirror-based optogenetic photostimulation with voltage-sensitive dye imaging. Neurosci Res *75*, 76-81.

Tukker, J.J., Fuentealba, P., Hartwich, K., Somogyi, P., and Klausberger, T. (2007). Cell type-specific tuning of hippocampal interneuron firing during gamma oscillations in vivo. J Neurosci *27*, 8184-8189.

Tukker, J.J., Lasztóczi, B., Katona, L., Roberts, J.D.B., Pissadaki, E.K., Dalezios, Y., Márton, L., Zhang, L., Klausberger, T., and Somogyi, P. (2013). Distinct Dendritic Arborization and In Vivo Firing Patterns of Parvalbumin-Expressing Basket Cells in the Hippocampal Area CA3. J Neurosci *33*, 6809-6825.

Uhlhaas, P.J., and Singer, W. (2006). Neural synchrony in brain disorders: relevance for cognitive dysfunctions and pathophysiology. Neuron *52*, 155-168.

Uhlhaas, Peter J., and Singer, W. (2012). Neuronal dynamics and neuropsychiatric disorders: Toward a translational paradigm for dysfunctional large-scale networks. Neuron *75*, 963-980.

van Strien, N.M., Cappaert, N.L.M., and Witter, M.P. (2009). The anatomy of memory: an interactive overview of the parahippocampal-hippocampal network. Nat Rev Neurosci *10*, 272-282.

van den Pol, Anthony N. (2012). Neuropeptide transmission in brain circuits. Neuron *76*, 98-115.

Vanderwolf, C.H. (1969). Hippocampal electrical activity and voluntary movement in the rat. Electroencephalogr Clin Neurophysiol *26*, 407-418.

Varga, C., Golshani, P., and Soltesz, I. (2012). Frequency-invariant temporal ordering of interneuronal discharges during hippocampal oscillations in awake mice. Proc Natl Acad Sci U S A *109*, E2726-E2734.

Vertes, R.P. (1982). Brain stem generation of the hippocampal EEG. Prog Neurobiol *19*, 159-186.

Vertes, R.P., Albo, Z., and Viana Di Prisco, G. (2001). Theta-rhythmically firing neurons in the anterior thalamus: implications for mnemonic functions of Papez's circuit. Neuroscience *104*, 619-625.

Vida, I., Bartos, M., and Jonas, P. (2006). Shunting inhibition improves robustness of gamma oscillations in hippocampal interneuron networks by homogenizing firing rates. Neuron *49*, 107-117.

Viney, T.J., Lasztoczi, B., Katona, L., Crump, M.G., Tukker, J.J., Klausberger, T., and Somogyi, P. (2013). Network state-dependent inhibition of identified hippocampal CA3 axo-axonic cells in vivo. Nat Neurosci *16*, 1802-1811.

Vullhorst, D., Neddens, J., Karavanova, I., Tricoire, L., Petralia, R.S., McBain, C.J., and Buonanno, A. (2009). Selective expression of ErbB4 in interneurons, but not pyramidal cells, of the rodent hippocampus. J Neurosci *29*, 12255-12264.

Wang, D., and Maler, L. (1998). Differential roles of Ca2+/calmodulin-dependent kinases in posttetanic potentiation at input selective glutamatergic pathways. Proc Natl Acad Sci U S A *95*, 7133-7138.

Weiser, M., Bueno, E., Sekirnjak, C., Martone, M.E., Baker, H., Hillman, D., Chen, S., Thornhill, W., Ellisman, M., and Rudy, B. (1995). The potassium channel subunit KV3.1b is localized to somatic and axonal membranes of specific populations of CNS neurons. J Neurosci *15*, 4298-4314.

Wells, C.E., Amos, D.P., Jeewajee, A., Douchamps, V., Rodgers, J., O'Keefe, J., Burgess, N., and Lever, C. (2013). Novelty and anxiolytic drugs dissociate two components of hippocampal theta in behaving rats. J Neurosci *33*, 8650-8667.

Whittington, M.A., Cunningham, M.O., LeBeau, F.E.N., Racca, C., and Traub, R.D. (2011a). Multiple origins of the cortical gamma rhythm. Dev Neurobiol *71*, 92-106.

Whittington, M.A., Roopun, A.K., Traub, R.D., and Davies, C.H. (2011b). Circuits and brain rhythms in schizophrenia: a wealth of convergent targets. Curr Opin Pharmacol *11*, 508-514.

Wilson, M.A., and McNaughton, B.L. (1994). Reactivation of hippocampal ensemble memories during sleep. Science *265*, 676-679.

Witter, M.P. (2007). Intrinsic and extrinsic wiring of CA3: Indications for connectional heterogeneity. Learn Mem *14*, 705-713.

Witter, M.P., and Amaral, D.G. (1991). Entorhinal cortex of the monkey: V. Projections to the dentate gyrus, hippocampus, and subicular complex. J Comp Neurol *307*, 437-459.

Wittner, L., Henze, D., Záborszky, L., and Buzsáki, G. (2007). Three-dimensional reconstruction of the axon arbor of a CA3 pyramidal cell recorded and filled in vivo. Brain Struct Funct *212*, 75-83.

Wong, H.C., Sternini, C., Lloyd, K., De Giorgio, R., and Walsh, J.H. (1996). Monoclonal antibody to VIP: production, characterization, immunoneutralizing activity, and usefulness in cytochemical staining. Hybridoma *2*, 133-139.

Wong, R.K.S., and Prince, D.A. (1978). Participation of calcium spikes during intrinsic burst firing in hippocampal neurons. Brain Res *159*, 385-390.

Woodnorth, M.-A., and McNaughton, N. (2002a). Similar effects of medial supramammillary or systemic injection of chlordiazepoxide on both theta frequency and fixed-interval respondin. Cogn Affect Behav Neurosci *2*, 76-83.

Woodnorth, M.A., and McNaughton, N. (2002b). Benzodiazepine receptors in the medial-posterior hypothalamus mediate the reduction of hippocampal theta frequency by chlordiazepoxide. Brain Res *954*, 194-201.

Woodruff, A., Xu, Q., Anderson, S.A., and Yuste, R. (2009). Depolarizing effect of neocortical chandelier neurons. Front Neural Circuits *3*.

Woodruff, A.R., McGarry, L.M., Vogels, T.P., Inan, M., Anderson, S.A., and Yuste, R. (2011). State-Dependent Function of Neocortical Chandelier Cells. J Neurosci *31*, 17872-17886.

Wouterlood, F.G., Saldana, E., and Witter, M.P. (1990). Projection from the nucleus reuniens thalami to the hippocampal region: Light and electron microscopic tracing study in the rat with the anterograde tracer Phaseolus vulgaris-leucoagglutinin. J Comp Neurol *296*, 179-203.

Wyass, J.M., and Van Groen, T. (1992). Connections between the retrosplenial cortex and the hippocampal formation in the rat: A review. Hippocampus *2*, 1-11.

Yeckel, M.F., and Berger, T.W. (1990). Feedforward excitation of the hippocampus by afferents from the entorhinal cortex: redefinition of the role of the trisynaptic pathway. Proc Natl Acad Sci U S A *87*, 5832-5836.

Yeckel, M.F., and Berger, T.W. (1995). Monosynaptic excitation of hippocampal CA1 pyramidal cells by afferents from the entorhinal cortex. Hippocampus *5*, 108-114.

Ylinen, A., Bragin, A., Nadasdy, Z., Jando, G., Szabo, I., Sik, A., and Buzsaki, G. (1995a). Sharp wave-associated high-frequency oscillation (200 Hz) in the intact hippocampus: network and intracellular mechanisms. J Neurosci *15*, 30-46.

Ylinen, A., Soltész, I., Bragin, A., Penttonen, M., Sik, A., and Buzsáki, G. (1995b). Intracellular correlates of hippocampal theta rhythm in identified pyramidal cells, granule cells, and basket cells. Hippocampus *5*, 78-90.

Young, C.K., and McNaughton, N. (2009). Coupling of Theta Oscillations between Anterior and Posterior Midline Cortex and with the Hippocampus in Freely Behaving Rats. Cereb Cortex *19*, 24-40.

Zanos, T.P., Mineault, P.J., and Pack, C.C. (2011). Removal of spurious correlations between spikes and local field potentials. J Neurophysiol *105*, 474 -486.

Zar, J.H. (1999). Biostatistical analysis, 4 edn (Upper Saddler River: Prentice Hall).

Zemankovics, R., Veres, J.M., Oren, I., and Hájos, N. (2013). Feedforward inhibition underlies the propagation of cholinergically induced gamma oscillations from hippocampal CA3 to CA1. J Neurosci *33*, 12337-12351.

Zezula, J., and Sieghart, W. (1991). Isolation of type I and type II GABAA-benzodiazepine receptors by immunoaffinity chromatography. FEBS Lett *284*, 15-18.

Zhang, L., Chen, G., Niu, R., Wei, W., Ma, X., Xu, J., Wang, J., Wang, Z., and Lin, L. (2012). Hippocampal theta-driving cells revealed by Granger causality. Hippocampus *22*, 1781-1793.

Zhang, L., and McBain, C.J. (1995). Voltage-gated potassium currents in stratum oriens-alveus inhibitory neurones of the rat CA1 hippocampus. J Physiol *488*, 647-660.

Zhang, W.N., Pothuizen, H.H.J., Feldon, J., and Rawlins, J.N.P. (2004). Dissociation of function within the hippocampus: effects of dorsal, ventral and complete excitotoxic hippocampal lesions on spatial navigation. Neuroscience *127*, 289-300.

Zola-Morgan, S., and Squire, L.R. (1985). Medial temporal lesions in monkeys impair memory on a variety of tasks sensitive to human amnesia. Behav Neurosci *99*, 22-34.

Zola-Morgan, S., Squire, L.R., and Amaral, D.G. (1986). Human amnesia and the medial temporal region: enduring memory impairment following a bilateral lesion limited to field CA1 of the hippocampus. J Neurosci *6*, 2950-2967.